PERMEABILITY STUDIES OF WOOD FIBRE BEDS

By

ALEXANDER KWUN TO CHAN, B.A.Sc., M.A.Sc.

A Thesis

Submitted to the School of Graduate Studies

in Partial Fulfilment of the Requirements

for the Degree

Doctor of Philosophy

McMaster University

PERMEABILITY STUDIES OF WOOD FIBRE BEDS

Doctor of Philosophy (1994) McMaster University

(Chemical Engineering) Hamilton, Ontario

TITLE: Permeability Studies of Wood Fibre Beds

AUTHOR: Alexander Kwun To Chan, M.A.Sc. (University of Toronto)

B.A.Sc. (University of Toronto)

SUPERVISORS: Dr. R.H. Pelton

Dr. M.H.I. Baird

NUMBER OF PAGES: xviii, 290

ABSTRACT

The effect of polystyrene beads and nylon fibres on the permeability of bleached kraft pulp fibre beds was studied experimentally. Three types of experiments: 1) constant head filtration, 2) elastic permeation, and 3) fixed bed permeation were carried out. Four types of fibre beds were used: 1) pulp fibres only, 2) pulp fibres and plastic beads, 3) pulp fibres and nylon fibres, and 4) pulp fibres, nylon fibres and plastic beads. The beads used were 80 μm in diameter while the diameter and the length of the nylon fibre were 45 μm and 1.89 mm respectively. The beads were used as a model for dispersed air bubbles in pulp suspensions, while the nylon fibres were chosen because their specific surface area and specific swollen volume were close to those of the beads.

In a filtration experiment, a fibre bed was formed from the corresponding suspension while pressure drop across the bed and cumulative filtrate weight were recorded. Specific filtration resistance values for the suspensions were calculated from the filtrate weight data. It was observed that specific filtration resistance increased with bead content in the slurry while filtration resistance decreased with an increase in the content of nylon fibres in the suspension. A mathematical model based on permeation equations was derived to simulate the filtration process.

In a permeation experiment, the fibre bed formed in a filtration experiment was subjected to a complete recovery-compression cycle starting with the maximum pressure drop. Flowrate of water through the bed and the thickness of the bed were measured as a function of the pressure drop. Fibre beds of the

four different compositions all displayed hysteresis in both the flowrate and bed thickness data. Bed thickness data were correlated by regression analysis and under flow induced compression the thicknesses were found to be linear or nearly linear functions of the pressure drop acting across the bed. The presence of plastic beads did not affect the structure and thickness of the beds, suggesting that the plastic beads were able to fit into the pores of the pulp bed without disrupting the structure. By contrast, nylon fibres increased both the permeability and the thickness of the bed because of the formation of a more open network structure. The mathematical model proposed by Jonsson and Jonsson was used to predict compression behaviour; however, the concave form of plot of thickness versus pressure drop during recovery was not predicted by any of the current bed compressibility models.

Permeability of the compressed bed formed in the filtration experiment was measured in a fixed bed permeation experiment. Permeability of the bed was used to calculate the specific external surface area and specific swollen volume of the bed materials using the Kozeny-Carman equation. It was found that for both the pulp/bead system and the pulp/nylon fibre system, the specific surface area and specific swollen volume of the bed were linear functions of the content of polystyrene beads or nylon fibres. The specific surface area and specific swollen volume of beds that contained pulp fibres, nylon fibres and plastic beads were predicted, within 7%, by the linear supposition of the specific surface area and specific swollen volume of the bed constituents. This analysis is important because it permits estimation of the effect of air bubbles on the permeability of pulp pads in various processes in the pulp and paper industry.

Acknowledgments

I would like to express my most sincere gratitude and appreciation to all the people who have supported me through out the course of this thesis. In particular, I would like to acknowledge:

Professor R.H. Pelton and **Professor M.H.I. Baird**, my supervisors, for their patience, guidance, encouragement, and inspiration. I would also like to sincerely thank them for their considerable effort in reviewing this work. Without their generous support, persistence and dedication, this work is not possible.

Professor B. Latto, member of my supervisory committee, for his excellent service and advice.

Professor S. Zhu, for his help in both the experimental and theoretical aspects of this work. I would also like to thank him for his friendship and I have benefited tremendously from the many technical discussions as well as private conversations with him.

W. Warriner and **G.M. Slater**, for their excellent job of fabricating the experimental equipment and constructing the data acquisition system.

M. Ajersch, for his valuable assistance in the design and fabrication of the experimental equipment, operation of the video/image analysis equipment and many helpful discussions.

B. Grosse and **B. Wasmund**, for their friendship and help on image analysis.

Mr. M. Maric for measuring the length of the kraft pulp fibres on the Kajaani analyser.

Dr. S. Loewen for useful discussions, **Professor C. Bennington** for kindly supplying the nylon fibres and **Mr. W. Pichard**, PAPRICAN, for the preparation and characterization of the bleached kraft pulp fibres.

I would also like to acknowledge McMaster Centre for Pulp and Paper Research, Department of Chemical Engineering, McMaster University, Abitibi-Price, Natural Sciences and Engineering Research Council of Canada and the Chemimechanical Wood Pulps Network for their financial support.

Most of all, I would like to dedicate this thesis to my family for their continual support and encouragement for my long years of study. Without their understanding, this work would not have been possible.

LIST OF FIGURES

LIST OF TABLES

1. INTRODUCTION

1.1 Background

Paper and paper products are involved in almost every area of human activity. Paper is widely used for dissemination of information and all writing and printing is done on paper. Paper is also used as packaging material with possibilities in structural applications [Smook, 1982]. Due to the vast spectrum of applications of paper, it plays an extremely important role in the economy of Canada. Pulp and paper products are the highest value added exports of Canada [CPPA Reference Tables, 1986].

In the pulp and paper industry, there are a number of processes that involve the formation of a pulp fibre pad and subsequent permeation of water through the pad. Examples of the processes include papermaking, brownstock washing, and deckering. In the papermaking process on a traditional Fourdrinier paper machine, water is removed from a suspension of pulp fibres by filtration under gravity or vacuum suction so that the pulp fibres form a paper mat. Further dewatering of the wet fibre mat is achieved mainly by suction from drainage devices under the paper machine wire. In a rotary vacuum brownstock washer, the cylindrical washer drum rotates in a vat that contains a suspension of cooked pulp fibres. Vacuum is applied inside the washer when it rotates into the suspension and a thick pulp fibre mat is therefore left adhering to the washer drum when it emerges from the suspension in the vat. Wash water is sprayed onto the layer of pulp on the cylinder to displace the black liquor. Deckering is

the process by which pulp suspensions are thickened after low consistency operations such as cleaning and screening [Smook, 1982]. In the deckering process, the gravity thickener is used to increase the consistency of the pulp suspension to the 4 to 8% range. The decker consists of a vat that contains the low consistency pulp suspension and a rotating cylinder. Water flows into the cylinder so that a layer of pulp is retained on the rotating cylinder. The layer of pulp is then couched off by a rubber roll before the thickened pulp is discharged.

Air bubbles are entrained into pulp stock in various operations in a paper mill due to agitation of the stock, cascading of the flow and free-draining water [Smook, 1982]. Air in wood pulp suspensions exists in three states: 1) free air, 2) residual air and 3) dissolved air [Boadway, 1956; Sedivy, 1969; Miller, 1977; Barkowski, 1978; Kurtz, 1983]. Free air refers to bubbles that are neither adhering to the pulp fibres nor mechanically entrapped by fibre flocs in the slurry. Residual air represents dispersed air bubbles that are either mechanically entrapped by fibre flocs or bubbles that adhere to the surface of the pulp fibres with a contact angle. Residual air tends to cause the fibres to float and flocculate and thereby hinders dewatering of the slurry. Dissolved air is air that is dissolved in the pulp suspension which does not have any effect on pulp drainage.

It is known by pulp and paper researchers that the presence of dispersed air bubbles in pulp suspensions influences all three of the operations (papermaking, brownstock washing and deckering) mentioned above. For example, pinholes and weak spots in paper are attributed to the presence of dispersed air in the pulp stock. Also, the reduction in drainage rate of water through the paper machine wire is a consequence of the presence of dispersed air. In brownstock washing, workers believe that the presence of dispersed of

entrained air bubbles in the fibre mat reduces the mass flux of wash water. Therefore, chemical defoamers are added to the pulp slurry in quantities of up to 2 pounds per ton of stock to remove the troublesome bubbles [Morton, 1986]. Also, Kurtz [1983] reported improvement in stock washing productivity due to deaeration of the pulp stock.

Although it is accepted by papermakers that the presence of dispersed air in pulp furnishes causes problems in papermaking and brown stock washing, published research results in this area are extremely lacking. No mathematical model or theory on the filtration and permeation of pulp slurries in the presence of dispersed air has been published. Therefore, fundamental studies on the effects of dispersed air on drainage of pulp suspensions will provide the much needed insight into this phenomenon of dispersed air in pulp suspensions. This thesis is an attempt to correlate dispersed air content with the drainage properties of pulp suspensions by applying results from fundamental filtration and permeation experiments using model suspensions containing pulp fibres, nylon fibres and plastic beads.

1.2 Objectives

The overall objective of this work is to study the effect of dispersed particles on the drainage of pulp suspensions. Filtration and permeation characteristics of pulp suspensions are the two drainage parameters chosen for study. Initial experimentation showed that air bubbles were too difficult to work with because it is extremely difficult to generate air bubbles in a reproducible manner and because bubbles easily coalesce. Instead, plastic beads of a size range that

corresponds to bubbles found in typical headbox stock (an average diameter of 112 μm) were used in place of air bubbles in the experiments. Well-characterized bleached kraft pulp fibres were used to prepare suspensions for the experiments while various amounts of nylon fibres were also added to the suspensions to allow investigation of the effect of fibre rigidity on pulp drainage. The objectives of the work described in the thesis are:

Objective 1: To determine the effects of polymer particles on the drainage characteristics of pulp suspensions by performing filtration and permeation experiments with suspensions that contain a fixed amount of pulp with variable concentrations of plastic beads.

Objective 2: To measure the effects of rigid nylon fibres on the drainage characteristics of pulp suspensions by performing filtration and permeation experiments with suspensions that contain a fixed amount of pulp with variable concentrations of nylon fibres.

Objective 3: To develop mathematical models to predict the filtration and permeation behaviour of pulp suspensions as a function of the properties of the materials in the pad.

Objective 4: To use the experimental and theoretical results to predict the effect of air on: 1) the freeness and specific filtration resistance of pulp suspensions, and 2) the wash water flux in a typical brownstock washer.

1.3 Organization of Thesis

Chapter 2 of the thesis presents a review of the literature relevant to this work. The chapter begins with a summary of the literature on the effects of dispersed air bubbles on papermaking. Existing theories on fluid permeation through porous media are presented next followed by a review of the work on permeation through beds consisting of synthetic fibres, pulp fibres and binary mixtures. A general flow model of fluid permeation through a compressible bed is then reviewed. Summary of the research on filtration of suspensions and in particular, wood pulp suspensions, is presented next. The chapter concludes with a summary on the status of research on pulp drainage and a summary of the important equations.

Chapter 3 gives a detailed description of the materials used and the apparatus used to carry out the experiments. Description of the experimental procedures follows and the chapter concludes with a summary of the procedure for analysis of the filtrate and the composition of the fibre pad resulting from the experiments.

Chapter 4 reports the results from fixed bed permeation experiments. In this work, the mass of pulp in the pad was kept constant while seven different bead concentrations (0, 0.025, 0.05, 0.1, 0.2, 0.3 & 0.4 kg/m^3) and nine different nylon fibre concentrations (0, 0.05, 0.1, 0.15, 0.2, 0.25, 0.3, 0.36 & 0.5 kg/m^3) were used. Ternary systems consisting of pulp fibres (at a fixed concentration of 0.1 kg/m^3), nylon fibres (at a fixed concentration of 0.36 kg/m^3) and plastic beads (at 3 possible concentrations of: 0, 0.05 & 0.1 kg/m^3) were also studied in the experiments. Permeability data of the pads are analyzed using the Kozeny-

Carman equation. Mixing rules are described which correlated permeability of the pads to the properties of the fibres and beads as well as the content of the constituents. Discussion of the results and the conclusions follow.

Results from elastic permeation experiments are presented in Chapter 5. A mathematical model is used to correlate the experimental data. The validity of the model and its accuracy in prediction of elastic permeation is investigated after discussion of the experimental data is presented.

Chapter 6 is a presentation of the results from the filtration experiments. Presentation of the experimental results is followed by the data obtained by numerical simulation. A numerical scheme that makes use of permeation equations and properties of the bed materials is developed to simulate the filtration behaviour of the various pulp suspensions. Discussion of the results and conclusions drawn from the results complete the chapter.

Chapter 7 discusses the implications of the results from this study on pulp and paper operations. The effect of dispersed air bubbles on the specific filtration resistance of pulp suspensions predicted from the properties of the pad materials is presented. The correlation between dispersed air content and the freeness of air-containing pulp suspensions is presented next. The chapter concludes with discussions on: 1) the effect of dispersed air content on the mass flux of wash water in a typical brownstock washer, and 2) the effect of rigid fibres on the dewatering of pulp suspensions.

Chapter 8 summarizes the conclusions drawn from the results and concludes the thesis by listing the recommendations for future work.

2. REVIEW OF RELEVANT LITERATURE

Papermaking consists of the dispersion of pulp fibres in water followed by the removal of water from the suspension to obtain the sheet of paper. A key part of the process involves filtration of the pulp suspension and permeation of water through the pulp fibre mat. Papermakers believe that the presence of dispersed air in pulp suspensions interferes with filtration and permeation which causes problems in machine efficiency and paper quality.

The overall objective of this work is to study the effect of dispersed particles on the drainage of pulp suspensions. The polystyrene spheres are used as models for air bubbles because it is extremely difficult to produce air bubbles in a reproducible manner. The existing literature on the effects of dispersed air on papermaking, filtration of suspensions and permeation through porous media will be reviewed in this chapter.

2.1 Dispersed Air in Papermaking

In a modern paper machine, air is mixed into the pulp suspensions during various stages of agitation and flow cascading in the complicated flow system [Smook, 1982]. Therefore, air bubbles are usually present in the pulp stock feeding headboxes.

Air in wood pulp suspensions exists in three states: 1) free air, 2) residual air, and 3) dissolved air [Boadway, 1956; Sedivy, 1969; Miller, 1977; Barkowski, 1978; Kurtz, 1983]. Free air refers to dispersed air bubbles in the pulp suspension that are

neither adhering to the pulp fibres nor mechanically entrapped by fibre flocs in the slurry. Therefore, free air will rise to the top of the pulp suspension if the stock is left standing. Residual air collectively represents dispersed air bubbles that are either mechanically entrapped by fibre flocs or bubbles that are adhered to the surface of the pulp fibres with a contact angle. Residual air, in either form, tends to cause the fibres to float and flocculate thereby resulting in a retardation in the drainage rate of the slurry. Dissolved air is air that is dissolved in the pulp suspension which does not have any effect on pulp drainage unless the slurry becomes supersaturated with air and the dissolved air begins to turn into either free or residual air. Isler and Widmer [1979] demonstrated that large non-adhering free bubbles in a pulp suspension tend to rise to the surface in horizontal flow of pulp suspensions through experimental flow channels while small bubbles remain either adhered to or trapped in the fibre network.

Currently, there is no established industrial standard equipment for measuring the total air content in wood pulp furnishes. Several attempts have been made by various groups to design and develop air sensors [Woodworth, 1990]. An on-line air sensor based on ultrasonic principles [Karras et al., 1988] has been designed to measure the dispersed air content in pulp suspensions. An automated piston type of on-line air sensor that gives an estimate of the total air content of pulp by measuring the compressibility of the pulp suspension is commercially available [Process Air Measurement by Product And Process Engineering Concepts, Sumner, WA, U.S.A.]. A hand-held device that made use of the compressibility principle [Entrained Gas Tester by G.B. Machining Inc., Puyallup, WA, U.S.A.] is available to provide quick and crude estimates of the total air content in pulp slurries. Recently, papers by Ajersch et al. [1992a, 1992b] documented the use of a U-tube

densitometer to measure the amount of dispersed air in newsprint pulp suspensions. Excellent agreement was achieved between results obtained by the densitometer measurements and direct measurement by a commercial process air measurement sensor.

Although the devices mentioned above appear to be promising candidates for the measurement of dispersed air content in pulp furnishes, none is capable of providing any information on the size of bubbles in the pulp suspensions. Little is known about typical bubble size distributions and bubble loci in pulp furnishes. Few attempts have been made to measure sizes of bubbles. Isler and Widmer [1979] measured the size of air bubbles in pulp suspensions and reported that free air bubbles had diameters in the range of 80 to 300 μm while 60 μm was the upper limit to the diameters of air bubbles bound to fibres. Photographs by Jacobsson [1981] showed that bubble diameters were in the range of 10 to 100 μm. Size distribution of bubbles in pulp suspensions were determined optically by image analysis by Ajersch et al. [1992a, 1992b] who reported number average bubble diameters in the range of 50 to 120 μm for air bubbles in a newsprint paper machine. The U-tube densitometry method had also been applied to measure the bubble size distribution in addition to the total dispersed air content in a dispersion of air bubbles in water [Zhu et al., 1993]. A mass transfer model was derived to give the bubble size distribution of the dispersion in response to a step change in pressure. Reasonable agreement was achieved when the results were compared against bubble size distribution measured by image analysis technique. Volume average bubble diameters in the range 67 to 109 μm were reported.

It has long been recognized by papermakers that dispersed air bubbles in headbox pulp suspensions cause weak spots and pinholes in the paper sheet [Mardon & Gavelin, 1955]. Also, the presence of dispersed air bubbles in pulp suspensions interferes with water removal on the paper machine wire and results in poor drainage efficiency as well as poor paper machine performance. Brecht and Kirchner [1961] have shown with British handsheet studies that with increasing air content, drainage time and air permeability increased while tensile strength, wet-web strength and smoothness decreased. Regrettably, no information on the size of the bubbles in the suspensions was given. Although papermakers recognize the adverse effects of dispersed air on the papermaking process and actions are being taken to remove the air, there are few publications on air in papermaking besides the work of Brecht and Kirchner because direct and quantitative analysis of the influence of dispersed air on paper machine performance is difficult. Articles on this topic were reviewed by May and Buckman [1975]. In these papers [De Cew, 1935; Boadway, 1956; Sedivy, 1969; May & Buckman, 1975; Barkowski, 1978; Isler & Widmer, 1978; Jacobsson, 1981; Kurtz, 1978, 1983, 1987; Lorz, 1986], the problems caused by air were usually just mentioned as recognized phenomena while no quantitative correlation between total air content and the various affected parameters in papermaking had been proposed. No experimental work had been reported in the articles to back up the statements on the effects of dispersed air; the work of Brecht and Kirchner was always cited as the only experimental proof of the effects of air on papermaking although Kurtz reported improvement in stock washing [1983] and paper machine efficiency as well as paper quality [1987] due to deaeration of the pulp stock.

In addition to the paper by Brecht and Kirchner and the two articles by Kurtz, only one recent article is found in this research area of pulp drainage in the presence of dispersed air [Karras & Springer, 1989]. This paper reported a study on the drainage of kraft pulp slurry using a modified dynamic drainage jar tester instead of conventional filtration equipment. The filtration resistance of pulp suspension was studied as a function of the air content and/or polymer flocculant dosage in the slurry. It was shown that the presence of air caused an increase in the specific filtration resistance of the pulp slurry. Formation and tensile strength of the resulting paper was also adversely affected especially in the presence of polymer flocculants.

In the general area of filtration in the presence of dispersed air, there is an article on the study of the effects of entrapped air bubbles on fine coal dewatering via filtration [Chi et al., 1985]. Filtration and dewatering experiments were carried out with three types of coal slurries: 1) deaerated cake: the coal slurry was deaerated under vacuum for 15 minutes before filtration, 2) normal cake: no special treatment was applied to the coal slurry before the experiment, and 3) aerated cake: air bubbles were introduced into the coal slurry by a gas sparger (60 – 100 μm pore size) before filtration. After the filtration experiments, samples of the filter cakes were prepared by vacuum impregnation using epoxy resin. The vacuum impregnated cake samples were studied under the microscope and image analysis with quantitative stereology was applied to measure mean particle size, pore size distributions and average bubbles size in the filter cake. Experimental results showed that: 1) the surface-volume mean diameter of air bubbles ranged from 50 to 350 μm, 2) deaerated cakes exhibited higher permeabilities than aerated cakes, 3) filtration rate and cake permeability

decreased with increasing mean bubble size, 4) filtration flux and cake permeability decreased with an increase in the volume percent of air bubbles, and 5) average bubble diameter increased with increasing volume percent of air in the cakes. In summary, the work by Chi et al. has demonstrated that the presence of air causes a reduction in the rate of filtration and dewatering of coal slurries.

Papermakers have adopted various methods in an attempt to rectify the problems in papermaking caused by the presence of air in pulp. The two most common practices are the installation of deculators [Smith, 1952; Duskin & Jenkins, 1953; Jacobsson, 1958] in the stock system feeding paper machines and the application of chemical defoamers to the pulp furnishes. Deculators are large vacuum compartments into which pulp suspensions enter before being fed to the paper machine. The vacuum inside the deculator is usually held at 0.4 to 1.1 kPa below the boiling pressure of the incoming stock [Casey, 1980]. When the pulp slurry is pumped into the deculator, the stock impinges on a plate to break the suspension into a finely divided spray such that mechanically entrapped residual air bubbles can be easily removed. Entrained air in the pulp furnish is then flashed off due to the vacuum inside the deculator. Defoamers are chemical additives for removing foam, preventing foam from forming and eliminating existing entrained air from pulp slurries [Barrett & MacKay, 1986]. Chemical defoamers work by one of the following four mechanisms: 1) reducing the effectiveness of foam stabilizers, 2) displacing foam formers, 3) destabilizing foams, and 4) forming localized weak spots in the foams. Currently, these two methods of installation of deculators and defoamer usage are commonly adopted by most papermakers. However, little is known of the effectiveness of

either method although Ajersch et al. [1992b] concluded from their mill trial that defoamers appeared to be capable of removing all dispersed air bubbles from a headbox stock. Although defoamers and deculators appear to be effective means of dispersed air removal, they represent a substantial capital and operating cost because of the pumping, cleaning and maintenance required [Casey, 1980]. Therefore, understanding of the effects of dispersed air on papermaking in a quantitative manner will help in the decision of investment on deaeration measures and optimization of the deaeration process if air removal from stock is deemed necessary.

2.2 Permeation

Fluid flow is extremely important in the papermaking industry. Fluid transport is involved in different facets of the papermaking process such as the conveying of pulp fibres in the mill, brownstock washing where lignin is displaced by water, and suspension drainage on a paper machine. In the context of papermaking, suspension drainage refers to the removal of water from the pulp suspension during the sheet forming process in a paper machine. Drainage on a paper machine is a complex process that involves filtration of the pulp fibre suspension under gravity, filtration under vacuum, and the flow of water through the wet fibre web formed by filtration. Therefore, understanding of the fundamental principles of fluid permeation and filtration will help elucidate the mechanisms involved in drainage on a paper machine and thereby enable optimization and better control of the process.

2.2.1 General Permeation Behaviour in Porous Media

Fluid flow through conduits is a well studied subject. With the definitive work of Poiseuille, Reynolds, von Karman, Prandtl and many other researchers, the flow process is well understood and it is possible to make predictions about flow parameters such as frictional pressure drop and flowrates. Permeation is the flow of fluid through a bed of solid particles while the particles can be either rigid or compressible. However, permeation through porous media is a more complex phenomenon than the flow of fluid in conduits. Basic flow equations that describe flow through conduits still apply but the complexity is caused by the complicated geometry of channels in the bed.

Darcy's original experiment [Darcy, 1856] is probably the best known early attempt in the study of permeation in porous beds. In 1856, Darcy studied permeation of water through sand filters in connection with the fountains in the city of Dijon, France [Bear, 1972]. Darcy carried out experiments using a column that contained a vertical homogeneous sand bed with the flow of water driven by a hydrostatic head. Darcy concluded from the results of his experiments that the volumetric flowrate of fluid through the sand bed was directly proportional to the pressure drop driving the flow and the cross sectional area of the bed; and inversely proportional to the thickness of the bed. Therefore, based on Darcy's conclusions, a simple equation that is linear in all its parameters can be used to relate the pressure drop to the flowrate through a porous bed. This resulting equation is called Darcy's law and the proportionality constant in the equation is called the permeability coefficient:

$$Q = \frac{dV}{dt} = \frac{K \cdot A \cdot \Delta P}{\mu L} \quad ....(2.2.1)$$

where Q is the volumetric flowrate of fluid permeating through a porous bed with a thickness of L and an area of A under a driving force of ΔP. μ is the dynamic viscosity of the fluid and K is the permeability of the porous bed in m^2. In summary, Darcy's law relates the volumetric flowrate of the fluid to parameters that characterize the flow conditions as well as the microstructure in the porous medium (through the permeability coefficient, K) and it is the best known equation that describes permeation of fluids through porous media.

Although Darcy's law is simple and easy to use, it has limitations. Subsequent experiments by other researchers have demonstrated that Darcy's law is not obeyed at higher flowrates. According to Darcy's law, the flowrate of water through a porous bed is proportional to the first power of the pressure drop. However, as the flowrate of water increases past a certain threshold, usually in terms of a critical Reynolds number defined for porous media [Dullien, 1979], flowrate becomes proportional to an increasing power of the pressure drop. The value of the exponent increases from unity to a maximum value of two indicating a transition in the flow regime in the porous bed. The transition is analogous to the laminar to turbulent transition in pipe flow except that in porous media flow, the transition is caused by the gradual dominance of inertial effects over viscous effects while the totally random, chaotic turbulent regime exhibited in pipe flow is not observed until extremely high flowrates [Happel & Brenner, 1973]. A number of equations have been proposed to correlate flowrate and pressure

drop data beyond the range of validity of Darcy's law and the best known among them is probably the Ergun equation:

$$\frac{D_p \varepsilon^3 \Delta P}{\rho u^2 (1-\varepsilon) L} = \frac{150\mu(1-\varepsilon)}{D_p u \rho} + 1.75 \quad ....(2.2.2)$$

where ρ is the density of the fluid that flows through a porous bed with a depth of L and a porosity of ε at a superficial velocity of u. D_p is the diameter of the particles in the bed. A list of these flow equations can be found in standard fluid dynamics texts like Bird et al. [1960].

The value of the permeability coefficient in Darcy's law is a function dependent on the geometry of the network of materials that make up the bed [Robertson & Mason, 1949]. Numerous attempts, both theoretical and empirical, have been made to propose equations that relate properties of the bed materials to overall permeability of the bed. However, rigorous analytical studies of permeation through porous media are possible only under the streamline flow regime because of the random nature of turbulent flow. Following Darcy's work, many different approaches have been taken to model single-phase flow in a porous medium in the laminar regime to come up with permeability functions. Among all these attempts, there are two common approaches: 1) fluid flow inside a conduit is extended to the analogous case of flow through a porous bed, and 2) flow around solid particles immersed in the fluid is applied to analyze porous media flow. For porous beds that have low to medium porosities, the conduit approach is more appropriate while the latter approach, which is often termed "drag theory", depicts the flow regime much more closely in beds with high

porosities. In between the two extremes, however, it is "a gray area where neither approach seems to have a clear advantage over the other" [Dullien, 1979].

Considerable research efforts using the conduit flow approach have been made in the area of porous media flow [Dullien, 1979]. The Kozeny-Carman equation [Carman, 1956], which is often called the "hydraulic radius theory", is probably the best known mathematical expression describing streamline flow through a porous medium based on the conduit flow model. This equation was first proposed by Kozeny [1927] and later modified by Carman [1937, 1938c, 1956]. The Kozeny-Carman equation relates the permeability of a porous bed to the physical properties of the material that makes up the bed. Such properties include the specific surface area, specific volume and shape factor of the bed materials as well as the tortuosity of the flow paths within the bed.

In the Kozeny-Carman model, the random and irregular way in which different capillaries inside the bed were connected with each other was ignored. The porous medium was assumed to be equivalent to a conduit with a channel diameter given by four times the hydraulic radius. The hydraulic radius was defined as the ratio between the void volume of the medium and the hydrodynamic surface area of the channels in the medium. The superficial fluid velocity was corrected to give the average velocity inside the channel by incorporating the porosity of the bed. Tortuosity of the bed was included in the model to give an estimate of the actual length of the path traveled by the fluid. Along with a shape factor for the particles making up the bed, all the above information was applied to the Hagen-Poiseuille equation [Bird et al., 1960] for flow through a cylindrical tube with a radius of r and a length L:

$$Q = \frac{\pi r^4 \Delta P}{8\mu L} \quad ....(2.2.3)$$

and the outcome was an equation that related the flowrate of fluid through a porous medium to the properties of the constituent particles of the bed. By comparing this equation to Darcy's law, the subsequent equation for the permeability of the bed was called the Kozeny-Carman equation:

$$K = \frac{1}{K''S^2} \frac{\varepsilon^3}{(1-\varepsilon)^2} \quad ....(2.2.4)$$

where K'' was the dimensionless Kozeny coefficient, ε was the porosity in the bed and S was the specific surface area of the bed materials. The validity of the Kozeny-Carman equation has been confirmed by various experimental works using materials that include powders, sand and glass spheres [Carman, 1937, 1938c, 1939b, 1948, 1956; Fowler & Hertel, 1940; Hatch, 1940; Sullivan & Hertel, 1940] and the equation has been widely used for measuring surface areas of powders and different particles [Carman, 1938c, 1939b, 1948; Ingmanson, 1952, 1954].

If the Kozeny-Carman equation is combined with Darcy's law, the resulting equation relates the flowrate through a bed to the structural properties of the bed materials,

$$Q = \frac{dV}{dt} = \frac{A \cdot \Delta P}{\mu L} \frac{1}{K''S^2} \frac{\varepsilon^3}{(1-\varepsilon)^2} \quad ....(2.2.5)$$

The Kozeny-Carman equation applies to flow through an incompressible porous medium as long as the flow is in the laminar regime. Nevertheless, it is possible to apply the Kozeny-Carman equation to permeation through compressible media such as fibre beds although modifications to the equation are necessary. For pulp pads, since wood pulp fibres swell in water, the volume of solid material in the porous medium is given by the product of the mass and specific swollen volume of the material in the bed. If the mass concentration of fibres in the bed is used in place of the mass of solid, the product becomes the volume fraction of solid material in the bed. Therefore, the following equation gives the void fraction in the bed [Robertson & Mason, 1949],

$$\varepsilon = 1 - \alpha c \quad ....(2.2.6)$$

where α and c are the specific swollen volume and mass concentration of the material in the bed respectively. In the Kozeny-Carman equation, S is the surface area to volume ratio of the bed material. That is, S is the ratio of external surface area offered by all the solid material to the total volume of the material. Since fibres swell in water, it is more convenient and more appropriate to use a specific surface area that is defined on a mass basis. Therefore, a new parameter, σ, the specific surface area of fibres (area per unit mass of fibre) is introduced. σ is given by,

$$\sigma = \alpha \cdot S \quad ....(2.2.7)$$

K", the Kozeny coefficient, combines both the shape factor of the bed material and the tortuosity of the flow channels inside the bed. For perfect spheres, K" has a value of 5 and for fibres, K" is found to be 5.55 [Fowler & Hertel, 1940; Sullivan &

Hertel, 1942]. However, it had been demonstrated by Davies [1952] and Ingmanson et al. [1959] that for fibrous bed having a porosity exceeding 0.8, the value of K″ was no longer constant. Instead, it became a strong function of porosity and it obeyed the following empirical equation for porosities up to 0.96,

$$K'' = 3.5\frac{\varepsilon^3}{(1-\varepsilon)^{1/2}}\left[1+57(1-\varepsilon)^3\right] \quad ....(2.2.8)$$

After introducing K″ and σ into the Kozeny-Carman equation and rearranging the terms, the following equation is obtained for highly compressed beds with porosities below 0.8 [Ingmanson, 1952, 1954; Robertson & Mason, 1949],

$$K = \frac{(1-\alpha c)^3}{5.55\sigma^2 c^2} \quad ....(2.2.9)$$

By rearranging the terms, the Kozeny-Carman equation becomes,

$$\left(Kc^2\right)^{1/3} = \left(\frac{1}{5.55\sigma^2}\right)^{1/3}(1-\alpha c) \quad ....(2.2.10)$$

The above equation is the linearized form of the Kozeny-Carman equation. If the concentration of solid materials in the bed and the permeability of the bed at that concentration are known, a straight line will be obtained when $(Kc^2)^{1/3}$ is plotted against c if the Kozeny-Carman equation is obeyed. From the intercepts on the two axes, the specific external surface area, σ, and the specific swollen volume, α, can be found. This is a method of measuring the specific surface area and specific swollen volume of bed materials that has been frequently used. It has been well documented that this method yielded reproducible and

accurate results; close agreement was achieved when the specific surface areas of glass spheres, glass fibres, cotton fibres and wool fibres measured by the permeability method were compared with specific surface areas calculated from dimensions of the particles measured by microscopic techniques [Sullivan & Hertel, 1942]. The specific external surface area of the bed material is the area that the fluid has to cover when it permeates through the porous bed, and the specific swollen volume of the bed material is the volume occupied by the bed material that is denied to flow. Knowledge of these parameters is useful because paper strength has been related to the specific surface area of the constituent pulp fibres [Ingmanson & Andrews, 1959; Thode & Ingmanson, 1959].

There is a potential pitfall in obtaining the specific surface area and specific swollen volume using the linearized form of the Kozeny-Carman equation. The concentration of solid materials in the bed is the independent variable in the equation. When the linearized equation is plotted, solid concentration is not only the independent variable but it also appears in the predicted variable (which appears as the ordinate variable in the plot). As a result, by plotting the Kozeny-Carman equation in the linearized form, the independent variable is being plotted against a function of itself. It is only logical to expect some degree of correlation between the independent variable and the predicted variable regardless of whether the data follow the relationship expressed by the equation [Rowe, 1963]. Also, plotting the independent variable against itself will have the probable effect of masking deviation of the experimental data from the Kozeny-Carman equation. Therefore, in order to obtain accurate estimate of the specific surface area and specific swollen volume, nonlinear regression analysis using Equation (2.2.9) was applied to the data in this work. Analysis of the data using

linear regression method based on the linearized equation (Equation (2.2.10)) provides an excellent initial estimate of the specific surface area and specific swollen volume for the nonlinear regression analysis.

2.2.2 Permeation Behaviour in Fibrous Beds

Most of the earlier works on permeation through porous media are carried out using granular beds and studies of flow through fibrous beds are relatively less extensive in volume. Nevertheless, fibrous beds have been studied because of their application as gas filters and of their capability to form stable structure of high porosity [Dullien, 1979; Jackson & James, 1986].

It has been reported that flowrate and pressure drop data for fibrous beds are correlated satisfactorily by the Ergun equation (Equation (2.2.2)) [MacDonald et al., 1979]. The applicability of the Kozeny-Carman equation to fibrous media has been demonstrated experimentally for textile fibres and wood pulps [Sullivan & Hertel, 1942; Robertson & Mason, 1949]. Robertson and Mason [1949] applied a linearized form of the Kozeny-Carman equation to determine the specific external surface area and the specific hydrodynamic volume of the fibres used.

Less than twenty papers exist as the experimental database on permeation through fibrous media. Many fibrous materials have been used in these experiments including stainless steel wire crimps, glass rods, copper wire, glass wool, fibreglass, yarn, goat wool, human hair, cotton, rayon, kapok, down, filter pads, nylon fibres, and kapron fibres. Empirical correlations for permeability of fibrous beds are described in a review article by Jackson and James [1986]. Among all these works, the research carried out by Kyan et al. [1970] is worth

noting because it is the only one that had studied the effect of fibre rigidity on permeability of the bed.

In their paper, Kyan et al. stated that although fibre beds had high porosities, "unexpectedly" high pressure drops were required to drive the flow through the beds. Two causes for the phenomenon were postulated: 1) dead space and dead channels must exist in the bed. Therefore, the effective porosity was much lower than the actual bed porosity; and 2) the flexibility or elasticity of the constituent fibres served as a means of flow pressure energy dissipation, thereby a higher pressure drop is required to compensate for the loss. Therefore, Kyan et al. proposed a new friction factor-Reynolds number correlation for fibrous beds. First, they assumed that the fluid did not flow in a significant portion of the pores in the bed. Using a geometric model of inclined fibres intercrossed with fibres perpendicular to flow, equations for bed porosity and effective porosity were derived. They then assumed that the total pressure drop was made up of viscous losses, form drag and fibre deflection. On the basis of modifications of existing equations for viscous losses, form drag and fibre flexural losses, an expression for the total pressure drop was derived. However, the term corresponding to form drag in the equation was actually representing the pressure drop due to total drag although the total drag included viscous shear losses. Therefore, the term corresponding to form drag was redundant and erroneous [Dullien, 1979]. Nevertheless, Kyan et al. combined all these expressions and obtained a final equation for the correlation. Experiments were carried out with glass, dacron and nylon fibres using water and glycerol solution. The correlation equation with three unknown parameters from the three pressure loss terms was fitted to experimental data. Although the elastic

modulus of the fibres used should have been measured separately, the modulus of elasticity was combined with the parameter for fibre deflection and estimated from the measured data. The equation was then applied to predict other experimental results. Agreement was achieved between experimental data and predicted results. Nonlinear behaviour was observed with the data at high flowrates. The authors attributed the nonlinearity to fibre deflection and concluded that fibre flexibility did have an effect on the permeability of the fibrous bed. However, this point has yet to be proven by comparing theoretical predictions using independently measured elastic moduli of the fibres with experimental results.

The volume of theoretical literature on permeation through fibrous media is smaller than that for experimental studies [Jackson & James, 1986]. The general approach taken by researchers is to model constituent fibres as rigid cylinders and the whole porous medium as a regular or random matrix of the cylinders. In order to obtain permeability expressions, the Navier-Stokes equations or equivalent flow equations are solved for the particular matrix geometry. The most commonly used matrix configurations are: 1) flow parallel to an array of cylinders; 2) flow perpendicular to an array of cylinders; and 3) flow through a random 3-D array of cylinders.

For flow parallel to an array of cylinders, the cylinders are usually arranged in an orderly periodic array and all the cylinders are parallel to the flow. The earliest work was done by Langmuir in 1942. Happel [1959] incidentally obtained the same result by using an identical approach but his work was quoted more often than that of Langmuir's. A unit cell approach was adopted in the derivation to account for the geometry of the porous media. In the unit cell, a single

cylinder was considered to be surrounded by a concentric cylindrical fluid envelope. The ratio of the volume of the void space in the unit cell to the volume of the whole unit cell was equal to the porosity of the bed. It was assumed that flow in the cell was representative of that in the porous medium. Creeping flow regime was assumed in the model derivation. To solve the fluid motion equation for the flow field, Happel used the boundary conditions of: 1) no slip at the surface of the cylinder, and 2) zero shear stress at the boundary of the unit cell. The resulting permeability equation for flow parallel to an array of cylinders was:

$$K = \frac{d^2}{16(1-\varepsilon)}\left[-\ln(1-\varepsilon) - 1.5 + 2(1-\varepsilon) - \frac{(1-\varepsilon)^2}{2}\right] \quad ....(2.2.11)$$

where ε was the porosity in the bed and d was the diameter of the cylinders. Predictions by Equation (2.2.11) had been compared to experimental data in a review paper by Jackson and James [1986] and close agreement was achieved.

Non-circular cells were also used in solution of the same problem. Sparrow and Loeffler [1959] used square and triangular arrays and solved the flow equations by a truncated power series technique. The Langmuir-Happel equation and Sparrow and Loeffler solution agree well with each other but these theoretical predictions tend to overestimate the permeability of fibre beds because the fibres in real beds are not perfectly aligned with flow [Jackson & James, 1986].

For the case of flow perpendicular to an array of cylinders, Happel [1959] applied the aforementioned unit cell approach and solved the problem by

specifying a boundary of zero shear at the cell outer surface. The resulting equation for permeability in an array of cylinders perpendicular to the flow is:

$$K = \frac{d^2}{32(1-\varepsilon)}\left[-\ln(1-\varepsilon) + \frac{(1-\varepsilon)^2 - 1}{(1-\varepsilon)^2 + 1}\right] \quad ....(2.2.12)$$

where ε was the porosity in the bed and d was the diameter of the cylinders. In the same year, Kuwabara solved the same problem using the same unit cell approach except that a boundary condition of zero vorticity was specified at the unit cell boundary. A totally different approach was used by Spielman and Goren [1968]. They modelled the permeation process by the flow around a single cylinder that was surrounded by a homogeneous porous medium. The Brinkman-Debye-Bueche equation, which is the superposition of the Navier-Stokes equation and Darcy's law, was used in place of the Navier-Stokes equation. Since the permeability of the medium was the unknown, the solution led to an implicit relation for the permeability. This approach of Spielman and Goren is usually referred to as the "swarm theory" and it has led to a series of works by Howells [1974], Neale and Masliyah [1975], and Guzy et al. [1983]. The Spielman and Goren solution demonstrated good agreement with experimental data.

There is much less work done in the case of flow through random 3-D arrays. Spielman and Goren had applied the swarm theory to 3-D arrays and come up with a solution for the permeability of the bed. The other work on 3-D arrays was that done by Jackson and James in 1982 [Jackson & James, 1986]. Both

of these models agree well with each other and agree well with experimental data.

2.2.3 Permeation Behaviour in Beds of Pulp Fibres

Robertson and Mason were among the first to study the permeation of water through pulp fibre beds. In 1949, Robertson and Mason [1949] carried out permeation experiments using a variety of fibres including sulphite pulp and kraft pulp. Fibre beds having masses of approximately 4 to 8 g were formed from pulp suspensions with a consistency of 0.2 to 0.5%. The Kozeny-Carman equation was applied to analyze the data and the specific external surface area as well as the specific swollen volume of the various fibres were calculated. The effect of beating on the specific surface area was studied but no useful correlation with sheet properties could be found. Nevertheless, specific swollen volume of the pulp fibres was found to be related to the burst strength of the paper. In another paper by Mason [1950], various methods for determining the specific surface area of fibres were reviewed and results from different researchers were presented. Particular emphasis was given to the pad permeation method that Robertson and Mason used in 1949.

In the 1950's, a number of researchers applied the fluid permeation method used by Robertson and Mason to determine the specific surface area of various fibres. Brown [1950] used the permeation method with air to determine the specific surface area of pulp fibres and glass wool. Ingmanson et al. applied the fluid permeation method to measure the specific surface area and specific swollen volume of the pulp fibres they used in the filtration studies [1952; 1954].

Ingmanson et al. also made use of the permeation method to measure the specific surface area of pulp fibres and correlate them with beating time, specific filtration resistance, and strength of the sheet [1959a; 1959b].

In a later article, Ingmanson et al. reported results for fluid permeation through fibre beds with high porosities [1959d]. For fibre beds with a high porosity (exceeding a porosity of 0.8), the Kozeny coefficient became a function of bed porosity and ceased to be constant at 5.55. Ingmanson suggested that the equation proposed by Davies (Equation (2.2.9)) should be used to obtain the value of the Kozeny coefficient. Higgins and DeYong [1965] had also carried out research in the permeation through fibres beds with high porosity. They pointed out that the Kozeny-Carman equation was no longer applicable at high bed porosities and they followed the drag theory proposed by Emersleben [1925] and Iberall [1950] and came up with an equation that related permeability to pad geometry as well as pore geometry.

2.2.4 Permeation Behaviour in Beds of Binary Mixtures

Filter-aids are solid particles that are added to slurries to enhance drainage during filtration. The enhancement in drainage is possible because the filter-aid particles provide a large number of pores for the liquid to flow through [Cain, 1979]. Carman [1938b; 1939a] concluded that the filter-aid particles contribute by providing extra porosity and a more rigid structure to the filter cake for enhancement in drainage. It was demonstrated by Carman [1938b, 1939a] that the Kozeny-Carman equation was still obeyed in permeation of a fluid through the mixture and a simple linear mixing rule could be applied to estimate the subsequent specific

surface area of the mixture from the specific surface area of the constituent particles.

In 1963, Shirato, Sambuichi and Okamura [1963] studied the filtration behavior of a mixture of two slurries. Shirato et al. predicted the filtration characteristics of the mixture based on an additive law. The resulting mathematical equations were complicated (required the knowledge of a large number of physical parameters). An important assumption was that each particle of either slurry would carry with it a pore volume that was specific to the original slurry in the mixture. Difficulties arose since filling of the pore volume of one material by small particles of the other could not be described. Heertjes and Zuideveld [1978] derived a mathematical model to predict the specific filtration resistance of a cake consisting of a mixture of particles. The model was based on the blocking model of a filter cloth. Unfortunately, the predictive power of the model was limited and the agreement between experimental and theoretical results was not good.

A series of papers on pressure drop across multi-component glass fibre filters was published by Clarenburg et al. [Clarenburg & Werner, 1965; Clarenburg & Schiereck, 1968]. Two mathematical models, each adopting a different approach, were proposed by the authors to correlate the data. One of the models [Clarenburg & Werner, 1965] was based on two effects proposed by the authors that were opposite in action: shadow effect and structural effect. Clarenburg and Werner stated that, in a two component filter consisting of fine fibres and coarse fibres, the shadow effect was caused by the screening of a fraction of the surface area of the coarse fibres from the flow by the fine fibres. The authors argued that screening reduced the effective contribution of the coarse fibres to the total

resistance of the filter. Since fine fibres had a much larger specific external surface area and hence a much higher resistance to flow than the coarse fibres, the shadow effect caused an increase in the resistance to flow which was manifested in an increase in pressure drop across the filter. However, the structural effect had a tendency to reduce the flow resistance. Clarenburg and Werner explained that in a single component filter consisting only of fine fibres, the pores formed between the fibres were small. Introduction of coarse fibres into the filter would perturb the small pores and resulted in a more open fibrous structure with larger pores that offered less resistance to flow. The other mathematical model [Clarenburg & Schiereck, 1968] was based on purely geometrical considerations of the pore size distributions and tortuosity in multi-component glass fibre filters of arbitrary composition. Experiments were carried out with multi-component filters of glass fibres having different lengths and diameters. Excellent agreement was achieved between experimental data and theoretical predictions. However, the models were derived for rigid and linear glass fibres. Therefore, the applicability of the models to filters consisting of flexible pulp fibres is questionable.

In 1979, Abe, Hirosue and Yokota [1979] developed a packed bed model to predict the specific permeation resistance of a binary mixture. Packing and permeation experiments were carried out using glass beads and calcite particles to test the validity of the model. The model predictions agreed well with experimental results. Experimental data had also shown that the model worked well for the non-spherical calcite particles. However, derivation of the model was not given nor was it referred to in the article.

In 1991, Ethier [1991] carried out a theoretical study of flow through mixed fibrous materials. In the study, creeping flow through porous beds consisting of two fibres which had widely different radii was modelled. The porous bed was treated as a porous matrix of fine fibres into which coarse cylindrical fibres were embedded. The flow was assumed to be governed by the Brinkman-Debye equation. A unit cell approach and a periodic lattice of coarse fibres were used to account for the geometry of the porous bed. Predictions based on the two idealized bed geometries were in good agreement with each other. Regrettably, no experimental data had been included to demonstrate the accuracy of the theoretical predictions.

Another binary system that has been studied consisted of pulp fibres and filler particles. Springer and Kuchibhotla [1992] reported an experimental study to determine the specific filtration resistance of hardwood eucalyptus pulp and various fillers with filler concentrations in the range of 10 to 40% by weight. The fillers used included clay, titanium dioxide, calcium carbonate and a blend of clay and titanium dioxide. Experiments were carried out using a modified drainage, vacuum and retention tester. Fillers were found to cause the specific filtration resistance to increase and calcium carbonate offered the highest filtration resistance, followed by clay, the clay/titanium dioxide blend and titanium dioxide. Increase in filler concentration caused a corresponding increase in the specific filtration resistance. This was consistent with the Kozeny-Carman equation which indicated that an increase in the total external surface area would result in a higher resistance to flow. Therefore, this study confirmed that the Kozeny-Carman equation was applicable to binary systems of pulp and fillers.

In 1992, the permeability of binary packings of spheres was studied by Andrade et al. [1992]. In this article, the packed beds were considered as microscopically disordered porous media and network models were employed to represent the pore space in the packing. Effective media approximation theory was used to calculate the macroscopic transport properties. Experiments were performed by measuring the pressure drop for air flow through packed bed of glass spheres. Agreement between the experimental data and theoretical predictions were good for particles having a small radius ratio (a particle radius ratio of 1.9) while model predictions at large particle radius ratio (a particle radius ratio of 4.2) underestimated the permeability and only displayed the observed trends.

2.2.5 Flow Model of Permeation Through Fibrous Beds

Considerable efforts have been made to model the flow of fluid through unconstrained pads [Gurnham & Masson, 1946; Andersson & Gardh, 1970; Caulfield et al., 1982; Carlsson et al., 1983; Hoering et al., 1983, Jonsson et al., 1987; El-Hosseiny, 1991; Roux & Vincent, 1991]. A mathematical model of the permeation process was recently proposed by the Swedish research group Jonsson and Jonsson [1992a, 1992b]. This is a good model of the flow process because it provides a general framework that enables the use of different mechanistic equations to account for the permeation and compressibility of the bed. An outline of the model is given below.

2.2.5.1 Mass Balance of Materials in The Bed

The volume of a compressible porous bed, V_{tot}, was made up of two components: the void volume, V_v, and volume of the solid plus any moisture adsorbed and immobilized by the solid material, V_{sa}. Therefore,

$$V_{tot} = V_v + V_{sa} \quad ....(2.2.13)$$

It was assumed that only the void volume was compressible. For non-swelling solids, such as sand or glass fibre, the amount of adsorbed moisture was insignificant. Therefore, V_{sa} of such solids is approximately equal to V_s, the volume of the solid material. Since the solids were assumed to be incompressible, V_{sa} could be expressed as:

$$V_{sa} = m_s \alpha_{sa} \quad ....(2.2.14)$$

where m_s was the mass of dried solid material in the bed while α_{sa} was the swollen volume per unit mass of dried solid material.

Porosity in the bed, ε, can be expressed in terms of the volumes defined above:

$$\varepsilon = \frac{V_v}{V_{tot}} = 1 - \frac{V_{sa}}{V_{tot}} \quad ....(2.2.15)$$

The void ratio was defined as the ratio between the void volume and the volume of the solid material plus adsorbed moisture. The following expression relates void ratio to porosity:

$$X = \frac{V_v}{V_{sa}} = \frac{\varepsilon}{1-\varepsilon} \quad \text{....(2.2.16)}$$

Since a porous bed was under compression by fluid stresses, the thickness of the bed would be changing according to the pressure drop. The normal coordinate system would make calculations difficult as the thickness of the bed kept changing in response to the change in pressure and there would be transport of water as well as fibres when the pad was compressed. The main feature of the work by Jonsson and Jonsson was to devise a pad coordinate system that would deform with the porous medium by assuming that there was no mixing of solid material between different layers in the solid matrix. Under this assumption, the mass of solid in any layer of the pad remained constant while compression and expansion of the pad were still possible. The new coordinate system which essentially described the normalized position in the pad was denoted as the y coordinate system in the paper by Jonsson and Jonsson. The variable y would vary from 0 at the septum surface of the bed to 1 at the free surface of the bed. The normal coordinate system that was based on the actual thickness of the bed was subsequently denoted as the z coordinate system. The two coordinate systems are shown in Figure 2.2.5.1.

The volume of solid material plus adsorbed water was ΔV_{sa} for an elemental volume of the bed with a thickness of Δy. Since V_{sa} was assumed to be constant,

$$\frac{\Delta V_{sa}}{\Delta y} = \text{constant} = \frac{dV_{sa}}{dy} \quad \text{....(2.2.17)}$$

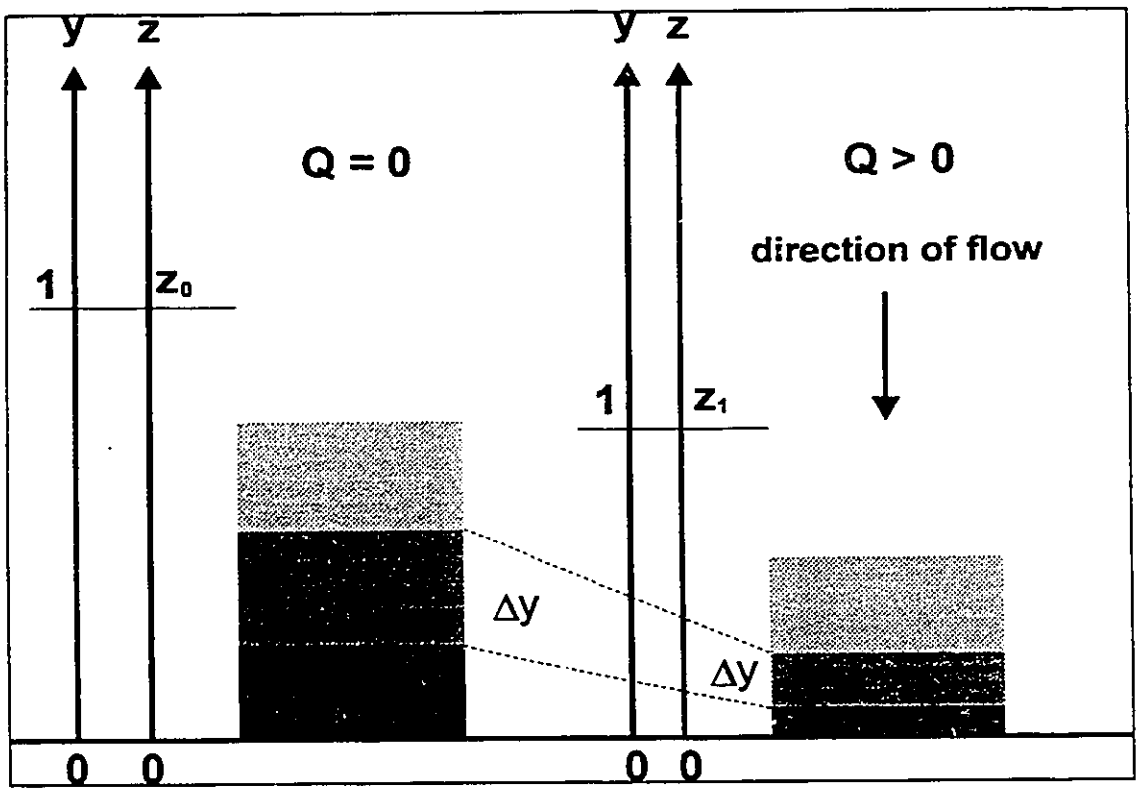

Figure 2.2.5.1 Schematic diagram of the z– and y– coordinate systems.

The mass of solid material present in a volume element of thickness Δy was given by:

$$\Delta m_s = w \cdot A \cdot \Delta y \quad ....(2.2.18)$$

where w was the weight of solid material per unit cross-sectional area of the pad and A was the cross-sectional area of the bed. According to Equation (2.2.14), ΔV_{sa} could be expressed as:

$$\Delta V_{sa} = \Delta(m_s \alpha_{sa}) = \Delta m_s \cdot \alpha_{sa} \quad ....(2.2.19)$$

A mass balance on the volume element yielded the following equation:

$$\Delta V_{sa} = \alpha_{sa} \cdot \Delta m_s = \frac{A \cdot \Delta z}{1+X} \quad ....(2.2.20)$$

By combining Equations (2.2.18), (2.2.19) and (2.2.20), the following relationship between the z- and y- coordinate systems was obtained:

$$\frac{dz}{dy} = w\alpha_{sa}(1+X) \quad ....(2.2.21)$$

2.2.5.2 Hydrodynamics of Permeation

When fluid flowed through a porous medium, the total pressure, P_{tot}, was divided into two components: the mechanical stress, P_m, which tended to compress the porous medium and the hydraulic pressure, P_h, which acted as the driving force to cause the flow. Both the mechanical stress and the hydraulic pressure developed their own profile within the porous medium but their sum always remained constant. Therefore, for any position within the porous bed:

$$P_{tot} = P_h + P_m = \text{constant} \quad ....(2.2.22)$$

Applying Darcy's law to a differential volume of the bed would result in the differential form of the Darcy's law equation:

$$\frac{Q}{A} = \frac{K}{\mu}\frac{dP_h}{dz} \quad ....(2.2.23)$$

Since the use of dimensionless quantities simplified calculations, a dimensionless permeability function, K(X), was defined as:

$$K(X) = \frac{K}{1+X}\left(\frac{S_s}{\alpha_{sa}}\right)^2 \quad ....(2.2.24)$$

where $S_s = \sigma_{solid} = \sigma_{sa}$; $\alpha_{sa} = \alpha_s$ and both of these quantities were based on mass of the solid material only. Therefore, the equation became:

$$K(X) = \frac{K}{1+X}\left(\frac{\sigma_{sa}}{\alpha_{sa}}\right)^2 \quad ....(2.2.25)$$

Combining Equations (2.2.21), (2.2.22) and (2.2.25) resulted in an equation for the flow through the porous medium:

$$\frac{Q}{A} = \frac{\alpha_{sa}}{\mu w \sigma_{sa}^{\ 2}} K(X) \frac{dP_h}{dy} \quad ....(2.2.26)$$

Since the sum of P_h and P_m was a constant, Equation (2.2.26) could be re-written as:

$$\frac{Q}{A} = -\frac{\alpha_{sa}}{\mu w \sigma_{sa}^{\ 2}} K(X) \frac{dP_m}{dy} \quad ....(2.2.27)$$

At steady state, the flow within the porous medium was constant. Therefore, Q/A was constant in the porous bed. Integration of Equation (2.2.27) yielded the following flow equation for permeation through a porous bed:

$$\int_0^y \frac{Q(y)}{A} dy = \left(\frac{Q}{A}\right)_{SSF} y = -\frac{\alpha_{sa}}{\mu w \sigma_{sa}^{\ 2}} \int_{P_m(0)}^{P_m(y)} K[X(P)] dP \quad ....(2.2.28)$$

If y was set to be equal to 1, then Equation (2.2.28) provided a prediction of the overall flowrate of fluid through the porous bed. Successful evaluation of the integral in equation (2.2.28) required knowledge of the mechanical stress at y = 0 and y = 1. y = 1 corresponded to the free surface of the bed where there was no mechanical stress acting on the bed. Therefore $P_m(y = 1)$ was equal to zero. At y = 0, this was the position where the fluid left the bed, all the pressure was converted into mechanical stress. Therefore, P_m was equal to P_{tot}. Consequently, Equation (2.2.28) could be re-written as:

$$\left(\frac{Q}{A}\right)_{SSF} = \frac{\alpha_{sa}}{\mu w \sigma_{sa}^{\,2}} \int_0^{P_m+P_h} K[X(P)]dP \quad ....(2.2.29)$$

Equation (2.2.29) was the model equation for permeation through an unconstrained compressible fibre pad according to Jonsson and Jonsson. Successful evaluation of the integral on the right hand side of the equation enables prediction of the flowrate of water permeating through the bed. However, in addition to the knowledge of the physical properties of the bed materials, information on the compressibility and permeability function of the fibre bed is also needed for the solution of the integral in Equation (2.2.29). Therefore, it is of vital importance that the appropriate permeability and compressibility functions be used in the solution of the model equation (2.2.29). Summaries of the existing permeability functions and compressibility functions in the literature are given in Sections 2.2.5.3 and 2.2.5.4 below followed by comments on the validity of the model by Jonsson and Jonsson in Section 2.2.5.5.

2.2.5.3 Permeability Functions

Equations (2.2.4), (2.2.11) and (2.2.12) were expressed by Jonsson and Jonsson in terms of void ratio instead of porosity,

$$\text{Kozeny-Carman:} \quad K(X) = \frac{X^3}{K''(1+X)^2} \quad \text{....(2.2.30)}$$

$$\text{Happel (perpendicular):} \quad K(X) = -0.5 + 0.5\ln(1+X) + \frac{1}{(2+2X+X^2)} \quad \text{....(2.2.31)}$$

$$\text{Happel (parallel):} \quad K(X) = \ln(1+X) - \frac{X(1+1.5X)}{(1+X)^2} \quad \text{....(2.2.32)}$$

Either one of the three permeability functions can be used in the integral in Equation (2.2 29) to solve for the permeation rate.

2.2.5.4 Compressibility of Pulp Beds

A fibre bed is a compressible porous medium. Since the fluid stresses in the bed during permeation have a cumulative effect, the fibre bed is compressed in such a way that a concentration profile will develop in the direction of flow. In addition to the fact that the porous medium is compressed by fluid stresses during permeation, it has been reported by numerous researchers that a fibrous medium under fluid stresses exhibits hysteresis when the fibre bed goes through compressive cycles [Ingmanson et al., 1959; Wilder, 1960; Jones, 1963; Elias, 1967; Samson, 1971; Hoering et al., 1983; Carnaby & Pan, 1989]. Consequently, to solve Equation

(2.2.29), a compressibility relation for viscoelastic media that display hysteresis is needed to account for the compression behaviour of fibre bed and to provide the functionality between void ratio and compressive pressure acting on the bed material.

A number of empirical compressibility functions are available from the literature. These compressibility functions can be found in the pulp and paper science literature and the textile science literature. Almost all of the compressibility functions from the textile industry are theoretical models. Komori et al. have a series of paper on the study of compression of fibre assemblies [1977, 1978, 1979, 1991a, 1991b, 1992]. Komori's group started by first mathematically modelling the fibre network and then applying the network model to study the effect of mechanical compression on the fibre assemblies. Carnaby and Pan [1989] published a paper on hysteresis in fibrous assemblies but the compressibility function alone involved a number of complicated equations. Although science from the textile industry had taken the effect of bed hysteresis into account in the theoretical models, these equations were all derived for mechanical compression of the fibre assemblies. Therefore, the compressive response of fibre assemblies to fluid stresses resulting from flow was not addressed.

Equations from the pulp and paper science literature are mainly empirical correlations based on the compressive response of fibre bed to static loads added. A widely used empirical compressibility function was that given by Quiller [1938] and Campbell [1947]:

$$c = MP_m^{\,n} \quad \ldots.(2.2.33)$$

Jonsson and Jonsson considered pad hysteresis to be a 2-step process. Compression was divided into the first compression cycle and all subsequent cycles. The pad was assumed to be more compressible in the first cycle than in the subsequent cycles and all the irrecoverable deformation took place during the first cycle. Jonsson and Jonsson cited the classical definition of compressibility given in a physical chemistry text by Moore,

$$\beta = -\frac{1}{V}\left(\frac{\partial V}{\partial P_m}\right)_T \quad ....(2.2.34)$$

Since Jonsson and Jonsson assumed that only the void volume was compressible, the compressibility of a pulp pad could be described by:

$$\beta_v = -\frac{1}{V_v}\left(\frac{\partial V_v}{\partial P_m}\right) \quad ....(2.2.35)$$

and Grace's equation [Grace, 1953] was used to describe the compressibility factor, β:

$$\beta = NP_m^{-b} \quad ....(2.2.36)$$

Both N and b are compressibility parameters specific to the material. For most materials, b is equal to 1 [Jonsson & Jonsson, 1992]. Substitution of Equation (2.2.35) into Equation (2.2.34) using a b value of 1 gave:

$$NP_m^{-1} = -\frac{1}{V_v}\left(\frac{\partial V_v}{\partial P_m}\right) \quad ....(2.2.37)$$

After integration and algebraic manipulation of the equation, the following relation for pad compressibility was obtained:

$$X = X'\left(\frac{P_m}{P_m'}\right)^{-N} \quad ....(2.2.38)$$

In subsequent compression cycles, since pad hysteresis was present, compressibility for subsequent cycles should be less. Jonsson and Jonsson assumed that there was only one single compressibility function for all subsequent cycles. In this compressibility function, the value of N was lower than that in the first cycle and β was independent of pressure although it was a function of the maximum pressure that the pad had been exposed to. Therefore, the compressibility function had the form:

$$\beta_v = NP_{max}^{-1} \quad ....(2.2.39)$$

After integration, the following equation resulted:

$$X = X(P_{max})\exp\left(N - \frac{NP_m}{P_{max}}\right) \quad ....(2.2.40)$$

Therefore, Equation (2.2.38) coupled with (2.2.40) describe the compressive behaviour of pulp pads in all compressive cycles and the two equations offer an alternative to the widely used empirical power law compressibility relationship (Equation (2.2.33)).

2.2.5.5 Comments on The Validity of The Jonsson and Jonsson Model

According to the model by Jonsson and Jonsson (Equation (2.2.29)), if the total pressure is known, use of the appropriate compressibility function and permeability function enables the prediction of permeation rate through a porous bed. A schematic flow diagram of the mathematical model involving the main equations is shown in Figure 2.2.5.2 below.

The versatility of this mathematical model is that different compressibility functions and permeability functions can be applied to the general framework of the model to predict elastic permeation results. However, the compressive response data in Figure 9 [Jonsson & Jonsson, 1992a] of the article were erroneous. In the figure, part of the data was supposed to represent a complete first compressive cycle with a maximum compressive stress of 100 kPa. The data in the figure displayed the expected response that the flowrate of water through the pad at zero and 100 kPa were consistent for both the compression and recovery steps. However, when calculations were carried out independently using the equations given in the article, different results were obtained. The flowrate of water at the maximum compressive stress of 100 kPa was different for the compression step and the recovery step. This seemed to indicate that there were problems with the compressibility equations proposed by Jonsson and Jonsson. Therefore, the choice of compressibility function is of vital importance in this mathematical model. Nevertheless, the Jonsson and Jonsson model is an excellent framework for modelling permeation through fibrous beds.

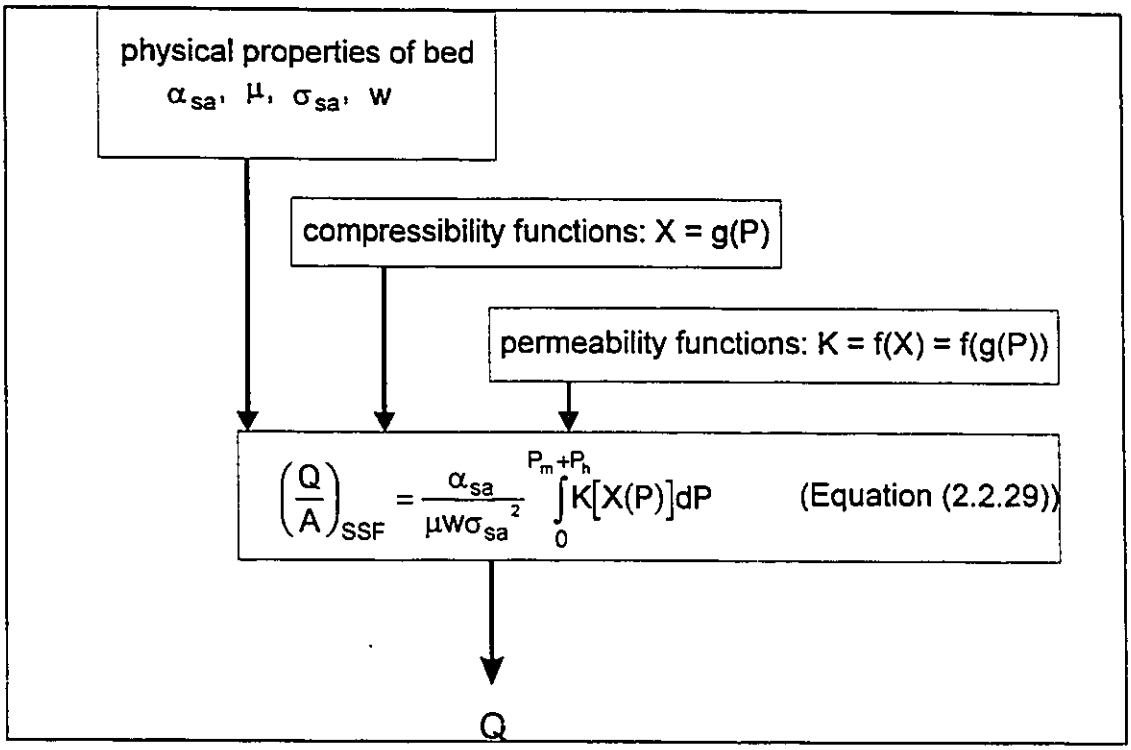

Figure 2.2.5.2 Schematic flow diagram of the model by Jonsson and Jonsson showing the information necessary for solving the model equation (Equation (2.2.29)) which includes: 1) physical properties of the bed such as the specific surface area and specific swollen volume of the bed material, viscosity of the fluid and weight of the fibre bed, 2) the appropriate compressibility equation, and 3) the appropriate permeability function.

2.3 Filtration

2.3.1 Filtration Behaviour of Suspensions

Filtration processes can be classified into three main categories: cake filtration, depth (or deep bed) filtration, and surface filtration [Cain, 1979].

In a cake filtration process, a suspension of solid particles is forced through a porous medium. Sizes of the pores in the filter cake are smaller than the solid

particles in the suspending medium. Therefore, the liquid will flow through the pores while the solid particles are retained such that a layer of filter cake is left on the surface of the filter medium. The thickness of the filter cake increases as filtration progresses. A prerequisite for cake filtration is that the resulting filter cake has a high enough permeability to enable the passage of liquid as filtration proceeds.

In depth filtration, the liquid suspension is forced through a bed of porous materials that acts as the filter medium. Interstices in the porous bed are coarse and the solid particles are trapped within the structure of the bed as filtration progresses. As a result, the total channel area available to flow is steadily decreasing. The filtration will ultimately be stopped when either the flowrate drops to an extremely low value or that some solid particles are forced out into the filtrate stream by the flow. At this stage, either bed regeneration or replacement is necessary. Typical examples of depth filtration are sand filtration and cartridge filtration.

General theories of cake filtration are well established. Mathematical models of the filtration process were first presented by Lewis and Almy [1912], Sperry [1916], and Ruth et al. [1933a, 1933b]. Reference books on this subject are available [Brown, 1950; McCabe & Smith, 1976; Bennett & Myers, 1982]. Carman [1938a], Heertjes [1950], and Miller [1951] have all presented reviews on the fundamental principles of filtration. In Carman's article, development of the fundamental governing equations for the filtration process was reviewed. Heertjes presented a review on the methods to correlate and analyze filtration data and introduced a specific filtration resistance which was defined as "the resistance of a cake of unit weight per unit of filtering area". Heertjes went on to state that the specific

filtration resistance was not constant for the whole cake and he introduced a point resistance, the differential specific resistance, which was useful in the analysis of filtration data from compressible cakes. A summary of the governing equations for cake filtration is outlined in the following paragraphs.

Although Darcy's law (Equation (2.2.1)) is a mathematical description of fluid permeation through a porous medium and thus it is not an equation primarily for filtration, many early researchers in the area of filtration came up with empirical equations that have the same form as Darcy's law. The governing equation for cake filtration is defined in a classical chemical engineering manner: the flowrate of fluid is directly proportional to the driving force of the flow process (the pressure drop across the filter cake, ΔP) divided by the total resistance offered by the cake, R. This relationship is described by the equation,

$$Q = \frac{A \cdot \Delta P}{\mu R} = \frac{A \cdot \Delta P}{\mu (L/K)} \quad ....(2.3.1)$$

If analogy is drawn between Equation (2.3.1) and Darcy's law (Equation (2.2.1)), one will notice that R is related to the parameter L/K where L and K are the thickness and permeability of the bed respectively. From the total resistance, a specific filtration resistance base on the mass of the filter cake, R_w, can be similarly defined. The relationship between the total resistance and specific resistance can be expressed mathematically as,

$$R_w = \frac{R \cdot A}{m_s} = \frac{R}{(CV)/A} \quad ....(2.3.2)$$

In Equation (2.3.2), m_s is the mass of the filter cake while V is the cumulative volume of filtrate collected and C is the mass of solid material filtered out per unit volume of filtrate collected. If the retention of solid material by the filtering medium is 100%, then C is equal to the concentration of solid material in the suspension that is being filtered. Introducing R_w into Equation (2.3.1) [Ingmanson, 1952; Ingmanson & Whitney, 1954] yields the following equation,

$$\frac{dV}{dt} = \frac{1}{R_w}\left[\frac{A \cdot \Delta P}{(CV / A)\mu}\right] \quad ....(2.3.3)$$

Equation (2.3.3) is a standard equation for filtration analysis. Assuming that R_w and ΔP are constant, integration of the ODE (Equation (2.3.3)) gives:

$$\frac{(t - t_1)}{(V - V_1)} = \frac{\mu C}{2A^2 \Delta P} R_w (V + V_1) \quad ....(2.3.4)$$

where t_1 and V_1 are the time and corresponding cumulative filtrate volume when the condition of constant pressure is attained. Consequently, plotting $(t - t_1)/(V - V_1)$ against $(V + V_1)$ gives a linear relationship if the equation is valid. From the slope of the line, the specific filtration resistance R_w can then be calculated.

Ruth [1935, 1946] and Carman [1938a] suggested the equivalence of specific filtration resistance and specific permeation resistance. Therefore, with the use of permeability equations such as the Kozeny-Carman equation that correlates permeability with physical properties of the filter bed materials, an increased understanding of the nature and mechanism of filtration could be achieved. Hoffing and Lockhart [1951] reported experimental data that supported and

confirmed Carman's argument of the equivalence of filtration resistance and permeation resistance for incompressible bed materials such as quartz and diatomaceous earth.

For compressible materials (such as pulp fibres), the application of permeability data obtained under static (preformed pulp bed) conditions to the dynamic (the bed is in the process of formation) conditions of filtration presents a problem. The problem is that with the compressibility of the bed material, there will be a variation in porosity throughout the bed under dynamic (filtration) conditions while there will be no such variation under static conditions.

Ruth [1935] and Carman [1938a] have shown that although the porosity and thus the point specific filtration resistance varied in the bed in filtration of compressible materials, an average specific filtration resistance could be obtained for the bed. Ruth [1946] later tested the correlation using calcium carbonate particles which were slightly compressible. Ruth found that the predicted permeation resistance differed from the filtration resistance calculated from experimental data by 10 to 15%. Walas [1946] developed an empirical equation that gave the average specific filtration resistance of compressible materials but his equation was not in agreement with the Kozeny-Carman equation. Grace [1953a, 1953b] adopted Ruth's compression-permeability technique to evaluate the filtration resistance of flocculated cakes formed from various subsieve and submicron materials. Grace showed that such beds did not obey the Kozeny-Carman equation because of the structural nonuniformity. However, Grace [1953b] later demonstrated that an average filtration resistance could still be calculated from compression-permeability results by integrating the point resistance over the whole bed. Theoretical predictions for constant

pressure filtrations were made and the predicted results agreed within 10% with experimental data.

2.3.2 Filtration Behaviour of Wood Pulp Suspensions

Filtration behaviour of pulp suspensions had been extensively studied to provide insight to pulp drainage on a paper machine. Ingmanson et al. [1952, 1954, 1955, 1957, 1959a, 1959b, 1959c, 1959d, 1963, 1964] had performed a thorough investigation on the filtration of deaerated pulp suspensions. He demonstrated the validity of applying permeability data to predict the specific filtration resistance of dilute pulp suspensions with a modified filtration equation. Ingmanson started with the classical filtration and permeability equations and modified them by taking into account the compressibility of the pulp pad to come up with the equation for specific filtration resistance. Experiments were then carried out to generate data on the compressibility of pulp fibres. Permeability experiments were also performed to generate data on the physical properties of the bed material needed for the Kozeny-Carman equation. Ingmanson followed the method of analysis suggested by Robertson and Mason [1949] and obtained the specific external surface area and specific swollen volume of the pulp fibres. Finally, filtration experiments were carried out to provide values of specific filtration resistances of dilute pulp suspensions. Theoretical predictions of specific permeation resistance were calculated using the compressibility and permeability data. Excellent agreement (an average error of 6%) was achieved between experimentally measured specific filtration resistance and specific permeation resistance predicted by theory. The theoretical model for prediction

of specific filtration resistance proposed by Ingmanson is outlined in the following paragraphs.

Assuming perfect retention of solids at the filter septum, a mass balance of the solid cake material can be written as,

$$CV = cAL = m_s \quad ....(2.3.5)$$

where m_s is the total mass of fibres in the bed and c is the mass concentration of fibres in the bed which has a thickness of L and an area of A. C is he solid concentration in the suspension that is being filtered and V is the volume of filtrate collected. Substitution of Equations (2.3.5) and (2.2.4) (Kozeny-Carman equation) into Equation (2.3.1) yields the following equation,

$$Q = \frac{dV}{dt} = \frac{A \cdot \Delta P(1-\alpha c)^3}{5.55 \cdot \mu(CV/A)\sigma^2 c} \quad ....(2.3.6)$$

According to Ingmanson [1952, 1954], the mass concentration of solid materials in a compressible bed, c, was a function of the pressure inside the bed. Since a pressure profile existed in the compressible bed, Equation (2.3.6) should be applied to a differential volume of the bed and then integrated over the whole bed in order to get the relationship for flow through the whole bed. The differential form of Equation (2.3.6) is:

$$Q = \frac{dV}{dt} = \frac{A\left[(1-\alpha c)^3 / c\right] \cdot dP}{5.55 \cdot (\mu C/A)\sigma^2 \cdot dV} \quad ....(2.3.7)$$

Since Q is constant in the bed, the differential equation can be solved by separating the variables. After integration the following equation is obtained,

$$Q = \frac{dV}{dt} = \frac{A\int_0^{\Delta P}\left[(1-\alpha c)^3 / c\right]dP}{5.55 \cdot \mu(CV/A)\sigma^2} \quad ....(2.3.8)$$

Comparing Equation (2.3.8) with Equation (2.3.3) gives,

$$R_w = \frac{5.55 \cdot \sigma^2 \cdot \Delta P}{\int_0^{\Delta P}\left[(1-\alpha c)^3 / c\right]dP} \quad ....(2.3.9)$$

For compressible materials, knowledge of the compressibility of the cake will permit evaluation of the integral. Thus, with data on the specific surface area and specific swollen volume of the cake material, prediction of the specific permeation resistance of the cake is possible.

The same result can be obtained from the flow model proposed by Jonsson and Jonsson which was described in the previous section. Starting with the flow equation by Jonsson and Jonsson, substitution of the Kozeny-Carman equation (Equation (2.2.30)) into Equation (2.2.29) and replacing the void ratio, X, by the porosity, ε, through Equation (2.2.16) results in an equation that is identical to Equation (2.3.8). Therefore, Equation (2.3.9) is again obtained as the equation for the evaluation of specific filtration resistance. This result has demonstrated that Equation (2.3.9) is consistent with existing theories on permeation and filtration. Also, since Equation (2.3.9) can be derived from a steady state permeation model (the flow model by Jonsson and Jonsson), the significance of

Equation (2.3.9) is that it enables one to predict dynamic filtration characteristics from steady state permeation results.

In summary, two equations for evaluating the specific filtration resistance of filter cakes have been presented. One of the two equations is Equation (2.3.3), which is based on an analysis of experimental filtration data while the other, Equation (2.3.9), is a theoretical prediction of the specific filtration resistance based on permeation parameters of the cake material. Ingmanson et al. [1952, 1954] had applied Equation (2.3.9) to predict specific filtration resistance of filter cakes of various pulp fibres and close agreement was achieved between experimental results and theoretical predictions. However, Ingmanson's work was restricted to beds consisting of a single type of pulp fibres and the accuracy of the theoretical prediction with systems consisting of more than one component remains unknown.

The research carried out by Ingmanson et al. on the filtration and drainage of pulp suspensions was comprehensive and thorough. Research work on the filtration of pulp suspensions that follows concentrates on the advent of new or modified filtration equipment that will more closely resemble the conditions on a paper machine [Gertjejansen, 1964; Pires et al., 1989]. In these research works, analysis of data is carried out using the theory given in Ingmanson's original paper. Therefore, with the work of Ingmanson, the theory and study on the drainage behavior of dilute air-free pulp suspensions was well established.

2.4 Summary

It is generally agreed that air in pulp furnishes causes problems in paper machine efficiency and final paper product quality. Based on this literature review, the quantitative effects of dispersed air on pulp drainage in paper mills have not been measured or theoretically described. Semi-empirical treatment of the permeability and compressibility of pulp pads are well established. Numerous articles on experimental studies of the filtration of pulp suspensions are available from the pulp and paper literature. However, data on the permeability and filtration of pulp suspensions containing a 2nd or even a 3rd component are lacking. In addition, empirical predictions of the relationship between dispersed air content and pulp drainage is virtually nonexistent in the literature. Therefore, fundamental studies on the effects of dispersed particles (air bubbles or solid particles) on the filtration and permeation behaviour of pulp suspensions will provide the much needed insight to the problem of dispersed air on pulp drainage. Results from such studies will thereby contribute towards an efficient and cost-effective remedy to this problem of dispersed air in the papermaking process.

2.5 Summary of Important Equations

Darcy's law

$$Q = \frac{dV}{dt} = \frac{K \cdot A \cdot \Delta P}{\mu L} \quad ....(2.2.1)$$

Happel's model (flow parallel to an array of cylinders)

$$K = \frac{d^2}{16(1-\varepsilon)}\left[-\ln(1-\varepsilon) - 1.5 + 2(1-\varepsilon) - \frac{(1-\varepsilon)^2}{2}\right] \quad ....(2.2.11)$$

Happel's model (flow perpendicular to an array of cylinders)

$$K = \frac{d^2}{32(1-\varepsilon)}\left[-\ln(1-\varepsilon) + \frac{(1-\varepsilon)^2 - 1}{(1-\varepsilon)^2 + 1}\right] \quad ....(2.2.12)$$

Kozeny coefficient

$$K'' = 3.5\frac{\varepsilon^3}{(1-\varepsilon)^{1/2}}\left[1 + 57(1-\varepsilon)^3\right] \quad ....(2.2.8)$$

Kozeny-Carman equation

$$K = \frac{(1-\alpha c)^3}{5.55\sigma^2 c^2} \quad ....(2.2.9)$$

Linearized Kozeny-Carman equation

$$\left(Kc^2\right)^{1/3} = \left(\frac{1}{5.55\sigma^2}\right)^{1/3}(1-\alpha c) \quad ....(2.2.10)$$

Differential form of Darcy's law

$$\frac{Q}{A} = \frac{K}{\mu}\frac{dP_h}{dz} \quad ....(2.2.23)$$

The model equation by Jonsson and Jonsson for permeation through an unconstrained pad

$$\left(\frac{Q}{A}\right)_{SSF} = \frac{\alpha_{sa}}{\mu w \sigma_{sa}^{\ 2}} \int_0^{P_m+P_h} K[X(P)]dP \quad ....(2.2.29)$$

Compressibility equation (Campbell)

$$c = MP_m^{\ n} \quad ....(2.2.33)$$

Compressibility equation for the first compression cycle by Jonsson and Jonsson

$$X = X'\left(\frac{P_m}{P_m'}\right)^{-N} \quad ....(2.2.38)$$

Compressibility equation for subsequent compression cycles by Jonsson and Jonsson

$$X = X(P_{max})\exp\left(N - \frac{NP_m}{P_{max}}\right) \quad ....(2.2.40)$$

Filtration equation

$$\frac{dV}{dt} = \frac{1}{R_w}\left[\frac{A \cdot \Delta P}{(CV/A)\mu}\right] \quad ....(2.3.3)$$

Integrated form of the filtration equation

$$\frac{(t - t_1)}{(V - V_1)} = \frac{\mu C}{2A^2 \Delta P} R_w (V + V_1) \quad ....(2.3.4)$$

Specific filtration resistance from permeation data

$$R_w = \frac{5.55 \cdot \sigma^2 \cdot \Delta P}{\int_0^{\Delta P}\left[(1 - \alpha c)^3 / c\right] dP} \quad ....(2.3.9)$$

3. EXPERIMENTAL PROCEDURE

3.1 Materials

The wood pulp fibres used were fully bleached softwood kraft pulp originating from Boise Cascade Canada Limited in Fort Francis Ontario. Flash-dried pulp was beaten in a Valley beater to a final Canadian Standard Freeness (CSF) of 452 mL at the Pulp and Paper Research Institute of Canada. The mean fibre length of the pulp was measured to be 3.6 mm using a Kajaani FS-100 fibre length analyzer. The fibre length distributions measured in two runs on the FS-100 are given in Table 3.1.1.

The average diameter of wet, swollen kraft pulp fibres was determined from a sample of 96 fibres using image analysis techniques. The kraft pulp fibres were immersed in water for 3 hours before they were viewed with a Wild M420 Zoom Macroscope working at a magnification of 32×. Images of the fibres were captured on video tape in Super-VHS format with a Dage MT165 video camera that was connected to a Panasonic AG-1960 video cassette recorder. Video images of the fibres were then transferred from video tape to a Kontron Electronik Image Analyzer via a JVC BR-S601 MU Super-VHS video cassette recorder. The images were processed on the image analyzer running IBAS (Kontron) release 2 software supplied by Zeiss. The optics were calibrated by carrying out image analysis on the video image of a hemocytometer (a glass slide with a 50 μm grid) taped under the same condition as the fibres. Since the pulp fibres were not perfectly cylindrical in shape, fibre diameter varied along the

length of the fibre. Therefore, line segments across the fibres, which were estimates of the fibre diameter, were manually drawn using the image analysis software at different locations along the length of the fibre. The lengths of the line segments were then calculated by a software macro to give an estimate of the fibre diameter at the various locations on the fibres. A complete listing of the macro is given in Appendix A.6. The number average diameter of the pulp fibres was found to be 26.2 μm with a standard deviation of 8.1 μm. The fibre diameter distribution is plotted in Figure 3.1.1 and data on the complete diameter distribution is presented in Appendix A.4.

After beating, the pulp fibres were dried to a moisture content of 11.19 g dry pulp per 100 g of sample for storage in a refrigerator to avoid rotting of the pulp.

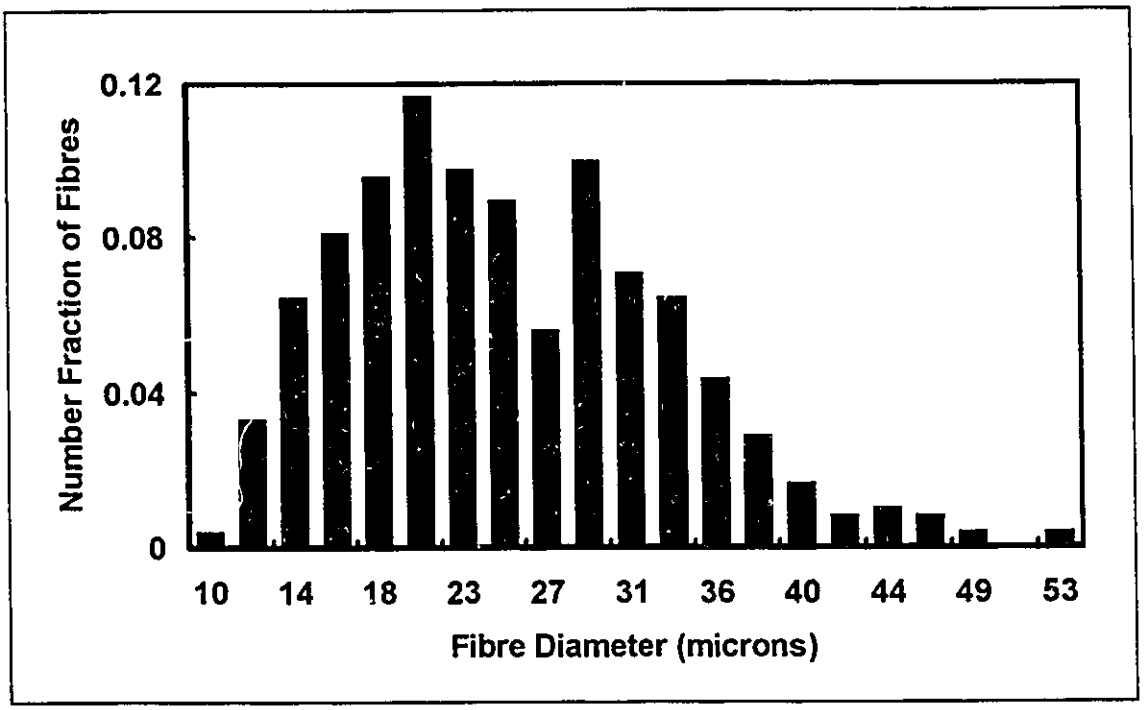

Figure 3.1.1 Distribution of pulp fibre diameter as measured by image analysis techniques.

fibre length (mm)	no. of fibres: run 1	no. of fibres: run 2
0	495	340
0.2	594	379
0.41	464	294
0.61	324	241
0.82	245	181
1.02	213	174
1.23	168	138
1.44	167	107
1.64	141	102
1.85	148	99
2.05	136	72
2.26	105	80
2.67	210	98
3.08	149	104
3.5	118	83
3.91	106	62
4.32	75	53
4.73	60	38
5.14	51	27
5.55	37	13
5.97	28	11
6.38	8	10
6.79	7	1
> 6.79	14	5

Table 3.1.1 Fibre length distribution of bleached softwood kraft pulp fibres as measured in Kajaani FS–100.

The plastic beads used in the experiments were manufactured by Bangs Laboratories, Inc. in Indiana, U.S.A. The beads were made from polystyrene cross-linked with 2% of divinyl benzene. When examined under the microscope, the beads were perfectly spherical. The density of the beads given by the

manufacturer was 1050 kg/m^3. The average diameter of the beads reported by the manufacturer was 112 μm with a standard deviation of 37 μm.

The particle size distribution was determined independently from a sample of 476 beads using image analysis techniques. The image analysis procedure was similar to that used in measuring the diameter of pulp fibres. Samples of the plastic beads were viewed with a Wild M420 Zoom Macroscope working at a magnification of 32×. Images of the beads were captured on video tape in Super-VHS format with a Dage MT165 video camera connected to a Panasonic AG-1960 video cassette recorder. Video images of the beads were then transferred from video tape to a Kontron Electronik Image Analyzer via a JVC BR-S601 MU Super-VHS video cassette recorder. The images were processed on the image analyzer running IBAS (Kontron) release 2 software supplied by Zeiss. The optics was calibrated by carrying out image analysis on the video image of a hemocytometer (a glass slide with a 50 μm grid) taped under the same condition as the beads. The software macro used to measure the particle size distribution of the beads was written by Mr. B. Grosse. A listing of the macro is included in Appendix A.6. The number average diameter of the beads was measured at 80.4 μm with a standard deviation of 29 μm. The total size distribution is presented in Table 3.1.2 and plotted in Figure 3.1.2.

Possible reasons for the discrepancy between the two average diameters were the differences in the nature of the methods of measurement. The size distribution provided by the manufacturer was most probably obtained by using sieves. Therefore, the beads were classified into fractions at different ranges of mesh sizes. In calculation of the average bead size, the average sizes of the ranges were used. Therefore, the detail size distribution of beads within the

fractions were lost and the accuracy of the average bead size calculated was limited by the fineness of the size ranges. Since every individual bead was used in the determination of the average size using image analysis, the image analysis result is more accurate.

size range (μm)	nominal size (μm)	fraction of beads
15 - 30	22.5	0.132
30 - 45	37.5	0.071
45 - 60	52.5	0.013
60 - 75	67.5	0.038
75 - 90	82.5	0.269
90 - 105	97.5	0.374
105 - 120	112.5	0.084
120 - 135	127.5	0.008
135 - 150	142.5	0
150 - 165	157.5	0.006
165 - 180	172.5	0.004

Table 3.1.2 Particle size distribution of PS beads as measured by image analysis techniques for a total of 476 beads.

The nylon fibres were provided by Dr. C.P.J. Bennington of the University of British Columbia. The average length of the fibres was 1.89 mm and the fibre diameter was 0.045 mm. Density of the dry nylon fibres was 1140 kg/m^3 and the elastic modulus of the fibres was 1.76×10^9 Pa. A detailed description of the fibre properties was given in Dr. Bennington's paper [Bennington et al., 1990].

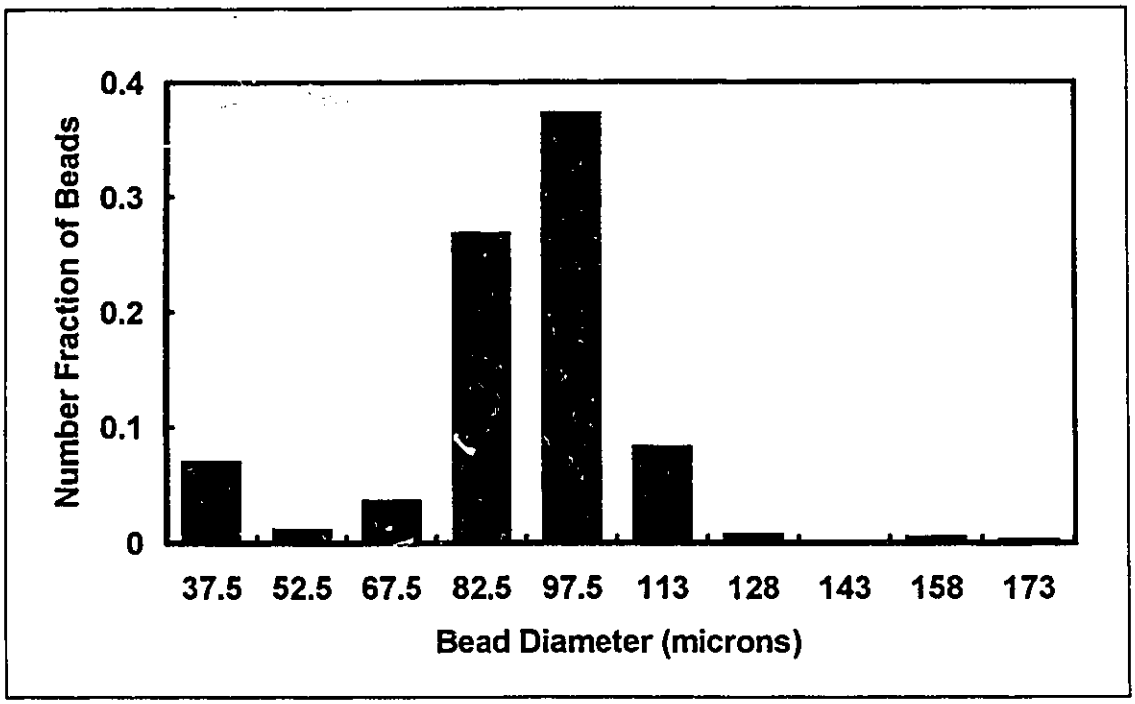

Figure 3.1.2 Plastic bead size distribution as measured by image analysis techniques.

3.2 Preparation Of Pulp Suspensions

Four different suspensions, prepared using kraft pulp, nylon fibres and plastic beads, were used in this work. All the suspensions had the same mass concentration of kraft pulp (0.01% consistency) and sodium chloride (10^{-3} M). Sodium chloride was added to the suspensions at a concentration of 10^{-3} M to provide a constant ionic strength in the suspending medium. Beaten kraft pulp fibres were dispersed in distilled water to a constant mass concentration of 0.1 ± 0.005 kg/m^3 (0.01% consistency).

The first suspension contained kraft pulp at 0.1 kg/m^3 and sodium chloride at 10^{-3} M. The second type of suspensions contained kraft pulp, plastic beads,

and sodium chloride. Mass concentration of the kraft pulp was 0.1 kg/m^3 while plastic beads were added at six different concentrations: 0.025, 0.05, 0.1, 0.2, 0.3 and 0.4 kg/m^3. The third type of suspensions was a mixture of kraft pulp fibres, nylon fibres and sodium chloride. Eight concentrations of nylon fibres were used: 0.05, 0.1, 0.15, 0.2, 0.25, 0.3, 0.36 and 0.5 kg/m^3. The last type of suspensions consisted of all four components: beaten kraft pulp fibres, nylon fibres, plastic beads and sodium chloride. The mass concentration of nylon fibres was held constant at 0.36 kg/m^3 while two different bead concentrations (0.05 kg/m^3 and 0.1 kg/m^3) were used.

3.3 Apparatus

A constant head filtration unit was used for the filtration and permeability experiments. A schematic diagram of the apparatus is shown on Figure 3.3.1. The filtration cell was a Plexiglas® cylinder with an inner diameter of 5 cm. The total length of the cell was 880 cm. A piece of paper machine wire was used as the filtering medium and it rested on top of a perforated stainless steel support plate. The stainless steel support plate had a diameter of 5.47 cm and a thickness of 1 mm. There was a total of 178 holes on the plate. All the holes had the same diameter of 2.54 mm (0.1 inch) which made 38.4% of the total area open to flow. The flow was driven by a constant hydrostatic head of approximately 107 cm.

For some experiments the fibre pad was constrained between the paper machine wire and a brass plunger. The brass plunger consisted of a brass rod and an assembly of porous plates. The assembly of porous plates included a

porous brass plate, a coarse wire mesh and a piece of paper machine wire. The diameter of the brass plate was 4.95 cm with a thickness of 4.76 mm (3/16 inch). 173 holes each having a diameter of 1.59 mm (1/16 inch) were drilled on the brass plate to enable flow through the plunger. The percentage of area open to flow was 17.8%. Both of the coarse mesh wire and the paper machine wire had the same diameter as the brass plate at 4.95 cm with a total thickness of 0.2 cm. The assembly of porous plates was arranged such that in permeation experiments, water would first permeate through the brass plate followed by the coarse mesh wire and finally the paper machine wire. The two pieces of wires improved the flow distribution of the brass plate which had a relatively low percentage of open area.

The brass rod had a length of 0.61 m with a diameter of 6.35 mm. The free end of the brass rod went through a 6.35 mm (0.25 inch) brass pipe fitting at the top of the filtration cell. By adjusting the brass rod and then tightening the pipe fitting, the position of the plunger could be fixed. During pad formation, the plunger was raised to the top so as not to interfere with pulp flow and the plunger remained in the raised position in elastic permeation experiments. For fixed bed permeation experiments, the plunger was lowered to confine the fibre pad to a known thickness. The pad thickness was determined by measuring the distance between marks on the brass rod using a vernier scale.

Two ports, one above and the other below the fixed paper machine wire, were drilled on the wall of the filtration cell. Hydraulic lines connected these two ports to a Celesco DP-30 differential pressure transducer which measured the differential pressure over the range 0 to 2 psi. The pressure transducer was connected to a Celesco CD10D carrier demodulator that produced signals in the

range of 0 to 10V DC. Two additional ports directly opposite the transducer ports were connected to water manometers. The pressure transducer was calibrated using the Series 65-120 Portable Pneumatic Calibrator manufactured by the Wallace & Tiernan Division of Pennwalt Corporation. After calibration, a sand bed was introduced into the filtration cell. Water was allowed to permeate through the sand bed at different flowrates. The corresponding pressure drops across the bed were recorded by both the pressure transducer and the manometer. Measurements from both devices were compared and excellent agreement was obtained. The results are included in Appendix A.2.

Filtrate was collected by a 22 L container resting on a Mettler PM-16 electronic balance. The balance measured the accumulation of filtrate with time. Electrical output signals from both the transducer and the electronic balance were sent to the OPTO 22 data acquisition system. The OPTO system was consisted of an AC7A adapter card, a B2 Analog Brain Board on a PB8AH Analog I/O Rack, an AC31 Intelligent Interface Adapter card and a 0 to 10V DC I/O module for the PB8AH I/O board. Signal from the Mettler PM-16 balance went to the AC31 adapter card through a RS-232 null modem cable while signal from the Celesco pressure transducer/demodulator unit was sent to the PB8AH I/O board directly. The AC31 board processed the serial signal from the balance and sent it to the AC7A board. Similarly, the B2 brain board on the PB8AH analog I/O rack took the signal coming from the transducer demodulator and sent it to the AC7A board. The AC7A adapter card was connected to the serial port of an IBM AT compatible computer and the signal was sent from the AC7A board to the computer via a RS-232 null model cable. A program was written in BASIC to control the data exchange between these devices. The program

enabled the initialization of the OPTO data acquisition system and the transfer of output data from both the pressure transducer and the balance to the computer memory for storage. Pressure data were taken at intervals of approximately 0.2 seconds while data from the balance were recorded once every 0.16 second. All these data were stored in "comma separated values" format in the output file generated by the program for future analysis. A complete listing of the data acquisition program is included in Appendix A.6.

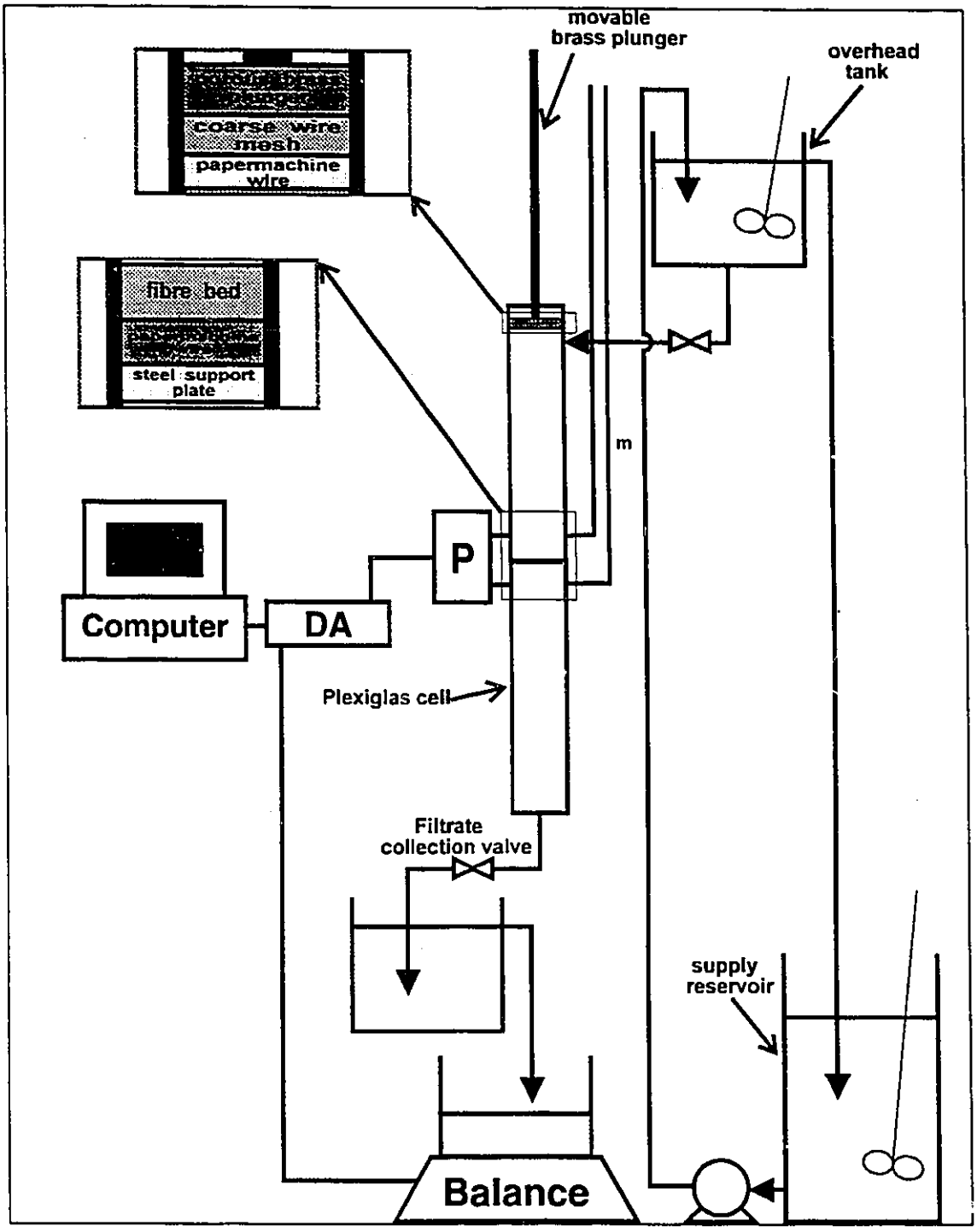

Figure 3.3.1 A schematic drawing of the constant head filtration/permeation apparatus. **P**: differential pressure transducer; **DA**: OPTO 22 data acquisition system; **m**: water manometer.

3.4 Testing Of Equipment: Constant Head Filtration/Permeation Unit

The constant head filtration equipment was tested by carrying out a sand bed permeation run. A sand bed consisting of dry coarse sand beads (Wedron 460 round grain) was introduced into the filtration cell. The density of the beads was measured to be 2650 kg/m^3 using a pycnometer. The bead particles were spheroidal in shape with irregular, rough surfaces. An analysis of the particle size distribution using standard sieves gave the information summarized in the following table.

US mesh size	nominal size (μm)	Weight % retained
30	600	1
40	425	60
50	300	34
70	212	4
>70	<212	1

Table 3.4.1 Particle size distribution of glass sand used for equipment testing.

88.25 g (dry weight) of beads were soaked in 1 L of distilled water for 30 minutes. The suspension of sand beads was stirred with a metal rod to remove any air bubbles that adhered to the beads. The suspension of sand bead was then carefully poured into the filtration cell with stirring. After the sand had settled, a bed having a thickness of 2.8 cm and a void fraction (by volume) of 0.4 was obtained. A stainless steel screen was used with the stainless steel support plate to support the sand bed. The stainless steel screen was a type 100R

perforated metal screen supplied by Paper Research Materials, Inc. in Syracuse, New York. The type 100R screen had the same diameter as the stainless steel support plate and the thickness of the screen was 0.071 mm (0.0028 inch). The size of the holes on the screen was 76.2 μm in diameter and the percentage of open area was 8%.

Water was allowed to permeate through the sand bed at different water flowrates. The flowrate of water was controlled by varying the position of the filtrate collection valve. The pressure drop across the sand bed was measured by both the water manometers and the pressure transducers. The filtrate rate was calculated from the change in filtrate weight with time as monitored by the electronic balance. A plot of the filtrate rate at various corresponding pressure drops is shown in Figure 3.4.1.

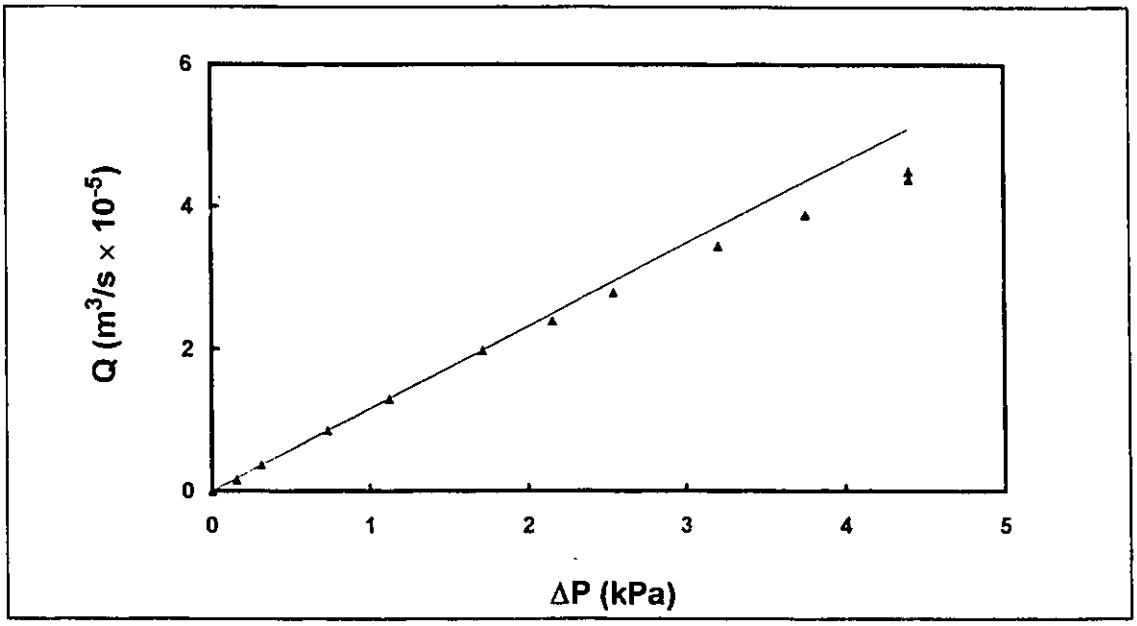

Figure 3.4.1 Darcy's law plot of the sand bed results. **ΔP:** pressure drop driving the flow; **Q:** flowrate of water through the sand bed. ▲: experimental data; —: Darcy's law fit based on data with ΔP values below 2 kPa.

According to Darcy's law, the flowrate of a fluid through a porous medium should be proportional to the pressure drop across the porous bed. The validity of Darcy's law was limited to low permeation rates when the flow in the porous medium was laminar. As the flowrate increased, inertial effects began to predominate over viscous effects and the higher subsequent pressure losses caused the flowrate/pressure drop relationship to deviate from the simple linearity that was exhibited in the laminar regime. Therefore, as demonstrated by the experimental results, flowrate data with ΔP values below 2 kPa did follow the linear relationship and the deviation from linearity gradually became more pronounced at higher flowrates.

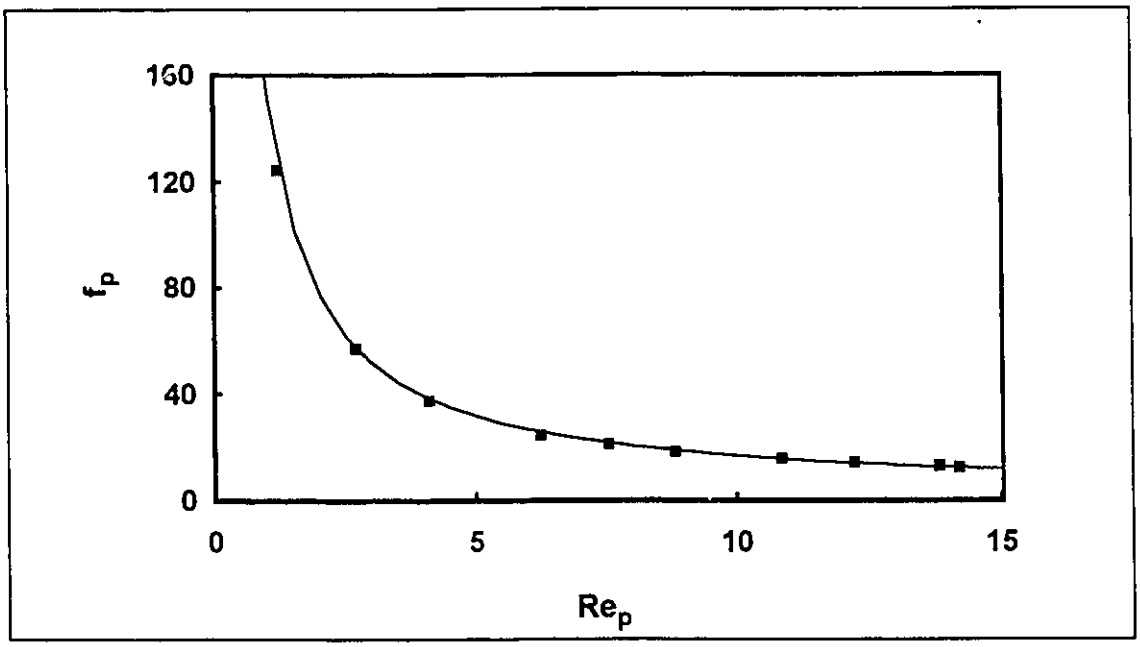

Figure 3.4.2 Sand bed data plotted in the dimensionless coordinates. f_p: friction factor for porous media; Re_p: Reynolds number .for porous media. ■: experimental data; —: Ergun equation fit.

For flow through a porous medium, Ergun proposed an equation that related the pressure drop to the flowrate of permeant through two dimensionless parameters [Dullien, 1979]: a modified friction factor, f_p and a modified Reynolds number, Re_p. The two parameters were defined as followed:

$$f_p = \frac{D_p \varepsilon^3 \Delta P}{\rho u^2 (1-\varepsilon) L} \quad ....(3.4.1)$$

$$Re_p = \frac{D_p u \rho}{\mu (1-\varepsilon)} \quad ....(3.4.2)$$

The Ergun equation was stated as:

$$f_p = \frac{150}{Re_p} + 1.75 \quad ....(3.4.3)$$

When Equations (3.4.1) and (3.4.2) were substituted into Equation (3.4.3), a different form of the Ergun equation in terms of particle diameter, fluid properties and bed porosity was obtained. The resulting expression was given as Equation (2.2.2) in Chapter 2.

When the data were plotted in the dimensionless groups proposed by Ergun for porous media flow, the curve exhibited the trend demonstrated by the Ergun equation. The result was presented in Figure 3.4.2.

When the experimental data were fitted to the Ergun equation by linear regression, a representative particle size of 432 μm, which was in agreement with the size range provided by the manufacturer of the sand particles, was obtained. Therefore, the experimental results confirmed that the equipment was

When the experimental data were fitted to the Ergun equation by linear regression, a representative particle size of 432 μm, which was in agreement with the size range provided by the manufacturer of the sand particles, was obtained. Therefore, the experimental results confirmed that the equipment was capable of carrying out permeation measurements and thus the validity of results from subsequent filtration and permeation experiments were established.

The pressure drop over the whole filtration equipment was comprised of three factors: 1) pressure drop across the fibre pad, 2) pressure drop across the filtering medium assembly (the steel support plate, paper machine wire and the porous plunger) and 3) pressure losses in pipes and fittings of the equipment. Pressure drops measured by the pressure transducer in all the experiments included both the pressure drop due to the fibre pad and the pressure drop caused by the filtering medium assembly. Therefore, knowledge of the pressure losses across the filtering medium assembly was important because they were needed to obtain the correct pressure drop across the fibre pad from the pressure drop measured. Pressure drop across the filtering medium assembly was measured by allowing water to permeate through the pulp pad assembly at various water flowrates. Pressure drop caused by the whole assembly was about 3 kPa at a flowrate of 135 g/s. In this research, flowrates in most of the permeation experiments were about 1 g/s. Pressure drops caused by the filtering medium assembly at this flowrate was about 0.2 kPa for a total hydrostatic head of 10.7 kPa. Therefore, the pressure loss caused by the plunger assembly was negligible compared to that caused by the pad. Pressure drop data of the plunger assembly are included in Appendix A.3.

At the start of filtration experiments, water flowrates as high as 120 g/s could be reached since the flow resistance of the filtering medium assembly was minimal and the fibre pad that was still in its initial stage of formation offered virtually no filtration resistance. However, substantial pipes and fittings pressure losses that were comparable in magnitude to the total hydrostatic head driving the flow were experienced at such a high flowrate. Therefore, it was useful to know the pressure losses in the piping as a function of the flowrate of fluid in the equipment. Normally, pressure losses in pipes are represented by a power law function:

$$\Delta P_{pipes} = f \cdot u^g \quad ....(3.4.4)$$

where u is the superficial flowrate of fluid through the pipes (in m/s) while f and g are numerical parameters. Pressure losses in the equipment at different flowrates had been determined experimentally and the power law function was found to be an adequate representation of the data. The experimental data are presented in Figure 3.4.3. At flowrates below 20 g/s, a change in the slope was observed, suggesting a transition in the flow regime. Since the lowest flowrate encountered in the filtration experiments was approximately 15 g/s, regression analysis was carried out only with data above 20 g/s. The parameters f and g were determined to be 1.294×10^6 and 1.786 respectively when the flowrate of fluid, u, was expressed in g/s and pressure drop in kPa.

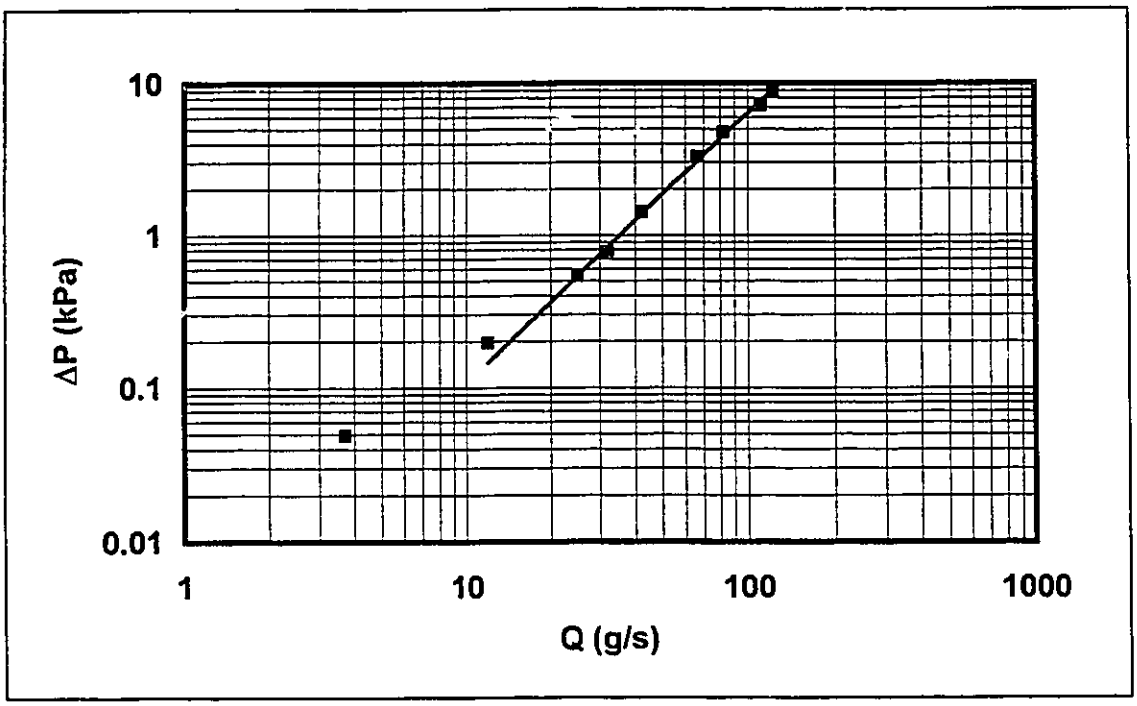

Figure 3.4.3 Pressure loss in the apparatus plotted against corresponding liquid flowrate. ΔP: pressure drop in apparatus; Q: flowrate of fluid in apparatus. Individual markers represent experimental data while the solid line is a linear regression fit of flowrate data above 20 g/s.

3.5 Experimental Procedure

3.5.1 Filtration Experiments

In filtration experiments, one of the four types of suspensions described in Section 3.2 was introduced to the supply reservoir (c.f. Figure 3.3.1). A stirrer in the supply reservoir kept the suspension well mixed. The suspension was continuously pumped from the supply reservoir to the overhead tank to keep the level in the tank and thereby the hydrostatic head driving the flow constant. Another stirrer in the overhead tank provide the necessary agitation. Before the

start of the experiment, the filtration cell was filled with distilled water and both the pressure transducer as well as the electronic balance were turned on. Just before the start of the experiment, the data acquisition system was turned on to begin data collection. The pressure drop across the filtering medium and weight of filtrate collected were measured by the pressure transducer and the electronic balance respectively and collected by the data acquisition system. Opening of the filtrate collection valve signified the actual start of the experiment. Well-agitated suspension entered the water filled filtration cell from the overhead reservoir and filtration of the pulp took place at the paper machine wire. Solid particles of the suspension (mainly fibres) were collected at the wire and the fibrous material gradually built up into a fibre pad until approximately 14 kg of filtrate was collected. Controlling the total amount of filtrate collected ensured that the amount of pulp fibres present in the pad remained constant from one run to another to allow direct comparison of results. From the cumulative filtrate weight versus time data, the specific filtration resistance was determined using the integrated filtration equation (Equation (2.3.4)).

3.5.2 Permeation Experiments

Two types of permeation experiments were carried out with the freshly formed pad after the filtration step during which the pulp pad was formed. Elastic permeation was conducted first followed by fixed bed permeation.

3.5.2.1 Elastic Permeation Experiments

After the filtration experiment, the pulp pad formed was left in the filtration cell and characterized first by an elastic permeation experiment. In this experiment, water was introduced into the supply reservoir and subsequently allowed to permeate through the pad. The filtrate collection valve was opened fully initially thus allowing maximum flowrate through the pad. This valve position was held constant for 5 minutes. During the 5 minute period, pressure drop across the pad and cumulative weight of permeate collected data were recorded both manually and by the data acquisition system. Manual measurements involved reading of the pressure drop from the water manometers and recording the weight of permeate collected in a time interval of 3 minutes. The pad thickness was measured by a vernier scale. Although it was possible to achieve an accuracy of 0.005 cm with the vernier scale, nonuniformity of the pad surface across the diameter of the wire reduced the accuracy of pad thickness measurements to $\pm$ 0.05 cm. The filtrate collection valve was adjusted manually to set a new flowrate and pressure drop for water after the 5 minutes interval. The pulp pad was free to respond to the change in pressure drop and adjust both thickness as well as the permeation rate since the porous plunger was not lowered to constrain the pad. Hence, this type of experiment was given the name elastic permeation. A total of 21 pressure drops (or flowrates) were used. 11 of them were in decreasing order from the maximum in the beginning to the minimum while the remaining 10 were carried out in reverse order so that a complete pressure drop cycle was achieved. Each successive pressure drop

was made in steps of approximately 1 kPa. Measurement of the same parameters were repeated for each pressure drop value.

3.5.2.2 Fixed Bed Permeation Experiments

After the elastic permeation experiments, fixed bed permeation experiments were carried out. The objectives of fixed bed permeation experiments were to obtain pressure drop across the pad as a function of flowrate to calculate the permeability of the pad as a function of solid concentration. The standard method was to compress the fibre pads in the permeability equipment to a certain thickness and allow water to permeate through the pad [Robertson & Mason, 1949; Ingmanson, 1952; Ingmanson & Whitney, 1954; Gertjejansen, 1964]. The pressure drop across the pad and the weight of filtrate collected were measured as functions of time. Permeability of the pads were low since they were highly compressed in fixed bed permeation experiments. Consequently, flowrates of water through the pads were extremely low, making it difficult to accurately measure the weight of filtrate by an electronic balance. Therefore, a novel technique was used in these fixed bed permeation experiments to measure the permeability of the fibre pad at various solid concentrations. The porous brass plunger was lowered to compress the pad to a fixed thickness. The position of the plunger was held constant by tightening the brass pipe fitting at the top of the filtration cell. Water was allowed to permeate through the pad with the filtrate collection valve opened fully. It would normally take approximately 3 minutes for the flow to become steady. The flow was stopped after it had become steady and the change in pressure drop across the pad was monitored by the pressure transducer with the data acquisition system running at a rate of 1 Hz.

Permeability of the highly compressed pad was low and usually about 3 minutes were required before enough water could permeate through the pad to enable the lower leg of the water manometer to return to the original level. Figures 3.5.2.2.1 to 3.5.2.2.3 were included to illustrate the pressure relaxation process. The data acquisition system was stopped after the pressure had relaxed completely and the plunger was then raised to allow free expansion of the pad for 5 minutes. This free expansion step was a precaution against a felting effect of the pad that was proposed by Robertson and Mason [1949]. The plunger was again lowered to compress the pad to a lower thickness after free expansion and the same pressure relaxation procedure was repeated. Usually four to six pressure relaxation runs were carried out with a single pad.

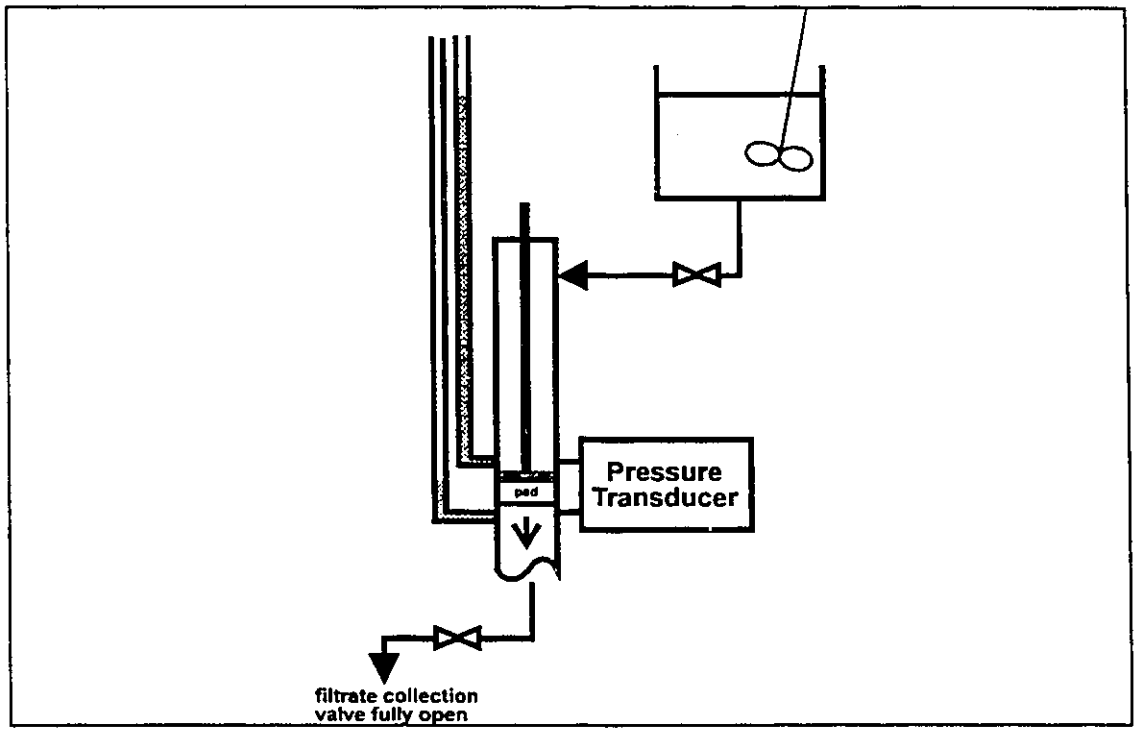

Figure 3.5.2.2.1 Schematic drawing of the apparatus before pressure relaxation when the flow was steady.

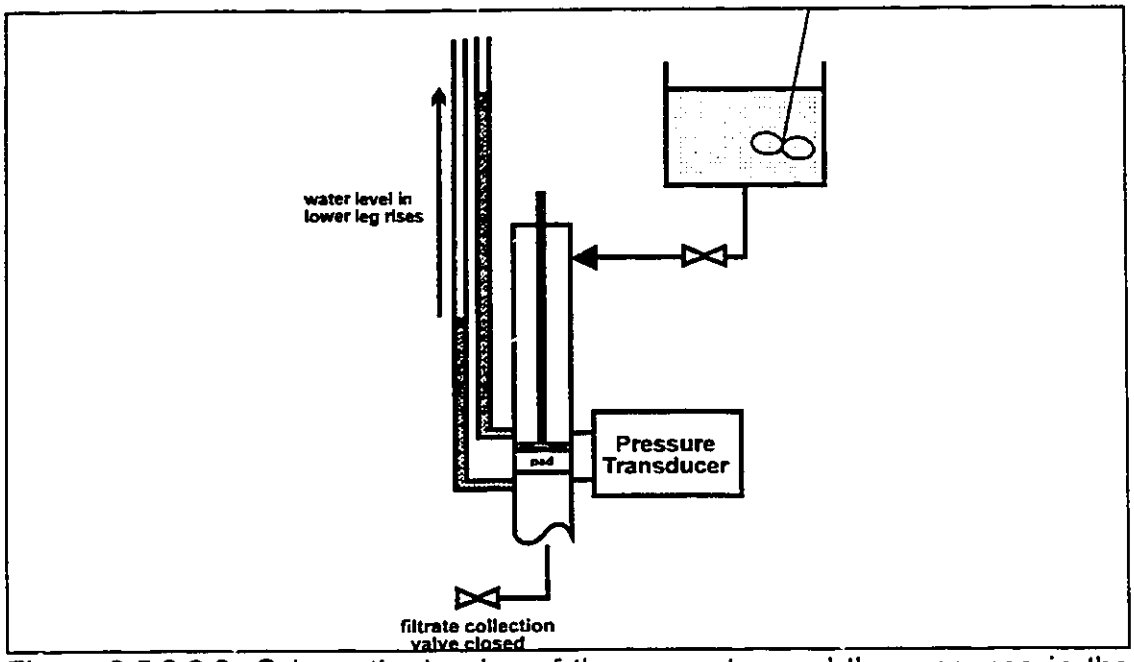

Figure 3.5.2.2.2 Schematic drawing of the apparatus and the response in the water manometer when the pressure relaxation had started.

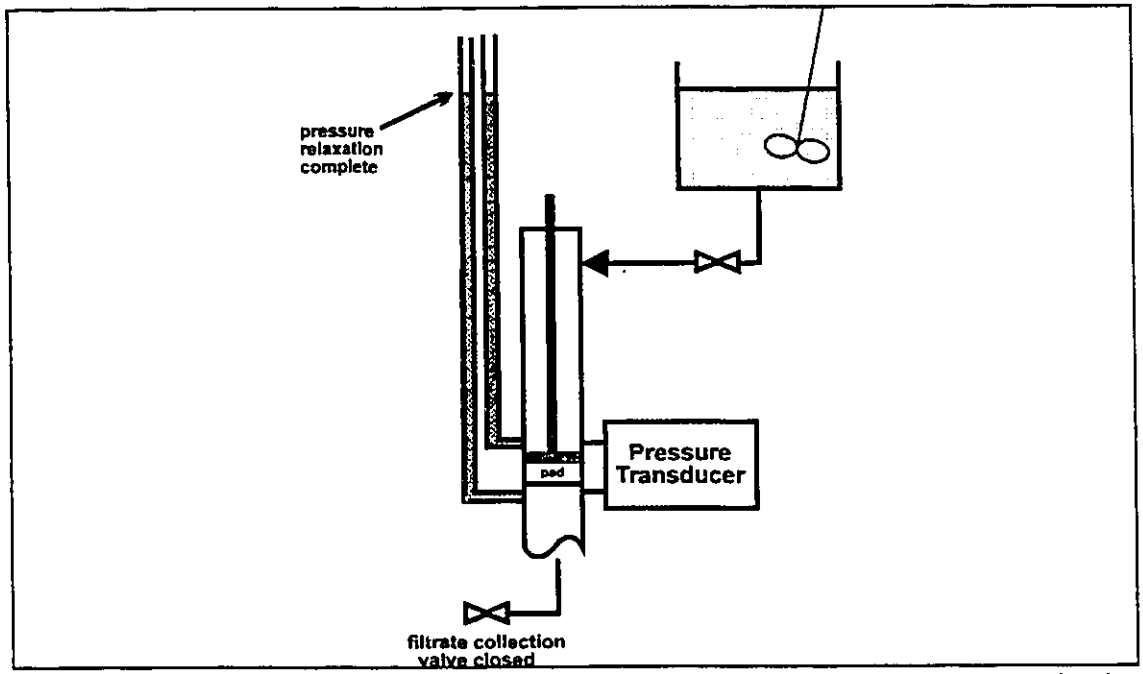

Figure 3.5.2.2.3 Schematic drawing of the apparatus and the response in the water manometer when the pressure relaxation was complete.

Applicability of Darcy's law was ensured in fixed bed permeation experiments because of the low flowrates which were a result of the highly compressed pad. Consequently, the pressure relaxation curve would provide a continuous spectrum of flowrate versus pressure drop data required for the determination of the permeability of the pad. Based on the principles of manometry, the rate of pressure relaxation across the fibre pad in the column was given by,

$$\frac{d(\Delta P)}{dt} = \rho g \frac{d(h - h_0)}{dt} = \rho g \frac{dh}{dt} \quad ....(3.5.1)$$

where ΔP was the pressure drop across the fibre pad, ρ was the density of water while h and h_0 were tne height of water in the lower leg and upper leg of the manometer respectively. The rate of pressure relaxation was related to the flowrate of water through the pad since the level of water in the lower leg of the manometer rose as pressure drop across the pad relaxed. The instantaneous flowrate of water was given by the following equation,

$$Q = -A_m \frac{dh}{dt} \quad ....(3.5.2)$$

where Q was the volumetric flowrate of water through the fibre pad and A_m was the cross-sectional area of the manometer tube. Therefore, flowrate of water through the pad was related to the rate of pressure relaxation by the equation, obtained by combining Equations (3.5.1) and (3.5.2):

$$Q = -\frac{A_m}{\rho g} \frac{d(\Delta P)}{dt} \quad ....(3.5.3)$$

Applying Darcy's law to the pad and relating that to the flowrate of water in the manometer tube resulted in the following equation:

$$Q = \frac{K \cdot A \cdot \Delta P}{\mu L} = -\frac{A_m}{\rho g}\frac{d(\Delta P)}{dt} \quad ....(3.5.4)$$

Solution of the above first order ODE with the initial condition: t = 0, $\Delta P = \Delta P_{max}$, gave the equation for the pressure relaxation curve. The solution of the ODE was,

$$\ln(\Delta P) = \ln(\Delta P_{max}) + (-\frac{K\rho gA}{\mu LA_m})t \quad ....(3.5.5)$$

Thus, semi-log plots of the pressure relaxation data were linear and the slope of the line gave the permeability of the pad at the particular compression.

3.5.3 Pulp Pad Composition Analysis

3.5.3.1 Filtrate Analysis

Retention of all the materials used in the experiments (pulp fibres, polymer beads and nylon fibres) were measured by analyzing the composition of filtrate. In the analysis, collected filtrate was filtered under vacuum. The filter papers used were Whatman no.1 qualitative filter papers having a diameter of 150 mm. The filtrates were filtered three times to ensure retention of all the solid materials on the filter paper. The filter paper was then dried and weighed to determine the

amount of solid materials that had passed through the paper machine wire during the course of the filtration experiment.

For kraft pulp fibres, filtrate analysis results showed that retention by the paper machine wire was 100%. The same was true for nylon fibres. However, for polymer beads, retention was not 100%. According to analysis, usually 1 to 3% by weight of the total amount of beads present in the original suspension were not retained. Using this information, mass balance on the beads could be carried out and the composition of all the pads containing beads could be determined.

3.5.3.2 Scanning Electronic Microscopic Analysis of Pad Composition

Permeation characteristics of the pads were determined by the arrangement of the constituent materials in the pad. Therefore, uniformity of the distribution of beads in pads was important. For pads made from suspensions that contained plastic beads, some representative ones were selected for Scanning Electronic Microscopy (SEM) studies. The dried pads were cut vertically into slices at different radial positions and the samples were mounted on metal stubs for SEM. The metal stubs were then sputter coated with gold for scanning electron microscopy. Scanning electronic micrographs of these samples were taken and the resulting pictures were enlarged using a colour laser photocopier. The enlarged prints were divided into grids and the number of beads in each grid was counted by hand. Distribution of the beads in the pads as a function of the vertical position and the radial position was determined from the results of the counts.

4. FIXED BED PERMEATION

4.1 Introduction

In this chapter, results from fixed bed permeation experiments are presented. In this work a fibre bed was first formed in the cake filtration experiment. The newly formed unrestrained bed was then subjected to permeation by water in the elastic permeation experiment. Fixed bed permeation was the experiment that followed elastic permeation. Fixed bed permeation data are presented ahead of the results from elastic permeation and cake filtration because bed parameters resulting from the analysis (specific surface area and specific swollen volume) are needed in analysis of elastic permeation and filtration data.

A novel technique was used to obtain pressure drop versus flowrate results in the fixed bed permeation experiments. A detailed description of the experimental procedure was given in Section 3.5.2.2. Permeability as a function of the solid concentration in the fibre pad was obtained from the raw data of fixed bed permeation experiments. The permeability data were then analyzed according to the theories outlined in Section 2.2.1 to obtain properties of the porous pad that included the specific external surface area and specific swollen volume.

Four types of fibre pads that differed in composition were used in fixed bed permeation experiments. The fibre pads contained either: 1) kraft pulp fibres only, 2) kraft pulp fibres and plastic beads, 3) kraft pulp fibres and nylon fibres,

or 4) kraft pulp fibres, nylon fibres and plastic beads. Results from experiments with the four types of fibre pads will be presented in the following sections of this chapter followed by discussion and conclusions from the results.

4.2 Results

4.2.1 Pads Consisting of Pulp Fibres

Experimental data for fixed bed permeation experiments of pads containing only kraft pulp are shown in Figures 4.2.1.1 to 4.2.1.3. In Figure 4.2.1.1, the pressure relaxation data for pulp pads are plotted in a semi-log fashion. The nine sets of experimental data presented in the figure were obtained at different levels of pad compression and thus, different pulp fibre concentrations. All nine sets of data display linearity in the plot. Regression analyses on all nine sets of data were carried out and the correlation coefficients for all the lines are larger than 0.99. The slopes of the lines exhibit a systematic trend; the lower the fibre concentration, the higher the slope of the line.

Permeability of the pads at different levels of compression were calculated from the slopes of the relaxation lines according to Equation (3.5.5) and are plotted against pulp fibre concentrations in Figure 4.2.1.2. In the figure, when pad permeability is plotted as a function of fibre concentration, the data follow the nonlinear trend predicted by the Kozeny-Carman equation (Equation (2.2.9)); as the fibre concentration increases, pad permeability decreases.

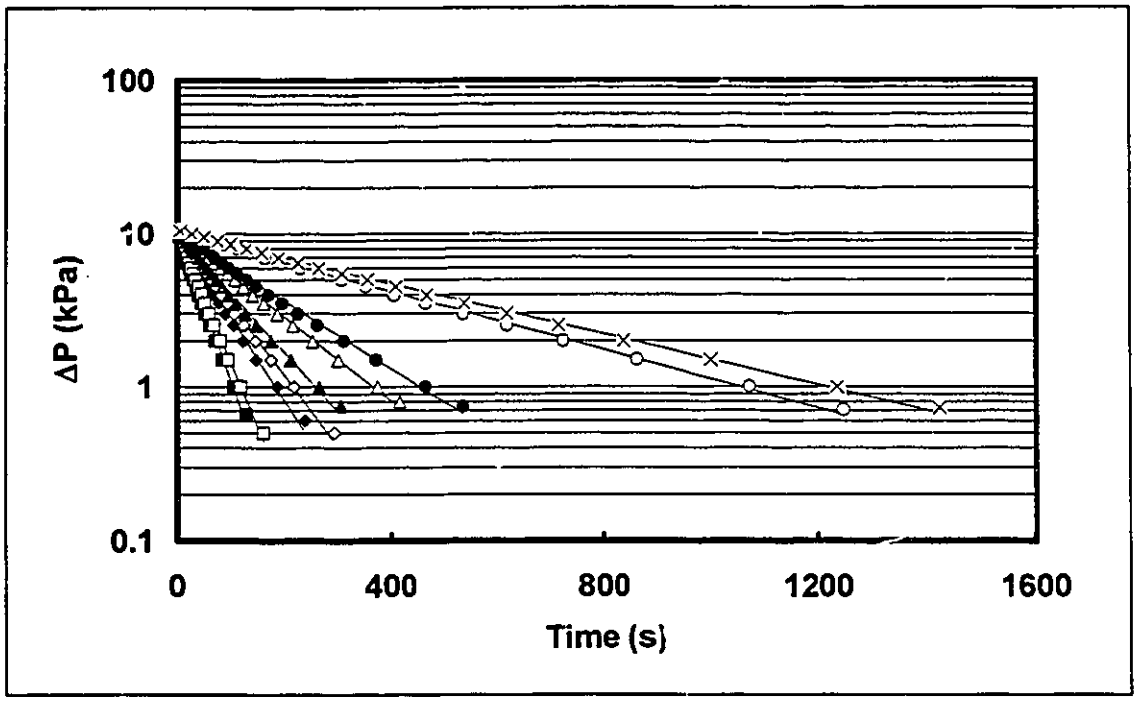

Figure 4.2.1.1 Pressure relaxation curves from kraft pulp pads compressed to different thicknesses. Each marker represents experimental measurement with a kraft pulp pad constrained to a specific pad solid concentration. The solid lines are linear regression fit of the experimental data to Equation (3.5.5). ■: pad solid concentration: 103.5 kg/m^3; □: 103.6 kg/m^3; ◆: 124.2 kg/m^3; ◇: 124.3 kg/m^3; ▲: 137.5 kg/m^3; Δ: 152.8 kg/m^3; ●: 155.4 kg/m^3; ○: 193.6 kg/m^3; ×: 203.8 kg/m^3.

A rectified Kozeny-Carman plot [Ingmanson, 1952, 1954] of the data for kraft pulp was constructed according to the linearized Kozeny-Carman equation (Equation (2.2.10)) and is shown in Figure 4.2.1.3. The data exhibit linearity as predicted by the linearized Kozeny-Carman equation and demonstrated by Robertson and Mason [1949].

The two intercepts of the rectified plot were used to calculate the specific external surface area and the specific swollen volume of the kraft pulp used. The specific surface area and specific swollen volume calculated were then

used as initial estimates in a nonlinear regression program to fit the data to the Kozeny-Carman equation. The program made use of the UWHAUS subroutine to carry out the regression analysis. The UWHAUS subroutine made use of the Marquart's compromise approach to obtain the best fit of the data. A listing of the program is included in Appendix A.6. A typical regression fit of the data is shown in Figure 4.2.1.2.

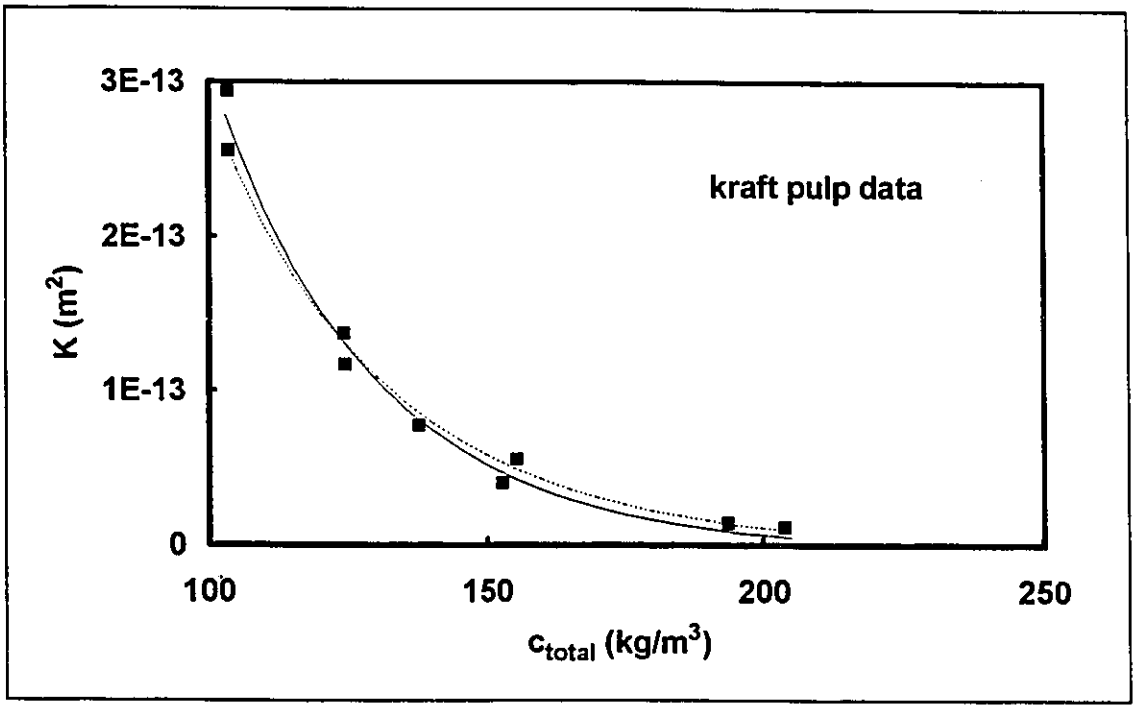

Figure 4.2.1.2 Permeability of kraft pulp pad at different degrees of compression (calculated from pressure relaxation data) plotted against the corresponding total solid concentration. The solid line shows the nonlinear regression fit of the experimental data to Equation (2.2.9). The dotted line is the permeability predicted by the Kozeny-Carman equation using specific surface area and specific swollen volume obtained from the linearized equation (Equation (2.2.10)).

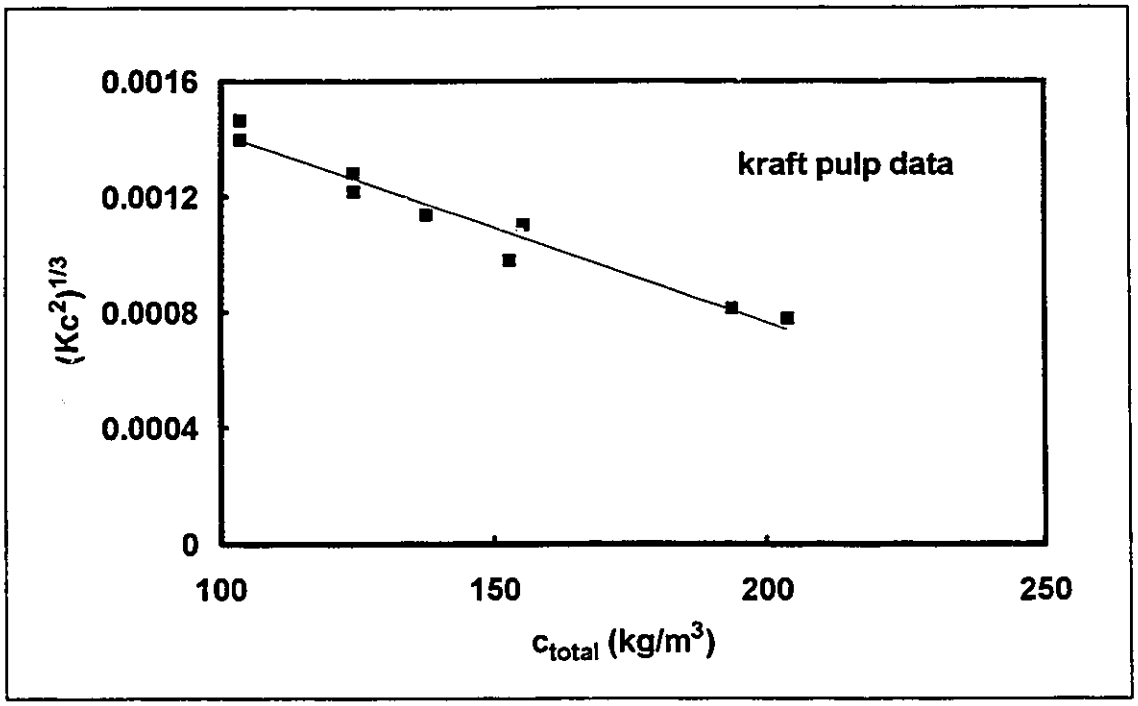

Figure 4.2.1.3 Rectified Kozeny-Carman plot of the permeability data of kraft pulp pads. The solid line is a linear regression fit of the data to the linearized Kozeny-Carman equation (Equation (2.2.10)).

The specific external surface area and the specific swollen volume of pulp fibres determined from the linearized Kozeny-Carman equation were 4485 m^2/kg and 0.003156 m^3/kg respectively. The same parameters determined by nonlinear regression using the Kozeny-Carman equation were 3918 ± 0.27 m^2/kg and 0.00358 ± 0.000115 m^3/kg. Typical published values for the specific surface area and specific swollen volume of wet kraft pulp beaten to a Canadian Standard Freeness of 454 mL are 3730 m^2/kg and 0.0047 m^3/kg [Robertson & Mason, 1949].

4.2.2 Pads Consisting of Pulp Fibres and Plastic Beads

Fixed bed permeation experiments had been carried out with pads containing kraft pulp and variable amounts of polystyrene beads. Specifications of the polystyrene beads were given in Section 3.1. Data for the pressure relaxation runs were all linear when the logarithm of the pressure drop was plotted against time. Since there were too many plots for all the systems used in the experiments and all the plots had the same feature as the plot for bead-free pulp (i.e., Figure 4.2.1.1), the plots will not be shown here. However, a list of the data files is given in Appendix A.7.

Permeability of the various pads at different thicknesses were determined from the pressure relaxation data by linear regression. In Figure 4.2.2.1, permeability of the pads at different levels of compression are plotted against total solid concentrations. Both the weight of the kraft pulp fibres and the weight of the plastic beads were used to calculate the total solid concentration. In the figure, each line gives data from pads having the same bead content. Data for all bead contents share the same feature: for each bead content, permeability of the pad decreases with an increase in the total solid concentration. Bead content is the other variable in Figure 4.2.2.1 that exhibits a systematic trend with pad permeability increasing with bead content. That is, for the same total solid concentration, the pad with the higher bead content displays a higher permeability than a pad that contains less beads. Therefore, the data from bead-free pulp pads lie below data from pads that contain beads.

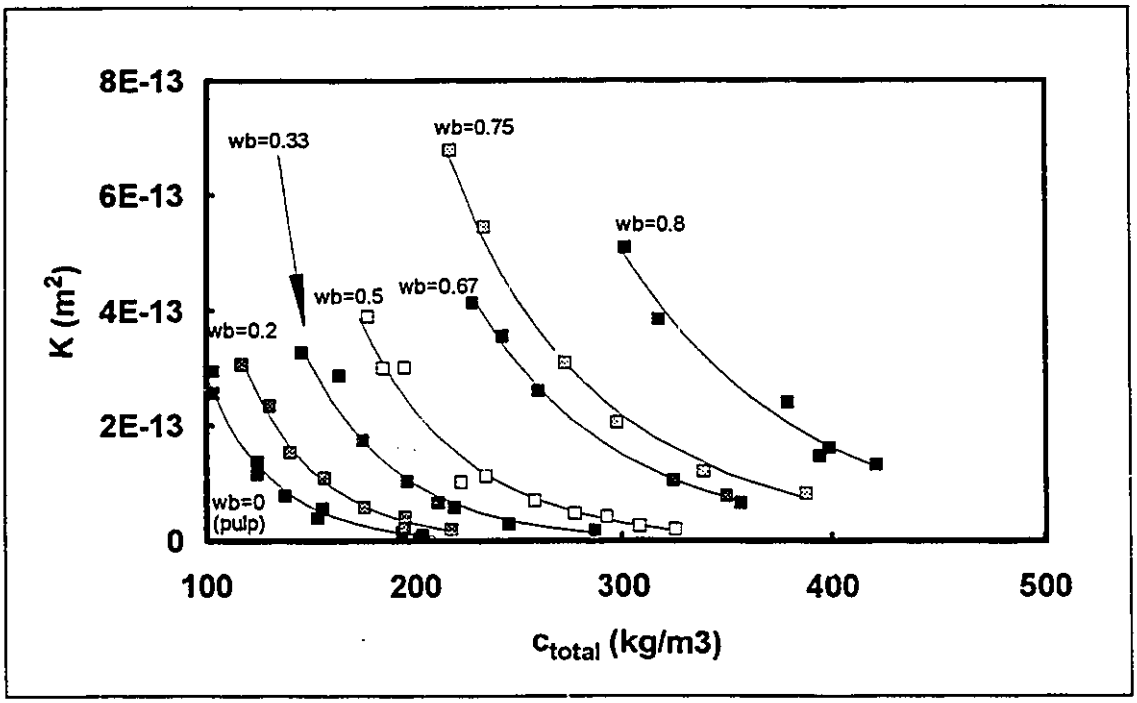

Figure 4.2.2.1 Permeability of kraft pulp pads containing plastic beads at different degrees of compression plotted against total solid concentration. Each data set represents experimental data from pads containing a fixed amount of beads. w_b is the weight fraction of beads in the fibre pad. Individual solid lines are results of nonlinear regression fit of the experimental data to Equation (2.2.9).

Since the beads serve as a model for air bubbles, it is reasonable to ignore bead weight in calculation of the solid concentration in pad. In Figure 4.2.2.2, the permeability of the pads are plotted against the concentration of kraft pulp fibres in the pad (i.e., the weight of the beads is NOT included in the calculation of the pad solid concentration). Permeability of pads at all bead contents decreases with pulp fibre concentration. A trend that is opposite to what is observed in Figure 4.2.2.1 is seen. The curve corresponding to the bead-free pad lies above all other curves. That is, for the same concentration of pulp

fibres, the pad with the higher bead content has a lower permeability and thus offers more resistance to flow.

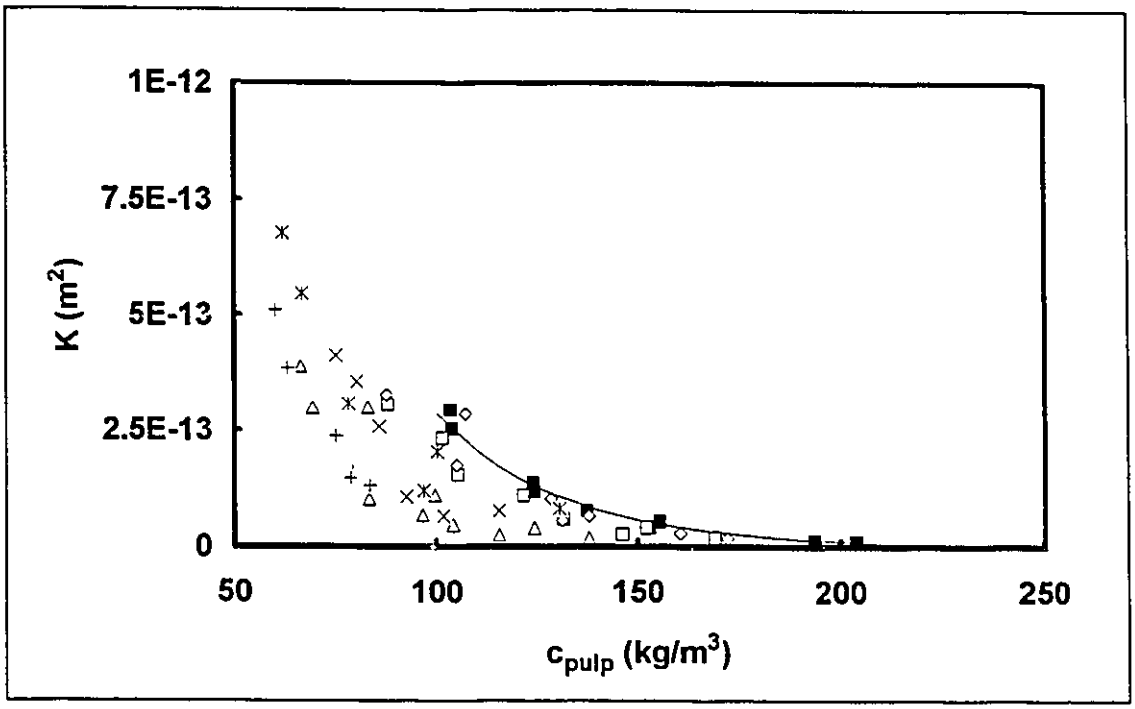

Figure 4.2.2.2 Permeability of kraft pulp pads containing various amounts of plastic beads plotted as a function of pulp fibre concentration. Individual markers are experimental data. ■: kraft pulp (solid line is nonlinear regression fit of kraft pulp data); □: weight fraction of beads in pad, w_b = 0.2; ◇: w_b = 0.33; △: w_b = 0.5; ×: w_b = 0.67; ✳: w_b = 0.75; +: w_b = 0.8.

Rectified Kozeny-Carman plots for pads having different bead contents are shown in Figure 4.2.2.3. Each line in the plot corresponds to a particular bead content in the pads. Data for the bead-free pulp pad lie below that of pads containing beads, which means that the data for bead-free pulp pad result in higher values of specific external surface area and specific swollen volume than pads that contain beads. The trend displayed by data from all the pads is that

an increase in the bead content results in a reduction in the specific surface area and specific swollen volume. Values of the specific surface area and specific swollen volume for pads with various bead contents were calculated from experimental data using nonlinear regression. The values are aggregate data which include contributions from both kraft pulp fibres and plastic beads. The specific surface area and specific swollen volume data for all bead contents are summarized in Table 4.2.2.1 except that the value for pure beads is a theoretical value calculated based on the average bead size of 112 μm.

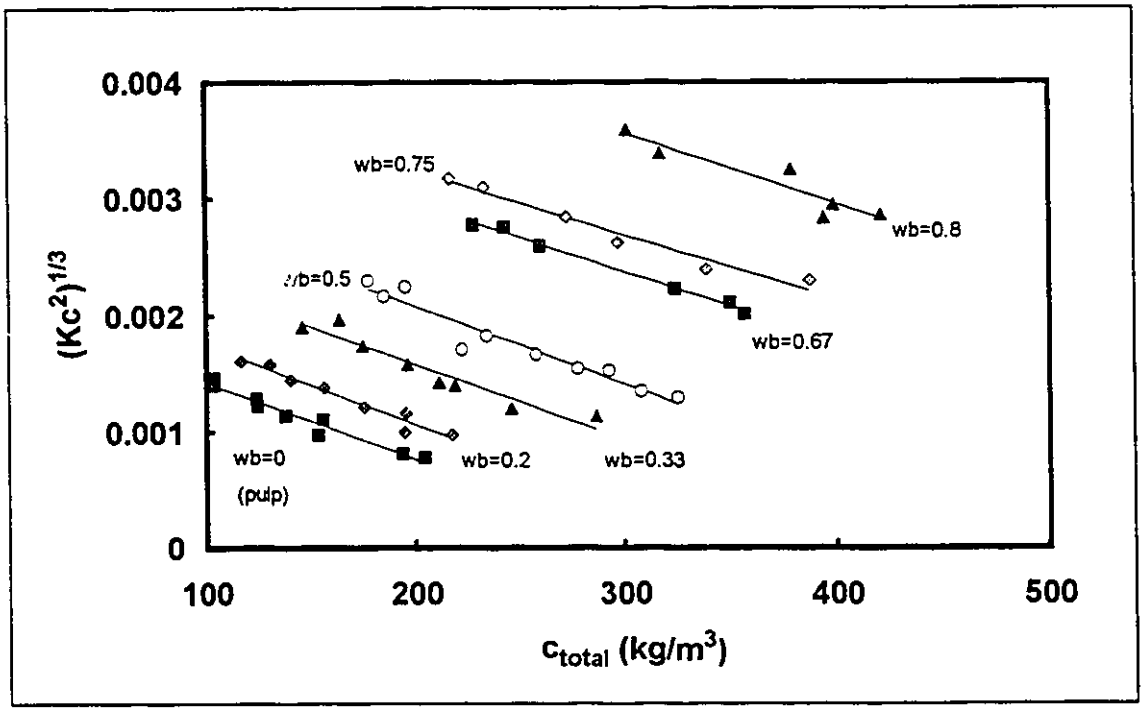

Figure 4.2.2.3 Rectified Kozeny-Carman plot of the permeability data of kraft pulp pads containing different amount of beads. w_b is the weight fraction of beads in the pad. The solid lines are linear regression fit of the data to Equation (2.2.10).

w_b	α (m^3/kg)	σ (m^2/kg)
0	0.003580	3918
0.2	0.002737	3637
0.33	0.002272	2688
0.5	0.002196	1846
0.67	0.001391	1613
0.75	0.001352	1411
0.8	0.001126	1074
1*	0.000952	51

Table 4.2.2.1 Summary of the effects of plastic beads on the overall specific surface area and specific swollen volume of pulp pads. w_b is the weight fraction of beads in a dried fibre pad. *: specific swollen volume and specific surface area of the plastic beads are calculated from the density and diameter of the beads.

4.2.3 Pads Consisting of Pulp and Nylon Fibres

Variable amounts of nylon fibres were mixed with 0.1 kg/m^3 kraft pulp suspensions to form pads that were used in fixed bed permeation experiments. Pressure relaxation data of the pads were all linear when plotted in a semi-log fashion. A list of the data files is given in Appendix A.7.

Permeability of the pads at different thicknesses were obtained from linear regression analysis of the pressure relaxation data. In Figure 4.2.3.1, permeability of the pads at different levels of compression are plotted as a function of total solid concentration. Both the weight of the kraft pulp fibres and the weight of the nylon fibres were used in the calculation of total solid concentration. Individual lines are the collection of data from different pads having the same nylon fibre content.

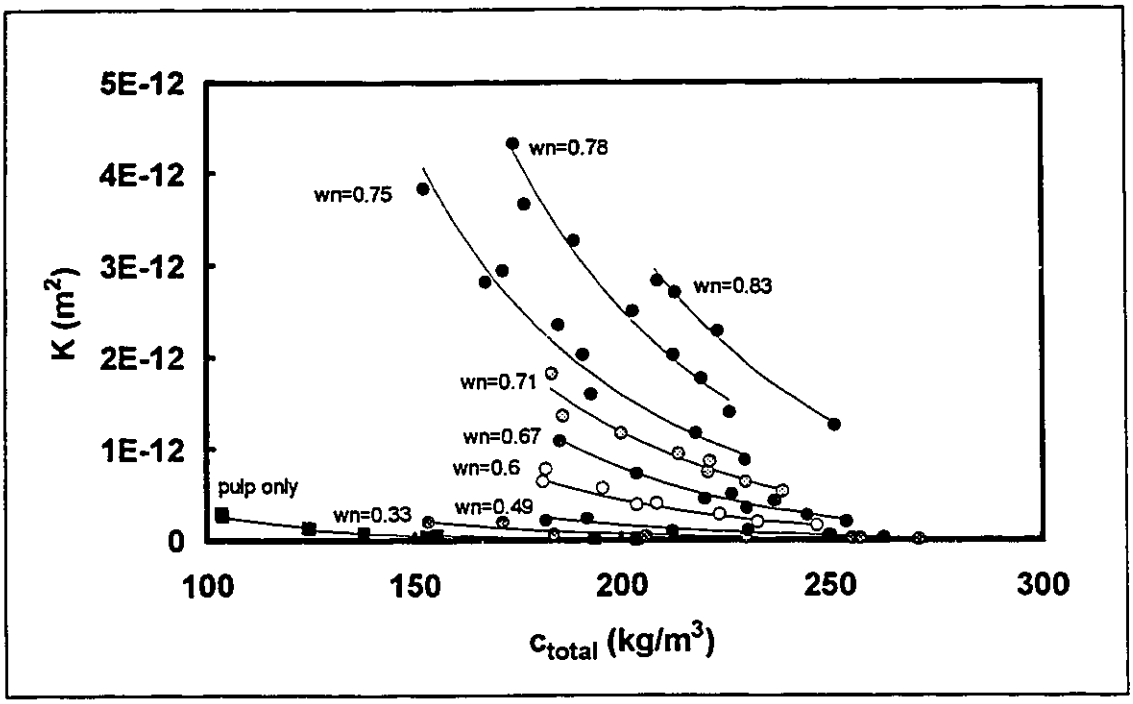

Figure 4.2.3.1 Permeability of kraft pulp pads containing different amount of nylon fibres plotted against total solid concentration. Each set of markers represents experimental data from pads containing a fixed amount of nylon fibres. w_n is the weight fraction of nylon fibres in the pad. The solid lines denote results of nonlinear regression fit of the experimental data to Equation (2.2.9).

Figure 4.2.3.1 shows that for any nylon fibre content, pad permeability decreases with an increase in total solid concentration. At a fixed total solid concentration, an increase in the nylon fibre content results in an increase in pad permeability. Therefore, data for the nylon fibre-free pad lies below data from all the other pads.

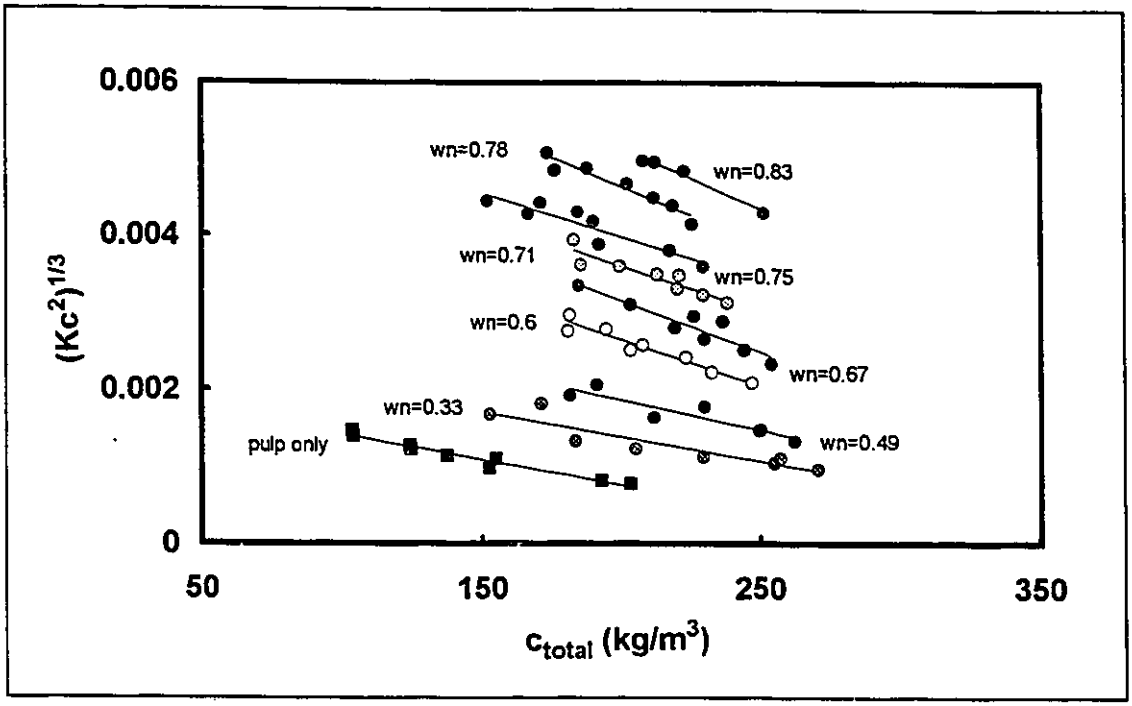

Figure 4.2.3.2 Rectified Kozeny-Carman plot of the permeability data of kraft pulp pads with different amount of nylon fibres. Markers represent experimental data. w_n is the weight fraction of nylon fibres in the pad. The solid lines denote linear regression fits of the data to Equation (2.2.10).

Rectified Kozeny-Carman plots of pads having different nylon fibre contents are shown in Figure 4.2.3.2. Data for all the different nylon fibre contents display linearity. The intercepts of the lines increase in value as the nylon fibre content increases resulting in a reduction of the overall specific swollen volume and specific external surface area. Values of the specific surface area and specific swollen volume for pads with various nylon fibre contents were calculated from nonlinear regression analysis results and summarized in Table 4.2.3.1 below.

w_n	α (m^3/kg)	σ (m^2/kg)
0	0.003580	3918
0.333	0.002511	2823
0.494	0.002160	2244
0.6	0.002340	1203
0.665	0.002243	981
0.714	0.001989	913
0.75	0.001651	912
0.783	0.001883	657
0.832	0.001875	568
1*	0.000877	78

Table 4.2.3.1 Summary of the effects of nylon fibres on the overall specific surface area and specific swollen volume of kraft pulp pads. *: specific swollen volume and specific surface area of the nylon fibres are calculated from the density and diameter of the beads instead of being measured experimentally.

4.2.4 Pads Containing Pulp/Nylon Fibres and Plastic Beads

Fixed bed permeation experiments were carried out with pads containing kraft pulp and nylon fibres at a fixed ratio (1:3.6 by mass) with a variable amount of polystyrene beads. Pressure relaxation data were all linear in semi-log plots and the list of data files is given in Appendix A.7.

Permeability of the various pads at different thicknesses were determined experimentally and plotted against total solid concentration in Figure 4.2.4.1. The weights of the kraft pulp fibres, nylon fibres and plastic beads were used in the calculation of the total solid concentration. In the figure, experimental data of the pads exhibit the same features that are observed with pads that contain pulp fibres and beads. At a fixed bead content, pad permeability decreases with increasing total solid concentration. At a fixed solid concentration, pad

permeability increases with increasing bead content. Permeability data for pulp pads are also included in the figure. Pads that contain nylon fibres display much higher permeability than pulp pads.

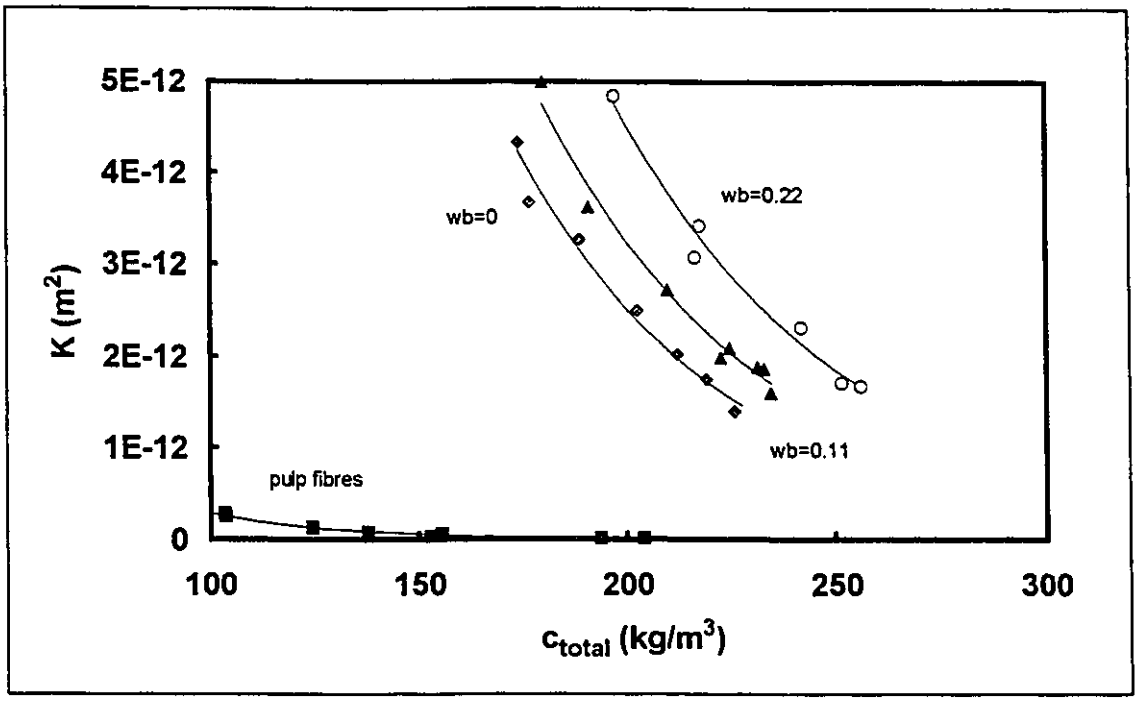

Figure 4.2.4.1 Permeability of kraft pulp/nylon fibre (1:3.6 by mass) pads containing different amount of plastic beads plotted against total solid concentration. Each set of markers represents experimental data from pads containing a fixed amount of beads. w_b is the weight fraction of beads in the pad. Individual solid lines are results of nonlinear regression fit of the experimental data to Equation (2.2.9).

In Figure 4.2.4.2, permeability of the pads are plotted as a function of the total FIBRE concentration in the pad (the weight of the beads is NOT included in the calculation of the pad solid concentration but the weight of both pulp and nylon fibres are included). The data presented show that pad permeability is inversely related to total fibre concentration. Data from the bead-free pulp/nylon

fibre pad lies above that from pads containing beads. However, permeability of pads that contain kraft pulp only is much lower than the permeability of pads containing pulp and nylon fibres.

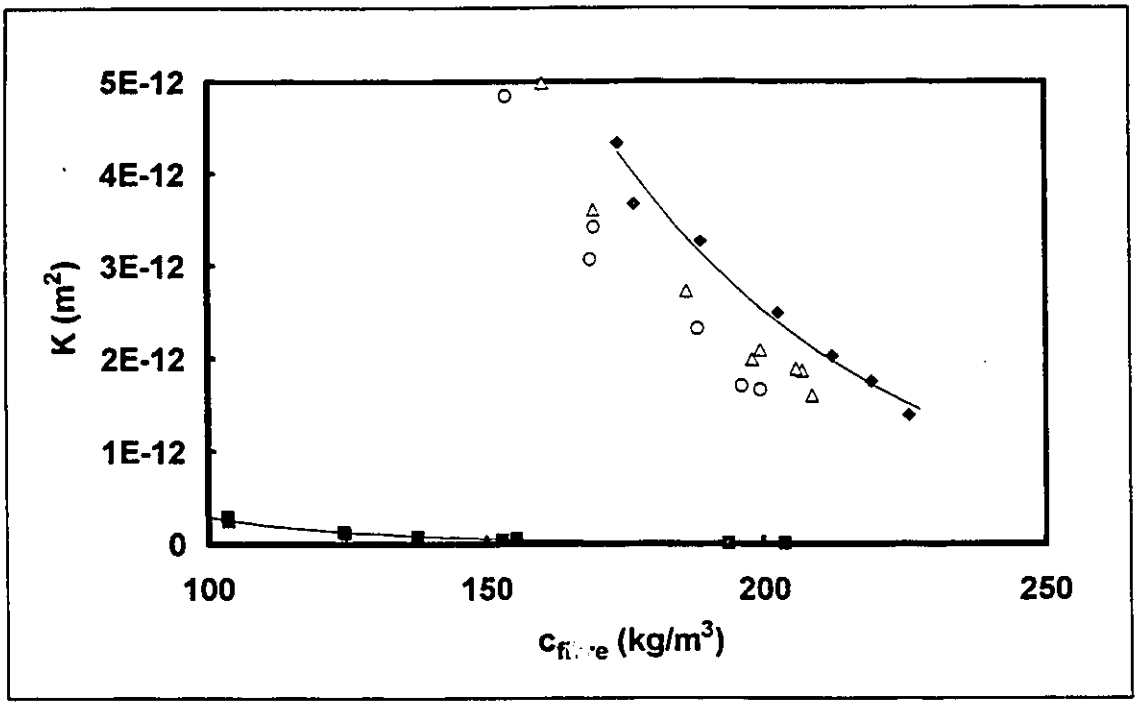

Figure 4.2.4.2. Permeability of kraft pulp/nylon fibre (1:3.6 by mass) pads containing various amount of plastic beads plotted as a function of total fibre concentration. Individual markers represent experimental data. The solid lines are nonlinear regression fit of the experimental data to Equation (2.2.9). ■: kraft pulp (solid line is a nonlinear regression fit of kraft pulp data); ◆: weight fraction of beads in pad, $w_b = 0$; △: $w_b = 0.11$; ○: $w_b = 0.22$.

Rectified Kozeny-Carman plots for pads having different bead contents are shown in Figure 4.2.4.3. Individual sets of data according to a particular bead content displays a strong linear relationship as predicted by the Kozeny-Carman equation. The effect of beads on the intercepts for pads containing pulp and nylon fibres is the same as in the case of pads containing kraft pulp fibres only.

The values of the specific surface area and specific swollen volume for pads with various bead contents were computed by nonlinear regression of the permeability data and summarized in Table 4.2.4.1.

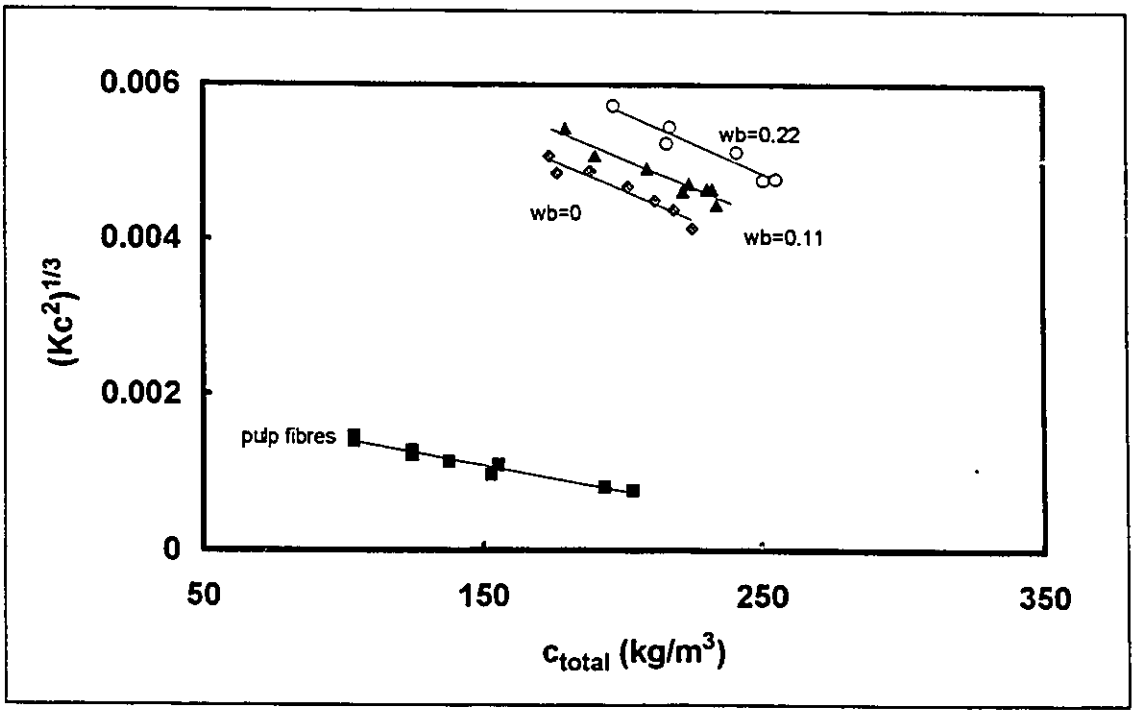

Figure 4.2.4.3 Rectified Kozeny-Carman plot of the permeability data of kraft pulp/nylon fibre (1:3.6 by mass) pads with beads. w_b is the weight fraction of beads in the pads. The solid lines are linear regression fit of the experimental data to Equation (2.2.10).

w_b	α (m^3/kg)	σ (m^2/kg)
0	0.001883	657
0.11	0.001912	570
0.22	0.001801	509

Table 4.2.4.1 Summary of the effects of plastic beads on the overall specific surface area and specific swollen volume of kraft pulp/nylon fibre pads with plastic beads.

4.3 Discussion

4.3.1 Pads Consisting of Pulp Fibres

Figure 4.2.1.1 demonstrates that the pressure relaxation data were linear with correlation coefficients for all the lines being larger than 0.99. This suggests that the flow regime in the fixed bed permeation experiments was laminar because the data exhibit the linearity predicted by Equation (3.5.5) which was derived assuming laminar flow in the porous pad. Robertson and Mason [1949] reported that Carman had proposed the following equation for the Reynolds number for flow in a porous medium:

$$Re = \frac{\rho Q}{A\mu S} = \frac{W}{A\mu S} \quad ....(4.3.1.1)$$

where Q is the volumetric flowrate of fluid through a porous pad that has a cross-sectional area of A while ρ and μ are the density and dynamic viscosity of the fluid respectively. S, in Equation (4.3.1.1), is the surface to volume ratio of particles in the porous pad and W is the mass flowrate of fluid through the pad. Carman stated that if Re was less than 2, flow in the porous medium was laminar. In the fixed bed permeation experiments, water was the fluid that flowed through the pad that had a radius of 5 cm. At room temperature, water has a viscosity of 8.5×10^{-4} Pa.s. The specific surface area and specific swollen volume of the pulp fibres were found to be 3918 m^2/kg and 0.00358 m^3/kg (see Section 4.2.1). Therefore, for a Re of 2, the resulting mass flowrate of water is 3.65 kg/s which implies that the flow through a pulp pad is laminar for any

flowrate that is less than 3.65 kg/s. In all the experiments carried out, the maximum flowrate was only 0.1 kg/s suggesting that the flows through the pads were laminar.

The experimental permeability were fit to the Kozeny-Carman equation (Equation (2.2.9)) and were shown in Figure 4.2.1.2. The Kozeny-Carman equation provides a close fit to the experimental data, indicating that the equation is a good correlation for permeability data. In Figure 4.2.1.3, the set of data displayed the linear relationship predicted by the linearized Kozeny-Carman equation.

The specific surface area and specific swollen volume obtained from the rectified plot were 4485 m^2/kg and 0.003156 m^3/kg respectively. These values are different from the values obtained by nonlinear regression by approximately 15%. The specific surface area and specific swollen volume estimated from the rectified plot were substituted in the original Kozeny-Carman equation (Equation (2.2.9)) to predict the permeability of pulp pads and the result was presented in Figure 4.2.1.2 as the dotted curve. Permeability predicted by the parameters obtained from the rectified plot are close to the nonlinear regression fit of the experimental data except at the two extremes of the concentration range. This indicates that although the linearized Kozeny-Carman equation appears to provide a good correlation of the experimental data, since the total solid concentration is included in both the abscissa and ordinate of the rectified plot, regression analysis using the linearized Kozeny-Carman equation puts too much emphasis on the high concentration range and thus overestimates the specific surface area and underestimates the specific swollen volume. Consequently, this error was manifested at the extremes of the concentration range when the

"rectified" parameters were used in the original Kozeny-Carman equation to predict pad permeability. Therefore, use of the linearized Kozeny-Carman equation and the rectified plot is a good method to obtain initial estimates of the specific surface area and specific swollen volume but only nonlinear regression of the data using the original Kozeny-Carman can provide accurate values of the two parameters.

In Figure 4.3.1.1, the permeability of a kraft pulp pad predicted by theoretical flow models are compared with the experimental data. Happel developed two flow models for porous media consisting of cylindrical particles [Happel, 1959]. A brief description of Happel's derivation was given in Section 2.2.1 and the results of the derivation were presented in the same section as Equation (2.2.2) and (2.2.3). In Happel's derivation, perfect cylindrical particles were assumed. In order to apply Happel's results to pulp fibres which are not perfect cylinders, the diameter of the cylinder in Happel's equations has to be replaced by the specific surface area and specific swollen volume of the pulp fibres. The diameter of a cylinder is related to its specific surface area and specific volume by the following equation if end effects are neglected,

$$\frac{4}{d} = \frac{\sigma}{\alpha} \quad \text{....(4.3.1.2)}$$

where d is the diameter of the cylinder while σ and α are the specific surface area and specific swollen volume. Substitution of Equation (4.3.1.2) into Equations (2.2.2) and (2.2.3) results in the following equations which are applicable to pulp fibres,

flow parallel to an array of cylinders

$$K = \frac{\alpha^2}{\sigma^2}\frac{1}{\alpha c}\left[-\ln(\alpha c) - 1.5 + 2\alpha c - \frac{(\alpha c)^2}{2}\right] \quad ....(4.3.1.3)$$

and flow perpendicular to an array of cylinders

$$K = \frac{\alpha^2}{\sigma^2}\frac{1}{2\alpha c}\left[-\ln(\alpha c) + \frac{(\alpha c)^2 - 1}{(\alpha c)^2 + 1}\right] \quad ....(4.3.1.4)$$

In both of the equations above, c is the total solid concentration in the bed and K is the permeability of the fibre bed.

Values of α and σ obtained from nonlinear regression analysis of experimental data for kraft pulp were used in Equations (4.3.1.3) and (4.3.1.4) to calculate the permeability of the pulp pad at different solid concentrations. The results are plotted with experimental data in Figure 4.3.1.1. The curves in the figure show that when the bed materials are aligned with the flow, resistance to flow is much smaller than when the cylinders are lying perpendicular to the direction of flow. This agrees with intuition because when the cylinders are aligned, the streamlines are much less disturbed than in the other case and thus less energy is lost to divert the flow around the solid particle. When the two theoretical models are compared with the experimental data, the parallel model overestimates the permeability while the perpendicular model exhibits excellent agreement with the experimental results. Therefore, it is most probable that the pulp fibres in the pad are all lying in the direction that is perpendicular to the flow, or in other words, the fibres are all lying flat in the pad. This condition is confirmed by studies using scanning electron microscopy. Fibre pads were dried after the fixed bed permeation experiments and examined using the

scanning electronic microscope. The resulting scanning electron micrographs showed that the dominant orientation of pulp fibres in the pad was perpendicular to the direction of flow. Therefore, the pad can be treated as a random, 2 dimensional layered structure. This condition will greatly assist in later modelling of the pad structure for permeation studies.

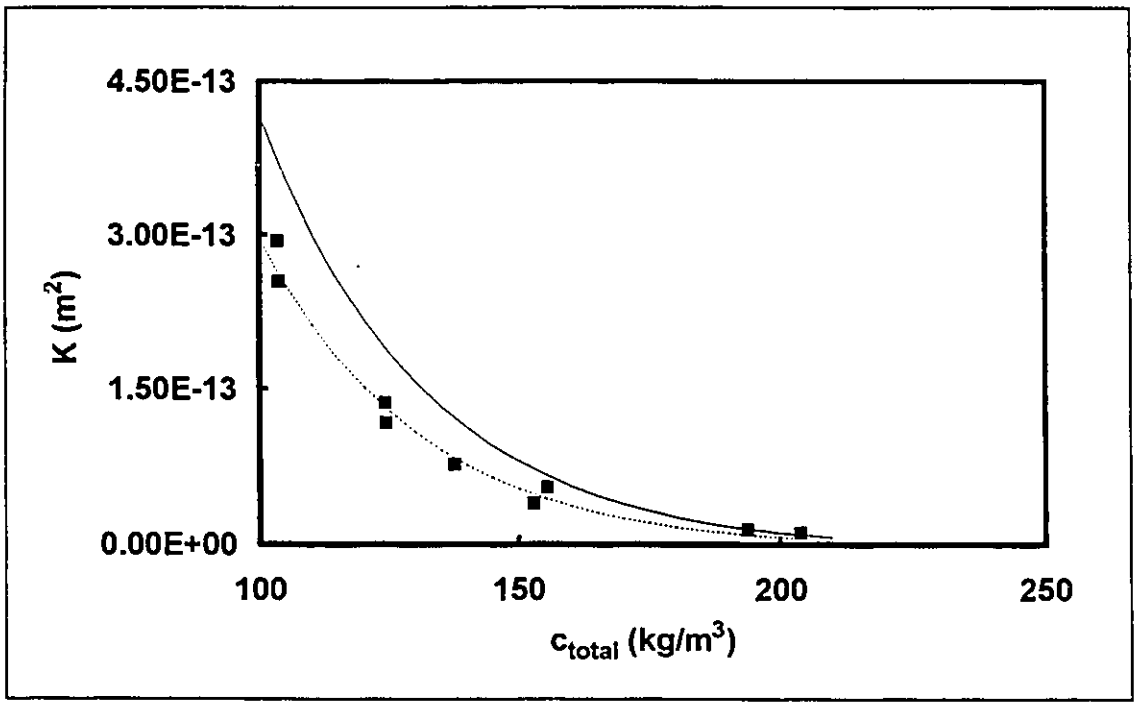

Figure 4.3.1.1 Plot of pad permeability as a function of total solid concentration. Individual markers represent experimental data with kraft pulp. The solid curve is theoretical prediction based on Happel's parallel flow model while the dotted curve is based on Happel's perpendicular flow model.

In summary, it has been shown with kraft pulp pads that Darcy's law applies in pressure relaxation experiments. The permeability calculated from pressure relaxation experiments obey the Kozeny-Carman equation. From the Kozeny-Carman plots, specific external surface area and specific swollen volume of pads

are determined by nonlinear regression. Values of the specific surface area and specific swollen volume obtained are of the same order of magnitude as values published in literature. However, estimation of the specific surface area and specific swollen volume of the pulp fibres from rectified plot produces erroneous results: overestimation of the specific surface area and underestimation of the specific swollen volume. Through comparison with existing theoretical models and scanning electron micrographs, it can be concluded that fibres in the pulp pad are lying in a direction perpendicular to flow and thus the pad can be approximated by a random, 2 dimensional layered structure.

4.3.2 Pads Consisting of Pulp Fibres and Plastic Beads

When pad permeability was plotted against total pad solid concentration in Figure 4.2.2.1, the curve that results from bead-free pads lies below the rest of the curves corresponding to pads containing beads. That is, for the same total solid concentration, pads having a higher bead content have a higher permeability. This reflects the low specific surface area and specific volume of the beads. The total specific surface area and specific swollen volume of the pad materials consist of contributions from both the kraft pulp and the beads. The Kozeny-Carman equation (Equation (2.2.9) indicates that both the specific surface area and the specific swollen volume are inversely related to the permeability of the pad. Since the beads have low contributions to both the area and volume, for the same total weight in a pad, the more beads there are, the lower the specific surface area and specific swollen volume will be, and thus the higher the permeability of the pad.

In Figure 4.2.2.2, pad permeability was plotted against mass concentration of pulp fibres (the mass of the plastic beads were neglected). The curve that corresponds to bead-free pads lies above the curves that represent data with pads containing beads. This means that at the same pulp fibre concentration, the pad that contains more beads has the lower permeability. This observation is consistent with intuition that the presence of a second component in the bed should actually hinder permeation. For a unit volume of the bed containing a fixed amount of pulp fibres, the pulp fibre concentration will remain constant regardless of the amount of plastic beads present. The presence of plastic beads in this volume of pad increases the total surface area presented to flow. This increase in surface area is given by the product of the mass of beads present and the specific external surface area of the beads. Therefore, at a fixed pulp fibre concentration, an increase in the bead content causes a proportional increase in the total external surface presented to flow which subsequently results in a decrease in the overall permeability of the pad.

The specific external surface area and specific swollen volume of the pads were summarized in Table 4.2.2.1. The specific swollen volume and the specific external surface area changed by approximately a factor of 3 when the weight fraction of beads increased from 0 to 0.8. It has been demonstrated in Figure 4.2.2.1, Figure 4.2.2.2 and Table 4.2.2.1 that the presence of the beads caused a systematic change in the effective specific swollen volume and effective specific surface area. Intuitively, one expects that the presence of plastic beads to cause an increase in the total surface area presented to flow and the total volume of material blocking the flow. Consequently, the effective specific surface area and specific swollen volume calculated based on the total weight of

solid materials should increase linearly with bead content since the beads have a specific volume that is much lower than that of the pulp fibres. That is, the effective specific swollen volume and specific surface area are sums of the contributions from the beads and the pulp fibres based on the weight fraction of the components present. However, if the introduction of plastic beads should cause any change in the structure of the pad by affecting the packing of the pulp fibres or the beads are blocking the external surface of the pulp fibres, the increase in effective external surface will cease to be linearly proportional to the amount of beads present. Therefore, it is possible to gain insights on the effect of beads on the microstructure of the pad by studying the total specific external surface area and specific swollen volume of the pad materials as a function of bead content. The total specific surface area and specific swollen volume of pads containing beads are plotted as a function of the weight fraction of beads in a dried pad in Figures 4.3.2.1 and 4.3.2.2.

In an effort to relate pad permeability to bead content, mixing rules were applied to the experimental results. The mixing rule equations for the specific surface area and specific swollen volume were derived as follows.

Mixing rules, which have found extensive usage in thermodynamics, are equations that relate an intensive property of a mixture to properties of the components. Properties such as length, area, and volume are all additive while all the different types of energies are not. A property being additive means that the mixing rule comprises of 1) a summation of the product between the component property and its composition (weight fraction or mole fraction) and 2) a term to account for nonlinearity. Since the unit of specific surface area is m^2, square root of the specific surface area is in the unit of m, designating a

characteristic length. Assuming that the square root of 1) the product of the Kozeny factor, 2) the weight fraction of the component (pulp fibre or bead) and 3) the specific surface area of the component is linearly additive (no nonlinear term is needed) to give the effective specific surface area, the following equation is obtained:

$$\sqrt{K''\sigma_m} = \sqrt{w_b K'\sigma_b} + \sqrt{w_p K''\sigma_p} \quad ....(4.3.2.1)$$

where w_b and w_p are the weight fraction of beads and pulp fibres in the pad. σ_m, σ_b and σ_p are the specific surface area of the mixture, the beads and the pulp fibres respectively. K′ and K″ in the equation are the Kozeny factors for beads (perfect spheres) and pulp fibres. Taking the square on both sides of Equation (4.3.2.1) and introducing a mixing parameter in the term with the square roots gives the mixing rule equation for specific surface area:

$$K''\sigma_m = w_b K'\sigma_b + w_p K''\sigma_p + 2\Omega\left[w_b w_p K'K''\sigma_b\sigma_p\right]^{1/2} \quad ....(4.3.2.2)$$

where Ω is the adjustable mixing parameter. If the specific surface area is linearly additive, Ω has a value of zero. The same approach is taken to derive the mixing rule equation for the specific swollen volume. Taking the cubic root of the specific swollen volume gives the following equation:

$$\sqrt[3]{\alpha_m} = \sqrt[3]{w_b\alpha_b} + \sqrt[3]{w_p\alpha_p} \quad ....(4.3.2.3)$$

where α_m, α_b and α_p are the specific swollen volume of the mixture, the beads and the pulp fibres respectively. Taking the cube on both sides of Equation

(4.3.2.3) and introducing two adjustable mixing parameters in the terms with the cubic roots gives the mixing rule equation for specific swollen volume,

$$\alpha_m = w_b\alpha_b + w_p\alpha_p + 3\lambda_b\left[(w_b\alpha_b)^2 w_p\alpha_p\right]^{1/3} + 3\lambda_p\left[(w_p\alpha_p)^2 w_b\alpha_b\right]^{1/3} \quad \text{....(4.3.2.4)}$$

where λ_b and λ_p are the mixing parameters for the beads and the pulp fibres. The specific external surface areas and specific swollen volumes from all the different pads were determined by nonlinear regression of the data and plotted against weight fraction of beads in the pads in Figures 4.3.2.1 and 4.3.2.2. Mixing rules (Equations (4.3.2.2) and (4.3.2.4)) were applied to the two sets of results to correlate the data. The mixing rule results are also included in the figures.

In Figure 4.3.2.1, a linear mixing rule and the result from a linear regression fit were shown with the experimental specific external surface area data. The mixing rule used was a linear one which meant that Ω in Equation (4.3.2.2) was set to be zero. A second order mixing rule in which Ω in Equation (4.3.2.2) was non-zero had also been tried to fit the experimental data. The two mixing rule models gave very close results and thus the second order mixing rule was not included in the figure. The first order model is therefore preferable to the second order model for representing the data since it is simpler in form. A linear regression fit also provided a reasonable fit correlated the data well, giving a correlation coefficient of 0.96. In the linear regression analysis, all the experimental points were used while the theoretical point for pure beads was not included. The resulting equation from regression analysis was:

$$\sigma_m = -3650 \cdot w_b + 4010 \quad r^2 = 0.96 \quad ....(4.3.2.5)$$

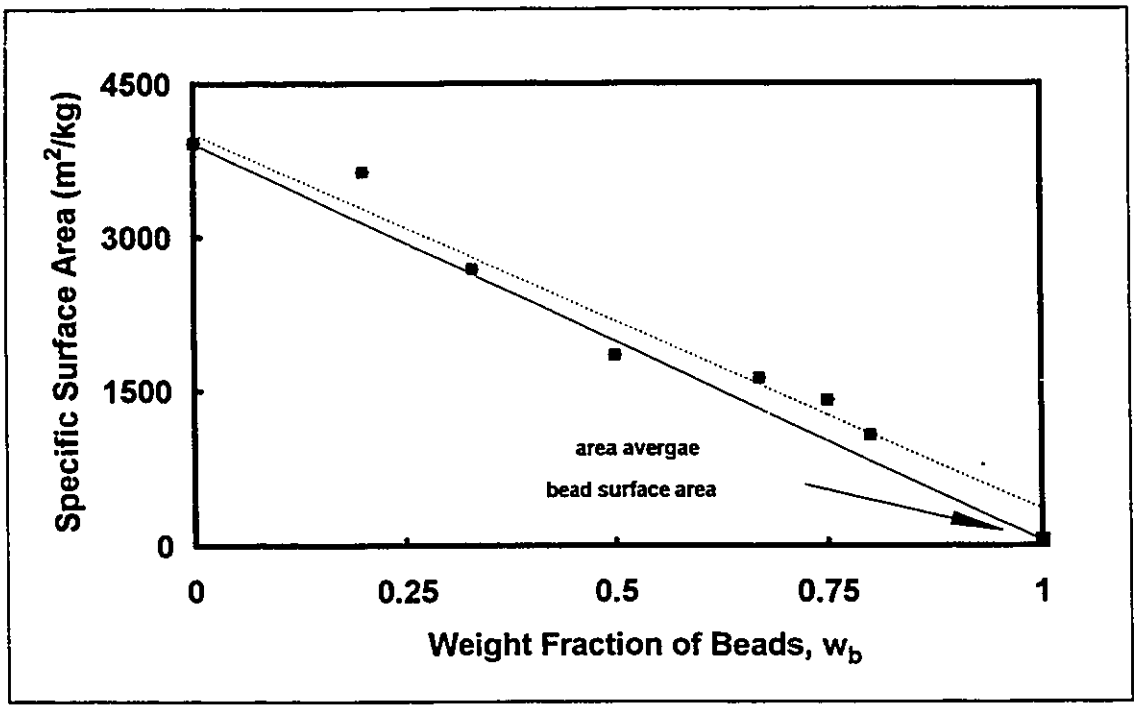

Figure 4.3.2.1 Specific surface area of pulp pads containing plastic beads plotted as a function of the weight fraction of beads. The solid line is the linear mixing rule (Equation (4.3.2.2)) with $\Omega = 0$ and the dotted line is a linear fit of the data.

When the first order mixing rule was compared to the linear regression model, the sum of square of errors (SSE) of the first order mixing rule was approximately 50% higher than that from the linear regression model; the first order mixing rule underestimated the effective specific surface area of the beads/pulp fibres system. Nevertheless, the specific surface area of plastic beads/kraft pulp system is linearly additive.

In Figure 4.3.2.2, two mixing rules and a linear regression fit were plotted with the experimental specific swollen volume data. One of the mixing rule models was first order (i.e., both λ_b and λ_p in Equation (4.3.2.4) were zero) while the other was third order (i.e., both λ_b and λ_p in Equation (4.3.2.4) attained values of –0.22 and 0.099 respectively). Both of the mixing rules provided correlation of the data while the higher order model predicted pronounced curvature in the data curve at high bead contents. The third order model exhibited closer agreement with the experimental data and thus seemed to be preferable to the first order model. However, since there were not enough data in the high bead content range to confirm the curvature, the first order model was preferable to the third order model. Linear regression analysis was carried out with the data. The resulting regression correlation equation was:

$$\alpha_m = -0.00288 \cdot w_b + 0.00343 \quad r^2 = 0.97 \quad \text{....(4.3.2.6)}$$

Similar to the case of the specific surface area, a linear correlation between specific swollen volume and bead content suggests that the effect of the bead is linearly additive.

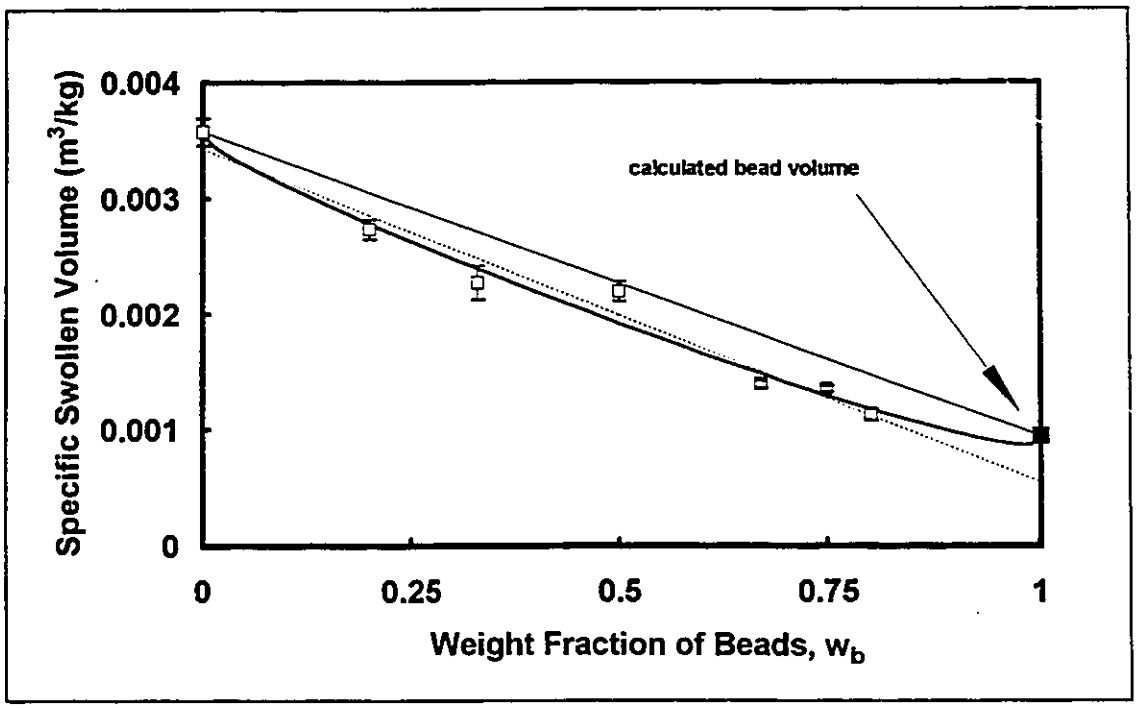

Figure 4.3.2.2 Specific swollen volume of pulp pads containing plastic beads plotted as a function of the weight fraction of beads. The solid line shows the linear mixing rule result (Equation (4.3.2.4)) with $\lambda_b = \lambda_p = 0$ while the solid curve is the result from the third order mixing rule (Equation (4.3.2.4)) with $\lambda_b = -0.22$ and $\lambda_p = 0.099$. The dotted line is a linear fit of the data.

According to the linear regression result (Equation (4.3.2.5)), the predicted specific external surface of the beads is higher than the theoretical value calculated from the average diameter of the bead. On the other hand, the regression equation of the specific swollen volume data (Equation (4.3.2.6)) gives a bead specific volume that is lower than the theoretical value. The quotient of the specific swollen volume and specific surface area is related to the equivalent bead diameter, D, by the following equation:

$$\frac{6}{D} = \frac{\sigma}{\alpha} \quad \text{....(4.3.2.7)}$$

Based on the specific surface area and specific volume of the beads predicted by the regression equations (Equations (4.3.2.5) and (4.3.2.6)), the predicted equivalent bead diameter is approximately 10 μm, which is 1/8 of the value based on the bead diameter measured by image analysis.

A possible reason for the change in equivalent diameter is the clogging of channels in the fibre bed. The effect of plugging the pores can be obtained by considering the following model. Suppose there are initially two channels in a porous bed and one of the channels becomes blocked. Flowrate of fluid through the bed with the plugged up channel is less than that when the bed is not clogged. Therefore, the permeability of the bed is reduced. There is now only one channel available to the flow. Consequently, the specific surface area, which is the surface area presented to flow in the porous bed, is reduced by half while the specific volume, volume in the porous bed that is denied to flow, is increased. According to Equation (4.3.2.7), the characteristic effective diameter of the bed material is increased. If the same argument is applied to the data from the plastic beads/pulp fibres system, since the effective diameter of the beads predicted by the linear regression is lower than the measured bead size, the plastic beads did not plug up the pores in the fibre bed. When specific surface area and specific swollen volume data presented in Figures 4.3.2.1 and 4.3.2.2 were examined, specific surface areas at all bead contents predicted by the first order mixing rule were almost always less than the experimental values, while the specific swollen volumes calculated from the first order mixing rule were always higher than the experimentally measured values. Therefore, the equivalent diameters at all bead contents are less than those predicted by the first order mixing rule according to Equation (4.3.2.7), suggesting not only that

the beads did not plug up the pores, but that the beads might have opened up the fibre bed structure to enhance fluid permeation. Alternatively, the beads may fit into the interstices of the fibre network without blocking any of the pores.

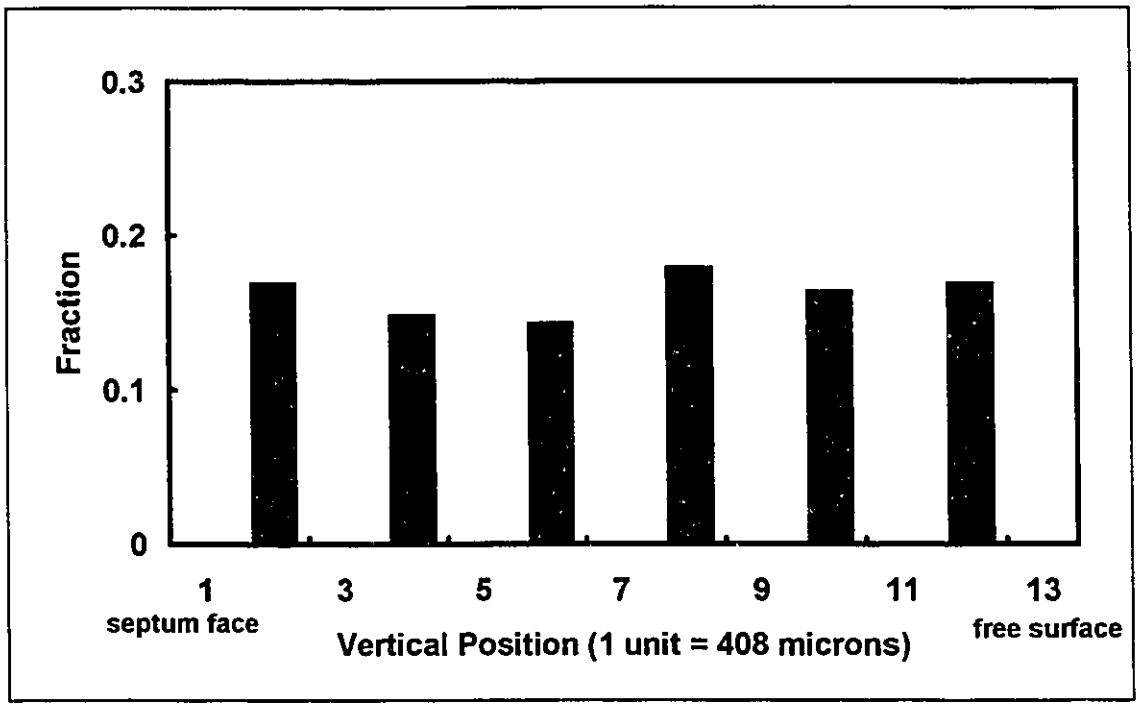

Figure 4.3.2.3 Distribution of plastic beads plotted as a function of vertical position in a fibre pad that has a bead weight fraction of 0.33. Bead distribution was estimated from scanning electron micrographs of pad section obtained from experiments.

Bead distribution in fibre pads was studied by scanning electron microscopy. Fibre pads containing various amount of plastic beads were dried and cut after fixed bed permeation experiments. Scanning electron micrographs of the pad sections were studied and the beads were found to be uniformly distributed in the pad. A typical bead distribution in a fibre pad that has a bead weight fraction of 0.33 was presented in Figure 4.3.2.3. Data in the figure

illustrate the uniformity in bead distribution. Scanning electron micrographs of sections from: 1) a pulp pad and 2) a fibre pad that has a bead weight fraction of 0.5 are shown in Figures 4.3.2.4 and 4.3.2.5. Figure 4.3.2.4 shows that the pulp fibres are predominantly oriented in the horizontal direction, illustrating the point made in Section 4.3.1 that the fibres are perpendicular to the direction of flow. Figure 4.3.2.5 illustrates the point that the beads are fitting into the pores in the network structure formed by the pulp fibres without blocking the channels.

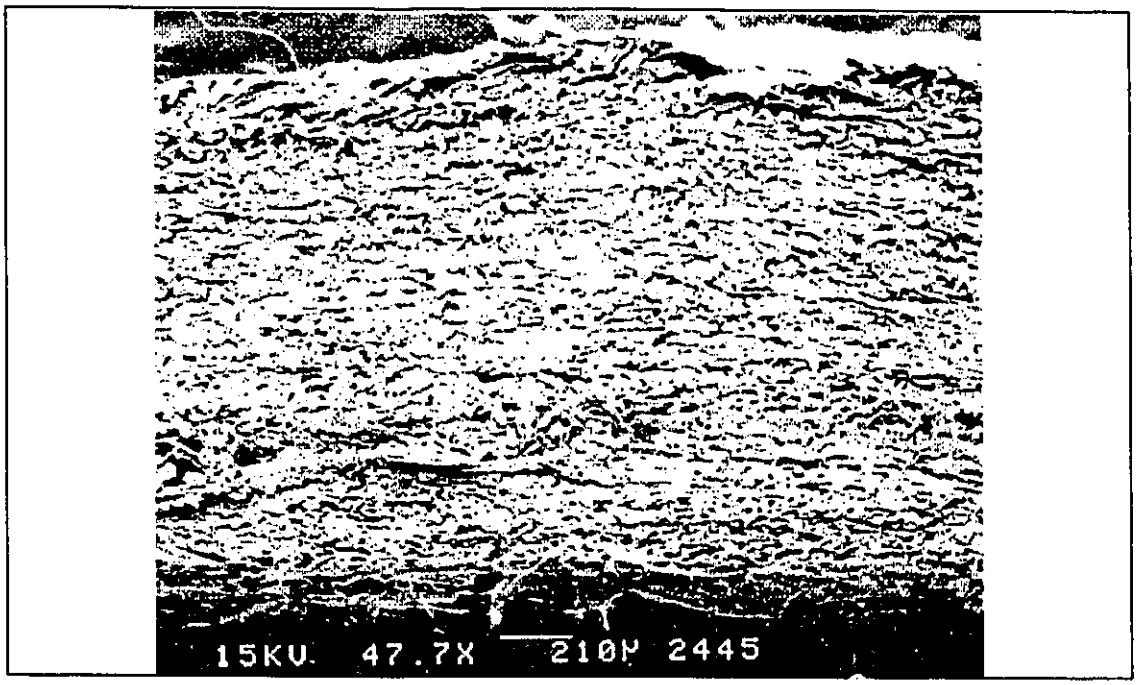

Figure 4.3.2.4 Scanning electron micrograph of a section of a pad that contains pulp fibres only.

In summary, both the specific surface area and specific swollen volume of pad materials were functions of bead content. An increase in bead content caused a decrease in both parameters. The effect of beads on both the specific surface area and specific swollen volume of the pad were linearly additive.

Therefore, the relationship between specific surface area, specific volume, and bead content can be represented by linear correlations. The plastic beads were uniformly distributed in the pulp pads and the beads did not plug up the pores in the fibre bed; the beads might have opened the pad structure to enhance permeation or fit into the pores in the fibre bed without blocking any of the pores.

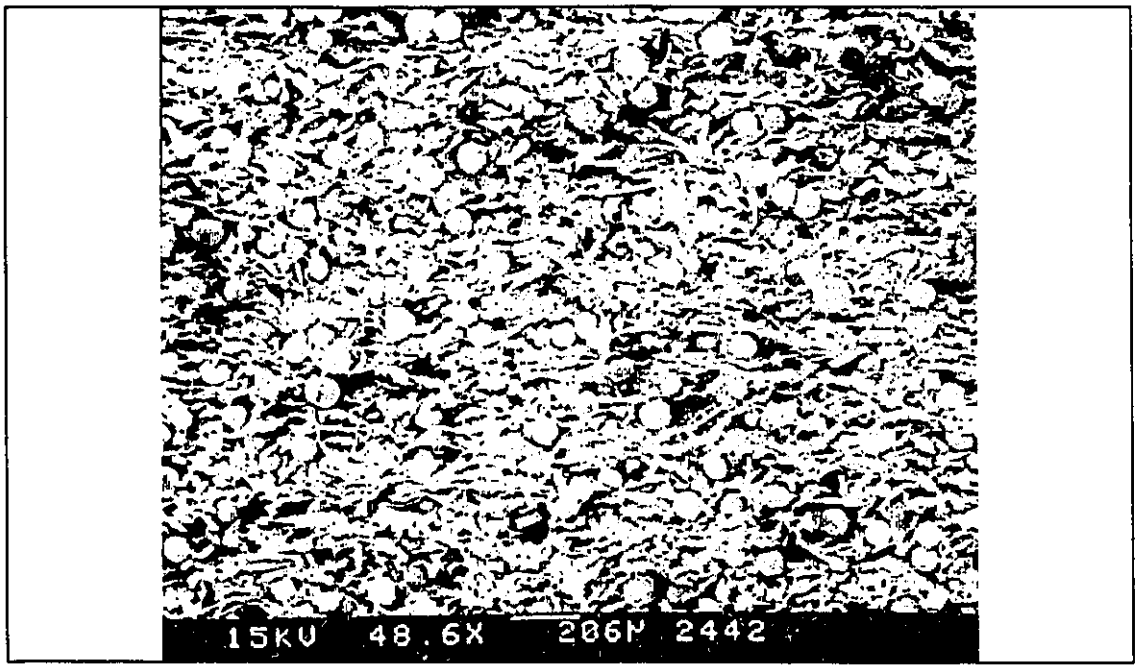

Figure 4.3.2.5 Scanning electron micrograph of a section of a pad that contains pulp fibres and plastic beads with a bead weight fraction of 0.5.

4.3.3 Pads Consisting of Pulp and Nylon Fibres

Permeability of pads containing various amounts of nylon fibres was plotted against total solid concentration in Figure 4.2.3.1. In the figure, the permeability of pads containing kraft pulp fibres only was lower than the permeability of pads that contained nylon fibres. That is, for the same amount of total solid material,

higher nylon fibre content resulted in higher pad permeability. This observation is expected because the nylon fibres have a specific surface area and a specific volume that are much lower than those of kraft pulp fibres. Therefore, the contribution from nylon fibres to the permeation resistance of the pad is less than that from kraft pulp fibres. If the overall permeation resistance is considered, higher nylon fibre content results in higher permeability. In addition to this effect of specific surface area and specific swollen volume, rigidity of the nylon fibres should also have contributed to the increase in overall permeability. The high rigidity of the nylon fibres should have the effect of opening up the pad structure because the nylon fibres tend to resist bending under stress. Consequently, the pad structure is more open and the pad becomes more permeable when more nylon fibres are present. Figure 4.3.3.1 is a scanning electron micrograph of a section from a pad that contains pulp fibres and nylon fibres. By comparing Figure 4.3.3.1 to Figure 4.3.2.4 which showed the scanning electron micrograph of a section of a pulp pad, it is clear that the rigid nylon fibres have the effect of opening up the network structure and making the fibre pad more permeable.

In the rectified Kozeny-Carman plot in Figure 4.2.3.3, the different sets of data displayed a systematic trend; as the nylon fibre content increased, the intercepts of the lines increased in value resulting in a reduction in the specific surface area and specific swollen volume of the pad materials. However, contrary to the case of pulp fibres and plastic beads, the slopes of the lines representing different nylon fibre contents were not the same, implying that the specific surface area and specific swollen volume of the pad materials were not

varying proportionally, suggesting that the nylon fibres were affecting the microstructure in the pads.

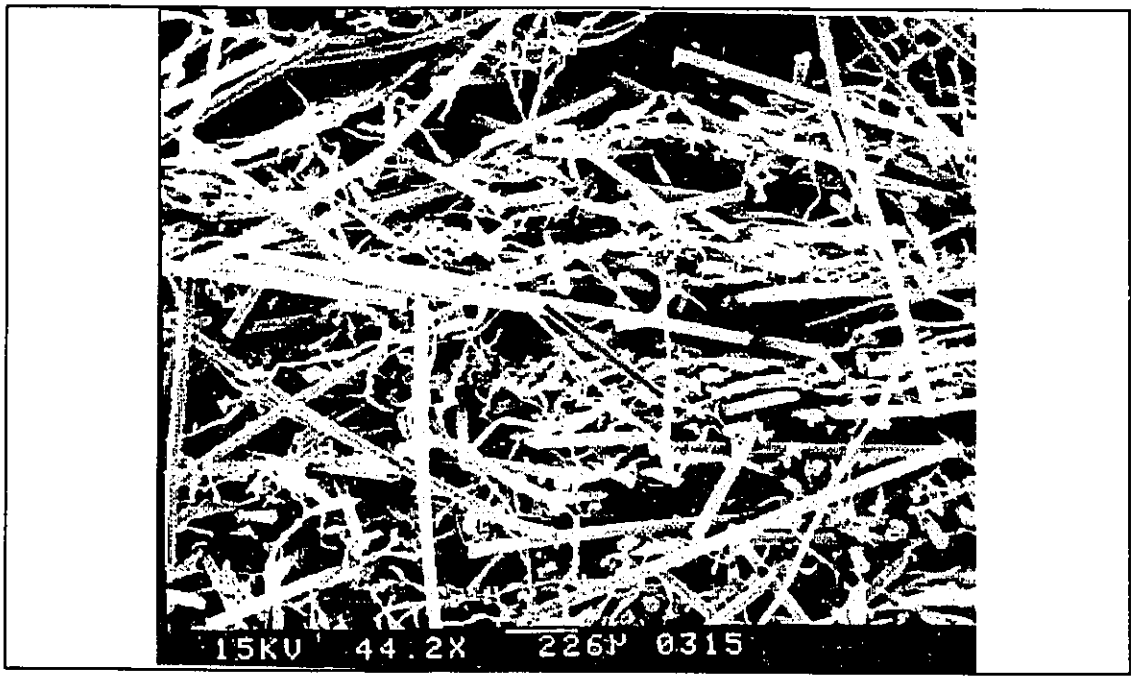

Figure 4.3.3.1 Scanning electron micrograph of a pad that contains pulp and nylon fibres. The weight fraction of nylon fibres in the pad is 0.783.

The specific surface area and specific swollen volume of pads at different nylon fibre content were calculated from nonlinear regression analysis results and presented in Table 4.2.3.1. The presence of nylon fibres caused reduction in both the specific surface area and specific swollen volume of the total pad materials as nylon fibre content increased. Contrary to the system of pulp fibres and plastic beads, the effect of nylon fibres on the specific swollen volume is not as pronounced as that on the specific external surface area. This is probably due to the fact that the difference in specific swollen volume between the two fibres are not as large as the difference in specific surface area. Consequently,

the presence of the nylon fibres have less effect on the specific swollen volume of the total pad materials.

Since both of the materials are fibres, a linear mixing rule should suffice to correlate the effect of nylon fibre content on overall pad permeability because of their similarity in shape. The specific external surface areas and specific swollen volumes from all the different pads were determined from the experimental data by nonlinear regression and plotted as a function of the weight fraction of nylon fibres in the pads in Figures 4.3.3.2 and 4.3.3.3. Linear mixing rules (Equations (4.3.2.2) and (4.3.2.4) with $\Omega = \lambda_b = \lambda_p = 0$) were applied to the two sets of results to correlate the data. Linear regression analysis was carried out with the experimental data. Mixing rule predictions and linear regression fits of the data are included in the figures.

In Figure 4.3.3.2, linear mixing rule results and the linear fit are shown with the experimental specific external surface areas. Since the specific surface area of pure nylon fibre was obtained by theoretical calculations based on the diameter of the fibre, it was not included in the linear regression fit. It is evident from Figure 4.3.3.2 that although linear mixing rule gives good prediction of the specific surface area, the mixing rule overestimates the parameter at higher nylon fibre contents. For the linear regression fit, since it is obtained through an error minimization procedure, the average accuracy of its prediction should be better than the linear mixing rule. Therefore, the linear regression fit is preferable to the mixing rule for predicting specific surface area and the regression equation is given by:

$$\sigma_m = -4300 \cdot w_n + 4050 \quad r^2 = 0.97 \quad ....(4.3.3.1)$$

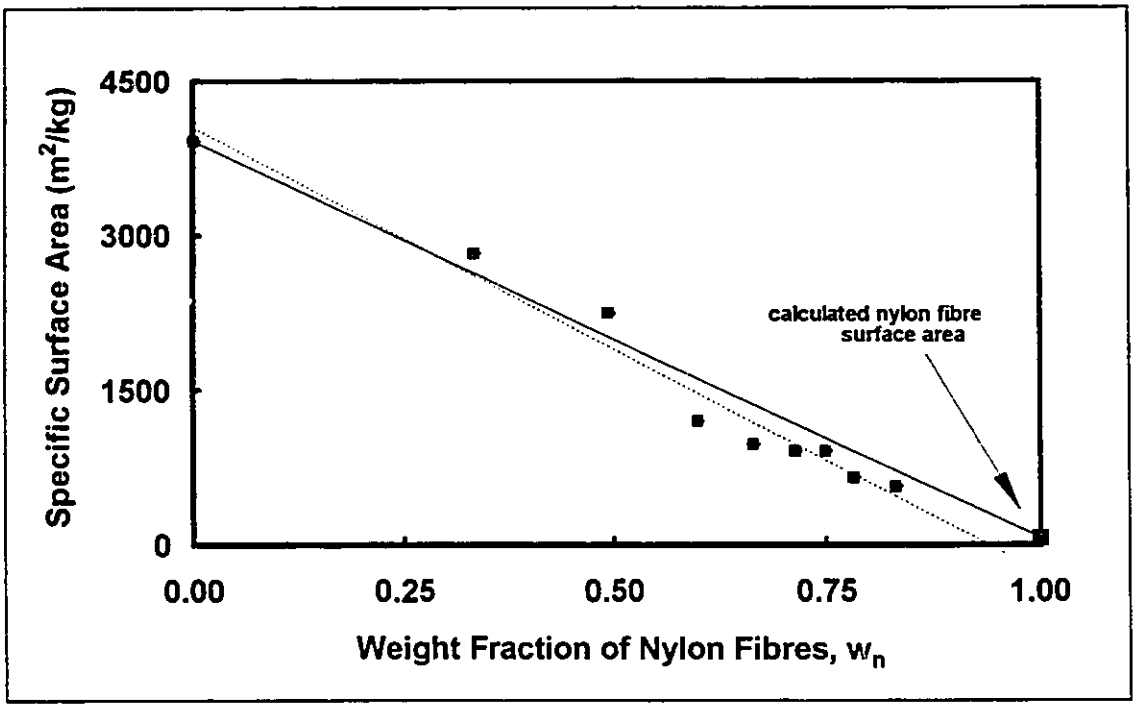

Figure 4.3.3.2 Specific surface area of pulp pads containing nylon fibres plotted as a function of weight fraction of nylon fibres. Solid line is the linear mixing rule and the dotted line is a linear fit of the data.

A linear mixing rule and a linear fit of the specific swollen volumes of pads containing pulp/nylon fibres are plotted as a function of nylon fibre content in Figure 4.3.3.3. Again, the linear fit is preferable to the first order mixing rule to represent the experimental data since the linear mixing rule underestimates the specific swollen volume with increasing magnitude at higher nylon fibre contents. The linear regression equation for specific swollen volume in pads containing pulp fibres and nylon fibres is:

$$\alpha_m = -0.00201 \cdot w_n + 0.0034 \quad r^2 = 0.89 \quad ....(4.3.3.2)$$

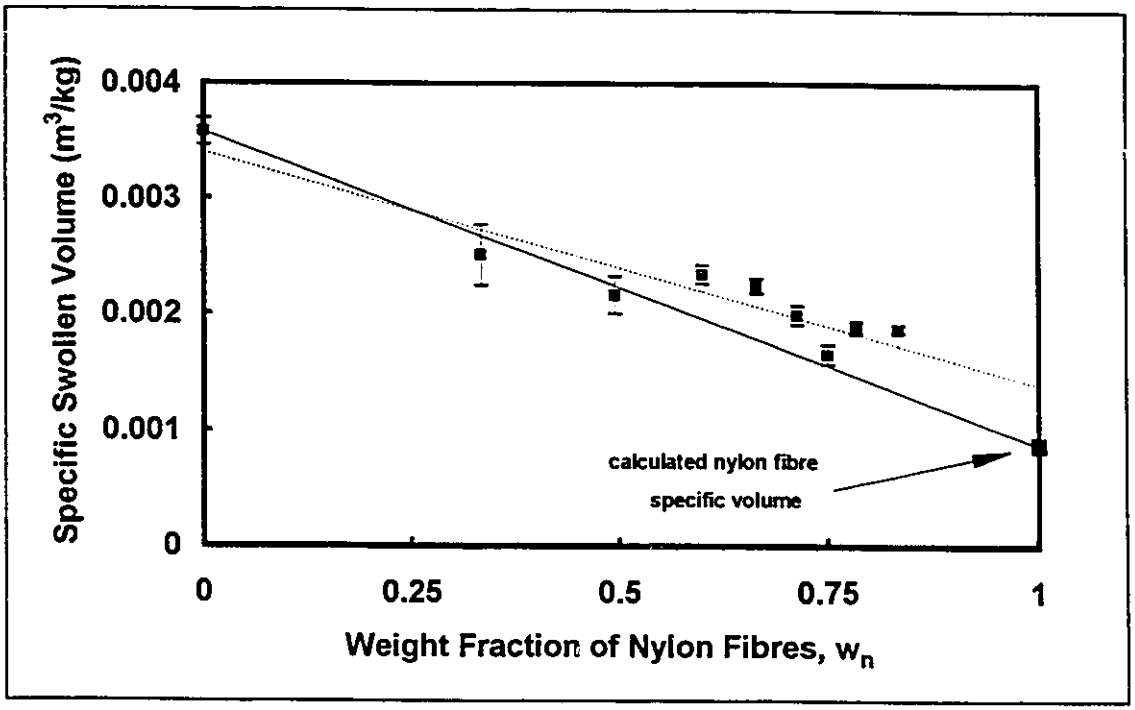

Figure 4.3.3.3 Specific swollen volume of pulp pads containing nylon fibres plotted as a function of weight fraction of nylon fibres. The solid line shows the linear mixing rule result while the dotted line is a linear fit of the data.

According to the regression models, the predicted specific surface area of the nylon fibre is lower than the theoretical value (a negative value is predicted) while the predicted specific swollen volume of the nylon fibre is approximately 60% higher than the theoretical value calculated from the diameter of the nylon fibre. The equivalent diameter of the nylon fibre is related to the quotient of the specific volume and the specific surface area by Equation (4.3.1.2). Therefore, using the specific surface area and specific swollen volume of nylon fibres obtained from linear regression models (assuming a specific surface area of 78 m^2/kg, instead of the negative value given by the linear regression equation), the equivalent diameter of the nylon fibre is found to be 71 μm, approximately 1.6 times of the actual value of 45 μm.

Permeability methods using the Kozeny-Carman equation had been widely applied to measure the specific surface area and size of particles with good accuracy (an error of less than 10%) [Sullivan & Hertel, 1942; Carman, 1948]. However, the authors also stated that if "the porous media were consolidated" or "bridging, agglomeration, or considerable channelling" existed in the porous media, the fraction of surface exposed to flow was uncertain and application of the Kozeny-Carman equation would lead to erroneous results. Therefore, a possible reason for the discrepancy between the equivalent and the actual nylon fibre diameter is that since the kraft pulp fibres are more flexible than the nylon fibres, the rigid nylon fibres are the predominant load bearing components of the network structure when the pad is formed. Although the rigidity of the nylon fibres opens up the fibre pad structure to allow higher fluid permeability, it is likely that flexible pulp fibres adjacent to nylon fibres conform to the contour of the rigid fibres and shield a fraction of the surface area of the nylon fibre. Therefore, the effective external surface area of the nylon fibres becomes lower, making the equivalent diameter of the nylon fibres larger than the theoretical value. The point made here about pulp fibres conforming to the nylon fibres is also evident from the scanning electron micrograph presented in Figure 4.3.3.1.

The specific surface area and specific volume of nylon fibres and the plastic beads used in the experiments are very close: 1) the specific surface area of plastic beads is 51 m^2/kg while the specific surface area of the nylon fibres is 78 m^2/kg and 2) the specific volume of beads is 0.000952 m^3/kg while it is 0.000877 m^3/kg for the nylon fibres. Therefore, it is reasonable to expect similar effects on total pad permeability when these two components were added to pulp fibres separately. The effects of beads and nylon fibres on the effective

specific surface area and specific swollen volume were similar; specific surface area and specific swollen volume decreased with increasing bead or nylon fibre content. However, the increase in pad permeability caused by the presence of the beads is not as pronounced as that caused by the nylon fibres. The reason for the difference, although the specific surface area and specific volume of the two components are so close, is the shape or aspect ratio of the particles. The plastic beads were perfectly spherical while the nylon fibres were cylindrical in shape. Therefore, it was possible for the nylon fibres to form open networks in the pads and cause further increase in pad permeability while the beads, although they did not plug up the pores in the pad, could only help in enhancing permeability by reducing the effective specific surface area and the specific swollen volume.

Pads containing pulp and nylon fibres were subjected to analysis by scanning electron microscopy. Nylon fibres were found to be uniformly distributed through out the pad and the elastic modulus of the nylon fibres was much higher than that of the pulp fibres. The nylon fibres were holding a network structure in the pad while the flexible pulp fibres stayed in the interstices of the network and curled around the nylon fibres.

In summary, both the specific surface area and specific swollen volume of pad materials were functions of nylon fibre content. An increase in nylon fibre content caused a decrease in both parameters. Effects of nylon fibres on both the specific surface area and specific swollen volume of the pad were linearly additive. Therefore, the correlation between specific surface area, specific volume, and nylon fibre content could be represented by linear regression. The

mixture of pulp fibres and nylon fibres exhibited higher overall pad permeability because of the rigidity of the nylon fibres.

4.3.4 Pads Containing Pulp/Nylon Fibres and Plastic Beads

In Figure 4.2.4.1, pad permeability data of pads containing various amounts of kraft pulp fibres, nylon fibres, and plastic beads are plotted against total pad solid concentration. The curve representing bead-free pads lies below the rest of the curves that correspond to pads containing various amounts of beads and a fixed amount of both fibres. Therefore, at the same total solid concentration, pads having a higher bead content have higher permeability, which is consistent with the results obtained with kraft pulp and beads system.

Pad permeability is plotted as a function of total fibre concentration (weight of the beads was excluded while the weights of both nylon and pulp fibres were included) in Figure 4.2.4.2 and a trend consistent with what was observed in the pulp/bead systems is shown: the curve corresponding to the pad that contains fibres only lies above all other curves. That is, for the same concentration of fibres, the pad with the higher bead content has lower permeability and thus more resistance to flow for the same reason as that for the pulp/bead system.

In Figure 4.2.4.3, the data exhibited linearity and the expected effect of beads was observed: intercepts of the lines increase in value with increases in bead content. Specific swollen volume and specific surface area of the various pads were calculated from nonlinear regression results and plotted against bead content in Figures 4.3.4.1 and 4.3.4.2. Linear mixing rules (Equations (4.3.2.2)

and (4.3.2.4) with $\Omega = \lambda_b = \lambda_p = 0$) and linear regression fits were applied to the two sets of results to correlate the data.

In Figure 4.3.4.1, results from a linear mixing rule and a linear fit were shown with the experimental specific external surface area data. Both the linear mixing rule and the linear regression fit give extremely close results. Due to the lack of data to cover the whole bead content range, it is not possible to decide which method correlates the data better. From the figure, it can be concluded that the specific surface area is additive linearly and the linear mixing rule prediction is close to the experimental value.

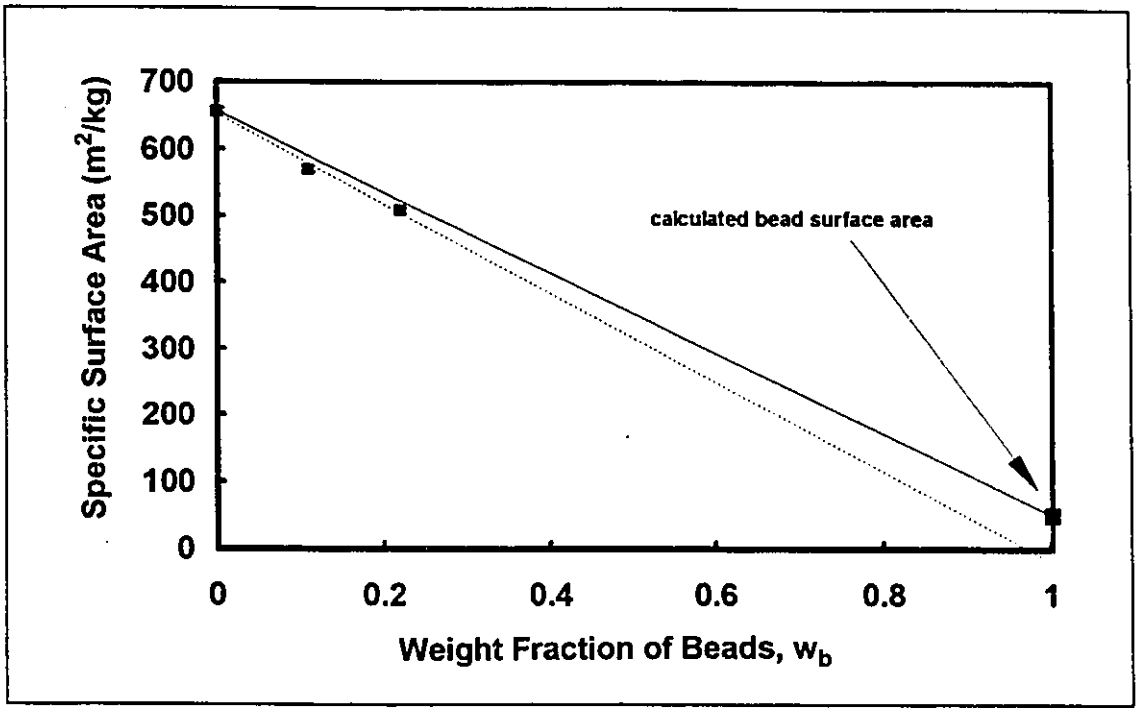

Figure 4.3.4.1 Specific surface area of kraft pulp/nylon fibre pads containing plastic beads plotted as a function of the weight fraction of beads. The solid line is the linear mixing rule and the dotted line is a linear fit of the data.

In Figure 4.3.4.2, a linear mixing rule and a linear fit were plotted with the experimental specific swollen volume data. Contrary to the data for specific surface area, the data for specific swollen volume is not correlated very well by the linear mixing rule. The data is showing a linear trend but the experimental data deviate from the linear mixing rule.

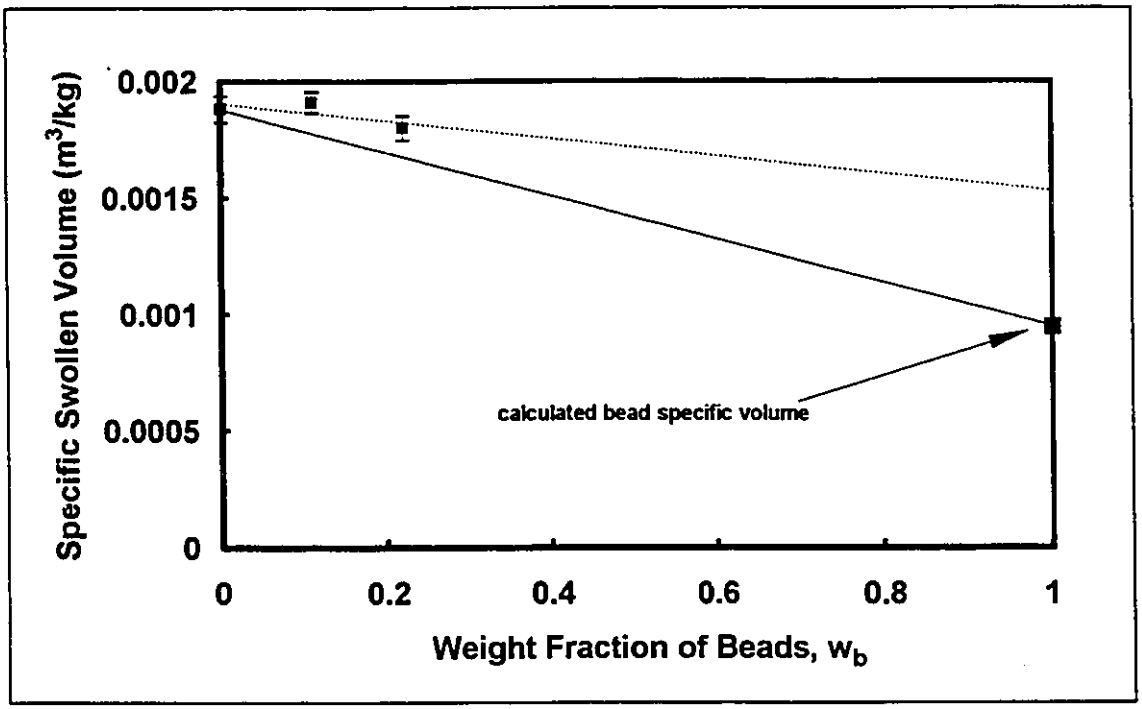

Figure 4.3.4.2 Specific swollen volume of kraft pulp/nylon fibre pads containing plastic beads plotted as a function of the weight fraction of beads. The solid line shows the linear mixing rule result while the dotted line is a linear fit of the data.

A comparison of the experimentally measured specific surface area and specific swollen volume to the values predicted by linear mixing rule provides insight into how linearly additive the two parameters are. Such a comparison had been carried out with the data for the ternary system. The linear mixing rule had the following form:

$$\beta_m = w_f\beta_f + w_b\beta_b \quad ....(4.3.4.1)$$

where β is the property of interest (i.e., either the specific surface area or the specific swollen volume) and w is the weight fraction of the component in the pad. The subscripts m, f and b represent the overall mixture, the fibres (both pulp and nylon fibres together) and the plastic beads. The results for the kraft pulp/nylon fibre/beads system calculated from Equation (4.3.4.1) are summarized in Table 4.3.4.1.

wt fraction of beads	α expt. (m^3/kg)	α predicted (m^3/kg)	% error in α	σ expt. (m^2/kg)	σ predicted (m^2/kg)	% error in σ
0	0.001883	0.001883	0	657	657	0
0.11	0.001912	0.001781	-6.85	570	590	+3.51
0.22	0.001801	0.001678	-6.83	509	524	+2.95
1	0.000952	0.000952	0	51	51	0

Table 4.3.4.1 Summary of the effects of plastic beads on the overall specific surface area and specific swollen volume of kraft pulp/nylon fibre pads with plastic beads predicted by the linear mixing rule (Equation (4.3.4.1)).

The regression equations reported in the previous sections for pulp/bead system and pulp/nylon fibre system were also used to predict the specific surface area and specific swollen volume of the ternary pulp/nylon fibre/bead system. Since all the regression equations were obtained from binary data, an assumption had to be made before the binary regression equations could be applied to predict the specific surface area and specific swollen volume of ternary systems. The specific surface area and specific volume of the plastic beads and the nylon fibres are close in value: 51 m^2/kg (beads)/78 m^2/kg (nylon) and 0.000952 m^3/kg (beads)/0.000877 m^3/kg (nylon). Therefore, it was

assumed that the effect of the two components on the effective specific surface area and specific swollen volume of the pads were similar. The ternary system was then approximated by the binary system of pulp fibres and nylon fibres. Calculation of the specific surface area and specific swollen volume of the ternary system was carried out as follows: weight fraction of nylon fibres under the assumption was equal to the sum of the weight fractions of beads and nylon fibres in the actual ternary system used in the experiment. Consequently, regression equations for the pulp/nylon fibre system, Equations (4.3.3.1) and (4.3.3.2), were used to predict the specific swollen and specific surface area of the ternary pads. Results of the predictions are presented in Table 4.3.4.2.

wt fraction of beads	equivalent wt fraction of nylon fibres	α expt. (m^3/kg)	α predicted (m^3/kg)	% error in α	σ expt. (m^2/kg)	σ predicted (m^2/kg)	% error in σ
0	0	0.001883	0.00183	-2.81	657	696	+5.94
0.11	0.81	0.001912	0.00177	-7.43	570	567	-0.53
0.22	0.83	0.001801	0.00173	-3.94	509	481	-5.50

Table 4.3.4.2 Summary of the effects of plastic beads on the overall specific surface area and specific swollen volume of kraft pulp/nylon fibre pads with plastic beads as predicted by regression equations (4.3.3.1) and (4.3.3.2).

It has been demonstrated by the results shown in Table 4.3.4.1, the predictions made in the lower range of bead content based on the linear mixing rule were accurate to within ± 7% while if the regression equations for pulp/nylon fibre system were used, the predictions were also accurate to within ± 7%. Therefore, both methods are equally accurate in prediction of the specific swollen volume and specific surface area of ternary pads.

In summary, both the specific surface area and specific swollen volume of pad materials decreased with increasing bead content. The effects of beads on both the specific surface area and specific swollen volume of the pad were additive. Overall specific surface area and specific volume of the ternary pad materials could be predicted by either a simple linear mixing rule or the regression equations for the pulp/nylon fibre system.

4.4 Conclusions

The following are conclusions drawn from the results of fixed bed permeation data:

1. The Kozeny-Carman equation has been successfully applied to the study of permeation through multi-component systems.
2. Pulp fibres in the pads used in the experiments were perpendicular to the direction of flow. Therefore, the pads can be viewed as a random 2D layered structure.
3. In pads containing pulp fibres and plastic beads, the higher the pad bead content, the lower were the effective specific surface area and specific swollen volume.
4. The presence of beads enhances the permeability of the pad because of the low specific surface area and specific volume of the beads compared to those of kraft pulp fibres. The beads did not plug up the pores in the pad. The beads are probably opening up the pad structure or they can fit in the pores of the fibre network.

5. In pads containing pulp and nylon fibres, the higher the nylon fibre content, the lower the effective specific surface area and specific swollen volume.
6. The presence of the nylon fibres increases the permeability of the pad because of its lower specific surface area and specific volume compared to those of kraft pulp fibres. In addition, the rigidity of the nylon fibres aids in opening up the pad structure to further enhance overall pad permeability.
7. Fibre pads consisting of kraft pulp, nylon fibres and plastic beads display trends that are same as those observed in kraft pulp/beads systems; effective specific surface area and specific swollen volume decreased with increasing bead content.
8. A linear mixing rule or regression equation for pulp/nylon fibre system could be used to predict the specific surface area and specific swollen volume of the kraft pulp/nylon fibre pads with low bead contents (weight fraction of beads less than 0.22) to within 7%.

5. ELASTIC PERMEATION

5.1 Introduction

Elastic permeation is the term used in this thesis to describe the flow of water through a fibre bed that is not constrained by a porous plunger. In elastic permeation, the fibre bed is free to expand or contract in its thickness according to the pressure exerted by the flow and therefore the term "elastic". Elastic permeation regime is found in brownstock washing and wet-end paper machine operations. In brownstock washing, water is used to displace lignin containing residual liquor from cooked pulp that comes from digestors. A common method of washing is the use of rotary vacuum washers. In the washer, vacuum is applied to a rotating wire-covered cylinder in a vat that contains the pulp slurry. A layer of pulp adheres to the wire on the cylinder as it emerges from the vat. Wash water is sprayed onto the pulp pad to displace the lignin containing black liquor in the sheet of pulp. During this displacement process, water has to permeate through an open, unconstrained pulp pad.

Drainage on a paper machine refers to the process of water removal from the pulp suspension to form a coherent network of pulp fibres. Water removal in traditional fourdrinier machines is achieved by the action of various drainage elements such as hydrofoil assemblies, table rolls, vacuum boxes and Dandy rolls, while in twin-wire paper machines, pulp dewatering is driven by drainage elements as well as pressure set up by the tension in the two wires [Smook, 1982]. When the pulp suspension proceeds along the paper machine, dewatering and

formation of the pulp mat takes place continuously. Elastic permeation takes place in the paper machine at the later stages of drainage when a coherent pulp pad is formed. Therefore, knowledge of the elastic permeation process can serve as the tool to optimize and make predictions on both pulp washing and paper machine drainage.

Elastic permeation was second in the order of the three experiments carried out in this work. In the first part of each experiment a fibre bed was formed in the cake filtration experiment. In the second experiment the newly formed unrestrained bed was then subjected to water flow. Detailed description of the experimental procedure was given in Section 3.5.2.1. Four types of fibre pads that differed in composition were used in elastic permeation experiments. The fibre pads contained either: 1) kraft pulp fibres only, 2) kraft pulp fibres and plastic beads, 3) kraft pulp fibres and nylon fibres, or 4) kraft pulp fibres, nylon fibres and plastic beads. Flowrates of water through the pads and thicknesses of the pads were measured as a function of pressure drop driving the flow.

If a porous bed is constrained by a porous plunger such that the solid concentration in the bed is known (i.e., fixed bed permeation), Darcy's law (Equation (2.2.1)) coupled with Kozeny-Carman equation (Equation (2.2.4)) suffices to predict the permeation rate from bed structure parameters. However, for the case of permeation through an unconstrained compressible bed, fluid stresses due to the flow will compress the bed and cause a change in bed thickness. Thus a more complicated model including functions to describe the compressibility of the bed are needed to describe the elastic permeation process mathematically. The theory outlined in Section 2.2.5 was used as the basis for data analysis. Results from experiments with the four types of fibre pads are

presented in the following sections of this chapter followed by discussion and conclusions.

5.2 Experimental Results

Elastic permeation experiments consisted of measuring flowrates through and thicknesses of pads as a function of pressure drop. The applied pressure went through a cycle to study hysteresis of pad properties. Detailed descriptions of the apparatus and experimental procedure were given in Section 3.3 and Section 3.5.2.1 respectively. Bed thickness was measured with a vernier scale. Although it was possible to achieve an accuracy of ± 0.005 cm with the vernier scale, nonuniformity of the pad surface across the diameter of the wire reduced the accuracy of pad thickness measurements to ± 0.05 cm. The accuracy of flowrate measurement was ± 0.014 g/s. A fibre pad was first formed in the filtration experiment under a constant hydrostatic head. Therefore, the pad was always under stress throughout the filtration experiment. After a fixed amount of filtrate had been collected so that a known amount of pulp fibres was present in the fibre pad, the filtration experiment was stopped and consequently the pressure acting on the pad became zero. The beginning and end of the filtration experiment caused compression and relief of stress on the fibre pad. Therefore, the filtration experiment itself constituted the 1st complete compression and recovery pressure cycle on the fibre pad.

After the filtration experiment, water was allowed to permeate through the fibre pad before the start of the elastic permeation experiments to ensure that all the apparatus was filled with water and no pulp fibre was left in the filtration cell.

In this purging step, water was allowed to permeate through the pad under the maximum hydrostatic head of approximately 10.6 kPa until a total of about 15 L of water had flowed through the pad. Since the pulp pad was under maximum compression at the start of the purging step and the stress on the pad was totally removed when the purging step ended, the purging step made up the 2nd complete compression and recovery cycle of the pad.

After purging, the elastic permeation experiments began by allowing water to permeate through the pad at the highest possible flowrate under the maximum pressure drop. Therefore, at the beginning of the elastic permeation experiment, the pad immediately went through its 3rd compression. The flowrate of water through the pad was gradually decreased over the course of the experiment until the lowest flowrate was achieved. When this point was reached, the flowrate was brought back up again until the maximum pressure drop was attained. The gradual decrease and increase in pressure drop acting across the fibre pad were the 3rd recovery and 4th compression of the fibre pad. Flowrate and pad thickness data from the 3rd recovery and 4th compression of the pad are the results that will be discussed in this chapter. A typical output from the data acquisition system for a pulp pad containing 75% by weight of beads is shown in Figure 5.2.1.

Pressure drops of the compressive cycle used in the elastic permeation experiment were represented by horizontal lines in Figure 5.2.1. Length of individual lines was proportional to the duration of permeation at each pressure drop. This representation of pressure drop provides a graphic demonstration of a compressive cycle The rest of the lines in the figure were the cumulative weight of filtrate collected at each pressure drop. Linearity of the lines for

cumulative filtrate weight indicated that flow through the fibre pad had reached steady state. The slopes of the lines were then used to calculate the flowrate of water through the fibre pad at the particular pressure drop.

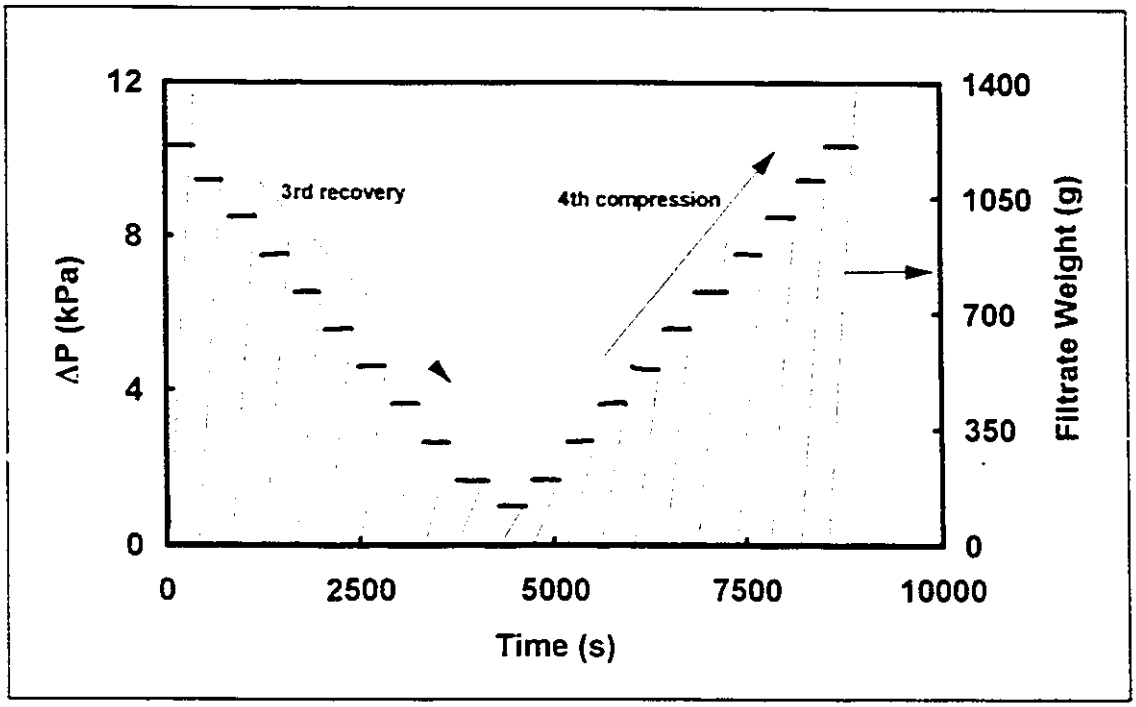

Figure 5.2.1 Elastic permeation data for a pulp pad containing 75% by weight of plastic beads. The left-side axis gives the pressure drops (horizontal lines) used in the experiment. The right-side axis represents cumulative filtrate weight collected during each pressure step.

5.2.1 Pads Consisting of Pulp Fibres

Elastic permeation experiments were carried out with pads containing only pulp fibres. Bed thickness of the pulp pad and flowrate of water through the pad are shown as a function of pressure drop in Figures 5.2.1.1 and 5.2.1.2. In both figures, data from the 3rd recovery and 4th compression are shown. In the 3rd

recovery, pressure drop across the pad was steadily reduced at intervals of approximately 1 kPa and the reverse was true in the 4th compression. Together, the two steps constitute a compressive cycle.

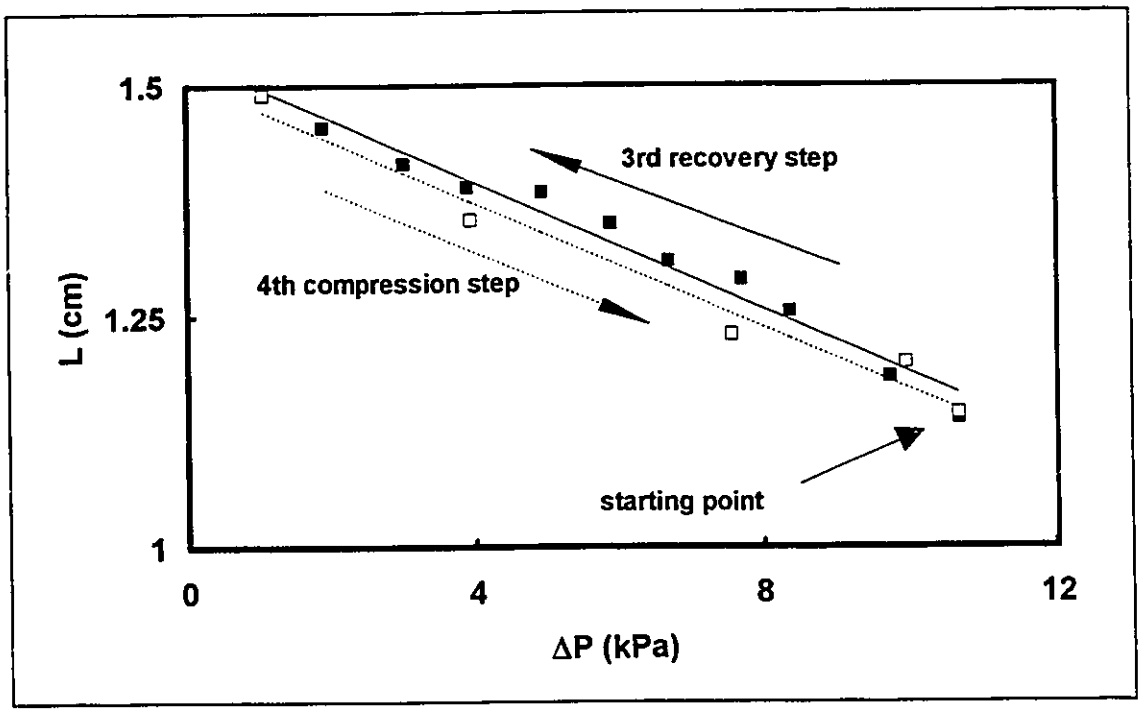

Figure 5.2.1.1 Thickness of the kraft pulp fibre bed plotted against the pressure drop across the fibre pad. Individual markers represent experimental data: ■: data from 3rd recovery step; □: data from 4th compression step. The solid lines are linear regression fit of the experimental results from both steps of the compressive cycle: ——: 3rd recovery step; – – –: 4th compression step.

Data in Figure 5.2.1.1 showed that the pulp pad displayed hysteresis when it went through a compressive cycle. Experimental data of pad thickness from the 3rd recovery step exhibited a linear trend up to the lowest pressure drop used. When pressure drop was increased again to approximately 4 kPa in the 4th compression step, thickness of the pad deviated from the line obtained from

the 3rd recovery step. Subsequent measurements of pad thicknesses at higher pressure drops during the 4th compression step also deviated from the line obtained for the 3rd recovery step.

Linear regression analysis was carried out with the experimental data from the 3rd recovery and 4th compression steps separately. The equations for pad thickness as a function of pressure drop in the 3rd recovery step were:

pulp fibres only:

3rd recovery: $L = -0.0341 \times \Delta P + 1.53$ $r^2 = 0.976$ ....(5.2.1.1)

4th compression: $L = -0.0335 \times \Delta P + 1.51$ $r^2 = 0.974$ ....(5.2.1.2)

where L was the thickness of the fibre bed in cm and ΔP was the pressure drop across the bed in kPa. Many researchers have proposed a power law model to describe the compressibility of fibre pads [van Wyk, 1946; Campbell, 1947; Ingmanson, 1952; Ingmanson & Whitney, 1954; Han, 1969; Jonsson & Jonsson, 1992]. Therefore, a power law model was fitted to the pad thickness data using regression analysis and the following results were obtained;

3rd recovery: $L = 1.56 \times (\Delta P)^{-0.103}$ $r^2 = 0.807$ ....(5.2.1.3)

4th compression: $L = 1.52 \times (\Delta P)^{-0.106}$ $r^2 = 0.949$ ....(5.2.1.4)

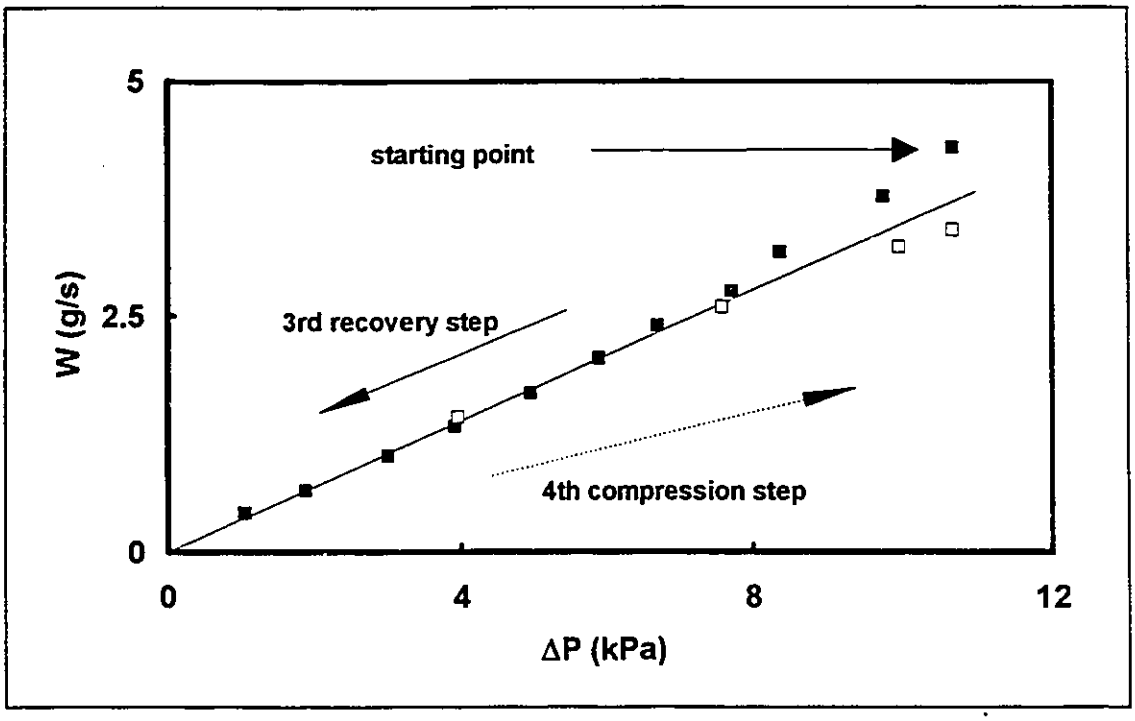

Figure 5.2.1.2 Flowrate of water through the kraft pulp fibre bed plotted against pressure drop across the fibre pad. Individual markers represent experimental data: ■: data from 3rd recovery step; □: data from 4th compression step. The solid line is a linear regression fit of the data at the lower pressure range.

In Figure 5.2.1.2, hysteresis effect was exhibited by the flowrate behaviour. At the start of the 3rd recovery step of the compressive cycle, the maximum pressure drop was used to drive the flow through the pad and thus a high flowrate was achieved. When the pressure drop was gradually reduced, the experimental data followed a curve with a slope that decreased as pressure drop was reduced. Data from the 3rd recovery step displayed a linear relationship when the pressure drop went below approximately 6 kPa. When the pressure drop was increased again in the 4th compression step, the linear relationship was followed until the pressure drop reached about 7 kPa. From that point on, the data followed a trend that was different from the 3rd recovery step. The

curve for data from the 4th compression step was opposite in shape to the curve followed by data from the 3rd recovery step in this pressure range: the curve had a slope that decreased with an increase in pressure drop.

5.2.2 Pads Consisting of Pulp Fibres and Plastic Beads

Elastic permeation experiments were carried out with kraft pulp pads containing various amounts of polystyrene beads. Six different beads contents were used: 20%, 33%, 50%, 67%, 75% and 80% by weight of beads in the pad. Pad thickness was measured at every pressure drop manually and plotted against the corresponding pressure drop across the pad in Figure 5.2.2.1. Flowrates of water through the pads were calculated from the cumulative filtrate weight data and plotted as a function of pressure drop in Figure 5.2.2.2. All experimental data were represented by markers in both figures while the solid lines were linear regression fit of the data from the 3rd recovery step.

In Figure 5.2.2.1, hysteresis was observed for the thickness of pads at all bead contents when the pads were subjected to the compressive cycle. However, the pads did not exhibit hysteresis at pressure drops below approximately 6 kPa except pads that had a bead content of 67%. Pads containing 67% by weight of beads displayed hysteresis even at the lowest pressure drop when the 4th compression step started.

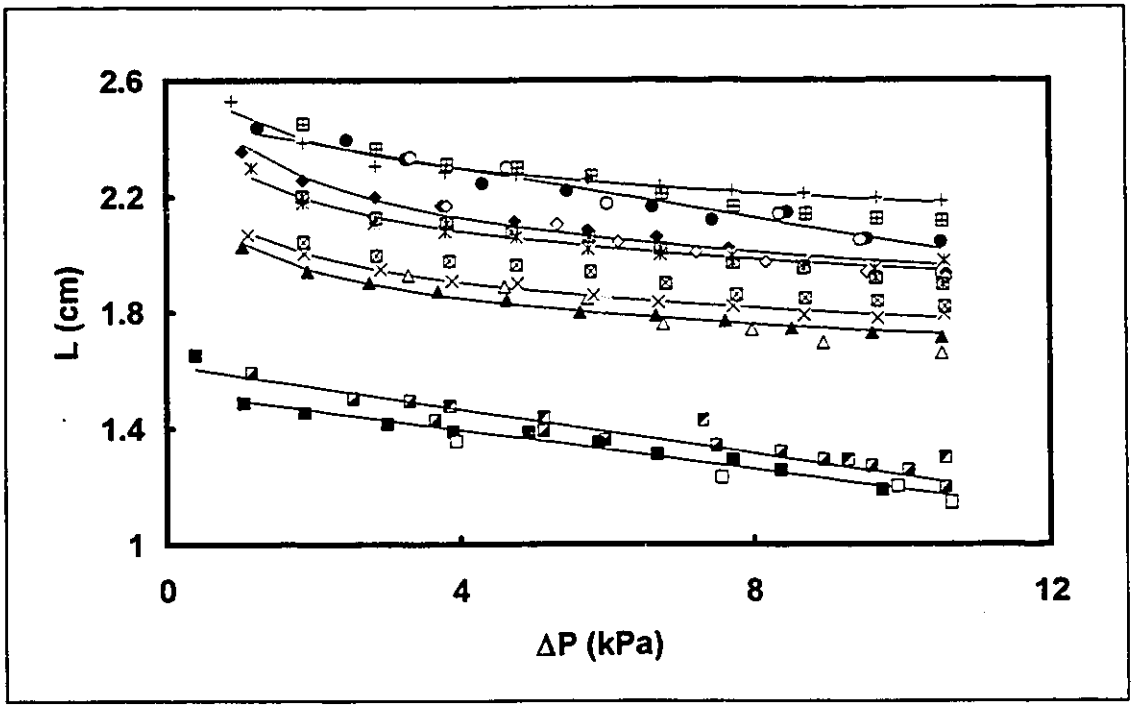

Figure 5.2.2.1 Thickness of kraft pulp pad containing various amount of plastic beads plotted against pressure drop across the pad. Individual markers represent experimental data. Data from 3rd recovery step: ■: kraft pulp; ◪: kraft pulp (repeat); ◆: 20% by weight of beads in pad; ▲: 33% beads; ●: 50% beads; ×: 67% beads; ✳: 75% beads; +: 80% beads. Data from 4th compression steps are represented by the symbols: □: kraft pulp; ◩: kraft pulp (repeat); ◇: 20% by weight of beads in pad; △: 33% beads; ○: 50% beads; ⊠: 67% beads; ⊠: 75% beads; ⊞: 80% beads.

The solid lines shown in Figure 5.2.2.1 were regression fits of experimental data from the 3rd recovery step in each test. Both linear and power law models were used to fit data from the 3rd recovery and 4th compression steps separately. The model that gave a better fit of the data was chosen to correlate the data. Correlation equations for a kraft pulp pad had already been given in Section 5.2.1 and the regression results for pads containing beads were:

20% beads:

3rd recovery: $L = 2.39 \times (\Delta P)^{-0.083}$ $r^2 = 0.973$ ....(5.2.2.1)

4th compression: $L = -0.0452 \times \Delta P + 2.36$ $r^2 = 0.959$ ....(5.2.2.2)

33% beads:

3rd recovery: $L = 2.04 \times (\Delta P)^{-0.072}$ $r^2 = 0.991$ ....(5.2.2.3)

4th compression: $L = -0.0405 \times \Delta P + 2.07$ $r^2 = 0.983$ ....(5.2.2.4)

50% beads:

3rd recovery: $L = -0.0426 \times \Delta P + 2.47$ $r^2 = 0.960$ ....(5.2.2.5)

4th compression: $L = -0.050 \times \Delta P + 2.51$ $r^2 = 0.964$ ....(5.2.2.6)

67% beads:

3rd recovery: $L = 2.09 \times (\Delta P)^{-0.068}$ $r^2 = 0.987$ ....(5.2.2.7)

4th compression: $L = -0.0266 \times \Delta P + 2.09$ $r^2 = 0.984$ ....(5.2.2.8)

75% beads:

3rd recovery: $L = 2.29 \times (\Delta P)^{-0.068}$ $r^2 = 0.970$ ....(5.2.2.9)

4th compression: $L = 2.33 \times (\Delta P)^{-0.081}$ $r^2 = 0.966$ ....(5.2.2.10)

80% beads:

3rd recovery: $L = 2.48 \times (\Delta P)^{-0.055}$ $r^2 = 0.969$ ....(5.2.2.11)

4th compression: $L = 2.55 \times (\Delta P)^{-0.076}$ $r^2 = 0.964$ ....(5.2.2.12)

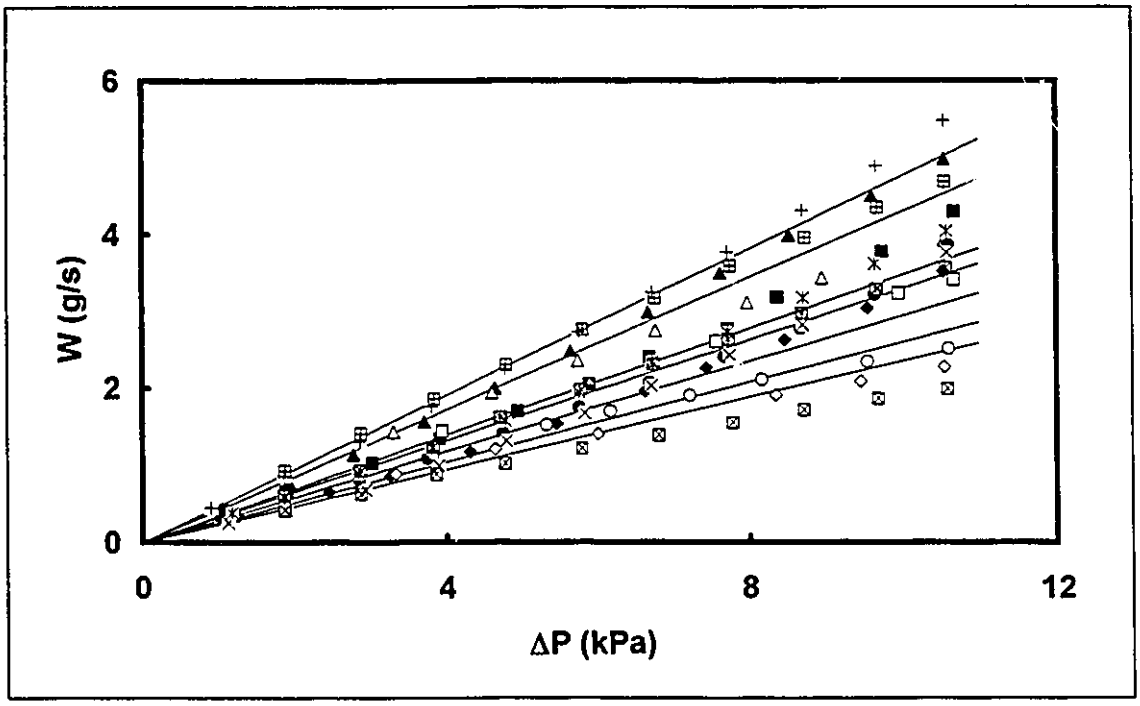

Figure 5.2.2.2 Flowrate of water through kraft pulp pads containing various amount of plastic beads plotted against pressure drop. Individual markers represent experimental data. Data from 3rd recovery step: ■: kraft pulp; ◆: 20% by weight of beads in pad; ▲: 33% beads; ●: 50% beads; ×: 67% beads; ✳: 75% beads; +: 80% beads. Data from 4th compression steps are represented by the symbols: □: kraft pulp; ◇: 20% by weight of beads in pad; △: 33% beads; ○: 50% beads; ⊠: 67% beads; ⊠: 75% beads; ⊞: 80% beads.

Flowrate data for pads at all bead contents were presented in Figure 5.2.2.2. Hysteresis was observed in the flowrate data for all pads. Pad hysteresis was not observed at low pressure drops; at low pressure drops,

flowrate data for all bead contents exhibited linearity. However, the pressure drop at which hysteresis began varied among pads with different bead contents and the pressure drop for the on-set of hysteresis fell in the range from 4 to 7 kPa.

5.2.3 Pads Consisting of Pulp and Nylon Fibres

Elastic permeation experiments were carried out with kraft pulp pads containing nylon fibres. 8 different nylon fibre contents have been used: 33%, 49%, 60%, 67%, 71%, 75%, 78% and 83% by weight of nylon fibres in the pad. Pad thickness data are plotted against pressure drop across the pad for all nylon content in Figure 5.2.3.1. Data of flowrate of water through the different pads are plotted as a function of pressure drop in Figure 5.2.3.2. Experimental data are represented in the figures by data markers and the solid lines show regression fits of data from 3rd recovery steps only.

In Figure 5.2.3.1, pad thickness data from all pads that contained nylon fibres were plotted as a function of pressure drop. Hysteresis was observed in data from all the pads as the thickness of the pads did not follow the same curve when the pads went through the compressive cycle. Another interesting trend was also displayed by the data in Figure 5.2.3.1. The thickness of the pads was proportional to the content of nylon fibres present; higher nylon fibre content resulted in a pad with a higher thickness.

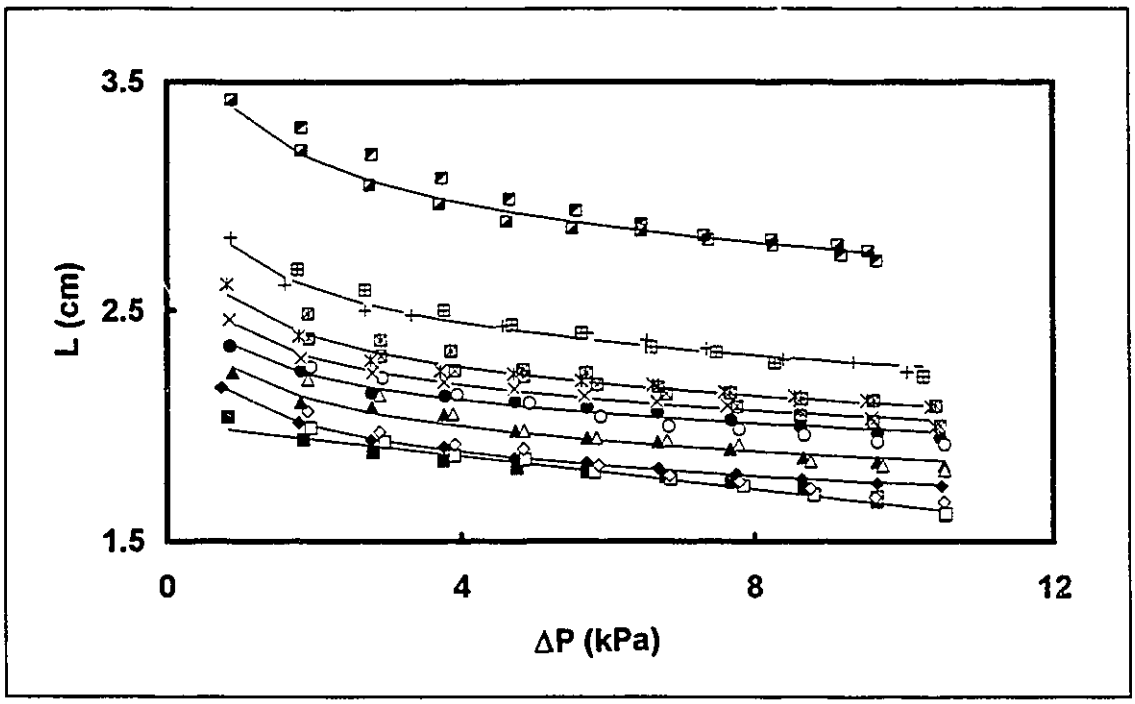

Figure 5.2.3.1 Thickness of kraft pulp pads containing nylon fibres as a function of pressure drop across the pad. Individual markers represent experimental data from the 3rd recovery step: ■: 33% by weight of nylon fibres in pad; ◆: 49% nylon fibres; ▲: 60% nylon fibres; ●: 67% nylon fibres; ×: 71% nylon fibres; ✳: 75% nylon fibres; +: 78% nylon fibres; ◪: 83% nylon fibres. Data from 4th compression steps are represented by the symbols: □: 33% nylon fibres; ◇: 49% nylon fibres; △: 60% nylon fibres; ○: 67% nylon fibres; ▨: 71% nylon fibres; ⊠: 75% nylon fibres; ⊞: 78% nylon fibres; ◩: 83% nylon fibres. Solid lines in the figure are regression fit of data from 3rd recovery steps.

Regression analyses had been carried out with data from pads containing nylon fibres. The results were as followed:

33% nylon:

3rd recovery: $L = -0.0363 \times \Delta P + 2.02$ $r^2 = 0.951$ ....(5.2.3.1)

4th compression: $L = -0.0406 \times \Delta P + 2.06$ $r^2 = 0.986$ ....(5.2.3.2)

49% nylon:

3rd recovery: $L = 2.12 \times (\Delta P)^{-0.082}$ $r^2 = 0.998$ ....(5.2.3.3)

4th compression: $L = -0.0485 \times \Delta P + 2.14$ $r^2 = 0.963$ ....(5.2.3.4)

60% nylon:

3rd recovery: $L = 2.23 \times (\Delta P)^{-0.080}$ $r^2 = 0.971$ ....(5.2.3.5)

4th compression: $L = -0.0449 \times \Delta P + 2.25$ $r^2 = 0.960$ ....(5.2.3.6)

67% nylon:

3rd recovery: $L = 2.33 \times (\Delta P)^{-0.070}$ $r^2 = 0.979$ ....(5.2.3.7)

4th compression: $L = -0.0433 \times \Delta P + 2.33$ $r^2 = 0.957$ ....(5.2.3.8)

71% nylon:

3rd recovery: $L = 2.42 \times (\Delta P)^{-0.076}$ $r^2 = 0.989$ ....(5.2.3.9)

4th compression: $L = -0.0466 \times \Delta P + 2.46$ $r^2 = 0.978$ ....(5.2.3.10)

75% nylon:

3rd recovery: $L = 2.53 \times (\Delta P)^{-0.082}$ $r^2 = 0.978$ ....(5.2.3.11)

4th compression: $L = 2.60 \times (\Delta P)^{-0.093}$ $r^2 = 0.987$ ....(5.2.3.12)

78% nylon:

3rd recovery: $L = 2.75 \times (\Delta P)^{-0.085}$ $r^2 = 0.981$ ....(5.2.3.13)

4th compression: $L = 2.82 \times (\Delta P)^{-0.098}$ $r^2 = 0.985$ ....(5.2.3.14)

83% nylon:

3rd recovery: $L = 3.36 \times (\Delta P)^{-0.088}$ $r^2 = 0.984$ ....(5.2.3.15)

4th compression: $L = 3.47 \times (\Delta P)^{-0.102}$ $r^2 = 0.968$ ....(5.2.3.16)

The flowrate data in Figure 5.2.3.2 showed the same important pad properties as the pad thickness results (Figure 5.2.3.1). That was, hysteresis effect was observed and that the flowrate increased with nylon content. Hysteresis was observed in data from all the pads as data from the 3rd recovery step and 4th compression step deviated from each other starting at a pressure drop of approximately 6 kPa. Flowrate data from the 4th compression step were lower than flowrates in 3rd recovery step at pressure drops above 6 kPa. The nylon content in the pads caused a systematic shift in flowrate of water through the pad at any given pressure drop. Higher nylon fibre contents in the pad resulted in higher flowrates at any pressure drop, suggesting that nylon fibres increased pad permeability which was also observed in fixed bed permeation results.

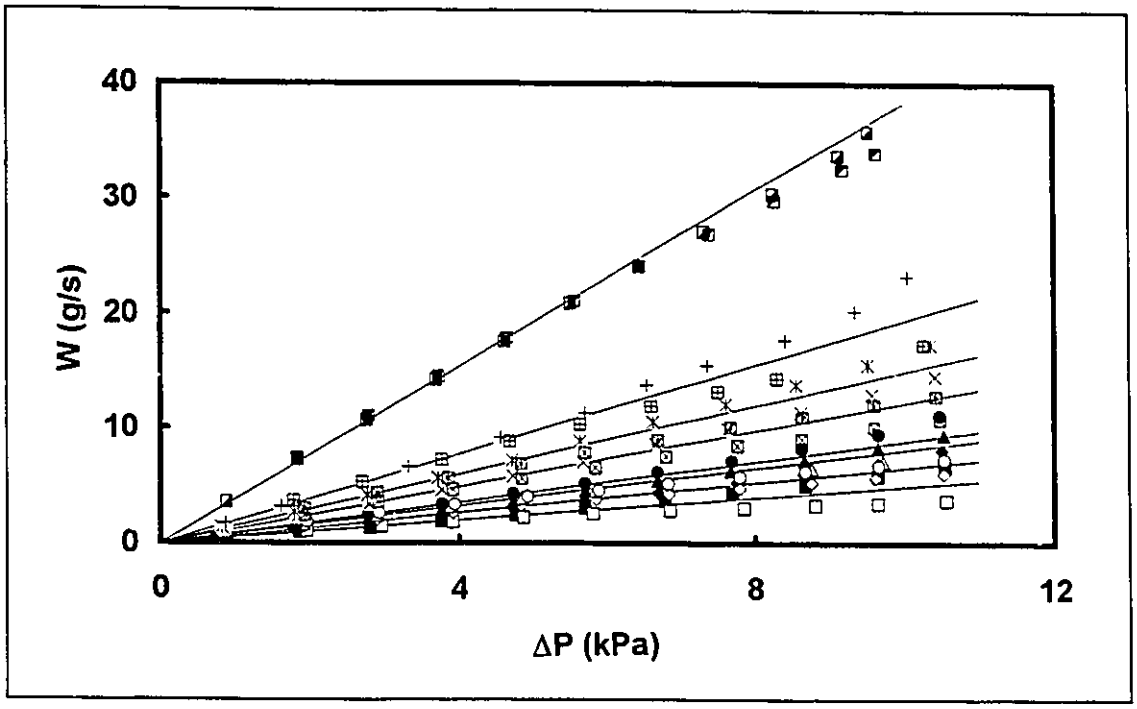

Figure 5.2.3.2 Flowrate of water through kraft pulp pads containing various amount of nylon fibres plotted as a function of pressure drop across the pad. Individual markers represent experimental data. Data from 3rd recovery steps: ■: 33% by weight of nylon fibres in pad; ◆: 49% nylon fibres; ▲: 60% nylon fibres; ●: 67% nylon fibres; ×: 71% nylon fibres; ✳: 75% nylon fibres; +: 78% nylon fibres; ◪: 83% nylon fibres. Data from 4th compression steps are represented by the symbols: □: 33% nylon fibres; ◇: 49% nylon fibres; △: 60% nylon fibres; ○: 67% nylon fibres; ⊠: 71% nylon fibres; ⊠: 75% nylon fibres; ⊞: 78% nylon fibres; ◩: 83% nylon fibres. Solid lines are regression fit of data from 3rd recovery steps.

5.2.4 Pads Containing Pulp/Nylon Fibres and Plastic Beads

Three component pads containing nylon fibres, wood pulp fibres, and polystyrene beads were investigated. The mixture of fibres had a composition that was fixed at a pulp to nylon fibre mass ratio of 1 to 3.6. This fibre mass ratio was chosen because at this ratio, the contribution to external surface area from

both types of fibres was the same. The bead contents used were: 0%, 11% and 22% by weight of beads in the pad.

Thickness data for all the pads are presented in Figure 5.2.4.1. Hysteresis was observed in all cases. Regression analysis was applied to correlate pad thickness data for the 3rd recovery and 4th compression steps separately. The results obtained were:

0% beads:

3rd recovery: $L = 2.75 \times (\Delta P)^{-0.085}$ $r^2 = 0.981$ ....(5.2.4.1)

4th compression: $L = 2.82 \times (\Delta P)^{-0.098}$ $r^2 = 0.985$ ....(5.2.4.2)

11% beads:

3rd recovery: $L = 2.89 \times (\Delta P)^{-0.078}$ $r^2 = 0.990$ ....(5.2.4.3)

4th compression: $L = 2.93 \times (\Delta P)^{-0.092}$ $r^2 = 0.970$ ....(5.2.4.4)

22% beads:

3rd recovery: $L = 2.77 \times (\Delta P)^{-0.092}$ $r^2 = 0.989$ ....(5.2.4.5)

4th compression: $L = 2.81 \times (\Delta P)^{-0.097}$ $r^2 = 0.946$ ....(5.2.4.6)

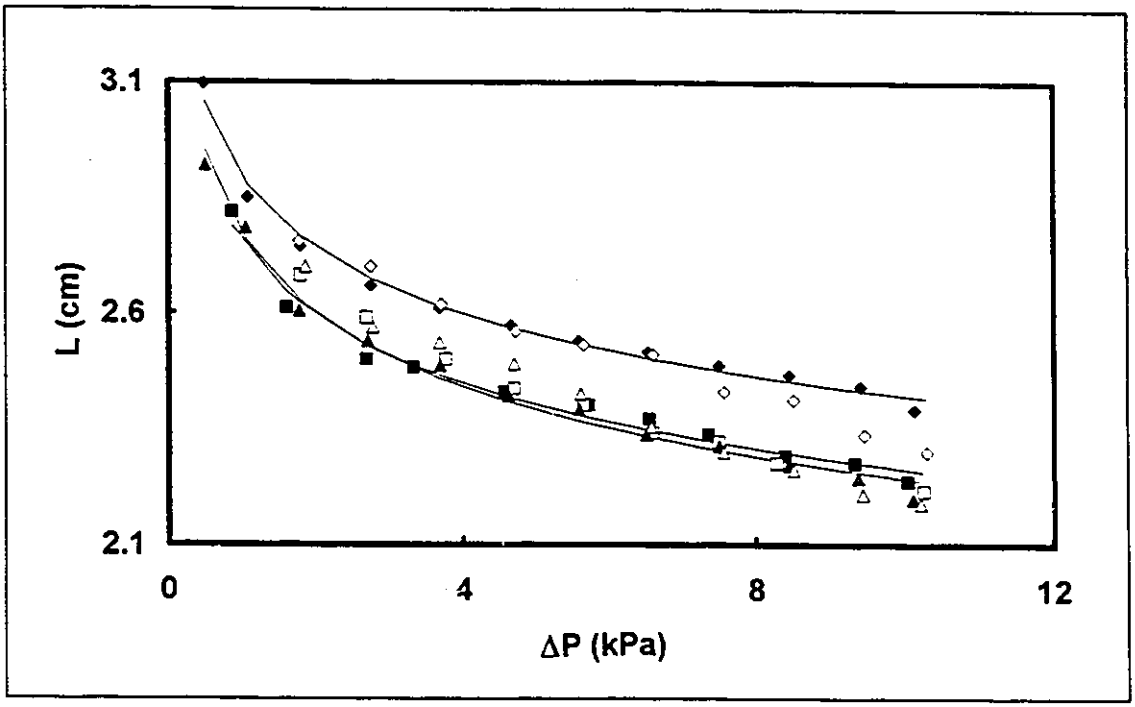

Figure 5.2.4.1 Thickness of kraft pulp/nylon fibre pad containing various amount of plastic beads plotted as a function of pressure drop across the pad. Individual markers represent experimental data. Data from 3rd recovery steps: ■: 0% by weight of plastic beads in pad; ◆: 11% plastic beads; ▲: 22% plastic beads. Data from 4th compression steps: □: 0% by weight of beads; ◇: 11% beads; Δ: 22% beads. Solid lines are regression fit of data from the 3rd recovery step.

The flowrates of water through the pads are plotted as a function of pressure drop across the pad in Figure 5.2.4.2. Hysteresis occurred at pressure drops above 4 to 6 kPa. Regardless of bead content, flowrate data from the 3rd recovery step and the 4th compression step traced different paths beyond the pressure drop of 4 to 6 kPa due to hysteresis. However, at pressure drops below 4 kPa, flowrate data from the recovery and compression steps merged into one line. The slopes of the lines for the three bead contents followed a trend: higher bead contents resulted in higher slopes, suggesting higher pad permeability.

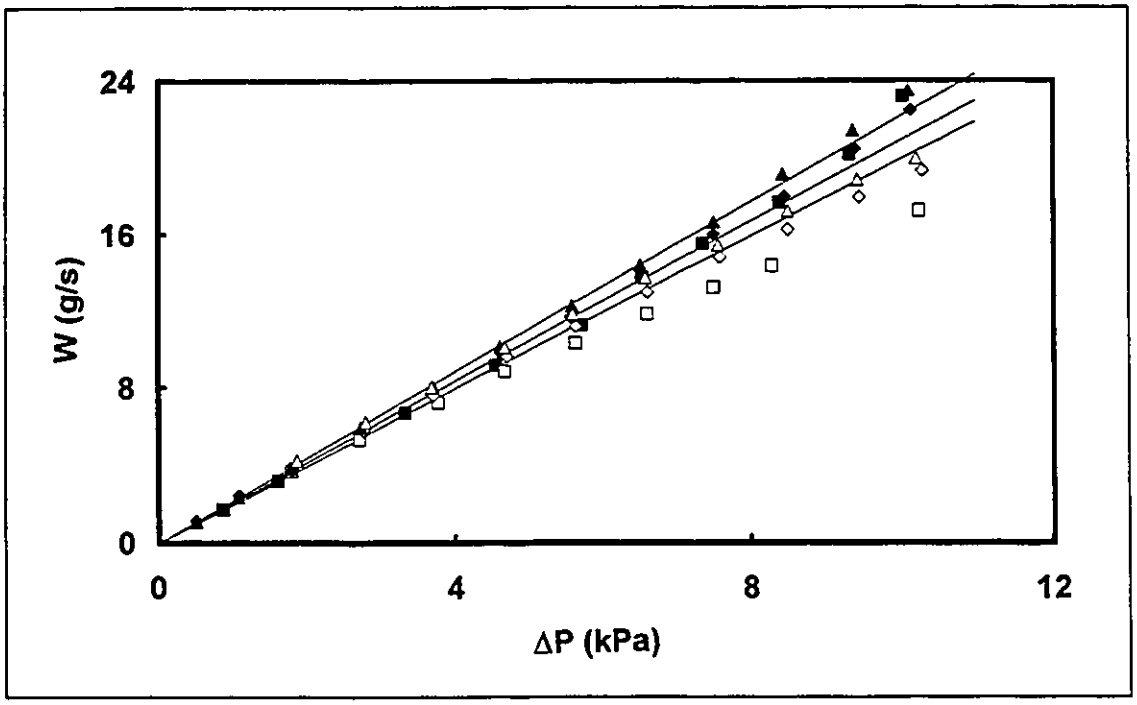

Figure 5.2.4.2 Flowrate of water through kraft pulp/nylon fibre pads containing various amount of plastic beads plotted as a function of pressure drop across the pad. Individual markers represent experimental data. Data from 3rd recovery steps: ■: 0% by weight of plastic beads in pad; ◆: 11% plastic beads; ▲: 22% plastic beads. Data from 4th compression steps: □: 0% by weight of beads; ◇: 11% beads; Δ: 22% beads. Solid lines are regression fits of data from the 3rd recovery step.

5.3 Discussion of Results

5.3.1 Pads Consisting of Pulp Fibres

Hysteresis was the main feature in Figures 5.2.1.1 and 5.2.1.2 where pad thickness and flowrate data from a kraft pulp pad were plotted as a function of pressure drop. Hysteresis is indicative of an irrecoverable change in pad

structure that had taken place during the compression step. When a pulp pad goes through compressive cycles, there are three possible mechanisms for the fibre pad to accommodate compressive stresses incurred by the flow [Gurnham & Masson, 1946; Han, 1969; Jonsson & Jonsson, 1992]: 1) repositioning of fibres in the pad and slippage of fibres at their contact points, 2) conformation of the fibres at the contact surfaces and 3) bending of the fibres. Mechanisms 1 and 2 describe irreversible changes and they have the effect of making the pad more compact while mechanism 3 describes elastic behaviour. Therefore, if the pad adopts either mechanisms 1 or 2 during a compression step, an irrecoverable change occurs in the pad structure to make it more compact. When a fibre pad is freshly formed, the pad structure is more open. When the pad goes through the 1st compression step, a combination of the three mechanisms takes place to make the pad structure more compact. During the 1st recovery step in which the stress is removed, the pad recovers but it never reaches the original level before the compression. When the pad goes through subsequent compressive cycles, the degree of recovery increases gradually from one cycle to the other until the compression-recovery behaviour of the pad becomes reproducible. The pad is said to be mechanically conditioned at this stage and it usually happens after the pad has gone through about six complete cycles [Wilder, 1960; Jones, 1963; Elias, 1967; Han, 1969]. Therefore, the results presented in this chapter correspond to the middle stages of the mechanical conditioning process.

Regression analysis was applied to the pad thickness data and linear and power law models were used to fit the experimental data. The linear model was chosen because of its simplicity while the power law model was the functional form that was used by most researchers in this area to correlate pad

compressibility data. The resulting equations had already been presented in Section 5.2.1 as Equations (5.2.1.1) to (5.2.1.4). Contrary to the power law model that was proposed by some researchers, data from both the 3rd recovery and 4th compression steps exhibited linearity as the correlation coefficient was close to 1. When the same set of data was fitted to the power law model, good correlation was achieved for the 4th compression step data although data from the 3rd recovery step was not fitted by the power law model well.

Another set of recovery-compression data obtained with a kraft pulp pad is presented in Figure 5.3.1.1. The set of data was obtained with a pulp pad that contained more pulp fibres (1.15 g of pulp fibres) than the pad (1.07 g of pulp fibres) with which the data in Figures 5.2.1.1 and 5.2.1.2 were obtained. Therefore, the pad thickness and flowrate data were different although they were in the same order of magnitude.

Regression analysis was carried out with data from the 3rd recovery and 4th compression steps using both the power law model and the linear model. The linear model gave the best fit to both the 3rd recovery and 4th compression data. The regression equations obtained were:

3rd recovery: $L = -0.0384 \times \Delta P + 1.62$ $r^2 = 0.958$ ....(5.3.1.1)

4th compression: $L = -0.0346 \times \Delta P + 1.64$ $r^2 = 0.941$ ....(5.3.1.2)

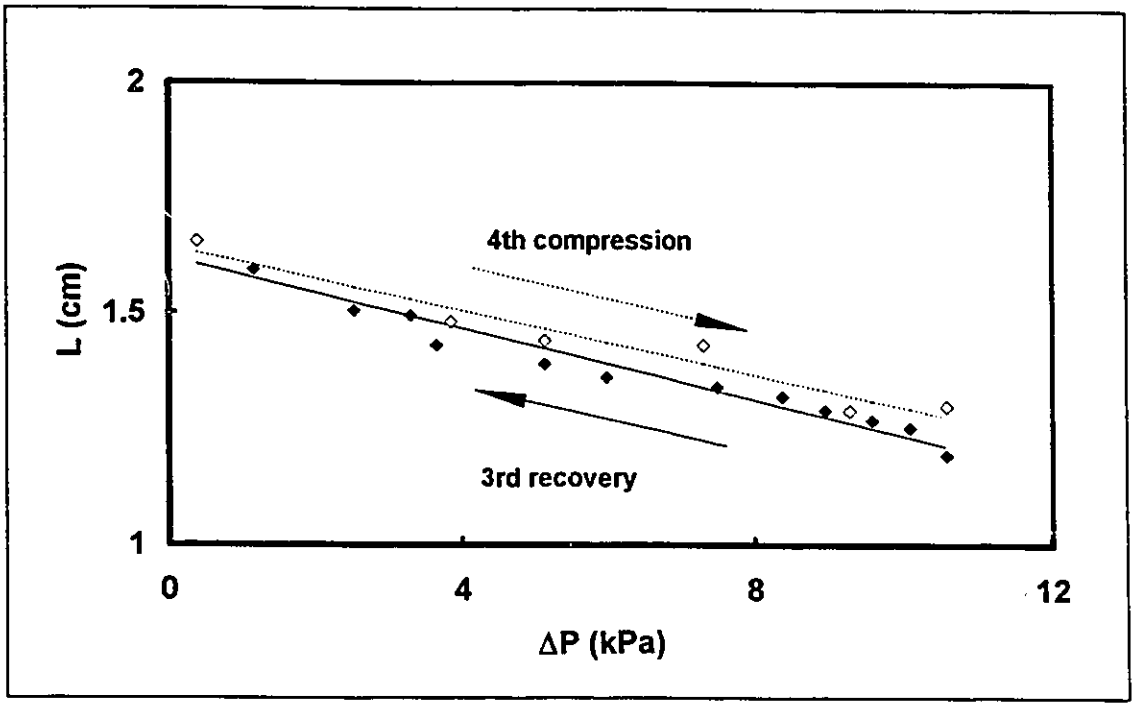

Figure 5.3.1.1 Thickness of the kraft pulp fibre bed plotted against the pressure drop across the fibre pad. Individual markers represent experimental data: ◆: data from 3rd recovery step; ◇: data from 4th compression step. The solid lines are linear regression fit of the experimental results from both steps of the compressive cycle: ——: 3rd recovery step; – – –: 4th compression step.

Since correlation coefficients of the linear model for both steps of the compressive cycle were closer to 1 than the correlation coefficients of the power law model for both fibre pads, the linear model was the preferable model for the compressibility of pure kraft pulp pad.

Several studies on the compressive response of pulp pads are available from the pulp and paper literature [Quiller, 1938; Campbell, 1947; Ingmanson & Whitney, 1954; Ingmanson et al., 1959; Wilder, 1960; Jones, 1963; Elias, 1967]. Empirical equations were developed to relate the concentration of pad materials to the compressive stress

acting on the pad. The best known empirical compressibility function among all is probably that given by Quiller [1938] and Campbell [1947]:

$$c = MP_m^{\ n} \quad ....(2.2.33)$$

where c is the fibre concentration in the pad, P_m is the compacting pressure acting on the pad while M and n are empirical constants. In Branion's work [1977], the values of M and n for various types of pulps were summarized. Typical M values for bleached kraft pulp pads range from 0.00191 to 0.0039 g·cm^{2n}/$dynes^n$·cm^3 while typical values of n fall in the range 0.25 to 0.368. For example, 3 compression curves are generated and plotted in Figure 5.3.1.2 using Equation (2.2.33) with a M value of either 0.00191 or 0.0039 g·cm^{2n}/$dynes^n$·cm^3 and a n value of either 0.25 or 0.368 with a constant pad weight of 0.0015 kg. Clearly none of the exponential curves in Figure 5.3.1.2 is a good fit of the data in Figure 5.3.1.1.

Higgins and DeYong [1966] had reported that values of the compressibility constants were dependent on the technique used in the measurement. In the pulp and paper literature, most of the compressibility constants were measured in cylindrical test cells equipped with pistons which were used to apply the compressive load. Higgins and DeYong observed that if the compressibility constants were measured using flow cells where the compressive stresses came from fluid drag, different values were obtained for the compressibility constants. A possible reason for the discrepancy caused by the method of measurement is that a pressure distribution exists along the thickness of the pad when the pad is under compression by fluid drag while a pad in a piston-type test cell exhibits a

uniform compressive stress. Therefore, the response of a pad under the compression by fluid drag is analogous to a pile of thin pulp pads each under the compression by a piston with the compressive loads corresponding to the pressure drop profile in the original pad. Consequently, the overall compressive response of the pad becomes linear.

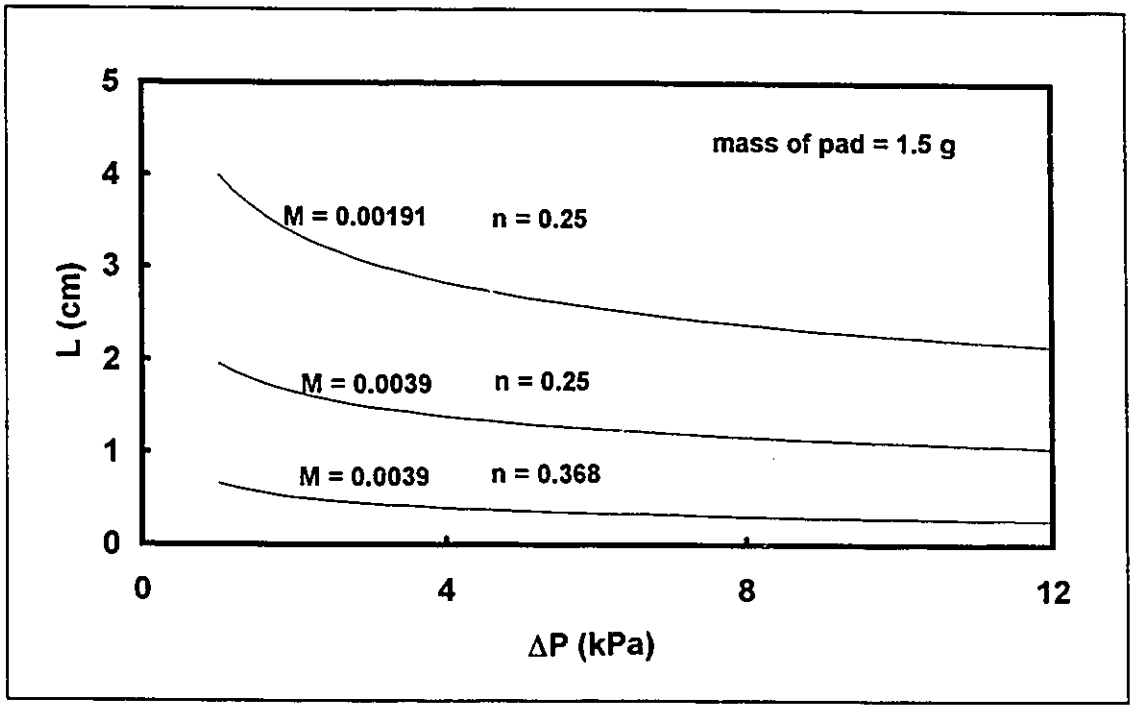

Figure 5.3.1.2 Thickness of a hypothetical kraft pulp fibre bed plotted against the pressure drop across the fibre pad. Equation (2.2.33) is used to calculate pad concentration using three sets of parameters: 1) M = 0.00191 and n = 0.25, 2) M = 0.0039 and n = 0.25, and 3) M = 0.0039 and n = 0.368. Pad thickness is calculated from pad concentration assuming a constant pad weight of 0.0015 kg. The unit of M is $g \cdot cm^{2n} \cdot dynes^{-n} \cdot cm^{-3}$ while n is dimensionless.

Hysteresis in pad thickness was mirrored by flowrate hysteresis. However, a pressure drop across the pad of 7 kPa was required to observe flowrate hysteresis. In Figure 5.2.1.2, the flowrate data followed a linear trend at the low

pressure drop range ($\Delta P < 7$ kPa). Experimental data from both the 3rd recovery and the 4th compression steps followed this line. Therefore, it suggested that irrecoverable structural changes that cause hysteresis occur mostly in the high pressure drop range. In other words, pressure drop below a certain value had negligible effect in causing irreversible structural changes in the pad.

5.3.2 Pads Consisting of Pulp Fibres and Plastic Beads

In Figure 5.2.2.1, experimental thickness data for all the different pads are shown. An attempt was made to keep the amount of pulp fibre in the pads constant and the weight of pulp fibres in the pads used in the elastic permeation experiments actually varied from 0.9 to 1.21 g. In the figure, compression data from the two repeats with kraft pulp only were included. The range of pad thickness with no beads was from 1.5 to 1.6 cm while the range of pad thickness for pads containing beads went from approximately 2 to 2.6 cm. Therefore, it is evident that the beads have an effect on the thickness of the pad. However, based on Figure 5.2.2.1, there was no correlation between the amount of beads in the pad and the thickness of the pad. For example, although the pad that consisted of kraft pulp only was the thinnest and the pad that contained the highest amount of beads (80% by weight of beads) was the thickest over the whole pressure range, all the pads that contained intermediate amounts of beads did not show any systematic trend and order in their thicknesses. The implication is that the beads do not have any systematic effect on the thicknesses of the pads. Since the beads are large (a diameter of 80 μm) compared to the average pulp fibres (a diameter of 26.2 μm. Please refer to

Section 3.1 for details) and since the pulp fibres are flexible, one expects the beads to increase the thickness of the pads. If the beads can be stacked up in a strong layered structure, higher bead content should result in thicker pads, making pad thickness proportional to bead content. However, the experimental observation was that bead content showed no correlation with pad thickness, suggesting that the beads were not stacked up in an orderly fashion. A possible explanation is that the pulp fibres were able to form a network structure in the pad that was so open that the beads were able to fit into the pores of the pad without blocking any of the flow channels. Therefore, the beads did not cause any disruption in the network structure and thus were not able to affect thicknesses of the pads regardless of the content of beads present.

Regression analysis was performed to fit a linear model and a power law model to pad thickness data. The resulting equation for a kraft pulp pad had already been shown in Section 5.2.1 as Equation (5.2.1.1) for the 3rd recovery step and Equation (5.2.2.2) for the 4th compression step. Equations for bead-containing pads were chosen from the model that gave the best correlation and the equations were listed in Section 5.2.2 as Equations (5.2.2.1) to (5.2.2.12). The linear model was preferable to the power law model to correlate thickness data from pure kraft pulp pads. For data from 3rd recovery steps with bead-containing pads, the linear model was the model of choice only for pads containing 50 weight % of beads. For the rest of the bead contents, the power law model correlated the pad thickness data better. Since there was a shift from linearity to a power law type of compressive response of the pads in the 3rd recovery step, it suggested that the presence of beads had caused some changes in the compressibility of the pad.

In the power law model, n is an indication of the compressibility of the pad [Casey, 1980]; high values of n correspond to high degree of compressibility because an n value of zero is possible only for incompressible materials. The linear model is a special form of the power law model with an n value of 1. Therefore, the 3rd compression response of the bead-containing pads shifted from an n value of 1 (kraft pulp pad) to values below 1. This phenomenon agrees with intuition because with a power law compressive response, the pad is more susceptible to compression at low pressure and much less so when the pressure gets into the higher range. This is probably due to the relatively large size of the beads and the flexibility of the pulp fibres. Scanning electron micrographs of pad sections that contained pulp fibres and plastic beads showed that the pulp fibres were following the contours of the beads. Therefore, since the pulp fibres conformed to the contours of the beads, the flexible fibres deform readily even under low pressure to bear the stress on the pad. However, when the pressure is high, the beads are closer to each other in the pad and thus more resistance to compression is offered by the pad due to the rigidity of the beads. In summary, the presence of the beads did not affect the thickness of the pad but there was a definite influence on the compressibility characteristics of the pad.

In Figure 5.2.2.2, hysteresis was observed with flowrate data. The point where hysteresis started varied from around 4 to 7 kPa and there was no definite trend to allow correlation between the start of hysteresis and bead content. Based on the results from fixed bed permeation experiments, one would expect that the permeability of the pad was directly proportional to the bead content. In other words, higher bead content would result in higher pad permeability. Since

the slopes of the lines in the figure was proportional to the permeability of the pad divided by the thickness of the pad, one would intuitively expect a systematic trend in the slopes. However, in Figure 5.2.2.2, such a trend was not observed since the beads did not have a systematic effect on the thickness of the pad as they did on the permeability. Table 5.3.2.1 is a summary of the slopes calculated from the flowrate data. The slopes of the lines did not follow any trend as expected. Nevertheless, if the permeability of the various pads were calculated at a fixed pressure drop knowing the pad thickness, the slopes of the flowrate plots would exhibit a trend that was consistent with the bead content in the pads.

Weight Fraction of Beads	Slope=Q/ΔP ($g \cdot s^{-1} \cdot kPa^{-1}$)
0	0.347
0.2	0.26
0.33	0.43
0.5	0.294
0.67	0.235
0.75	0.329
0.8	0.477

Table 5.3.2.1 Slopes of the flowrate data at low pressure drop range ($\Delta P < 6$ kPa) tabulated as a function of the weight fraction of beads.

5.3.3 Pads Consisting of Pulp and Nylon Fibres

In Figure 5.2.3.1, a systematic trend in the thickness of the pad was observed; as the nylon fibre content increased, the thickness of the pad increased. The possible cause was the aspect ratio and rigidity of the nylon fibres. The aspect ratio of a fibre is the ratio of the fibre length to the fibre

diameter. Aspect ratios of the nylon fibres and pulp fibres used in the experiments are: 42.1 and 137 respectively (refer to Section 3.1 for the dimensions of the fibres). Due to the relatively large aspect ratio of the nylon fibres, it was not possible for the nylon fibres to fit into the pores in the pulp fibre network as in the case of the plastic beads. In addition, the nylon fibres were in contact with each other to form a network structure because of the high aspect ratio. Due to the high elastic modulus (1.76×10^9 Pa) of the nylon fibres, this network structure was more resistant to bending and deformation. Thus, the more nylon fibres there were, the larger and the looser the structure was, making the pad thicker. The result was that thickness of the pad increased with nylon fibre content.

Results from regression analysis of the pad thickness data for nylon fibre-containing pads were presented in Section 5.2.3 as Equations (5.2.3.1) to (5.2.3.16). For 3rd recovery step data, only the pad that contained the least amount of nylon fibres (33% by weight of nylon) displayed linear compression response. This was the only pad that had pulp fibres as the major component. Fibre coarseness, which is the mass to length ratio of fibres, is one parameter used in pulp and paper literature to characterize fibres. It is possible to convert weight fraction of nylon fibres to length fraction of fibres by using fibre coarseness. Length fraction is a more realistic indication of the influence of the presence of nylon fibres in the pad on pad characteristics. A list of the physical properties and coarseness of the nylon fibres and pulp fibres used in the experiment are summarized in Table 5.3.3.1. Coarseness of the two types of fibre reported in Table 5.3.3.1 were estimated from the physical dimensions of the fibres assuming that the fibres were cylindrical.

Fibre Properties	Nylon Fibre	Pulp Fibre
diameter (m)	45×10^{-6}	26.2×10^{-6}*
density (kg/m^3)	1140	279**
length (m)	1.89×10^{-3}	3.6×10^{-3}
weight of dry single fibre (kg)	3.43×10^{-9}	5.42×10^{-10}
coarseness (kg/m)	1.81×10^{-6}	1.50×10^{-7}

Table 5.3.3.1 A list of the physical properties of nylon and pulp fibres. The weight of a single fibre was calculated from the physical dimensions and density of the fibre and coarseness of the fibre was calculated from the weight of single fibre. *: diameter of wet pulp fibre was measured by image analysis technique (refer to Section 3.1). **: density of pulp fibre used here was the reciprocal of the specific swollen volume of the pulp fibres estimated from pad permeability data in Chapter 4. It is the ratio of dried mass of pulp fibres to the wet swollen volume of fibres.

Fibre coarsenesses of typical North America pulpwoods have been given in pulp and paper literature [Smook, 1982] and the values range from 5×10^{-8} kg/m for Birch to 35×10^{-8} kg/m for redwood. Therefore, the estimated coarseness of the pulp fibres used here fell within the range of literature values. Nylon fibre length fractions results are converted from weight fractions and summarized in the following table:

Weight Fraction of Nylon Fibres	Length Fraction of Nylon Fibres
0	0
0.33	0.039
0.49	0.074
0.6	0.11
0.67	0.14
0.71	0.17
0.75	0.20
0.78	0.23
0.83	0.29

Table 5.3.3.2 Weight fraction of nylon fibres converted to length fraction.

Results listed in Table 5.3.3.2 indicated that nylon fibre was not the major component based on fibre length in the pad. Nevertheless, with a nylon fibre weight fraction of 0.33, the equivalent length fraction was only 0.039. Therefore, the fibre pad consisted of pulp fibres essentially and as a result, the compressive response of the pad was linear. When nylon fibre content in the pads exceeded a weight fraction 0.33, the compressive response of the nylon-containing pads shifted from linear to power law. In other words, when the amount of nylon fibres in the pads increased, the compressive response of the pad changed as the effect of the nylon fibres dominated. It has been mentioned in Section 5.3.2 that the linear model is a special form of the power law with n = 1. Since incompressible materials have an n value of zero, the shift of compressive response from linear to power law model suggests that the presence of nylon fibres makes the pads less compressible. This effect is probably a consequence of the rigidity of the nylon fibres. Since the nylon fibres have a stiffness (1.76×10^9 Pa) that is higher than the kraft pulp fibres (3.52×10^7 Pa [Bennington et al., 1990]), an increase in the nylon fibre content causes a corresponding increase in the resistance to compression and thereby resulting in a change in the compressive response.

A systematic trend was observed in Figure 5.2.3.2; at the same pressure drop, flowrate of water through the pad increased with an increase in the content of nylon fibres in the pad. Slopes of the data in the low pressure drop range ($\Delta P < 6$ kPa) where the data displayed linearity are listed in Table 5.3.3.3 below.

Weight Fraction of Nylon Fibres	Slope = Q/ΔP ($g \cdot s^{-1} \cdot kPa^{-1}$)
0.33	0.497
0.49	0.66
0.6	0.815
0.67	0.885
0.71	1.22
0.75	1.495
0.78	1.94
0.83	3.83

Table 5.3.3.3 Slopes of the flowrate vs pressure drop data at low pressure drop ($\Delta P < 6$ kPa) tabulated as a function of the weight fraction of nylon fibres.

The effect of nylon fibres on the permeability of fibre pads was another consequence of the rigidity of the nylon fibres. The nylon fibres resist bending even during network formation. Therefore, the resulting network is open and porous; the more nylon fibres there are, the more open and the thicker the structure will be. For the pulp fibres, since they are much more flexible than the nylon fibres, the pulp fibres tend to remain in the interstices of the network structure of nylon fibres and fill up the pores. With higher nylon content, even less pulp is present to fill up the pores, the open network structure is more permeable to water and thus allowing a higher flowrate of water through the pad. A scanning electron micrograph of a pad that contains pulp fibres and nylon fibres only is shown in Figure 5.3.3.1 to illustrate the point. In summary, the rigidity of the nylon fibres contributes to the thickness and permeability of the whole pad.

Pad hysteresis was observed in both the flowrate and pad thickness data from all the pads. The pressure drop at which hysteresis started varied from approximately 5 to 8 kPa. Although no definite correlation between the point at

which hysteresis started and the content of nylon fibres could be readily concluded from the current set of data, one would intuitively have anticipated that the onset of hysteresis should be related to the nylon fibre content in the pad; the higher the nylon fibre content, the higher the pressure for onset of hysteresis would be. The reason for such a correlation was that the more fibres there were, the more contact points there would be. As the network strength was dependent on the number of contact points between the fibres, higher nylon fibre content implied higher network strength. Also, due to the high elastic modulus of the nylon fibres, the nylon fibres would tend to resist bending and fibre conformation at the contact areas. Therefore, compression of the pad would cause more fibre slippage to effect hysteresis.

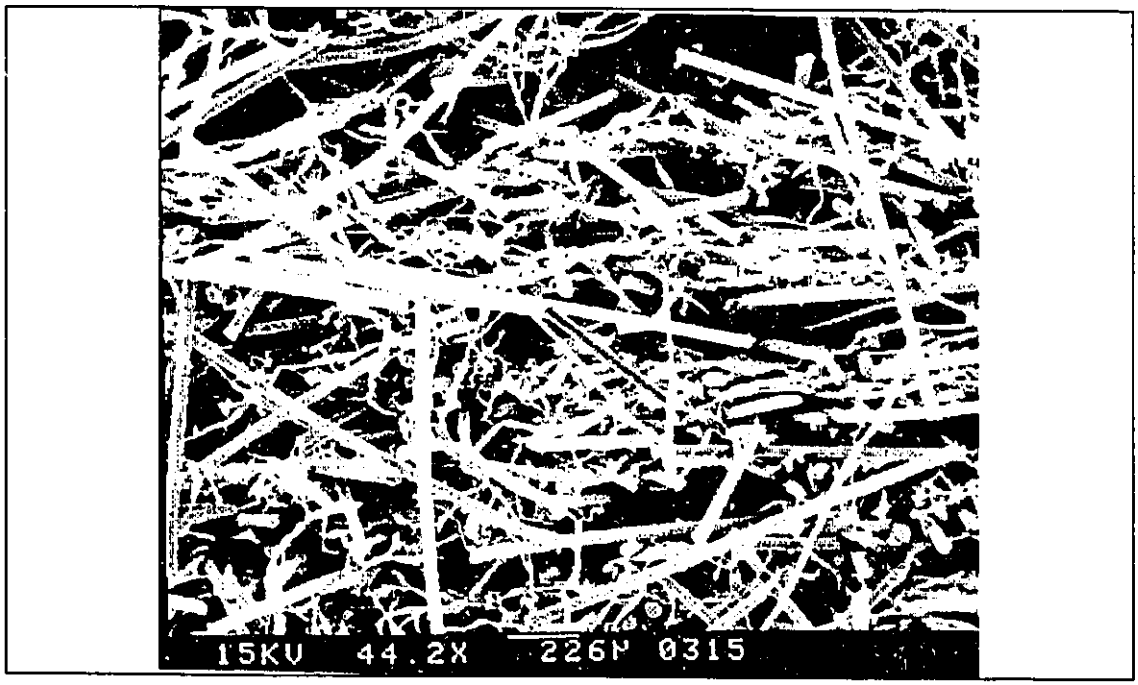

Figure 5.3.3.1 Scanning electron micrograph of a section of a pad that contains pulp fibres and nylon fibres only. The weight fraction of nylon fibres in the pad is 0.783.

5.3.4 Pads Containing Pulp/Nylon Fibres and Plastic Beads

In Figure 5.2.4.1, thickness data of individual pads displayed the power law trend that was typical of all the pads that consisted of a mixture of pulp and nylon fibres in their composition. Results from regression analysis of the pad thickness data were presented in Section 5.2.4 and pad thickness data from the 3rd recovery step were well-correlated by the power law model, giving correlation coefficients in excess of 0.98. Since the major component of the pads was the fibres, the pads exhibited compressibility characteristics that were the same as that found with pads that consisted only with pulp and nylon fibres. The bead content in the pad seemed to have no effect on the thickness of the pads. This is consistent with that observed for pads that contained only pulp fibres and beads. A possible reason was that as the nylon fibre content was high in the pad, the network structure was strong yet very open and porous. Therefore, it was easy for the beads to stay in the pores and not affect the thickness of the pad. In summary, the compressibility behaviour of the pad that consisted of all three components (pulp fibres, nylon fibres and plastic beads) could be presented by the power law model which was also the model that described the compressibility behaviour of pads containing pulp and nylon fibres.

Flowrate data is presented in Figure 5.2.4.2. Hysteresis was again observed in the data. The pressure drop for the onset of hysteresis was found at approximately 5 kPa. Flowrate data at low pressure drop exhibited linearity.

The slope of the data was proportional to the ratio of pad permeability to the thickness of the pad.

Weight Fraction of Beads	Slope at Low Pressure Drop ($g \cdot s^{-1} \cdot kPa^{-1}$)	Pressure Drop (kPa)	Flowrate (g/s)	Thickness (cm)	Estimation of Permeability (m^2)
0	1.99	2.69	5.36	2.55	2.21×10^{-11}
0.11	2.09	2.75	5.83	2.68	2.47×10^{-11}
0.22	2.22	2.74	6.12	2.54	2.47×10^{-11}

Table 5.3.4.1 Slope of flowrate data at low pressure drop range ($\Delta P < 5$ kPa) tabulated against bead content. Also included in the table are the flowrate and pad thickness data at a pressure drop of approximately 2.7 kPa. Permeability of the pads at the particular pressure drop were estimated from the data by using Darcy's law.

Slopes of the data from pads with the three bead contents were tabulated in Table 5.3.4.1. The slopes of the data displayed a correlation with the bead content; the slope increased with bead content in the pad. However, since slope of the flowrate data was proportional to the ratio of pad permeability to pad thickness, permeability of the pads were estimated from flowrate and pad thickness data at a pressure drop of approximately 2.7 kPa and included in Table 5.3.4.1. Results indicated that pad permeability was positively correlated with the bead content: higher bead content resulted in higher pad permeability, which was consistent with the observations from fixed bed permeation studies.

5.4 Mathematical Model

The mathematical model proposed by Jonsson and Jonsson that was outlined in Section 2.2.5 was used to predict the flowrate of water through the

different pads used in the experiment. Numerical calculations were performed by using a program in the commercial software MathCAD version 4.0. A sample output of the program is included in Appendix A.6 and results are presented in Figures 5.4.1 to 5.4.4.

The Jonsson and Jonsson model is general in the sense that any permeability function and any appropriate compressibility function could be used in the calculations. To produce the results in Figure 5.4.1, the Kozeny-Carman equation (Equation (2.2.30)) was used as the permeability function while three different compressibility relations were used. One was the equation obtained by linear regression analysis from the experimental data (Equation (5.2.1.2)) and the other two relations were the 1st cycle and 2nd cycle relations given by Jonsson and Jonsson (Equations (2.2.38) and (2.2.40)). The physical constants such as the specific external surface area and specific swollen volume all attained the values that were determined from fixed bed permeation experiment results. In order to fit the experimental data by the mathematical model, adjustable parameters were introduced into the compressibility equations used. One adjustable parameter was introduced into the regression equation (Equation (5.2.1.2)) and this parameter was a correction factor for the thickness of the pad. For the compressibility equations proposed by Jonsson and Jonsson, there were two adjustable parameters: the void ratio at a reference pressure, X_m, and the coefficient of compressibility, N. Therefore, the values of these parameters were chosen to ensure a close agreement between the simulation results and the experimental data.

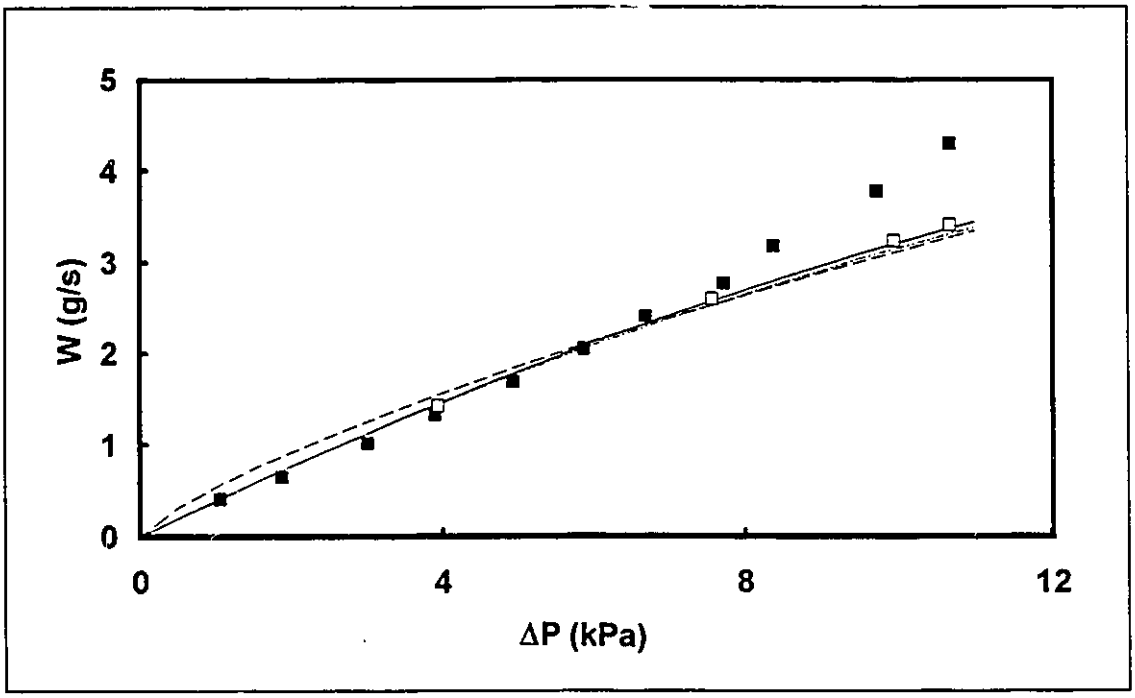

Figure 5.4.1 Flowrate through a pure kraft pulp pad plotted against pressure drop across the pad. Individual markers represent experimental data (■: 3rd recovery step data; □: 4th compression step data). The solid line is based on numerical simulation results using the regression compressibility relation. Dotted lines are numerical prediction obtained by using the Jonsson and Jonsson compressibility functions (– – –: 1st cycle model; – · ·–: 2nd cycle model). Equations used are (2.29), (2.30), (2.38) and (2.40).

In Figure 5.4.1, the pad thickness correction factor used was 0.606. The implication of this was that the pad was effectively thinner than the measured thickness and thus the pad had a much higher effective solid concentration. Consequently, the pad was offering much more flow resistance than what would be predicted if the measured thickness was used. Regarding the Jonsson and Jonsson compressibility relation for the 1st compression cycle, the reference void ratio used was calculated to be 2.53. Calculation of this parameter was based on experimental data with the pad thickness corrected by the effective

thickness factor of 0.606. A coefficient of compressibility of 0.17 was chosen to give a close fit of the data. For the Jonsson and Jonsson 2nd cycle compressibility equation, a compressibility coefficient of 0.38 was used to fit the experimental data. Since the compression and recovery data obtained in the experiment were 3rd recovery and 4th compression data, the Jonsson and Jonsson 2nd cycle compressibility is probably more appropriate for the model than the 1st cycle equation.

It was demonstrated in Figure 5.4.1 that the numerical results provided a good fit of data from the 4th compression step of the cycle. All three compressibility functions gave results that were within 1% of one another. Therefore, among the three compressibility equations, it seems that the regression model equation (Equation (5.2.1.2)) is preferable to both of the Jonsson and Jonsson equations because the regression equation is based on experimental data and it involves less adjustable parameters. However, there is one difficulty that has yet to be overcome; none of the compressibility functions could provide a fit to data from the 3rd recovery step. Simulation of permeation by all three compressibility equations failed to generate a curve with the trend (concave upwards) that was exhibited by data from the 3rd recovery step. Regardless of the value of the adjustable parameter, all three compressibility equations predicted flowrate curves that were concave downwards. Therefore, a better compressibility model, preferably a theoretical one, should be used in the numerical simulations.

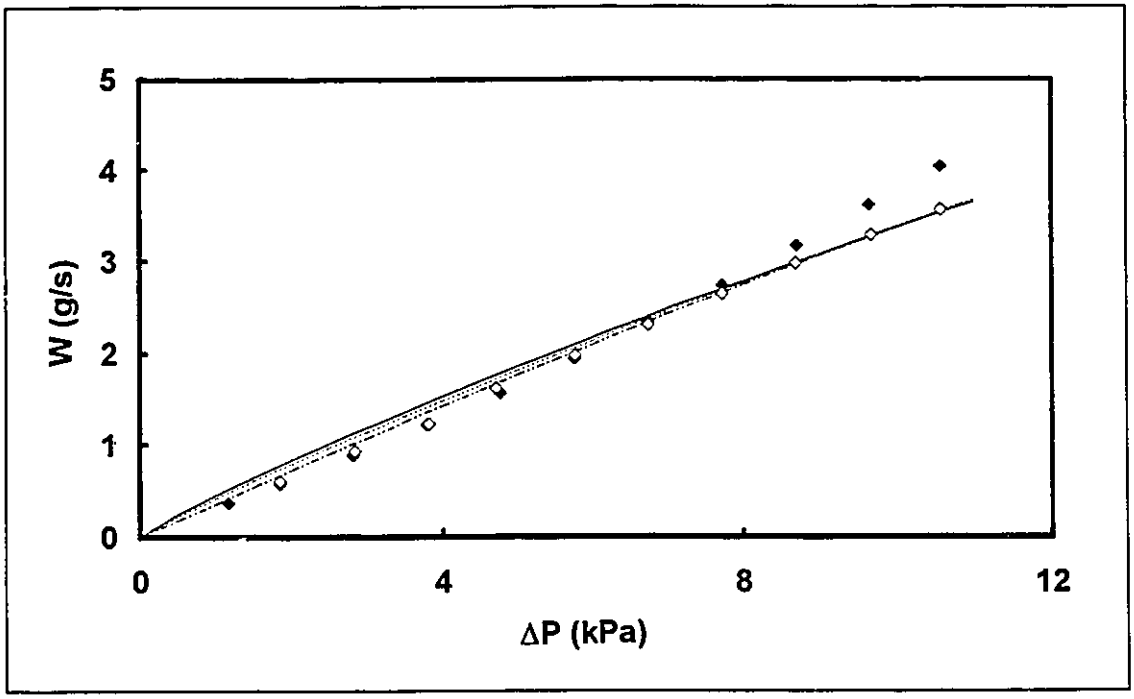

Figure 5.4.2 Flowrate through a pulp pad containing 75% by weight of beads plotted against pressure drop across the pad. Individual markers represent experimental data (♦: 3rd recovery step data; ◇: 4th compression step data). Solid line is based on numerical simulation results using the regression compressibility relation. Dotted lines are numerical prediction obtained by using the Jonsson and Jonsson compressibility functions (– – –: 1st cycle model; – · –: 2nd cycle model). Equations used are (2.29), (2.30), (2.38) and (2.40).

Flowrate data for the pulp fibres/plastic beads system is shown in Figure 5.4.2. The experimental data was obtained from the pad that contained 75% by weight of plastic beads. Again, three compressibility functions were used to generate three sets of prediction. The solid line was numerical results obtained using the power law model regression fit (Equation (5.2.2.10)). The dotted lines were results obtained using the Jonsson and Jonsson model. Similar to the case of pure pulp fibres, a thickness correction factor of 0.67 was used to get a good fit of the experimental data. The reference void ratio calculated based on

the correction factor was 3.64 and the coefficient of compressibility used in the 1st cycle equation was 0.075. The coefficient of compressibility for the 2nd cycle equation was 0.15. All compressibility functions provided results that were very close to each other. The similarity in the value of the thickness correction factor and the coefficient of compressibility for pads with and without beads implies that the beads are not affecting the structure of the pad and that the hydrodynamic characteristics of the pad is still governed by the pulp fibres as the beads can fit into the pores in the fibre pads.

In Figure 5.4.3, data from the pad that contained 75% by weight of nylon fibres and 25% by weight of pulp fibres is presented. Equation (5.2.3.12) was used as the regression compressibility function. Values of the adjustable parameters in the Jonsson and Jonsson 1st and 2nd cycle equations were: thickness correction factor = 1.16, reference void ratio = 4.8, 1st cycle coefficient of compressibility = 0.12 and 2nd cycle coefficient of compressibility = 0.23. Contrary to the case of pure kraft pulp fibres and pulp/beads mixture, the thickness correction factor in this case was larger than 1, indicating that the pad was effectively thicker than it actually was. An effectively thicker pad at the same weight implied that the pad had a lower solid concentration and thus a higher permeability. Therefore, from the model, it seemed to indicate that the presence of nylon fibres drastically enhanced the permeability of the pad. This agrees with and supports the hypothesis given in previous section that the nylon fibres form a network that is strong and yet very open.

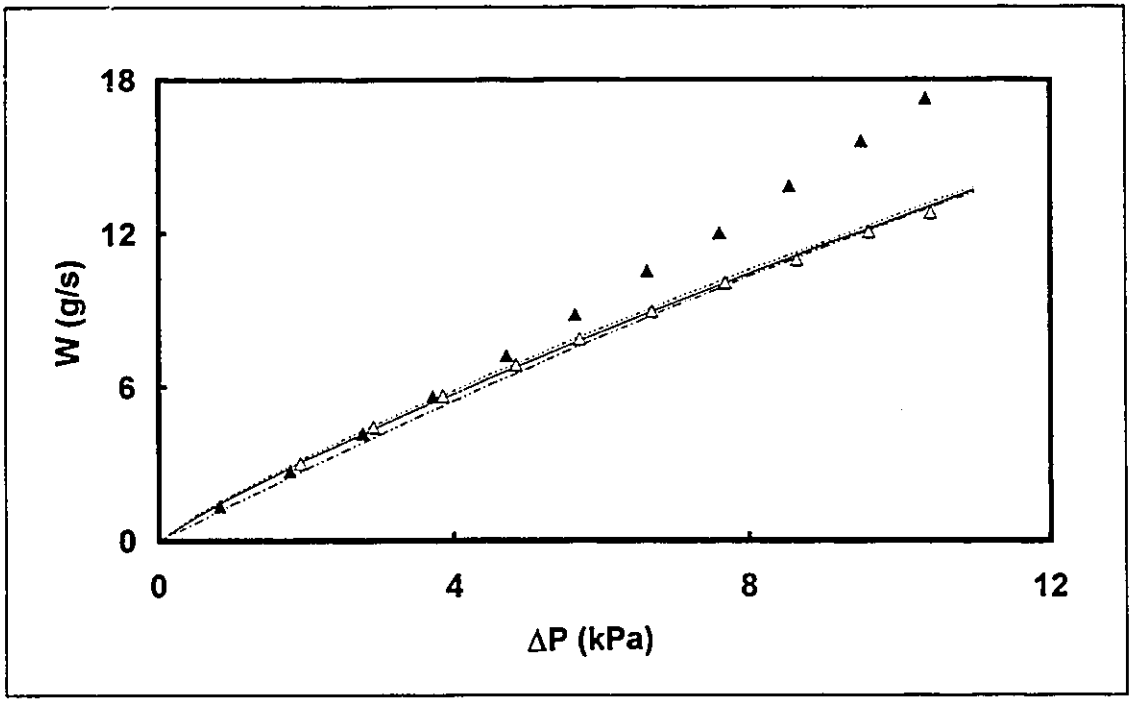

Figure 5.4.3 Flowrate through a pulp pad containing 75% by weight of nylon fibres plotted against pressure drop across the pad. Individual markers represent experimental data (▲: 3rd recovery step data; Δ: 4th compression step data). Solid line is based on numerical simulation results using the regression compressibility relation. Dotted lines are numerical prediction obtained by using the Jonsson and Jonsson compressibility functions (– – –: 1st cycle model; – · ·– : 2nd cycle model). Equations used are (2.29), (2.30), (2.38) and (2.40).

Figure 5.4.4 was chosen from the pulp fibres/nylon fibres/plastic beads system. The pad contained 11% by weight of beads and the rest of the pad was a mixture of pulp fibres and nylon fibres at a mass ratio of 1:3.6. The regression compressibility equation used was Equation (5.2.4.4). The value of the thickness correction factor was 1.18, which was the same as that for 75% nylon/25% pulp. The coefficient of compressibility for the 1st cycle was found at 0.15 while the reference void ratio was calculated at 3.29 and the coefficient of compressibility for the 2nd cycle was 0.32.

The thickness correction factor used in the mathematical model is just an adjustable parameter to modify the thickness of the pad such that the simulation results fit the experimental data. The value of the thickness correction factor reflected that the nylon fibres in enhanced permeability. Similarly, the value of the adjustable parameters for 75% nylon/25% pulp implied that the effect of the beads was not very pronounced and this was consistent with observations made with the pulp and beads systems.

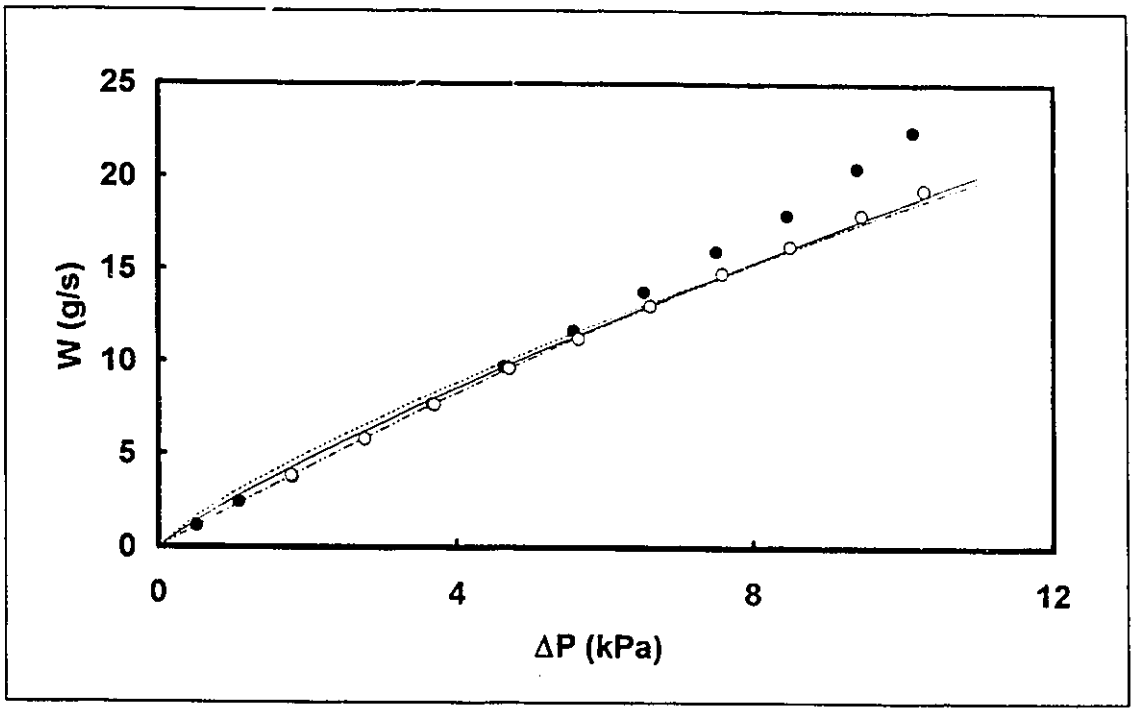

Figure 5.4.4 Flowrate through a pulp/nylon fibre pad containing 11% by weight of beads plotted against pressure drop across the pad. Individual markers represent experimental data (●: 3rd recovery step data; O: 4th compression step data). Solid line is based on numerical simulation results using the regression compressibility relation. Dotted lines are numerical prediction obtained by using the Jonsson and Jonsson compressibility functions (– – –: 1st cycle model; – · · – : 2nd cycle model). Equations used are (2.29), (2.30), (2.38) and (2.40).

5.5 Conclusions

The following is a list of the conclusions that are drawn from the analysis of the elastic permeation data:

1. All the pads exhibited hysteresis with flow induced compression.
2. Thicknesses of the pads under flow induced compression were linear or nearly linear functions of the pressure drop acting across the pad.
3. The presence of plastic beads did not affect the structure and thickness of the pads. The plastic beads were probably able to fit into the pores of the pulp pad without disrupting the structure.
4. The presence of nylon fibres increased the permeability of the pad because of the formation of a more open network structure.
5. The presence of plastic beads in kraft pulp/nylon fibre pads did not affect the thickness of the pad as they tend to stay inside the pores in the network structure formed by the nylon fibres.
6. The mathematical model proposed by Jonsson and Jonsson could be used to predict compression behaviour whereas the concave form of thickness versus pressure drop during recovery was not predicted by any of the current models.

6. PAD FORMATION: FILTRATION

6.1 Introduction

Drainage on a paper machine is the process of water removal from the pulp suspension to form a coherent network of pulp fibres as the pulp suspension proceeds through the sheet forming section. There are two possible mechanisms for the drainage of pulp suspensions on the paper machine wire: filtration and thickening [Parker, 1972]. Filtration is the predominant dewatering mechanism when the consistency of the pulp suspension is low. Therefore, the pulp fibres are free to move independent of one another in the original suspension because of its low consistency. Three zones develop after the start of filtration: 1) the fibre pad at the surface of the paper machine wire, 2) the dilute original suspension that is approaching the paper machine wire and 3) a transition zone between. The boundaries of the transition zone extend from the surface of the fibre pad (the face away from the paper machine wire) to the dilute suspension. In the transition zone, fibres gradually lose their mobility when they come into contact with the pulp pad. Fibre consistency in the three zones increases progressively from the dilute original suspension to the fibre pad at the wire surface. Due to this change in zones, fibres have more time to position themselves when they are deposited on the pulp pad. Consequently, fibres in pads that are formed by filtration tend to display a predominant orientation that is perpendicular to the direction of flow, resulting in a 2D, layered structure.

The mechanism of drainage by thickening is very different from that of drainage by filtration. It is a prerequisite that the consistency of the pulp suspension has to be much higher for thickening to take place. Fibres in the suspension have already formed a coherent network before the start of water removal because of the initial high consistency. Consequently, the fibres in the network behave as a thick compressible pad during dewatering and there is only one zone present. Since the thickening process starts with a coherent network of pulp fibres, the fibres usually display a random 3D orientation [Casey, 1980].

Radvan [1965] has studied the degree of layering in paper by measuring the "the number of over and under crossings of selected fibres in the interior of sheets" [Casey, 1980]. All the sheets that Radvan has studied indicated a predominantly layered structure although some degree of 3D fibre orientation was observed. Therefore, Radvan concluded that most papers are layered in structure and that they are formed mainly by the filtration mechanism, although it is not the only water removal mechanism in a paper machine. Since filtration is the predominant paper machine drainage mechanism, knowledge of the filtration characteristics of different suspensions permits prediction of the drainage behaviour of the suspensions on a paper machine.

Cake filtration was the first of three procedures carried out in an experiment. Pulp suspension that contained a specific amount of plastic beads and nylon fibres were subjected to cake filtration under a constant hydrostatic head to form the fibre pad. The newly formed unrestrained bed was then used in the elastic permeation experiments and the fixed bed permeation experiments. Four types of pulp suspensions that differed in composition were used in the filtration experiments. The suspensions contained either: 1) kraft pulp fibres

only, 2) kraft pulp fibres and plastic beads, 3) kraft pulp fibres and nylon fibres, or 4) kraft pulp fibres, nylon fibres and plastic beads. In this chapter, results from experiments with the four types of suspensions will be presented in the following sections followed by results from mathematical modelling. Discussion of the results and conclusions will then be presented to complete the chapter.

6.2 Results

Filtration experiments were conducted in which pressure drop across the growing fibre pad and the cumulative weight of filtrate collected were the two process parameters measured. Detailed descriptions of the apparatus and the experimental procedure were given in Section 3.3 and 3.5.1 respectively. Filtration experiments had been carried out with four systems: 1) kraft pulp only, 2) kraft pulp with plastic beads, 3) kraft pulp with nylon fibres, and 4) kraft pulp with nylon fibres and plastic beads. Pressure drop and filtrate weight data from all the systems were measured and recorded as functions of time. Typical experimental data from the four systems are plotted against time and presented in Figures 6.2.1 to 6.2.8. In Figures 6.2.1 and 6.2.2, pressure drop and cumulative filtrate weight data from the constant head filtration of suspensions containing kraft pulp fibres only are shown. Experimental data presented in the figures are results from five repeated experiments. Solid curves in the figures are results from mathematical simulation of the filtration process. Description of the numerical simulation scheme will be given in Section 6.3 of this chapter.

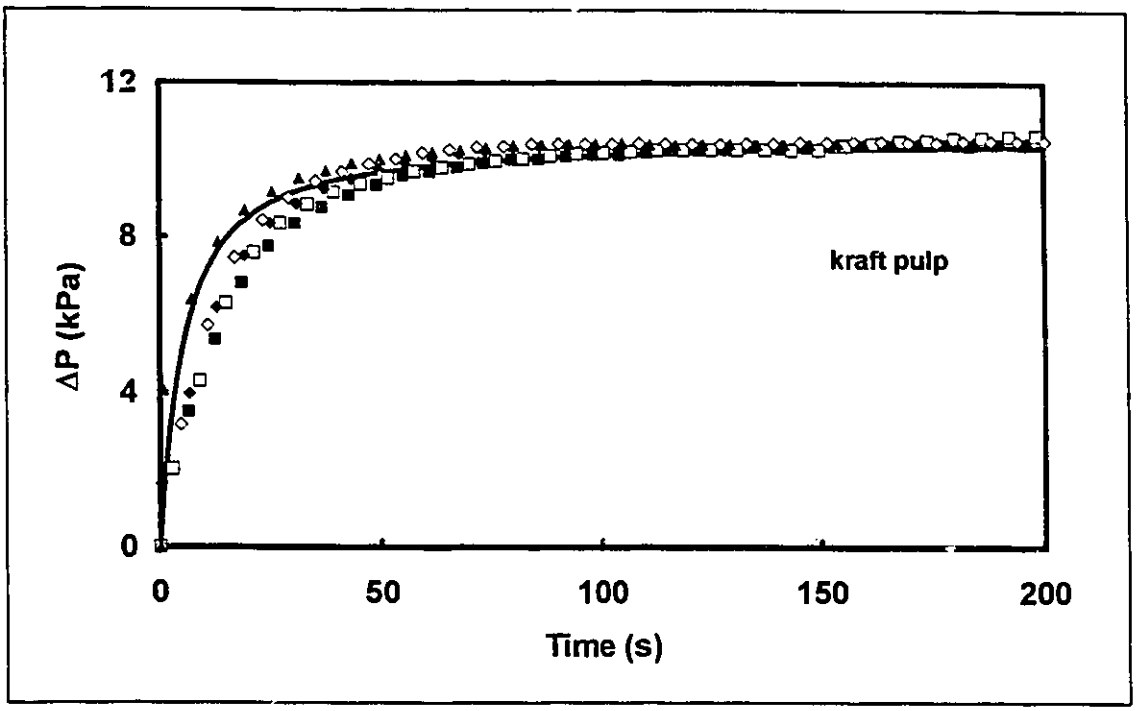

Figure 6.2.1 Pressure drop across the growing pad plotted as a function of time in a filtration experiment. Markers represent data from five repeated experiments. The solid line is a fit of the data by mathematical simulation. Model parameters: c_{min} = 0.08838 kg/m^3, c_{max} = 60 kg/m^3 and r = 0.8 using modified Kropholler's equation (Equation (6.3.4)) to represent the concentration profile in the fibre bed.

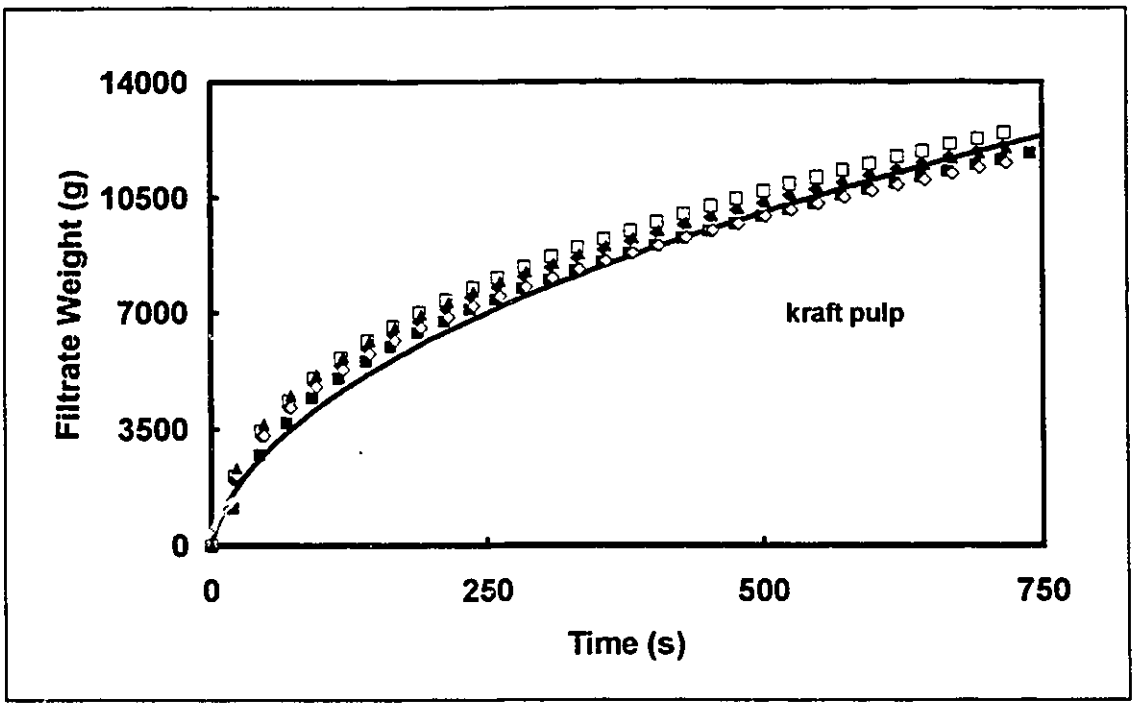

Figure 6.2.2 Cumulative filtrate weight data plotted as a function of time. Markers represent data from five repeated experiments. The solid line is a fit of the data by mathematical simulation. Model parameters: c_{min} = 0.08838 kg/m^3, c_{max} = 60 kg/m^3 and r = 0.8 using modified Kropholler's equation (Equation (6.3.4)) to represent the concentration profile in the fibre bed.

Since pressure drop and filtrate weight data from the filtration of all the suspensions display common trends and features, one set of data from each of the four systems was chosen to be presented in this chapter. The composition of the suspensions and the figure in which the data are presented are summarized in Table 6.2.1 below.

Composition (weight fraction)	Pressure Drop	Filtrate Weight
0.80 pulp/0.20 beads	Figure 6.2.3	Figure 6.2.4
0.40 pulp/0.60 nylon fibres	Figure 6.2.5	Figure 6.2.6
0.19 pulp/0.7 nylon/0.11 beads	Figure 6.2.7	Figure 6.2.8

Table 6.2.1 Summary of suspension compositions and locations where the corresponding filtration data are presented.

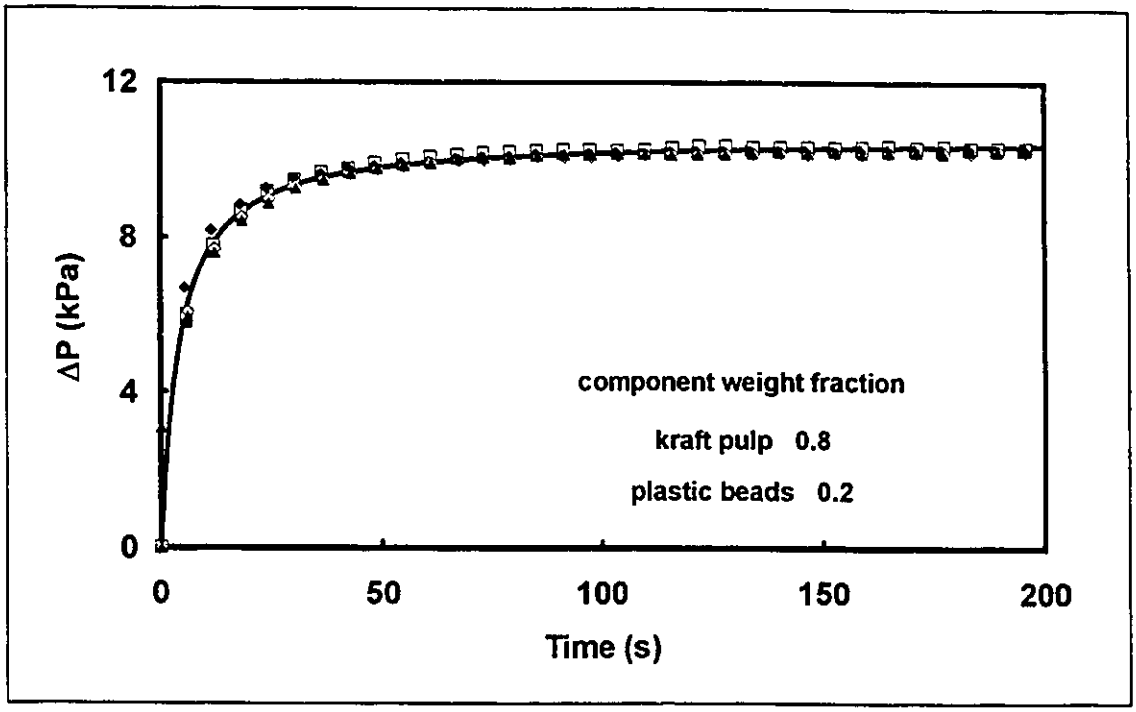

Figure 6.2.3 Pressure drop across the filter pad plotted against time. Composition of the fibre pad: dry weight fraction of kraft pulp = 0.8, weight fraction of beads = 0.2. Markers represent data from five repeated experiments. Solid line is the result of mathematical simulation. Model parameters: c_{min} = 0.1114 kg/m^3, c_{max} = 70 kg/m^3 and r = 0.8 using modified Kropholler's equation (Equation (6.3.4)) to represent the concentration profile in the fibre bed.

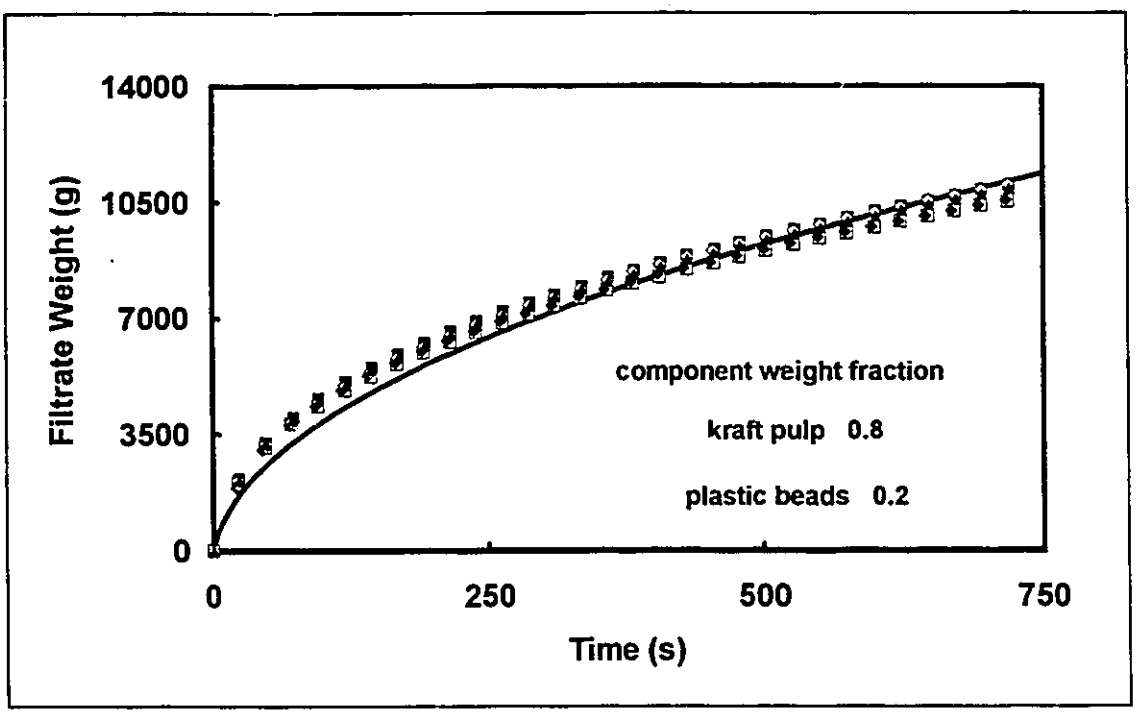

Figure 6.2.4 Cumulative filtrate weight collected plotted against time. Composition of the fibre pad: dry weight fraction of kraft pulp = 0.8, weight fraction of beads = 0.2. Markers represent data from five repeated experiments. Solid line is the result of mathematical simulation. Model parameters: c_{min} = 0.1114 kg/m^3, c_{max} = 70 kg/m^3 and r = 0.8 using modified Kropholler's equation (Equation (6.3.4)) to represent the concentration profile in the fibre bed.

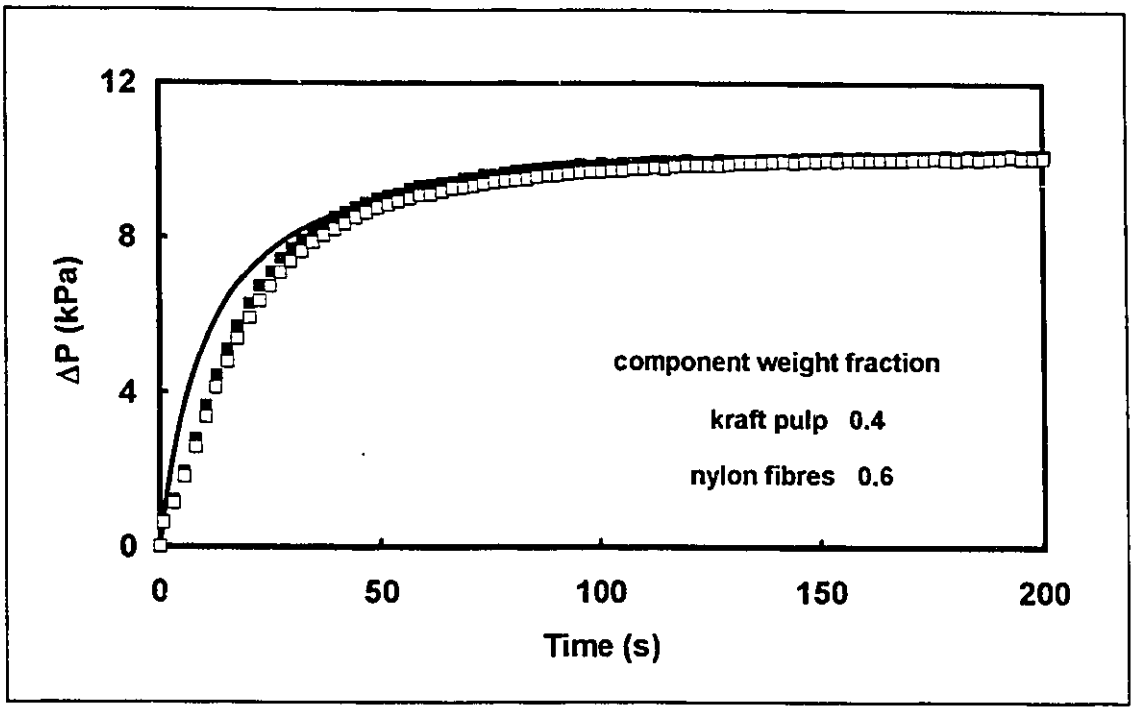

Figure 6.2.5 Pressure drop data plotted against time. Composition of the fibre pad: dry weight fraction of kraft pulp = 0.4, weight fraction of nylon fibres = 0.6. Markers represent experimental data from two repeated experiments. Solid line is the result of mathematical simulation. Model parameters: c_{min} = 0.2198 kg/m^3, c_{max} = 92 kg/m^3 and r = 0.38 using the original Kropholler's equation (Equation (6.3.2)) to represent the concentration profile in the fibre bed.

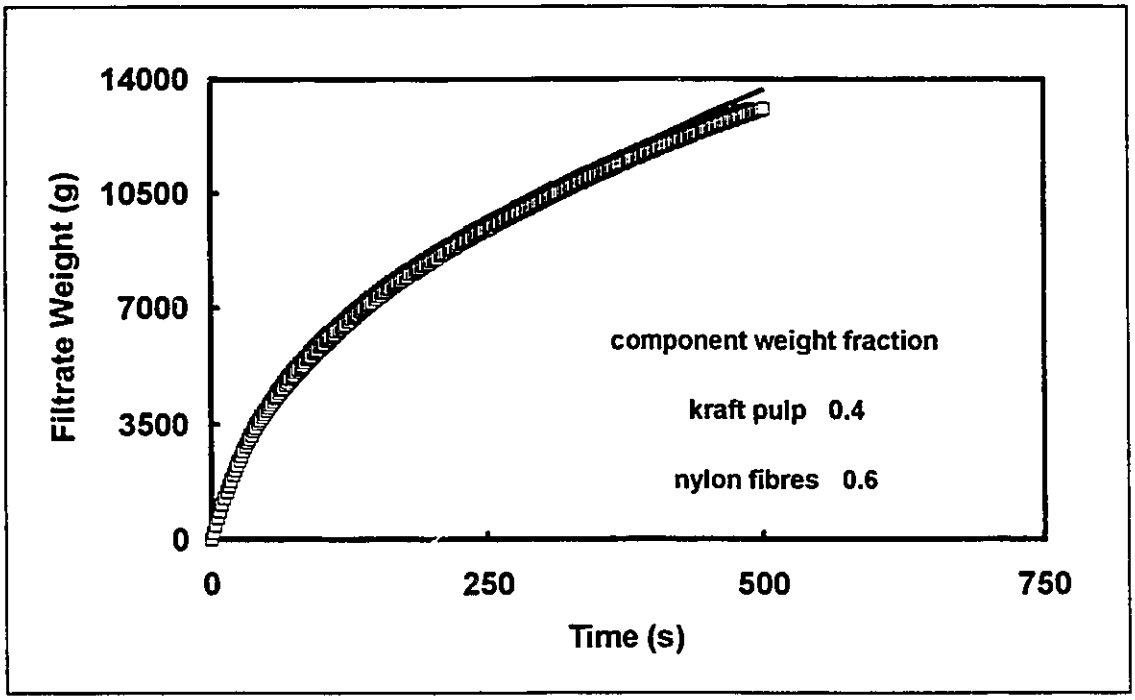

Figure 6.2.6 Cumulative filtrate weight data plotted against time. Composition of the fibre pad: dry weight fraction of kraft pulp = 0.4, weight fraction of nylon fibres = 0.6. Markers represent experimental data from two repeated experiments. Solid line is the result of mathematical simulation. Model parameters: c_{min} = 0.2198 kg/m^3, c_{max} = 92 kg/m^3 and r = 0.38 using the original Kropholler's equation (Equation (6.3.2)) to represent the concentration profile in the fibre bed.

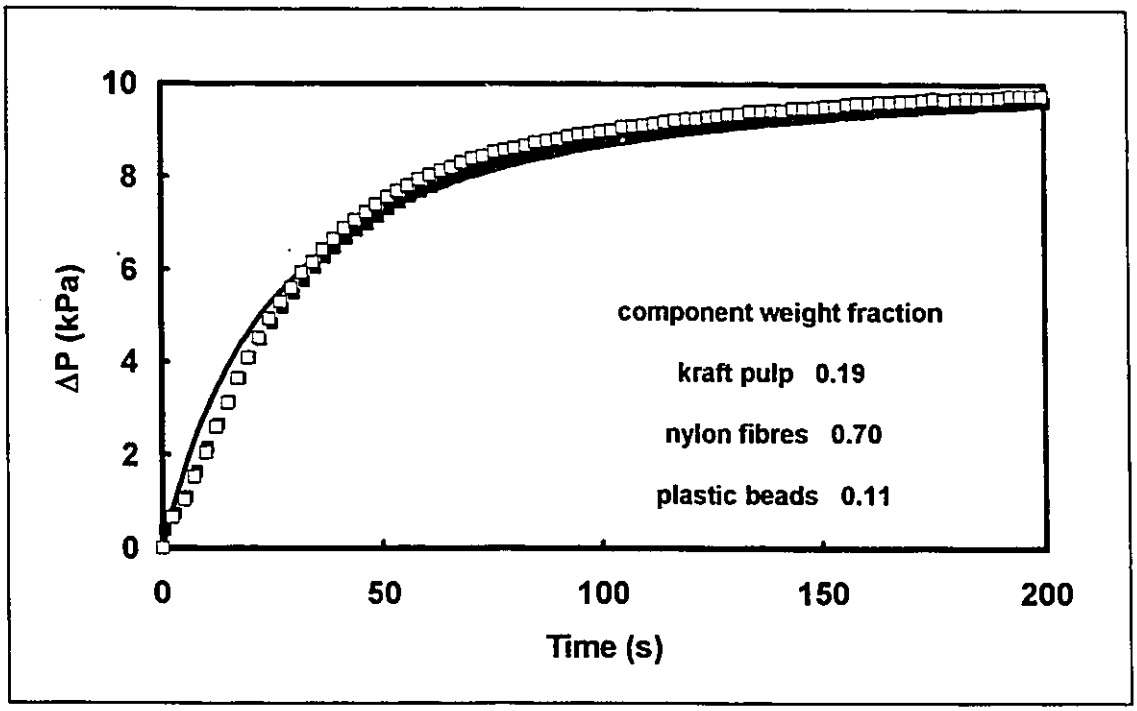

Figure 6.2.7 Pressure drop data plotted against time. Composition of the fibre pad: dry weight fraction of kraft pulp = 0.19, weight fraction of nylon fibres = 0.70 and weight fraction of plastic beads = 0.11. Markers represent experimental data from two repeated experiments. Solid line is the result of mathematical simulation. Model parameters: c_{min} = 0.4393 kg/m^3, c_{max} = 98 kg/m^3 and r = 0.38 using the original Kropholler's equation (Equation (6.3.2)) to represent the concentration profile in the fibre bed.

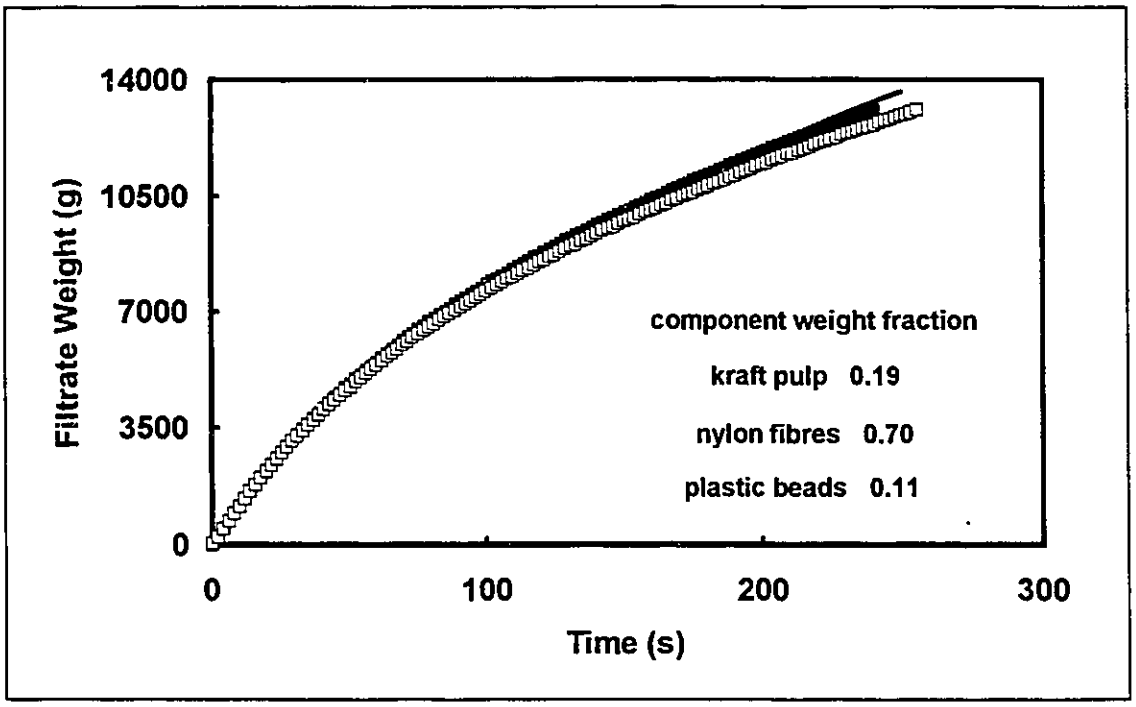

Figure 6.2.8 Cumulative filtrate weight data plotted against time. Composition of the fibre pad: dry weight fraction of kraft pulp = 0.19, weight fraction of nylon fibres = 0.70 and weight fraction of plastic beads = 0.11. Markers represent experimental data from two repeated experiments. Solid line is the result of mathematical simulation. Model parameters: c_{min} = 0.4393 kg/m^3, c_{max} = 98 kg/m^3 and r = 0.38 using the original Kropholler's equation (Equation (6.3.2)) to represent the concentration profile in the fibre bed.

The trends displayed by data in Figures 6.2.1 and 6.2.2 for filtration pure kraft pulp suspensions are common to rest of the figures. That is, at the beginning of the filtration experiment, pressure drop across the pad started at zero and increased quickly until it leveled off to a constant value when the pad

had attained approximately 20% of its final total thickness. Regarding the filtrate weight data, a parabolic relationship was observed in Figure 6.2.2. Since these features were common to all the data obtained regardless of the composition of the suspension, the eight figures above were chosen to represent data from the four systems in this chapter. A list of the files containing the experimental data is given in Appendix A.7.

Good reproducibility of the data had been observed for pure kraft pulp suspensions as it was demonstrated in both Figures 6.2.1 and 6.2.2. In Figure 6.2.1, the pressure drop data had some scattering in the beginning of filtration: pressure data from the repeated experiments varied by approximately 30%. However, data from the different experiments did converge to a single pressure drop value when the pressure started to level off. In Figure 6.2.2, the experimental data displayed some spread. However, the band of data was narrow and thus the experimental results were still highly reproducible. Similar comments could be made about the reproducibility in data displayed in Figures 6.2.3 to 6.2.8. Therefore, reproducibility in experimental data had, in general, been good. However, among the experimental data not included in Figures 6.2.1 to 6.2.8, more serious scattering was observed with suspensions at some specific compositions. Among those troublesome cases, two were selected and presented in the following figures, Figures 6.2.9 to 6.2.12.

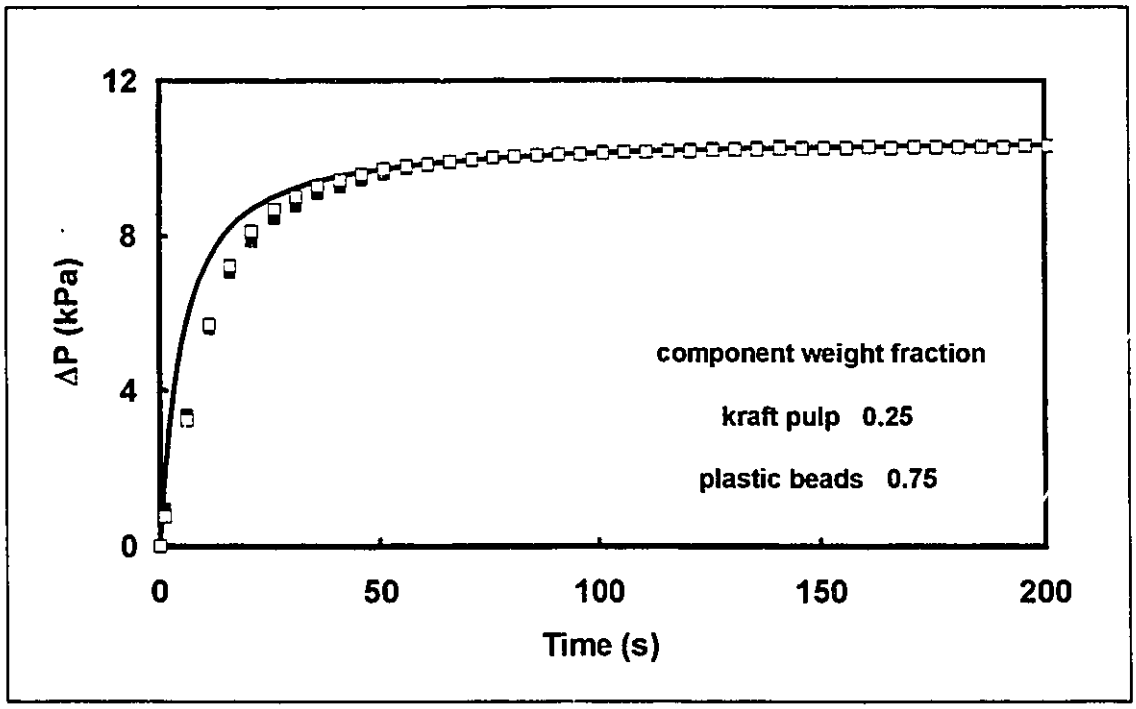

Figure 6.2.9 Pressure drop data plotted against time. Composition of the fibre pad: dry weight fraction of kraft pulp = 0.25 and weight fraction of plastic beads = 0.75. Markers represent experimental data from two repeated experiments. Solid line is the result of mathematical simulation. Model parameters: c_{min} = 0.271 kg/m^3, c_{max} = 160 kg/m^3 and r = 0.8 using the modified Kropholler's equation (Equation (6.3.4)).

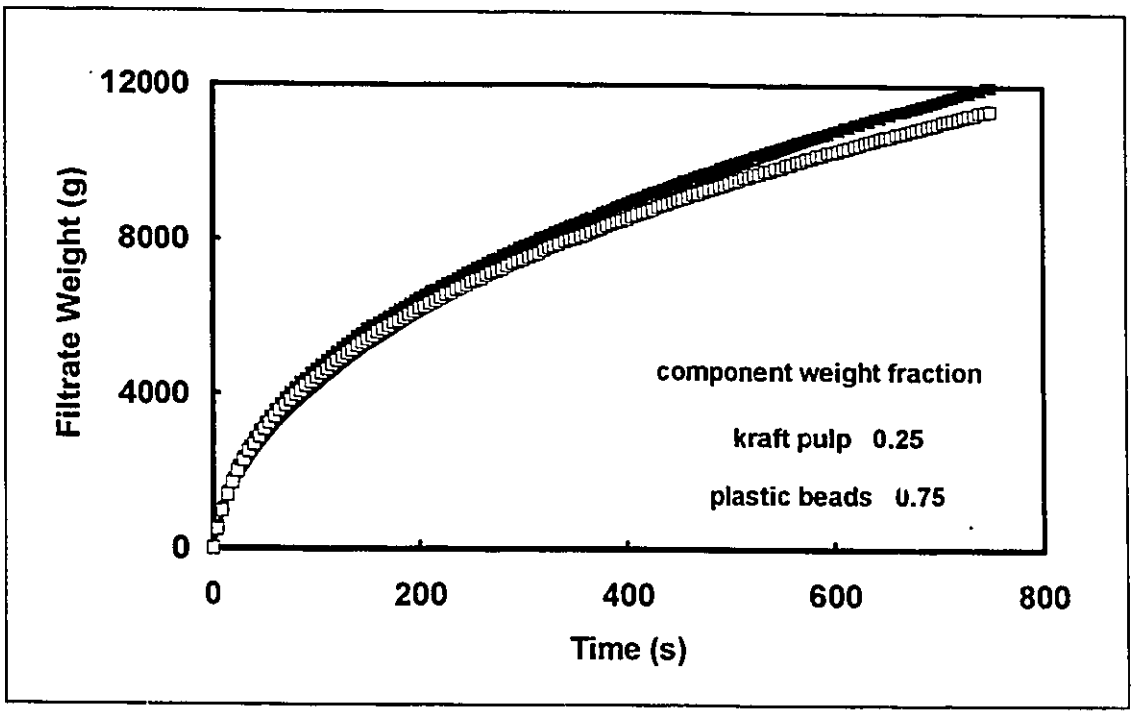

Figure 6.2.10 Cumulative filtrate weight data plotted against time. Composition of the fibre pad: dry weight fraction of kraft pulp = 0.25 and weight fraction of plastic beads = 0.75. Markers represent experimental data from two repeated experiments. Solid line is the result of mathematical simulation. Model parameters: c_{min} = 0.271 kg/m^3, c_{max} = 160 kg/m^3 and r = 0.8 using the modified Kropholler's equation (Equation (6.3.4)) to represent the concentration profile in the fibre bed.

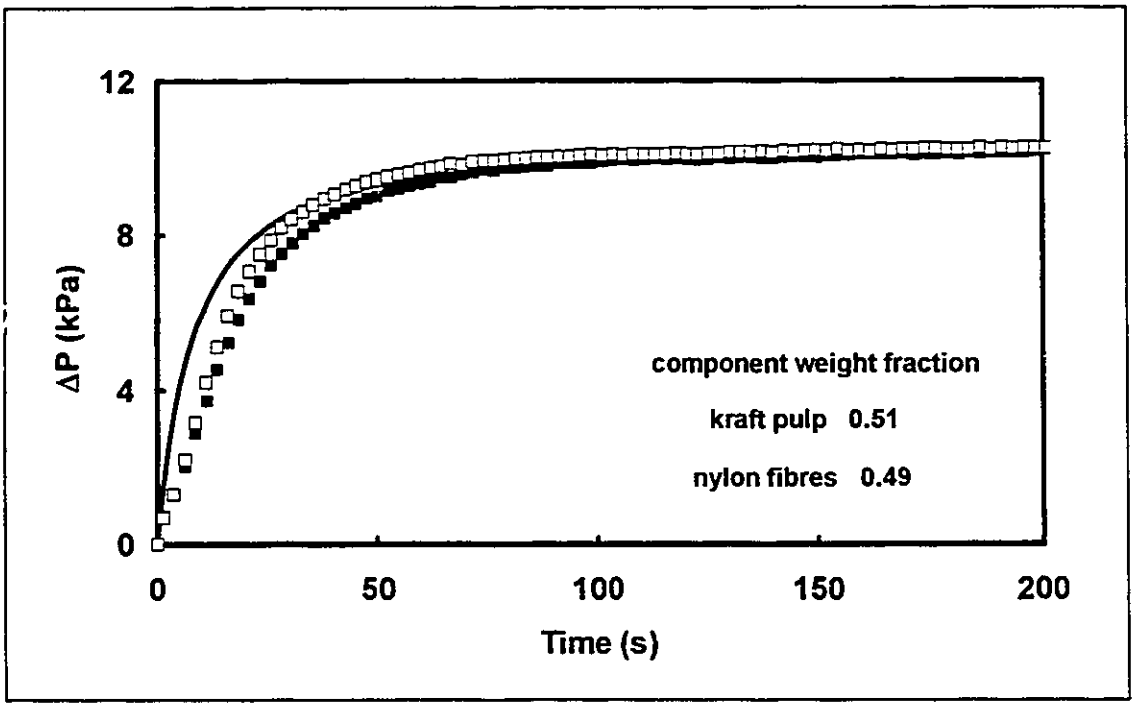

Figure 6.2.11 Pressure drop data plotted against time. Composition of the fibre pad: dry weight fraction of kraft pulp = 0.51 and weight fraction of nylon fibres = 0.49. Markers represent experimental data from two repeated experiments. Solid line is the result of mathematical simulation. Model parameters: c_{min} = 0.169 kg/m^3, c_{max} = 60 kg/m^3 and r = 0.38 using the original Kropholler's equation (Equation (6.3.2)) to represent the concentration profile in the fibre bed.

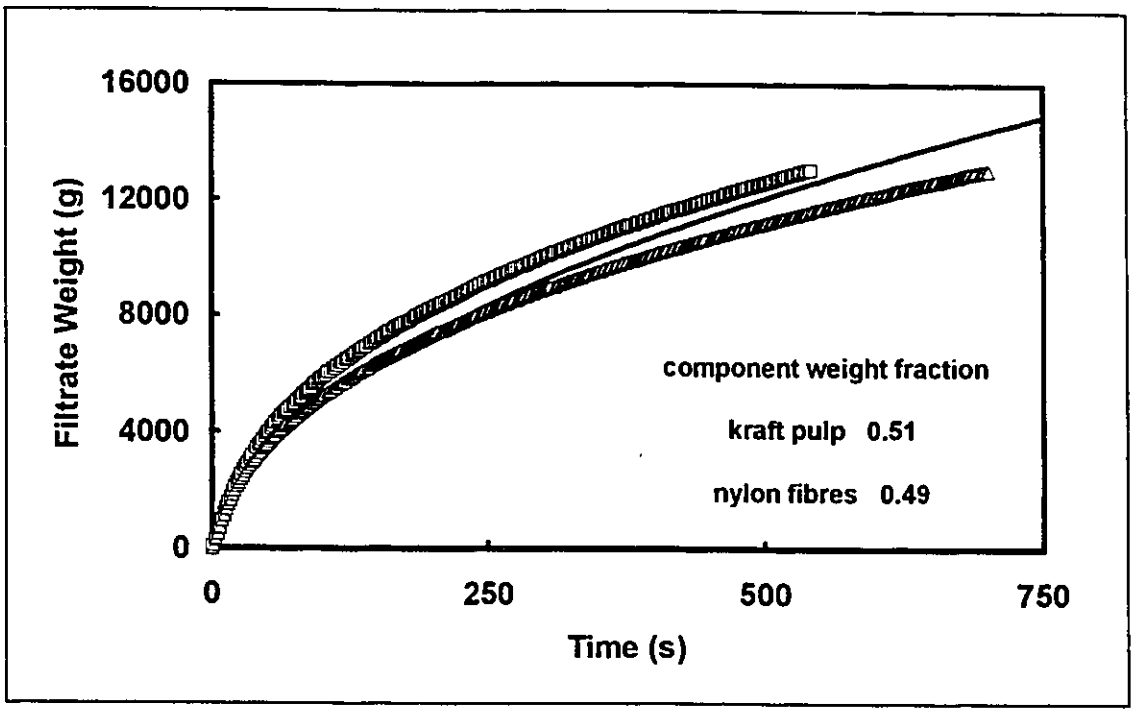

Figure 6.2.12 Cumulative filtrate weight data plotted against time. Composition of the fibre pad: dry weight fraction of kraft pulp = 0.51 and weight fraction of nylon fibres = 0.49. Markers represent experimental data from two repeated experiments. Solid line is the result of mathematical simulation. Model parameters: c_{min} = 0.169 kg/m^3, c_{max} = 60 kg/m^3 and r = 0.38 using the original Kropholler's equation (Equation (6.3.2)) to represent the concentration profile in the fibre bed.

In Figures 6.2.9 and 6.2.10, pressure drop and cumulative filtrate weight data for suspensions that contained 25% by weight of pulp fibres and 75% by weight of plastic beads are shown. Two filtration experiments had been performed under identical conditions with suspensions that had the same composition to produce the data shown in the figures. The reproducibility of

pressure drop data shown in Figure 6.2.9 was good. However, the reproducibility of filtrate weight data was worse. In Figure 6.2.10, the filtrate weight data from the two experiments were close at the initial stages of the experiment. When the experiment progressed, the two curves diverged, making the reproducibility bad at higher times. Similar problems were observed in Figures 6.2.11 and 6.2.12 for the pulp/nylon fibres system. Suspensions containing 51 weight percent of kraft pulp and 49 weight percent of nylon fibres were used to produce the data presented in Figures 6.2.11 and 6.2.12. The problem in reproducibility was similar to that observed in Figures 6.2.9 and 6.2.10 except that the effect was more pronounced. Among the 17 different suspension compositions that had been used, only 5 had displayed problem in reproducibility.

6.3 Modelling Pad Formation: Simulation of Filtration

The equations presented in Section 2.3.2 of this thesis enable prediction of the specific filtration resistance from permeation data. However, the use of those equations with some other auxiliary equations will also allow simulation of a filtration process driven by a constant hydrostatic head. The objective of the simulation is to predict the pressure drop across the filter cake and the cumulative weight of filtrate as a function of time. To model this filtration, the Kozeny-Carman equation, and equations giving the concentration profiles in the fibre bed and the mass balance of the growing fibrous filter cake are needed. In addition to the equations, values of several parameters that would remain

constant in a filtration experiment were needed. Such parameters included the specific external surface area and the specific swollen volume.

6.3.1 Hydrodynamics in The Filter Cake

Darcy's law governs the permeation of fluid through a porous medium. For a compressible bed, a pressure profile exists in the bed. Consequently, a concentration profile exists inside the bed. Therefore, the differential form of Darcy's law has to be applied to a section of the bed and then integrated over the whole bed to get the total flow across it. The differential form of Darcy's law has already been presented earlier as Equation (2.2.23). Separating the variables and integrating from the septum surface to the free surface of the pad gives the pressure drop across the pad that is driving the flow:

$$\Delta P_{pad} = \int_0^{\Delta P} dP = \frac{Q\mu}{A}\int_0^L \frac{d\ell}{K} = \mu \cdot u \cdot \int_0^L \frac{d\ell}{K} \quad ....(6.3.1)$$

To evaluate the integral in Equation (6.3.1), it is essential to know the permeability in the porous bed. The permeability of a bed is given by the Kozeny-Carman equation (Equation (2.2.9)). Since permeability is a function of the local solid concentration in the bed, information on the concentration profile will allow the expression of permeability as a function of location in the bed and thereby allowing the evaluation of the integral in Equation (6.3.1).

6.3.2 Concentration Profile in The Filter Cake

In batch filtration, since the driving force is continuously dropping, successive layers of the pad are formed at increasing porosities. Kropholler [1989] has suggested the following power law function to account for the porosity profile in a fibre pad:

$$c = c_{min} - (c_{min} - c_{max})\left(1 - \frac{\ell}{L}\right)^r \quad ....(6.3.2)$$

while the conditions at the two extreme surfaces of the pad were:

1) $\ell = 0$, $c = c_{max}$

2) $\ell = L$, $c = c_{min} = c_{slurry}$

In Equation (6.3.2), ℓ denotes the vertical position in the fibre bed. ℓ takes on a value that varies from 0 at the septum face of the pad to L at the free surface of the pad. Consequently, the parameter ℓ/L is the normalized pad position that varies from 0 at the septum face to 1 at the free surface of the bed. The two adjustable parameters in Kropholler's equation are c_{max}, the solid concentration at the septum face of the fibre bed and r, the exponent in the equation. The effects of c_{max} and r on the concentration profile predicted by Equation (6.3.2) are illustrated in Figure 6.3.1 by plotting local bed porosity against normalized pad position, ℓ/L. Bed porosity values were obtained from local solid concentrations predicted by Equation (6.3.2) using Equation (2.2.6).

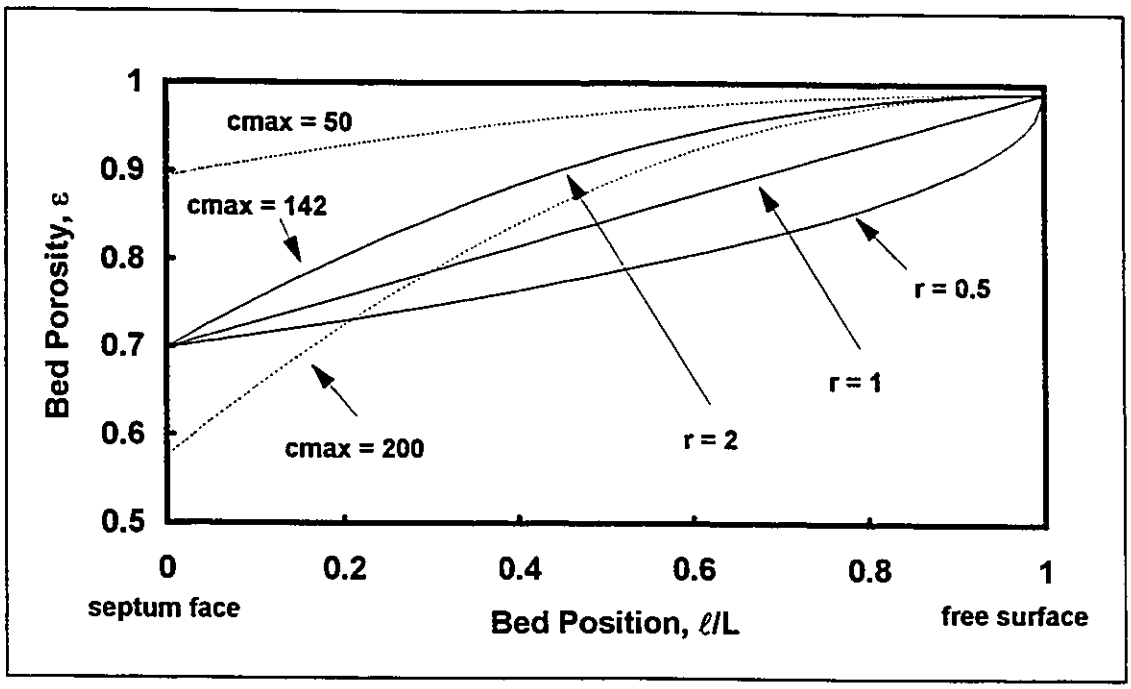

Figure 6.3.1 Porosity in a fibre bed plotted against normalized pad position. The porosity profiles are predicted by Equation (6.3.2) using the parameters: c_{min} = 4.72 kg/m^3, c_{max} = 142 kg/m^3 and r = 2 unless otherwise specified by the legends in the figure.

Three different values of r and three values of c_{max} were used in Equation (6.3.2) to generate the five porosity profiles in Figure 6.3.1. When r was fixed at a value of 2, porosity profiles obtained with the three different c_{max} values displayed the same general trend: porosity in the fibre bed increased with decreasing slopes as normalized pad position increased from 0 (septum face) to 1 (free surface). The effect of c_{max} was that porosity at the septum face of the fibre bed was reduced if c_{max} was increased while the general shape of the porosity profile remained the same. The effect of r on the shape of the porosity profile was more pronounced than that from c_{max}. With a fixed c_{max} value of 142 kg/m^3, bed porosity increased with an increase in pad position towards the free

surface for all three values of r. Porosity was a linear function of pad position when r was equal to 1. Bed porosity increased with decreasing slopes when r had a value of 2 while the opposite was true for a r value of 0.5.

Ingmanson et al. [1959] had studied the distribution of pressure in fibrous beds consisting of wood pulp fibres and synthetic fibres such as nylon, dacron and glass fibres. An equation was derived in the article to predict the pressure drop profile in a fibre bed from the compressive properties of the fibres:

$$\frac{\int_0^{\Delta P} \frac{d(\Delta P)}{c^{3/2}\left(1+57\alpha^3c^3\right)}}{\int_0^{\Delta P_{total}} \frac{d(\Delta P)}{c^{3/2}\left(1+57\alpha^3c^3\right)}} = 1-\frac{\ell}{L} \quad ....(6.3.3)$$

In the equation, L was the total thickness of the fibre bed and ΔP_{total} was the pressure drop across the whole bed. α was the specific swollen volume of the fibres while c and ΔP were the local solid concentration and pressure drop at a vertical position of ℓ in the fibre bed. To evaluate the integral to obtain pressure drop profiles in the fibre beds, Ingmanson et al. [1959] used the power law equation (Equation (2.2.33)) for solid concentration to account for the compressibility of the fibre beds. In the case of nylon fibres, because of the assumption that synthetic fibre beds had high porosities, the equation for the Kozeny coefficient (Equation (2.2.8)) could be simplified. Therefore, Equation (6.3.3) could be integrated analytically and the resulting equation predicted a parabolic pressure profile in the nylon fibre bed that was confirmed by experimental data. However, Equation (6.3.3) did not have an analytical solution

for the case of pulp fibres since the simplifying assumption for nylon fibres was no longer applicable. Nevertheless, numerical solution of the integral also resulted in a parabolic profile that was again confirmed by experimental data. Data on the pressure drop distribution in a pulp fibre bed measured by Ingmanson et al. [1959] and the pressure drop distribution predicted by Equation (6.3.3) using pulp compressibility data provided in the same article is presented in Figure 6.3.2 as an illustration. In the figure, the black markers represent experimental data measured by Ingmanson et al. and the solid line is the result of solving Equation (6.3.3) using the following set of parameters: α = 0.00212 m^3/kg, M = 0.00203 and n = 0.376, where M and n are the constants in the compressibility equation (Equation (2.2.33)).

From the knowledge of the pressure distribution in the fibre bed, it is possible to calculate the concentration profile in the fibre bed by the direct application of the compressibility equation (Equation (2.2.33)). Ingmanson et al. had carried out the calculation using M and n values obtained from compressibility experiments. Results of the calculations were presented in Figure 13 of the article [Ingmanson, 1959]. The calculation has been repeated for beds consisting of pulp fibres and nylon fibres and the results are presented in Figures 6.3.3 and 6.3.4 respectively. However, there was one limitation to the range of validity of the results; when the M and n values were evaluated by Ingmanson et al. from bed compressibility data, the data only covered the range of pressure drop from 978 to 9780 Pa. Therefore, values of local solid concentrations at bed positions close to the free surface where the pressure drops were lower than 978 Pa were results of extrapolation of the compressibility

equation. Consequently, accuracies of concentration data at these pad positions were questionable.

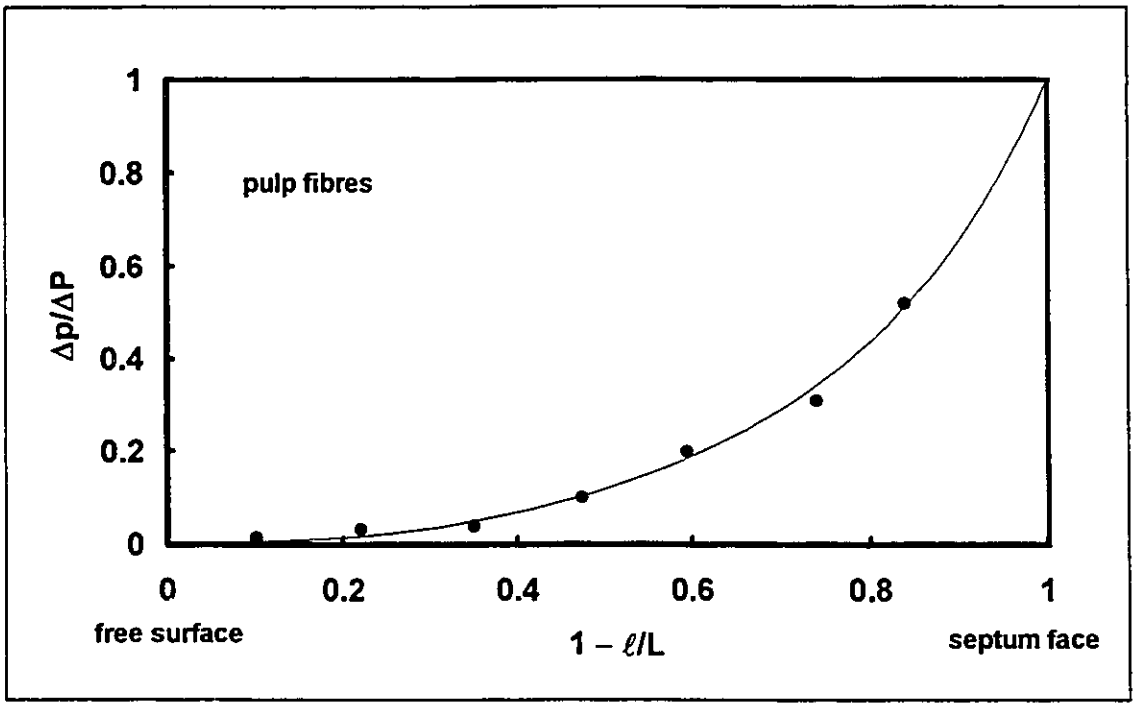

Figure 6.3.2 Pressure drop distribution in a pulp fibre pad measured by Ingmanson et al. Markers are experimental data measured by Ingmanson et al. that were presented in Figure 12 of the article: TAPPI, **42**, 10, 840-849, 1959. Solid line is the numerical solution of Equation (6.3.3) using parameters for pulp fibres that were given in the same article by Ingmanson et al. The value of the parameters used are: α = 0.00212 m^3/kg, M = 0.00203 and n = 0.376.

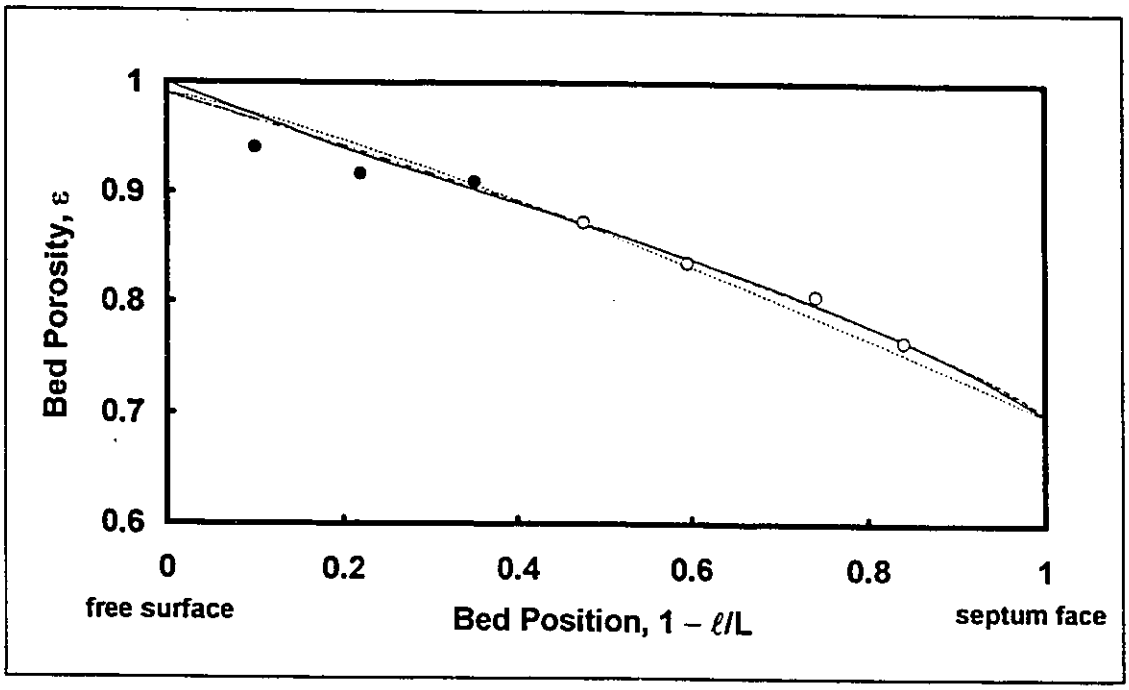

Figure 6.3.3 Porosity in a pulp fibre bed plotted against the normalized pad position. Markers represent experimental data obtained by Ingmanson et al. ○: concentration data calculated from pressure drop exceeding 978 Pa; ●: concentration data calculated from extrapolation of the compressibility equation. All the curves are prediction of the porosity profile by equations. ——: prediction of the porosity profile using Equation (6.3.3) and Equation (2.2.33) with α = 0.00212 m^3/kg, M = 0.00203, n = 0.376 and ΔP_{total} = 8050 Pa; – – –: prediction using Kropholler's equation (6.3.2) with c_{min} = 4.72 kg/m^3, c_{max} = 142 kg/m^3 and r = 1.2; – · –: prediction using modified Kropholler's equation (6.3.4) with c_{min} = 4.72 kg/m^3, c_{max} = 142 kg/m^3 and r = 0.8.

The porosity distribution in a pulp fibre bed measured by Ingmanson et al. was plotted in Figure 6.3.3. The equation (Equation (6.3.3)) proposed by Ingmanson et al. indicated curvature at pad positions that were close to the septum face although there were not enough experimental in that range to confirm the trend. Kropholler's original equation (Equation (6.3.2)) was used to predict the porosity profile using the boundary porosity values provided in Ingmanson's paper. The porosity profile predicted a curvature at pad positions

close to the free surface of the pad instead of near the septum face. Since the pressure gradient acting on the fibre bed at pad positions near the septum face is higher than pressure gradients near the free surface, it is highly possible that such a curvature in the porosity profile exists at such pad positions. Therefore, a modified Kropholler's equation was used to represent the porosity profile in a pulp fibre bed. The equation has the following form:

$$c = c_{max} - (c_{max} - c_{min})\left(\frac{\ell}{L}\right)^r \quad ....(6.3.4)$$

while the conditions at the two extreme surfaces of the pad are:

1) $\ell = 0$, $c = c_{max}$

2) $\ell = L$, $c = c_{min} = c_{slurry}$

The porosity profile predicted by Equation (6.3.4) was plotted in Figure 6.3.3 and the porosity profile was identical to that predicted by Equation (6.3.3) except at pad positions near the free surface; Equation (6.3.3) predicted a totally porous pad (porosity of 1) at the free surface while the porosity at the free surface was fixed in Equation (6.3.4). Therefore, since the free surface of pads should have finite porosities less than 1 and Equation (6.3.4) is much simpler mathematically than Equation (6.3.3) while both of them predict identical porosity profiles, Equation (6.3.4) is the equation of choice for representing porosity profiles in mathematical simulation of the filtration process of pulp fibre suspensions.

In the case of nylon fibre beds, porosity profiles predicted by the 3 equations (Equations (6.3.2), (6.3.3) and (6.3.4)) are presented in Figure 6.3.4 while the corresponding pressure distribution in the bed was calculated using

the data given in the article by Ingmanson et al. and the result is shown in Figure 6.3.5.

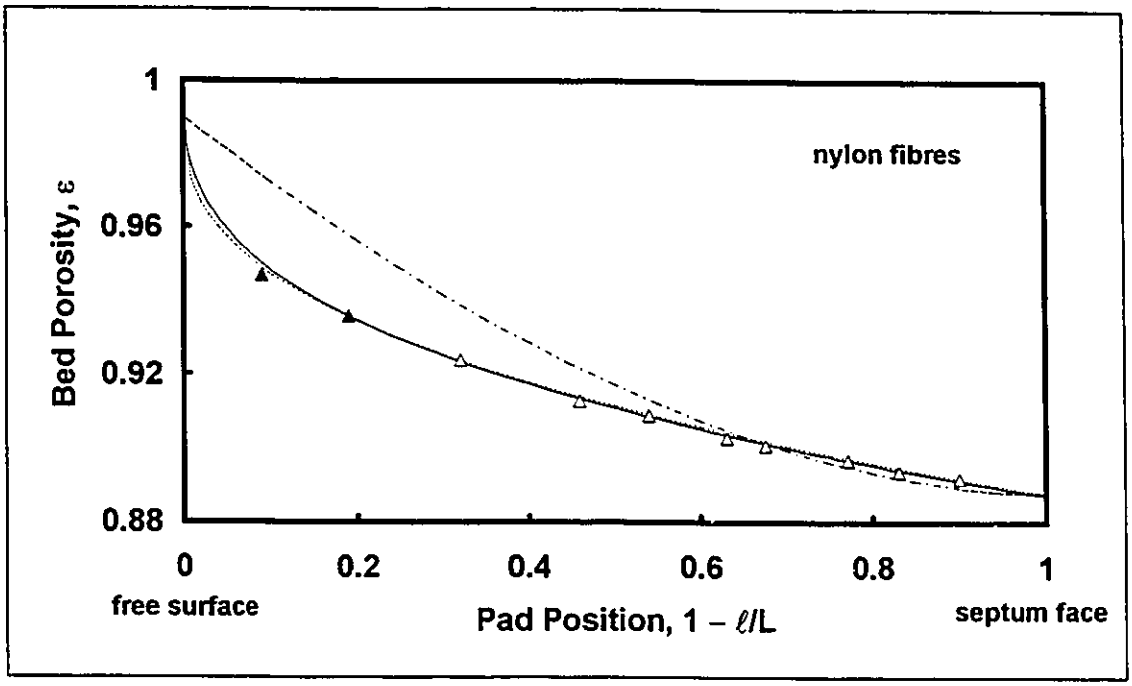

Figure 6.3.4 Porosity in a nylon fibre bed plotted against normalized pad position. Markers represent experimental data obtained by Ingmanson et al. Δ: concentration data calculated from pressure drop exceeding 978 Pa; ▲: concentration data calculated from extrapolation of the compressibility equation. All the curves are predictions of the porosity profile. ——: prediction of the porosity profile using Equation (6.3.3) and Equation (2.2.33) with α = 0.000904 m^3/kg, M = 0.0104, n = 0.225 and ΔP_{total} = 6220 Pa; – – –: prediction using Kropholler's equation (6.3.2) with c_{min} = 11 kg/m^3; c_{max} = 124 kg/m^3 and r = 0.38; – · –: prediction using modified Kropholler's equation (6.3.4) with c_{min} = 11 kg/m^3; c_{max} = 124 kg/m^3 and r = 1.8.

The shape of the pressure profile in Figure 6.3.5 was similar to that of a pulp pad (Figure 6.3.2). However, the shape of the porosity profile in a nylon fibre bed was markedly different from those found in pulp fibre pads (Figure 6.3.3). The curvature in the porosity profile was found at pad positions close to

the free surface of the bed instead of at positions close to the septum face. Equation (6.3.3) proposed by Ingmanson et al. predicted the curvature at pad positions close to the free surface of the fibre bed. Contrary to the case of pulp fibres, the modified Kropholler's equation (Equation (6.3.4)) failed to give a porosity profile that could fit the experimental data. Nevertheless, the original Kropholler's equation (Equation (6.3.2)) with a r-value of 0.38 predicted a porosity profile that was identical to that predicted by Equation (6.3.3) and provided an excellent fit to the experimental data. Consequently, Equation (6.3.2) is the equation of choice to be used in numerical simulation of the filtration of suspensions containing nylon fibres.

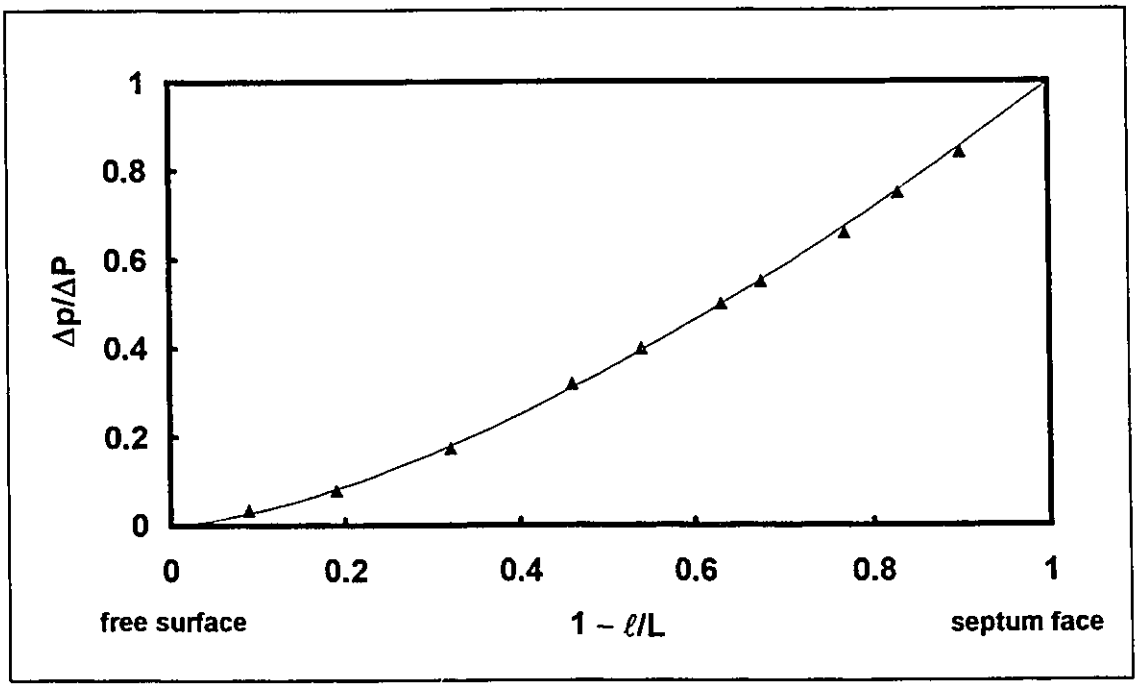

Figure 6.3.5 Pressure drop distribution in a nylon fibre pad measured by Ingmanson et al. Markers are experimental data measured by Ingmanson et al. that were presented in Figure 7 of the article: TAPPI, **42**, 10, 840-849, 1959. Solid line is the numerical solution of Equation (6.3.3) using the parameters: α = 0.000904 m^3/kg, M = 0.0104 and n = 0.225.

In summary, the concentration profile equations (Equations (6.3.2) and (6.3.4)) give reasonable estimates of the actual concentration profile in the bed and therefore, they can be used in numerical simulations of the filtration of suspensions. However, the applicability of the two equations is specific to the type of suspension; Equation (6.3.2) was found to be better for pads containing nylon fibres while Equation (6.3.4) was found to be better for pulp fibre pads. From the two concentration profile equations (Equations (6.3.2) and (6.3.4)), average concentrations in the fibre pads can be found by the following equations:

from Equation (6.3.2): $$c_{avg} = \frac{1}{L}\int_0^L c\,d\ell = \frac{r c_{min} + c_{max}}{r+1} \quad ....(6.3.5)$$

and

from Equation (6.3.4): $$c_{avg} = \frac{1}{L}\int_0^L c\,d\ell = \frac{r c_{max} + c_{min}}{r+1} \quad ....(6.3.6)$$

6.3.3 Mass Balance over The Fibre Pad

In the mathematical model for cake filtration of a suspension, a mass balance over the fibre pad and a definition of the filtrate flow rate are needed. The resulting equations are:

$$V \cdot c_{min} = A \cdot L \cdot c_{avg} \quad ....(6.3.7)$$

and

$$Q = \frac{dV}{dt} = u \cdot A \quad ....(6.3.8)$$

where V is the cumulative volume of filtrate collected, A and L are the area and thickness of the fibre bed respectively while u and Q are the superficial velocity and volumetric flowrate of fluid through the fibre pad. To complete the model, an expression relating pressure drop across the pad to the flow velocity is necessary.

Pressure drop over the whole filtration equipment is made up of two contributing factors: the pressure drop across the fibre pad and the pressure losses in the pipes and fittings of the equipment. Therefore, the pressure drop across the fibre pad is the difference between the total hydrostatic head driving the flow and the pressure loss in the pipes and fittings:

$$\Delta P_{pad} = \Delta P_{total} - \Delta P_{pipes} \quad ....(6.3.9)$$

It has already been discussed in Section 3.4 of the thesis that pressure losses in pipes can be represented by a power law function. Therefore, the above equation becomes:

$$\Delta P_{pad} = \Delta P_{total} - f \cdot u^g \quad ....(6.3.10)$$

where f and g are numerical parameters that have already been given in Section 3.4 for the present apparatus.

In summary, solution of Equations (6.3.1), (6.3.7), (6.3.8) and (6.3.10) with the appropriate concentration profile equation, the corresponding expression for the average concentration in the pad, and the permeability function enables prediction of the pressure drop across the fibre bed and the weight of filtrate as a function of time.

In the simulation of the filtration process, the two variables of interest are the cumulative filtrate weight, W, and the pressure drop across the fibre pad, ΔP_{pad}. The objective of the simulation is to get W and ΔP_{pad} as a function of time. In order to achieve that, all the above equations must be solved simultaneously. Since an analytical solution seems impossible, a numerical scheme was used to generate the results presented in this chapter. The numerical scheme centered around Equations (6.3.8) and (6.3.10). When Equation (6.3.1) was substituted into Equation (6.3.10), Equation (6.3.10) became an equation of only one variable, u, the superficial velocity of the filtrate. However, solution of the equation for u required an evaluation of the integral that came from Equation (6.3.1).

Equation (6.3.5) or Equation (6.3.6) gave the constant parameter of average solid concentration. With the knowledge of the average solid concentration, the specific swollen volume, the specific surface area, and the initial conditions of the filtration process, it was possible to solve Equation (6.3.7) for L, the instantaneous thickness of the pad. Using this value of L, the concentration profile equation (Equation (6.3.2) or Equation (6.3.4)) and the Kozeny-Carman equation (Equation (2.2.9)), the integral from Equation (6.3.1) was determined.

With the integral as a known quantity, Equation (6.3.10) was solved for u. Equation (6.3.10) was a non-linear algebraic equation. Therefore numerical algorithms such as the Newton-Raphson method had to be used to obtain the solution, u, the superficial velocity. After the value of u was obtained, ΔP_{pad} was calculated using Equation (6.3.1) and u was used by a linear ODE solver that returned V, the cumulative filtrate volume. The cumulative filtrate weight was

then calculated from V. After this step, the program would step up to a new time and repeat the procedure again to generate the values of W and ΔP_{pad} as a function of time.

The validity of the mathematical model was tested by application to the filtration of a suspension containing incompressible solids. The set of equations in the mathematical model were reduced to existing equations in literature that were derived for incompressible filter cakes. Therefore, the mathematical model is a valid extension for the filtration of suspensions of compressible solids. Details of the verification is given in Appendix A.5. A flow diagram of the numerical scheme is given below in Figure 6.3.6.

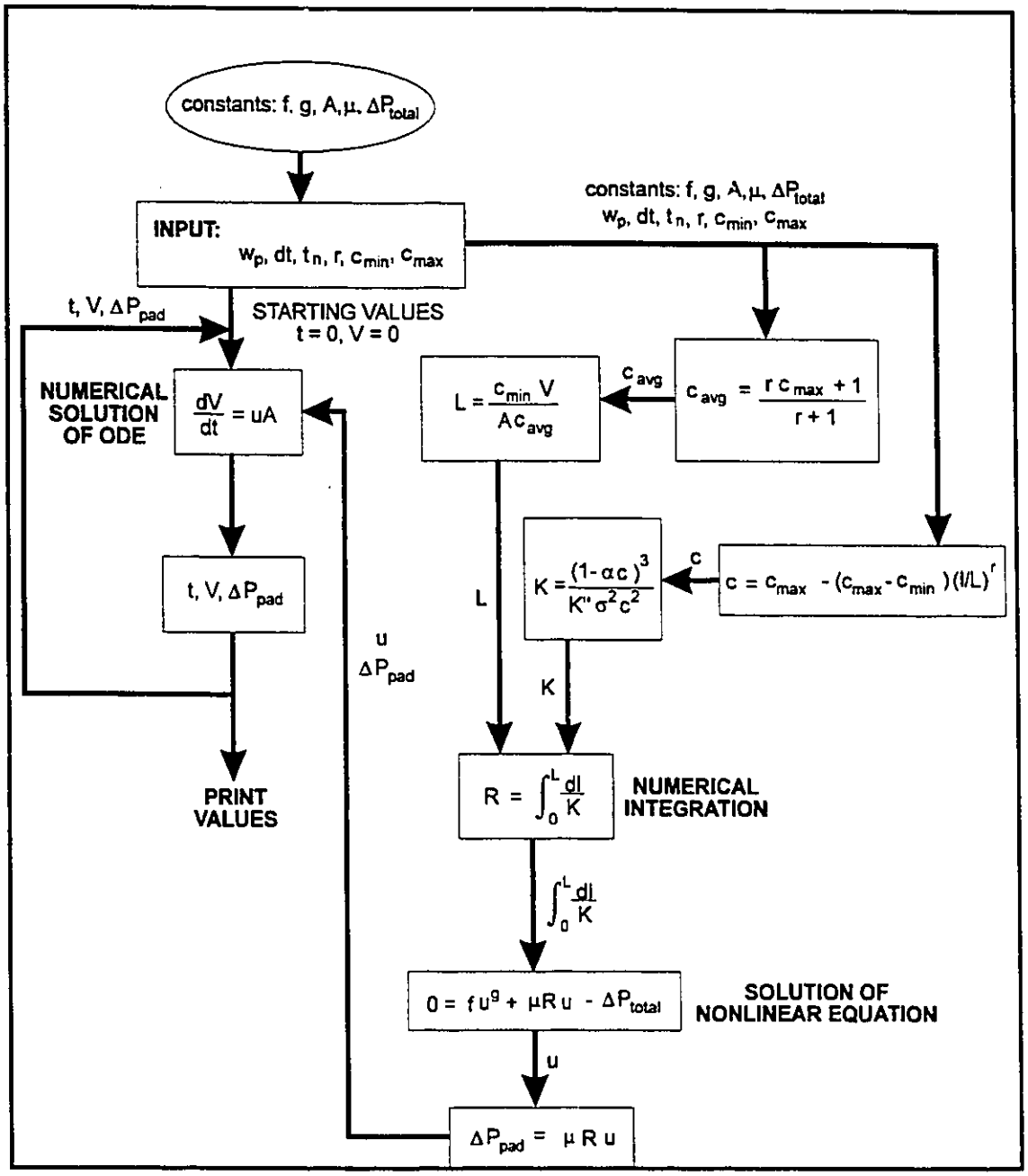

Figure 6.3.6 Flow chart of the numerical scheme for simulation of suspension filtration.

6.4 Discussion

A FORTRAN program based on the numerical scheme described in Section 6.3 was used to simulate the filtration of kraft pulp suspensions. A listing of the computer program is given in Appendix A.6. Specific external surface area and specific swollen volume of kraft pulp determined experimentally were used along with two adjustable parameters, r and c_{max}, which accounted for the compressibility of the pad. It has been illustrated in the previous section that the porosity profiles in pulp and nylon fibre beds were represented by Equations (6.3.4) and (6.3.2) respectively. Assuming that the shapes of the concentration profile in fibre beds with similar composition are identical, Equation (6.3.4) with a constant r value of 0.8 was used to simulate the filtration of pulp suspensions that contained plastic beads. Similarly, Equation (6.3.2) with a constant r value of 0.38 was used in the simulation for filtration of suspensions containing pulp and nylon fibres. For the simulation of the filtration of suspensions containing all three components, Equation (6.3.2) with a constant r value of 0.38 was used because nylon fibre was the major component by weight.

Since the value of r was fixed in all the simulations, c_{max} was the only remaining adjustable parameter. According to the equation proposed by Kropholler, c_{max} is the local solid concentration in the pad at the pad/filter medium interface or the septum face. In the experiments, all the pads were formed from suspensions having the same fibre consistency. Therefore, higher values of c_{max} indicated more compact pad structures that offered higher resistance to flow. The value of c_{max} was determined by the following procedure. A first approximation of c_{max} was chosen by estimating c_{max} and

seeing if the simulation provided a good fit to the experimental data. Simulation was then carried out using c_{max} values within $\pm$ 5 kg/m^3 of the first c_{max} value at increments of 1 kg/m^3. Therefore, a total of 11 sets of simulation results were obtained. The sum of square of errors for the 11 sets of results were calculated and the best c_{max} value was determined from the set of results that yielded the lowest sum of square of errors. Results from numerical simulation using the appropriate c_{max} values were shown in Figure 6.2.1 to 6.2.12 as solid lines.

In all the cases, the simulation pressure drop results were in excellent agreement with the experimental data. The cumulative filtrate weight curves predicted by the program displayed the same parabolic shape as shown by the experimental data but the agreement between the two sets of results was not always as good as with the pressure drop. Agreement was usually good in the initial part of the filtrate curve while the simulation results predicted flowrates that were approximately 5% higher than actual in the later stages of filtration when the process was running at a steady state. Faster filtrate rate meant lower resistance to flow. Therefore, the model was underestimating either the steady state filtration resistance or the total thickness of the fiber pad. A possible cause of this error was the assumption made for the concentration profile in the fibre pad. In the mathematical model, it was assumed that the concentration profile in the fibre pad remained the same throughout the filtration, regardless of the thickness of the pad and the pressure drop acting across the pad. Although the hydrostatic head driving the filtration was kept constant in all the experiments, the pressure drop across the fibre pad varied from zero at the start of the experiment to the final constant value that was approximately equal to the total hydrostatic head. Therefore, since the pressure acting on the forming fibre pad

was not constant, the assumption of a constant concentration profile might be oversimplifying the situation. Consequently, the discrepancy between the experimental data and the simulation results arose. More information on the change in concentration profile in fibre pad during filtration would make the mathematical model more accurate. However, study on such aspect of filtration was scarce. Nevertheless, with the simplicity of the compressibility equation considered, the mathematical model is capable of predicting qualitative trends in the filtration of suspensions with only one adjustable parameter and confirmed the assumption that permeation data could be applied to predict filtration behaviour of suspensions.

Since c_{max} was the only adjustable parameter left in the mathematical model. It would be interesting to find out how c_{max} varied with particle content in the fibre cake. In Figures 6.4.1 to 6.4.3, c_{max} values were plotted against the weight fraction of plastic beads or the weight fraction of nylon fibres.

In Figure 6.4.1, c_{max} is shown to increase with bead content for pads containing pulp fibres and plastic beads. This agreed with intuition because as bead content in the suspension was increased, there were more solid materials that would end up in the pad. Therefore, mass concentration of solid material in the pad should increase with bead content. Consequently, solid concentration at the septum face of the pad, c_{max}, should also be proportional to bead content in the pad. It has been demonstrated in Figure 6.4.1 that the c_{max} values followed a smooth curve with increasing slopes as bead content increased from zero except two of the experimental data points at bead weight fractions of 0.5 and 0.67. At a bead weight fraction of 0.5, the c_{max} value obtained was higher than expected while the reverse was true for the c_{max} at a bead fraction of 0.67. A

possible explanation for this phenomenon became apparent when Figure 6.4.1 was compared to Figure 6.4.4 where the specific filtration resistance for pulp fibres/plastic beads system was plotted against bead weight fraction. In Figure 6.4.4, specific filtration resistance of the suspensions dropped from a maximum at a bead fraction of 0.5 to an almost constant value at all subsequent bead fractions. This suggested a change in the pad microstructure due to the transition from having pulp fibres as the major component to having the beads as the major component. Therefore, sudden change in the c_{max} values in Figure 6.4.1 was probably a manifestation of this transition.

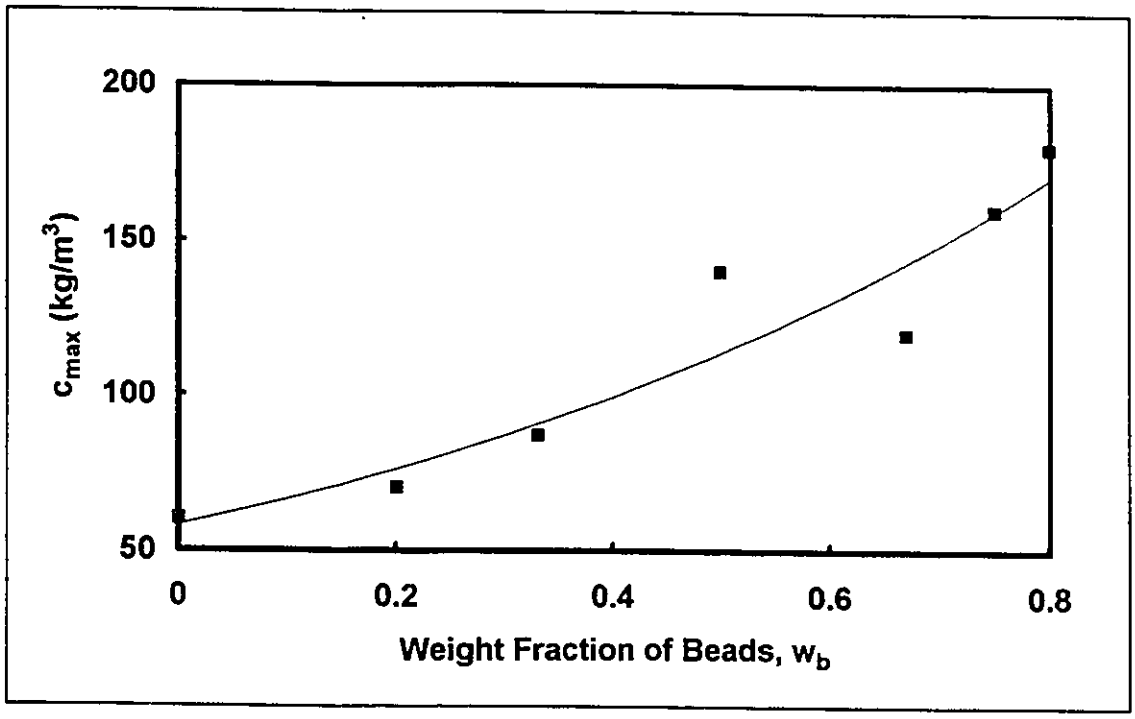

Figure 6.4.1 Value of c_{max} plotted against weight fraction of beads in the fibre cake for the pulp/beads system. Individual markers are actual values used in simulations.

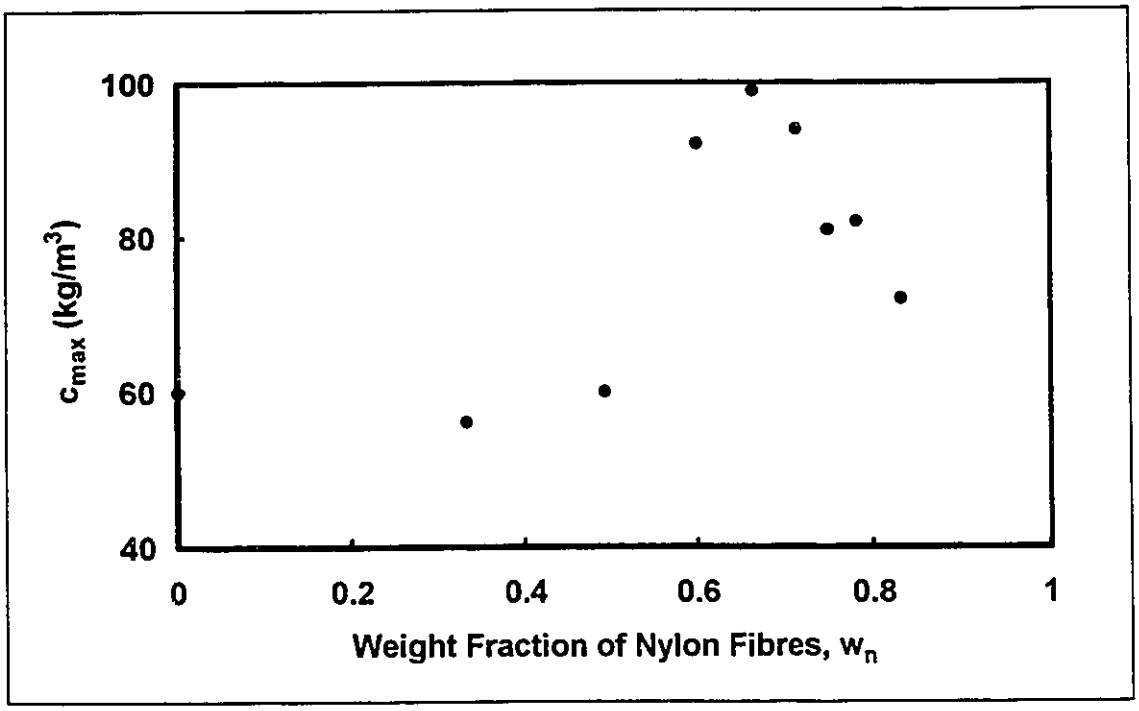

Figure 6.4.2 Value of c_{max} plotted against weight fraction of nylon fibres in the fibre cake for the pulp/nylon fibres system. Individual markers are actual c_{max} values used in simulations.

In Figure 6.4.2, the value of c_{max} increased with nylon fibre content until a nylon fibre weight fraction of about 0.665 was reached. Beyond this nylon fibre weight fraction, the value of c_{max} dropped gradually. Since c_{max} was the concentration of solids at the septum face of the fibre pad, reduction in the c_{max} value suggested less material in a fixed volume of pad and therefore a higher permeability to flow. Higher pad permeability and lower concentration implied a more open pad microstructure. A possible reason for this phenomenon was that the rigidity of nylon fibres was preventing the excessive accumulation and compaction of material at the septum face of the fibre pad. Although an increase in the weight fraction of nylon fibres meant that there would be more material present in the whole fibre pad, higher nylon fibre content resulted in a stronger

fibre network that was more resistant to compression by fluid pressure. Consequently, when the weight fraction of nylon fibres went beyond 0.5 so that the nylon fibres became the major component of the filter cake, the strong nylon fibre network restricted compression of materials at the septum face and thereby reduced c_{max}.

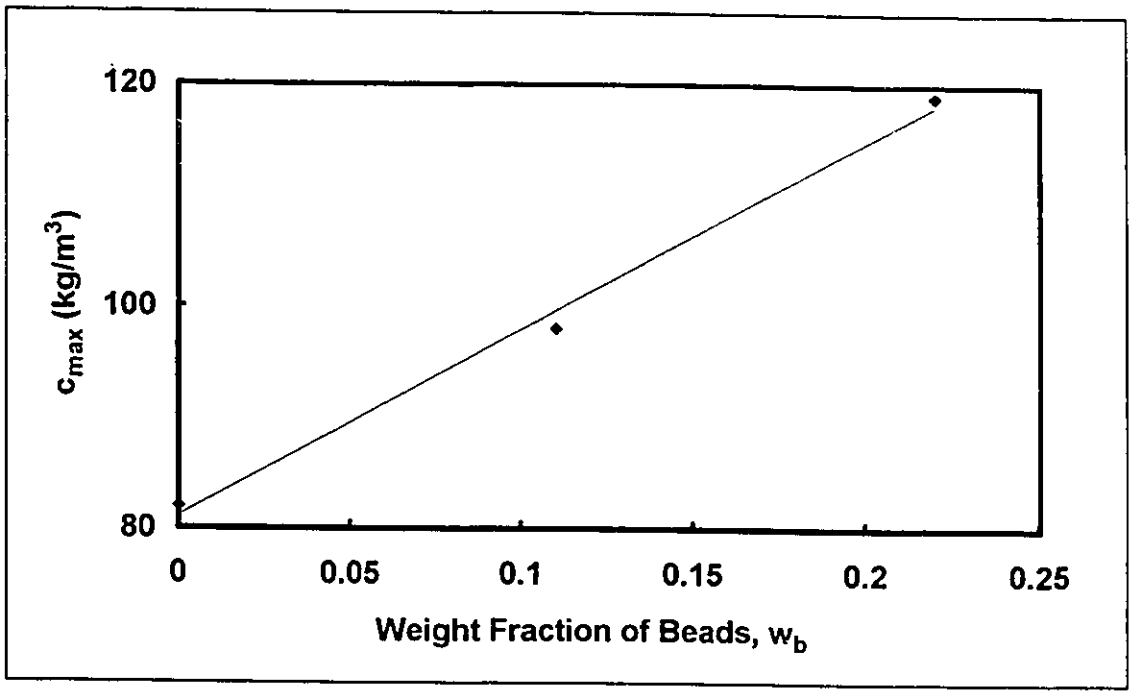

Figure 6.4.3 Value of c_{max} plotted against weight fraction of beads in the fibre cake for the pulp/nylon fibres/beads system. Individual markers are actual values used in simulations.

c_{max} values for pulp fibres/nylon fibres/plastic beads system were plotted against the weight fraction of plastic beads in the fibre pads in Figure 6.4.3. c_{max} values were found to increase with the weight content of plastic beads. It appeared that the c_{max} value was a linear function of the weight fraction of beads. However, it was difficult to come to a conclusion concerning the

functional form of the relation because of the size of the data set. Nevertheless, the trend observed was consistent with what was exhibited by the pulp fibres/plastic beads system in Figure 6.4.1. In both of the systems that contained plastic beads, the content of plastic beads was the only compositional variable. That was, in both systems, the mass of fibres remained constant. Therefore, it would be interesting to find out if the results from the pulp fibres/plastic beads system could be used to predict the effect of plastic beads on the c_{max} values for the pulp/nylon fibre/beads system. If a straight line was fitted to the c_{max} data in Figure 6.4.1, a bead weight fraction of 0.11 and 0.22 would cause the c_{max} values to increase from 60 to 67 and from 60 to 78. Therefore, one would expect the c_{max} value for the pulp/nylon fibres/beads system to exhibit the same effect. Consequently, c_{max} values for a bead weight fraction 0.11 and 0.22 predicted from the pulp fibres/beads system would be 89 and 100, which were approximately 10 and 15% lower than the actual values.

Specific filtration resistances of all the systems used in the experiments were calculated using Equation (2.3.4). Since at least two experiments were performed for each suspension composition, average specific filtration values were determined. These specific filtration resistance values were plotted as a function of the weight fraction of beads or weight fraction of nylon fibres in Figures 6.4.4 to 6.4.6.

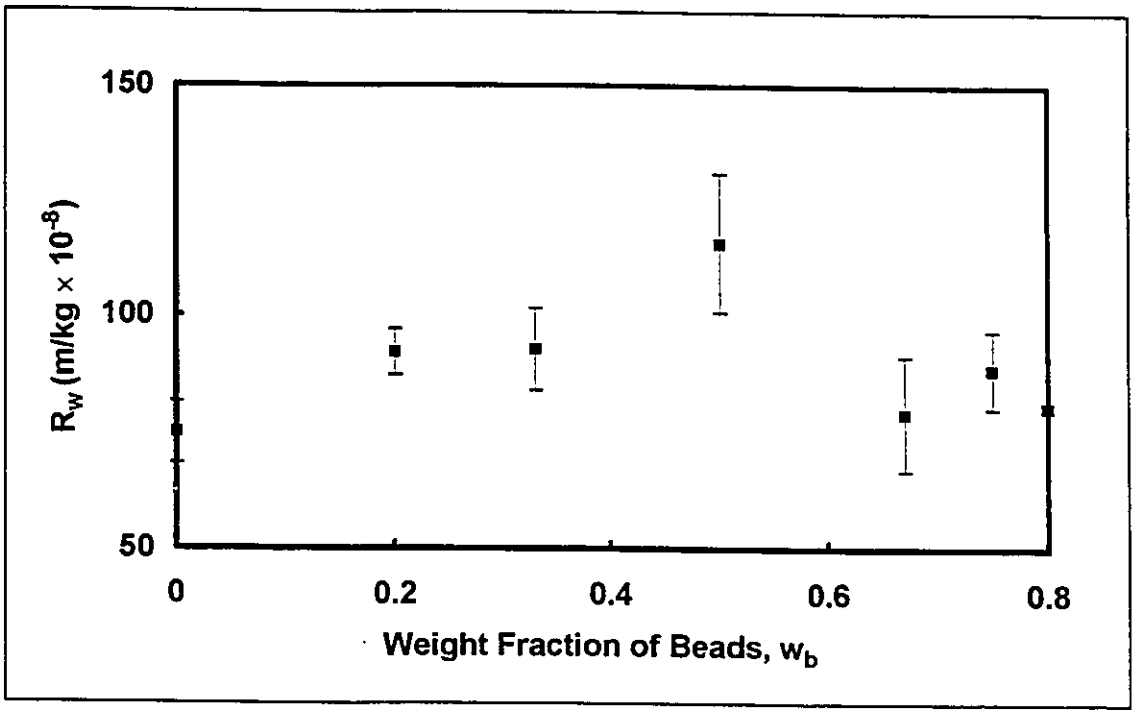

Figure 6.4.4 Specific filtration resistance plotted against weight fraction of beads in the fibre cake for the pulp/beads system. Individual markers are results calculated from experimental data. Each marker is the average filtration resistance of two suspensions (five suspensions in the case of slurries containing pulp fibres only) having the same composition. The error bars have the magnitude of one standard deviation of the average specific filtration resistance at the particular suspension composition.

In Figure 6.4.4, the experimentally determined steady state specific filtration resistances of suspensions having different bead contents were plotted against weight fraction of beads in the pad. The specific filtration resistance calculated was based on weight of the pulp fibres only. Up to a bead fraction of 0.5 the trend exhibited agreed with intuition that the specific filtration resistance of suspensions containing beads was higher than that of suspensions without beads. This observation agreed with and confirmed the common belief held by papermakers that the presence of a second dispersed particle increases the

filtration resistance and thus hinder the drainage of pulp suspensions. Quantitative effects of the dispersed particles which acted as a model of dispersed air bubbles on various aspects of papermaking will be discussed in detail in Chapter 7 of the thesis.

Although the specific filtration resistance increased with bead content initially, the specific filtration resistance dropped and remained essentially constant when bead weight fraction exceeded 0.5. A possible reason for this was that beyond a bead fraction of 0.5, the beads had become the major component in the pad. Therefore, there was a shift from the filtration characteristics of pulp fibres to the filtration characteristics of plastic beads. Consequently, the value of the filtration resistance dropped abruptly. Due to the rigid incompressible nature of the beads, further increase in bead fraction would not affect the microstructure of the filter cake and thus the filtration resistance remained almost constant.

Figure 6.4.5 for the pulp/nylon fibre system shows that an increase in the weight fraction of nylon fibres only results in a reduction in specific filtration resistance, regardless of whether the weight of the nylon fibres were included or not. This suggests that the extremely rigid nylon fibres had the effect of building an open network structure right at the start and thus the presence of the nylon fibres created channels for flow so that filtration was enhanced. This rigidity effect of the nylon fibres was so pronounced that the contribution of the pulp fibres to specific filtration resistance was overshadowed.

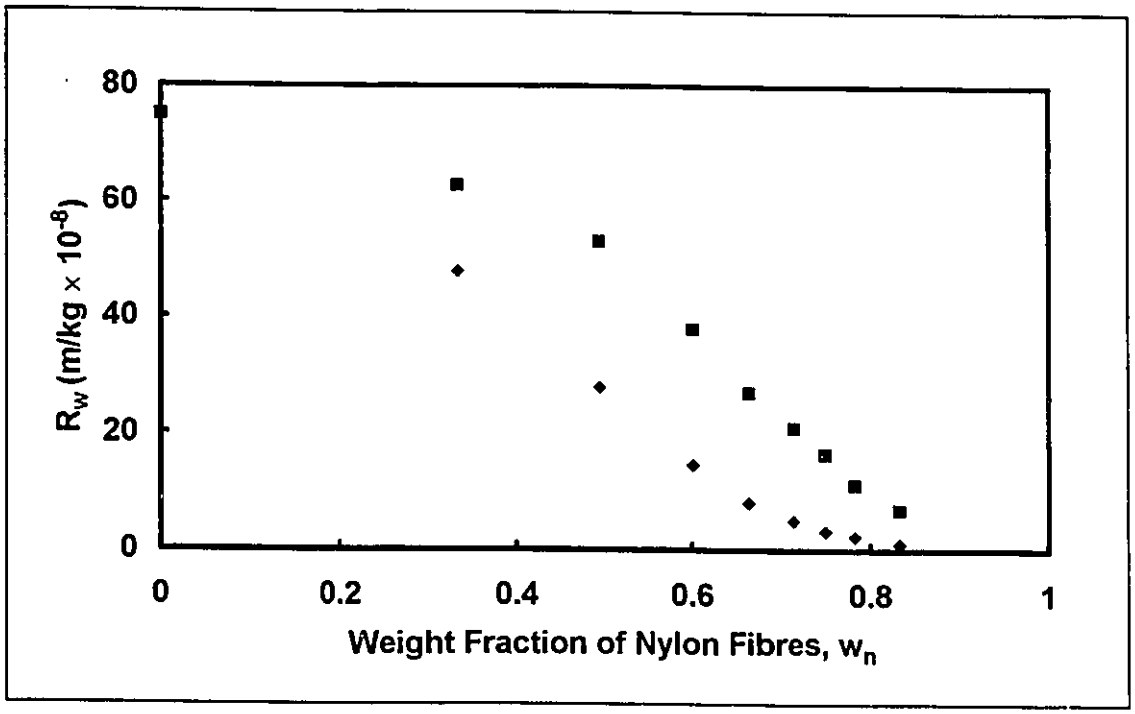

Figure 6.4.5 Specific filtration resistance plotted against weight fraction of nylon fibres in the fibre cake for the pulp/nylon fibres system. Individual markers are results calculated from experimental data. ■: specific filtration resistance calculated based on weight of pulp fibres only; ◆: specific filtration resistance based on total weight of solids.

In Figure 6.4.6, specific filtration resistance of the ternary system of pulp, nylon fibres and plastic beads is shown. Since the composition of fibres was constant in this system while the bead content was kept low, one would expect the behaviour to be similar to that exhibited by pulp/beads system at low bead content. That was, the presence of the plastic beads would cause an increase in the specific filtration resistance. The data in Figure 6.4.6 illustrates this point. An increase in bead content resulted in a systematic increase in the specific filtration resistance calculated based on weight of fibres alone. The relationship between weight content of beads and the specific filtration resistance appeared

to be linear. However, experimental data was limited to a bead weight fraction of 0.22. Therefore, no conclusion could be made about the linearity of the relationship. Otherwise, knowledge of the specific filtration resistance at high bead content would provide useful insight into the trend observed with pulp/bead system in Figure 6.4.4.

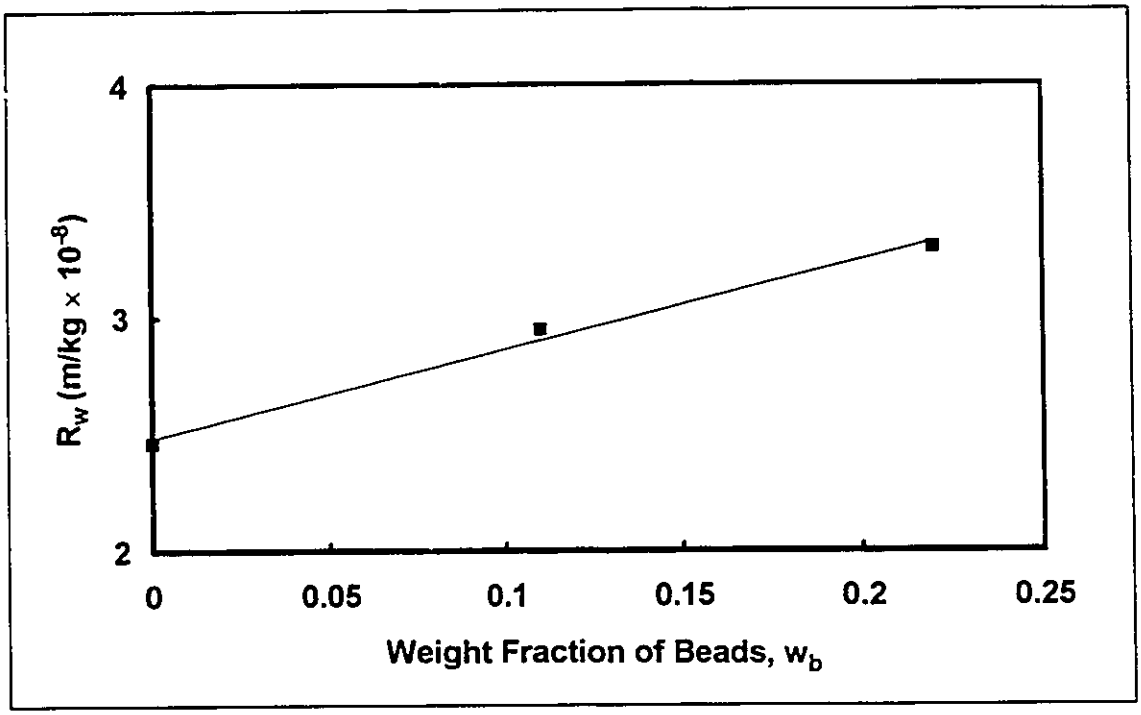

Figure 6.4.6 Specific filtration resistance plotted against weight fraction of beads in the fibre cake for the pulp/nylon fibres/beads system. Individual markers are results calculated from experimental data.

6.5 Conclusions

1. Excellent agreement between experimental data and a numerical simulation was obtained for the pressure drop data. The agreement between simulated and experimental filtrate weight data deteriorated towards later stages of the

filtration process. A possible cause of this discrepancy was that a constant concentration profile was assumed throughout the filtration experiment regardless of the compressive pressure acting on the fibre pad.

2. c_{max}, an adjustable parameter, was shown to be a function of the bead content and it increased with increasing bead content for both pulp/bead systems and pulp/nylon fibre/bead systems.
3. c_{max} for pulp/nylon fibres system was found to be a function of the nylon fibre content and it displayed a maximum at some intermediate weight fraction of nylon fibres.
4. For the pulp/beads system, experimental results shown that the presence of a second dispersed particle in the pulp suspensions caused an increase in specific filtration resistance as long as the beads remained the minor component.
5. For pulp/nylon fibres system, an increase in nylon fibre content resulted in a reduction in specific filtration resistance.
6. For bead weight fraction below 0.22, specific filtration resistance of suspensions containing pulp/nylon fibres and beads was proportional to bead content.
7. c_{max} values for the pulp fibre/nylon fibre/plastic bead system could be predicted from results of the pulp fibres/beads system to within 15% of the actual value.

7. IMPLICATIONS FOR PAPERMAKING

7.1 Introduction

The objective of this chapter is to illustrate the influence of dispersed air bubbles on pulp and paper manufacture by applying the results obtained in previous chapters on permeation and filtration of pulp fibres, plastic beads and nylon fibres systems to pulp dewatering and brownstock washing. The chapter begins with a discussion of the effects of entrained air bubbles on the specific filtration resistance of pulp suspensions. Since the predominant mechanism of pulp drainage on a paper machine is filtration [Radvan, 1965; Parker, 1972], the effect of dispersed air content on the specific filtration resistance of the pulp is of vital importance. Discussion on the effect of dispersed air on the freeness of pulp suspensions and the drainage of water through pulp pads under brownstock washing conditions is presented next. The chapter concludes with a presentation of the effects of rigid fibres on the dewatering of pulp suspensions.

7.2 Correlation Between Dispersed Air Content and Specific Filtration Resistance of Pulp Suspensions

Papermakers have long recognized that dispersed air bubbles in headbox pulp suspensions interfere with water removal on the paper machine wire and result in reduction of drainage rate as well as poor paper machine performance [Mardon & Gavelin, 1955]. Brecht and Kirchner [1961] have shown with British handsheet studies that with increasing air content, drainage time and air

permeability increased while tensile strength, wet-web strength and smoothness decreased. Although the handsheet studies by Brecht and Kirchner [1961] had shown that drainage time of pulp suspensions increased with increasing amount of dispersed air, no mathematical correlation describing the drainage characteristics of air-containing pulp on a paper machine is found in the pulp and paper literature. However, equations relating the dewatering of air-free pulp over drainage elements to the filtration resistance of the pulp slurry are available from the literature since the dewatering mechanism of pulp on a paper machine is primarily filtration [Radvan, 1965]. Therefore, knowledge of the filtration resistance of air-containing pulp suspension enables the prediction of pulp drainage in the presence of dispersed air on the paper machine. Consequently, filtration experiments using pulp suspensions that contain dispersed air are necessary to provide the information.

Unfortunately, it is difficult to study the effects of dispersed air on the filtration of pulp slurries in a reproducible and systematic manner because of the dynamic nature and instabilities of the bubbles; coalescence, dissolution or nucleation of bubbles due to pressure changes in the system are always possible and cannot be accounted for. An alternative approach to resolve the problem is to use plastic beads as a substitute for air bubbles in the experiments. There are some advantages of using plastic beads instead of dispersed air bubbles in filtration experiments: 1) the content of plastic beads always remains the same in the suspension while air bubbles may coalesce to form larger bubbles which rise to the surface of the suspension and escape to the atmosphere, 2) plastic beads neither dissolve nor grow in size in the suspension due to pressure changes and 3) at the conclusion of the experiments

when the fibre beds are dried, the plastic beads will remain in the fibre bed so that analysis of the position of the dispersed particles can be carried out while air bubbles will disappear rendering the analysis impossible. However, there are also limitations in using plastic beads as a model of air bubbles. The limitations are: 1) air bubbles are compressible while plastic beads are not. Therefore, the effect of bubbles on the compressibility of the fibre pad is not well simulated in the model system; 2) the plastic beads have a density higher than that of the bubbles. Therefore, the beads tend to sink in the suspension while the bubbles have the opposite tendency; and 3) air bubbles and plastic beads may not have the same degree of adhesion to pulp fibres. With full awareness of the limitations of using plastic beads, filtration and permeation experiments have been carried out using model suspensions of kraft pulp fibres containing plastic beads at different concentrations. Results from the permeation experiments and the filtration experiments were presented in Chapter 4 and Chapter 6 respectively.

According to Ingmanson et al. [1952, 1954, 1955, 1957, 1959a, 1959b, 1959c, 1959d, 1963, 1964], properties of the materials in the fibre bed (specific surface area and specific swollen volume of the pad materials) together with an appropriate equation describing the compressive response of the fibre pad can be used to predict the specific filtration resistance of the suspension by Equation (2.3.9) (derivation and discussion of the equation were presented in Section 2.3.2). Therefore, it is necessary to have an equation for the compressive response of a pulp pad and data on the pad properties in order to apply Equation (2.3.9).

Equation (5.2.1.2) which was obtained from regression analysis of the thickness data of a pulp pad under compression is the ideal equation for

describing the compressive response of the pulp pad. Data on the specific surface area and specific swollen volume of materials from pads containing various amounts of beads are available from Chapter 4. However, since the plastic beads are only a model of dispersed air bubbles, the weight of the beads should be neglected in the calculation of the specific filtration resistance so that the predicted results can illustrate the effect of dispersed air on filtration resistance. Therefore, data on the specific surface area and specific swollen volume were corrected for the weight of the beads and the corrected data based on the weight of pulp fibres only are presented in Figure 7.2.1.

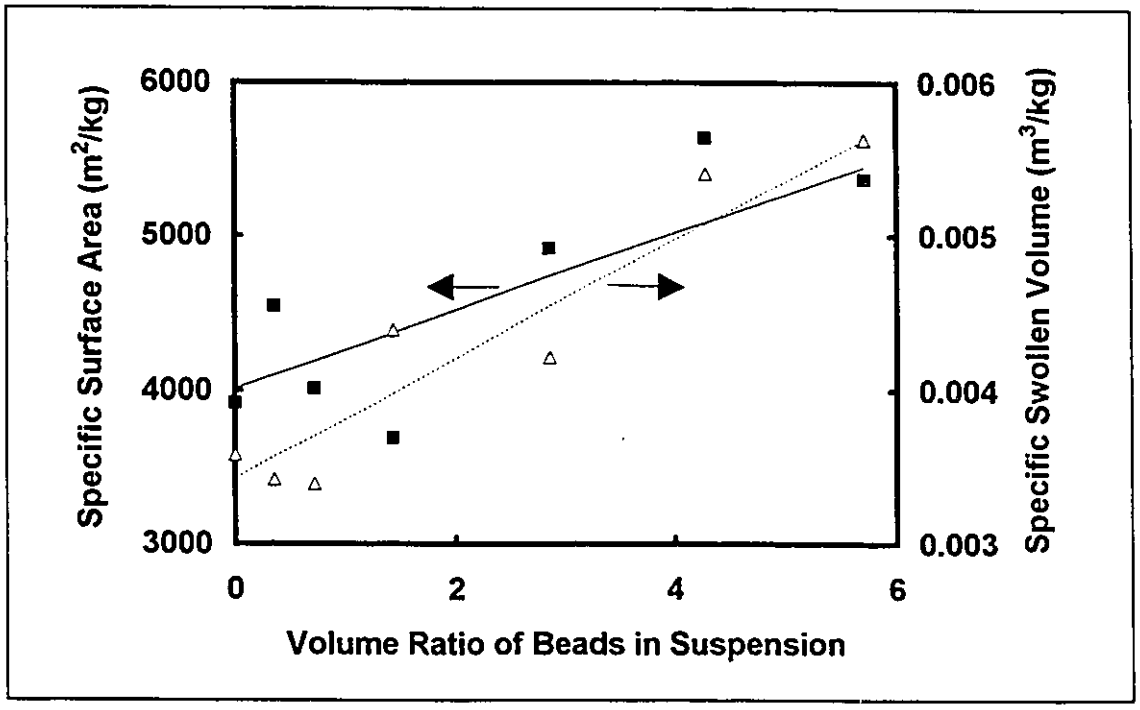

Figure 7.2.1 Specific surface area and specific swollen volume of bead-containing pulp plotted as a function of the volume ratio of beads in the suspension. ■: specific surface area; △: specific swollen volume; ——: linear fit of the specific surface area data; and – –: linear fit of the specific swollen volume data.

Data presented in Figure 7.2.1 show that both the specific surface area and specific swollen volume increase with an increase in the amount of beads in the suspension. Equation (2.3.9) was applied to predict the specific filtration resistance of bead containing pulp suspensions by using the corrected specific surface area and specific swollen volume data and Equation (5.2.1.2). Predicted specific filtration resistance of the suspensions is plotted as a function of the volume ratio of beads in the suspension in Figure 7.2.1. The volume ratio of beads used in Figure 7.2.1 was the ratio of bead volume to fibre volume in the suspension. The bead volume used in the calculation of volume ratio was computed based on a bead density of 1050 kg/m^3 while the fibre volume was calculated using a fibre density of 1500 kg/m^3.

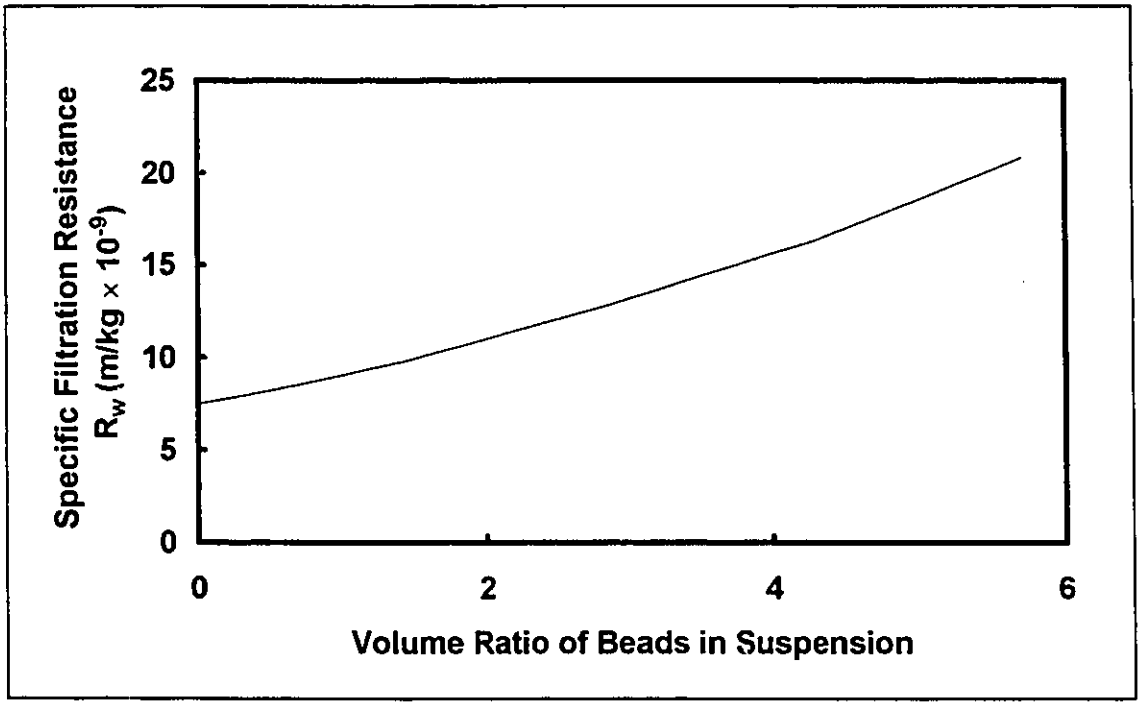

Figure 7.2.2 Specific filtration resistance of bead-containing pulp suspension plotted as a function of the ratio of bead volume to fibre volume in the suspension.

It is evident from Figure 7.2.2 that an increase in the amount of dispersed air bubbles leads to an increase in the specific filtration resistance of the pulp suspension. This phenomenon supports the observation by Brecht and Kirchner [1961] that drainage time of a pulp suspension in a handsheet machine increased with dispersed air content. In summary, the presence of dispersed air causes an increase in the filtration resistance of the pulp suspension and it is possible to predict the filtration resistance of air-containing suspensions by using properties of the pad materials. Therefore, with the predicted information on the specific filtration resistance of air-containing pulp suspensions, the effect of air bubbles on the drainage of pulp on a paper machine can be estimated using existing drainage equations from the pulp and paper literature.

7.3 Effect of Dispersed Air Bubbles on the Freeness of Pulp Suspensions

Freeness is the parameter that is widely used in the pulp and paper industry to characterize the degree of beating and refining of the pulp fibres [Casey, 1980]. Freeness tests measure how rapidly water drains away from a fixed volume of pulp suspension at a specific consistency and temperature. Therefore, in addition to being an indication of the degree of refining of the pulp fibres, the freeness test also serves as a measurement of the drainage properties of the pulp suspension. There are two standard instruments that are most widely used in the pulp and paper industry for measuring freeness: 1) the Canadian Standard Freeness tester (C.S.F.) which is used mainly in North America and is described in TAPPI standard T227 (also described in the

Canadian Pulp and Paper Association standard method (CPPA C.1)) and 2) the Schopper-Riegler (SR) wetness tester which used mainly in Europe and is described in ISO Specification TC 6/SC5-215E-1968 and the German standard Merkblatt 107. The Canadian Standard Freeness tester consists of a drainage chamber and a funnel-shaped receiver. Freeness measurement starts when 1 L of pulp suspension at 0.3% consistency is poured into the drainage chamber and water is allowed to drain from the chamber into the funnel receiver. The funnel receiver is constructed with a calibrated bottom orifice and a side overflow discharge. Water that exits from the side overflow is collected until drainage is complete. The volume of water collected is measured and corrected for temperature and consistency and it is called the Canadian Standard Freeness of the pulp. The great advantage of freeness tests is that they can be carried out easily in a short duration of time. Another advantage of the tests is that they are widely used by papermakers and the freeness results are accepted by papermakers. Therefore, freeness tests are the drainage measurement and pulp characterization method commonly used in paper mills today. If the correlation between freeness and specific filtration resistance is coupled with the correlation between the air content in pulp and specific filtration resistance, then it is possible to obtain air content information from freeness test results. An alternative way is that if the correlation between specific surface area and specific swollen volume of the pulp, which are pulp properties that can be measured easily in paper mills, is known and the relationship between dispersed air content and the specific surface area and specific swollen volume is available, the freeness test can again be used to provide information on the dispersed air content in pulp suspensions.

In the two papers by El-Hosseiny and Yan [1980], a drainage model for the Canadian Standard Freeness tester was derived from first principles using Darcy's law and the Kozeny-Carman equation. Two equations were obtained by the authors; one equation related freeness to the specific filtration resistance of the pulp suspension and the other related freeness to the specific surface area and specific swollen volume of the pulp fibres. The two equations are:

$$CSF = \frac{10^7}{10^4 + 1.11 \cdot c_0 \mu R} + \frac{1.11 \cdot c_0 \mu R}{10^4} \times \left[\frac{10^7}{10^4 + 1.11 \cdot c_0 \mu R} + 1000 \cdot \ln\left(1000 - \frac{10^7}{10^4 + 1.11 \cdot c_0 \mu R}\right) - 6907.76 \right] - 23.5$$

,,,,(7.3.1, derived from Darcy's law)

and

$$CSF = \frac{10^7 (1-\alpha c)^3}{10^4 (1-\alpha c)^3 + 6.164 \cdot c_0 \mu \sigma^2 c} + \frac{6.164 \cdot c_0 \mu \sigma^2 c^2}{10^4 (1-\alpha c)^3 c} \times \left[\frac{10^7 (1-\alpha c)^3}{10^4 (1-\alpha c)^3 + 6.164 \cdot c_0 \mu \sigma^2 c} + 1000 \cdot \ln\left(1000 - \frac{10^7 (1-\alpha c)^3}{10^4 (1-\alpha c)^3 + 6.164 \cdot c_0 \mu \sigma^2 c}\right) - 6907.7 \right] - 23.5$$

.... (7.3.2, derived from the Kozeny-Carman equation)

In the equations, α and σ are the specific swollen volume and specific surface area of the pulp fibres, c_0 is the initial consistency of the suspension in the drainage chamber, μ is the viscosity of the water, R is the specific filtration resistance of the suspension and c is an average concentration of pad materials through out the duration of the freeness test. Using Equations (7.3.1) and (7.3.2) with the data in Figures 7.2.1 and 7.2.2, the correlation between air content in pulp and freeness can be established, thereby enabling the prediction of air content from freeness values.

The specific surface area and specific swollen volume presented in Figure 7.2.1 were used in Equation (7.3.2) to estimate the freeness of air-containing suspensions. A c_0 value of 3 kg/m^3 (the fixed initial slurry consistency in a Canadian Standard Freeness tester), a water viscosity of 10^{-3} Pa.s and a constant arbitrary c value of 20 kg/m^3 were used in the calculations of the freeness of the suspensions. Results of the calculations are shown in Figure 7.3.1 to illustrate the correlation between bead content and the freeness of the pulp suspension.

Data in Figure 7.3.1 show that Canadian Standard Freeness is correlated with the amount of dispersed air bubbles in the pulp suspension; an increase in the dispersed air content results in a decrease in the freeness values. Reduction in the freeness value of a pulp indicates that the pulp suspension is less free, meaning that the pulp offers a higher resistance to flow. Therefore, the CSF calculation supports the observation with predicted specific filtration resistance results that the presence of dispersed air bubbles causes an increase in the resistance of the pulp suspension to dewatering.

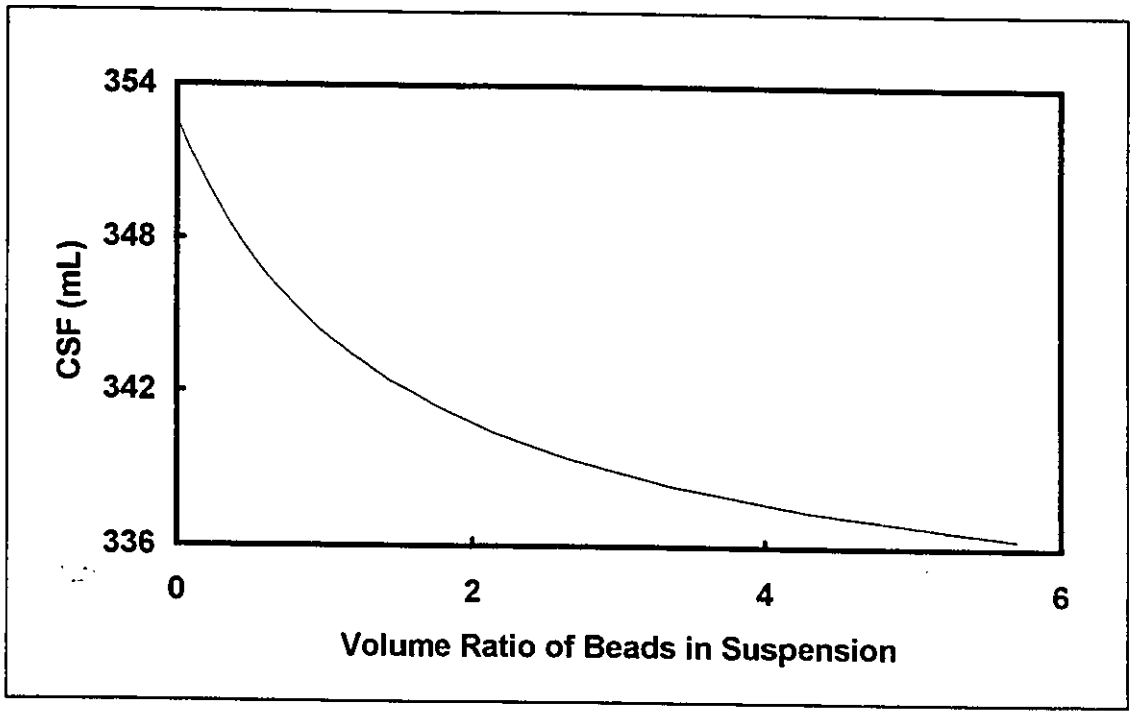

Figure 7.3.1 Canadian Standard Freeness of a bead-containing pulp suspension predicted by Equation (7.3.2) using corrected specific surface area and specific swollen volume data and the parameters of: c_0 = 3 kg/m^3, μ = 10^{-3} Pa.s and c = 20 kg/m^3.

7.4 Effect of Dispersed Air on Brownstock Washing

Brownstock washing is illustrative of pulp washing operations in a pulp and paper mill. In brownstock washing, a pulp bed is formed on the exterior of a rotating drum under the help from a partial vacuum inside the drum. Water is sprayed onto the top surface of the bed to displace black liquor, the solution of lignin fragments and spent pulping chemicals, from the mat by the wash water under the action of a vacuum applied inside the cylinder. Therefore, the operating principle of the washing process may be considered in terms of the fluid permeability of compressible fibrous media.

It has been demonstrated by experimental data in previous chapters that the presence of dispersed plastic beads in pulp fibre pads resulted in a decrease in pad permeability when the weight of the beds was neglected. Therefore, when the beads were replaced by dispersed air bubbles since the beads were only models of the bubbles, the permeability of a pulp pad that contained dispersed air was much lower than that of an air-free pad. In brownstock washing, air bubbles are present in the pulp suspension contained in the vat. When the pulp mat is formed on the surface of the cylinder due to the vacuum applied, both the pulp fibres and the entrained air bubbles are introduced into the mat. These bubbles stay in the pulp pad during the washing process and cause a reduction in the permeation rate of water through the pulp mat as well as a reduction in the efficiency in the brownstock washer. Therefore, brownstock washing is extremely susceptible to drainage impairment by dispersed air bubbles. This effect is illustrated by the following calculation. Assume that the pulp consistency in a mat on a brownstock washer is 10% (111 kg/m^3) and the pulp mat has a dispersed air content of 1% by volume. This situation corresponds to a volume ratio of plastic beads to pulp fibres of 0.13. From the results obtained in Chapter 4, the corrected specific surface area and specific swollen volume of the pad materials are 3925 m^2/kg and 0.00367 m^3/kg. The resulting permeability of the pad containing air calculated by the Kozeny-Carman equation (Equation (2.2.9)) is 1.98×10^{-13} m^2 while the permeability of the air-free pad is 2.08×10^{-13} m^2. Therefore, there is a 5% reduction in the permeability due to 1% entrained air. Using Darcy's law (Equation (2.2.1)) while assuming a pad thickness of 5 cm, an operating temperature of 50°C and wash water is driven through the mat under a vacuum of 15 kPa, the flux of wash

water through the air-free pad is 0.103 $kg \cdot m^{-2} \cdot s^{-1}$ and the flux of water through the pad containing 1% by volume of air is 0.098 $kg \cdot m^{-2} \cdot s^{-1}$. Similar calculations were carried out using the same assumptions for dispersed air content ranging from 1% to 10% and mat consistencies at 5, 7 and 10%. The results are plotted in Figure 7.4.1 to illustrate the effect of dispersed air on drainage over a brownstock washer.

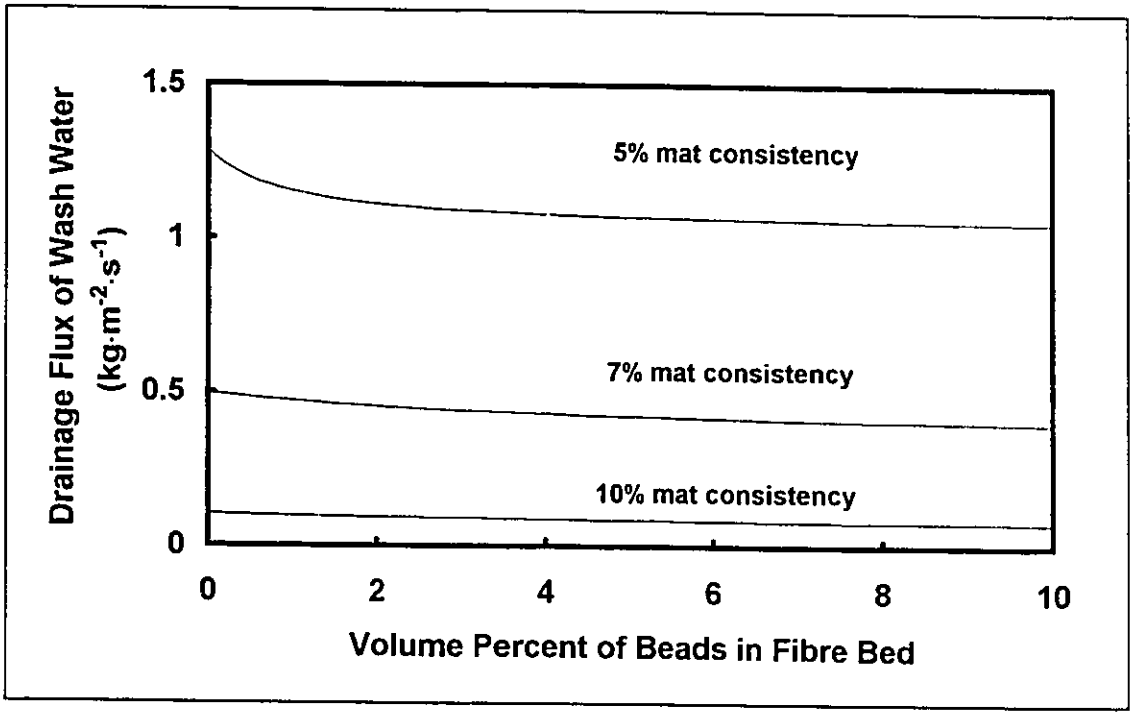

Figure 7.4.1 Flux of wash water through a 5 cm thick pulp mat under a pressure driving force of 15 kPa at a temperature of 50°C. Mat consistencies are 5, 7 and 10%. Corrected specific surface area and specific swollen volume of pad materials based on data obtained from permeation experiments using pads containing pulp fibre and plastic beads were used in the calculation of mat permeability using the Kozeny-Carman equation (Equation (2.2.9)). Mass flux of wash water through the pad was calculated using Darcy's law (Equation (2.2.1)).

7.5 Effect of Rigid Fibres on the Drainage of Pulp Suspensions

For the pulp/nylon fibre system, presence of the rigid nylon fibres has a different effect on the specific filtration resistance than the plastic beads. Figure 6.4.5 has clearly illustrated that as nylon fibre content in the suspension increased, the specific filtration resistance decreased. The reason for this phenomenon was that the nylon fibres were very rigid compared to the pulp fibres. Therefore, presence of nylon fibres in the suspension made the resulting fibre mat more open in structure and thus more permeable to flow. Consequently, a reduction in the specific filtration resistance was observed. From Figure 6.4.5, a nylon fibre content of 50% by weight in the suspension results in a specific filtration resistance of 52.2 m/kg. Compared to the value of 75 m/kg for kraft pulp, there is a 30% reduction in the specific filtration resistance. The presence of nylon fibres in the suspension has a drainage enhancing effect and other rigid fibres should produce the same result. Therefore, a possible method of drainage enhancement on the paper machine is to add either synthetic fibres or natural rigid pulp fibres to the stock suspension for the reduction in specific filtration resistance.

With the pulp/nylon fibres/plastic beads system, an increase in bead content resulted in an increase in the specific filtration resistance. This was consistent with the results exhibited by the pulp/bead system. However, specific filtration resistances of the nylon-containing suspensions were much lower than filtration resistances for nylon-free suspensions containing the same amount of beads. In summary, the effects of nylon fibres and plastic beads are additive. Therefore, in papermaking, knowledge of the content of dispersed air in the pulp

suspension allows formulation of the composition of a mixture of flexible and rigid fibres such that drainage impairment caused by the dispersed air bubbles can be compensated for by the drainage enhancing rigid fibres.

7.6 Summary

In summary, it has been demonstrated that the specific filtration resistances of dispersed air-containing pulp suspensions can be predicted by using Equation (2.3.9) and the specific filtration resistances of such suspensions increase with increasing bead (dispersed air) content. Therefore, presence of air adversely affects pulp drainage on a paper machine. Also, it is possible to predict the freeness of a pulp suspension through the use of Equations (7.3.1) and (7.3.2). Theoretical freeness of air-containing pulps indicate that increasing dispersed air content results in a decrease in the freeness value of the pulp. The presence of dispersed air bubbles in a pulp mat on a brownstock washer reduces the mass flux of wash water through the mat. The presence of rigid fibres in a mixture of pulp causes a reduction in the filtration resistance of the suspension and results in a fibre pad that has a much more open structure.

8. CONCLUSIONS AND RECOMMENDATIONS

8.1 Conclusions

Wood fibre pads having four different compositions were used in the experimental work of this research. The four different compositions were: 1) wood pulp fibres only; 2) wood pulp fibres and plastic beads; 3) pulp fibres and nylon fibres; and 4) pulp fibres, nylon fibres and plastic beads. Three different experiments: 1) constant head filtration; 2) elastic permeation; and 3) fixed bed permeation, were carried out in succession with each fibre pad.

Both SEM studies and analysis of fixed bed permeation results have shown that pulp fibres in the pads used in the experiments are perpendicular to the direction of flow, forming a random 2D layered structure. Also, all the pads, despite their composition, exhibit hysteresis when the pad goes through a complete compress-recovery cycle in the elastic permeation experiments. Thicknesses of the pads under flow induced compression during the elastic permeation experiments are linear or nearly linear functions of the pressure drop acting across the pad.

For pads containing pulp fibres and plastic beads, higher bead content in the pad results in lower effective specific surface area and lower specific swollen volume. The correlation between specific surface area and specific swollen volume of beads-containing pads can be represented by a simple linear mixing rule. Also, the presence of plastic beads does not affect the structure and thickness of the pads. Therefore, the plastic beads are probably able to fit into

the pores of the pulp pad without disrupting the structure. Experimental results for the pulp/beads system have shown that the presence of a second dispersed particle in the pulp suspensions causes an increase in specific filtration resistance as long as the beads remain as the minor component.

For pads containing pulp and nylon fibres, the higher the nylon fibre content, the lower are the effective specific surface area and specific swollen volume.. As in the case for the pulp/beads system, the effective specific surface area, specific swollen volume, and nylon fibre content in the pad is correlated by a simple mixing rule. The presence of the nylon fibres increased the permeability of the pad because the synthetic fibres had a lower specific surface area and specific volume compared to those of kraft pulp fibres. Furthermore, the rigid nylon fibres open up the pad structure to further enhance overall pad permeability.

Fibre pads consisting of kraft pulp, nylon fibres and plastic beads display trends that are the same as those observed in kraft pulp/beads systems; the effective specific surface area and specific swollen volume decrease with increasing bead content. The presence of plastic beads in kraft pulp/nylon fibre pads does not affect the thickness of the pad as the beads tended to stay inside the pores formed by the nylon fibres in the network structure. A linear mixing rule or regression equation for pulp/nylon fibre system can be used to predict the specific surface area and specific swollen volume of the kraft pulp/nylon fibre pads with low bead contents (weight fraction of beads less than 0.22) to within 7%. For bead weight fraction below 0.22, specific filtration resistance of suspensions containing pulp/nylon fibres and beads is proportional to bead content.

The Kozeny-Carman equation has been successfully applied to the study of permeation through both single component (pulp fibres only) and multi-component systems. The mathematical model proposed by Jonsson and Jonsson can be used to predict elastic permeation behaviour although concavity of the flowrate versus pressure drop curve is not predicted by any of the current models. The mathematical model for filtration pressure drop exhibited excellent agreement with experimental results. The agreement between simulated and experimental filtrate weight data deteriorated in the later stages of the filtration process. A possible cause of this discrepancy was the assumption that a constant concentration profile existed throughout the filtration experiment regardless of the compressive pressure acting on the fibre pad.

8.2 Recommendations

It has been demonstrated by the experimental data that pad specific surface areas and specific swollen volumes are linear functions of the content of beads or nylon fibres. However, there are not enough data to justify the same conclusion with the pulp/nylon/bead system. Therefore, more experiments using the ternary system should be performed to investigate the linearity of the parameters.

In this thesis research, plastic beads, due to their stability, have been used as a model replacement for dispersed air bubbles. Although the plastic beads were chosen such that their size was close to that of the bubbles, air bubbles have a tendency to adhere to pulp fibres. This tendency is not displayed by the plastic beads. Therefore, a possibility for future research is to add polymeric

flocculants to promote aggregation between plastic beads and pulp fibres so that the beads can better simulate the effects of dispersed air bubbles.

The Jonsson and Jonsson mathematical model has been used in this work to simulate elastic permeation through the fibre pads. It has been demonstrated that the numerical results provide a good fit of compression data. However, none of the compressibility functions could provide a fit to data from the recovery step; that is, the compressibility equations failed to generate a function with upward concave curvature that was exhibited by the data. In fact, all the available compressibility equations used predicted flowrate curves that were concave downwards. Therefore, improved theoretical compressibility equations are needed.

Although both the Jonsson and Jonsson model for elastic permeation and the mathematical model for filtration can be used to simulate the respective processes, none of them have accounted for the mechanisms involved in terms of the bed structures observed. Therefore, mechanistic models for the formation of the multi-component pads (filtration) and the permeation of uncompressed pads (elastic permeation) are needed to provide the necessary insights into the phenomena.

LIST OF SYMBOLS

A	cross-sectional area of a fibre bed, m^2
A_m	cross-sectional area of a manometer tube, m^2
b	parameter in Equation (2.2.36)
C, c_{slurry}	concentration of solids in the original suspension, kg/m^3
c	concentration of solid materials in a fibre bed, kg/m^3
c_{avg}	average concentration of solid materials in a fibre bed, kg/m^3
c_{max}	maximum solid concentration in a fibre bed, kg/m^3
c_{min}	minimum solid concentration in a fibre bed, kg/m^3
c_{pulp}	concentration of pulp fibres in a fibre bed, kg/m^3
c_{total}	concentration of all solid materials in a fibre bed, kg/m^3
c (Ch. 7)	average concentration of materials in a fibre bed, g/cm^3
c_0 (Ch. 7)	initial mass concentration of pulp slurry in freeness tester, g/cm^3
CSF	Canadian Standard Freeness, mL
D	diameter of a perfect sphere, m
D_p	diameter of particles in a porous bed, m
d	diameter of a perfect cylindrical fibre, m
f	parameter in Equation (3.4.4)
f_p	particle friction factor in Ergun Equation, dimensionless
g	gravitational accelaration (=9.81), m/s^2
g	exponent in Equation (3.4.4), dimensionless
h	height of water in a manometer, m
h_0	initial height of water in a manometer, m

K	permeability coefficient of a porous medium, m^2
K'	Kozeny constant for a perfect sphere (=5), dimensionless
K''	Kozeny constant for fibres (=5.55), dimensionless
L	total thickness of a fibre bed, m
L (Ch. 5)	total thickness of a fibre bed, cm
ℓ	vertical position in a fibre bed, m
M	parameter in Equation (2.2.33), $g \cdot cm^{2n} \cdot dynes^{-n} \cdot cm^{-3}$
m_s	mass of dried solid materials in a fibre bed or a filter cake, kg
N	compressibility coefficient in Equation (2.2.38), dimensionless
N	parameter in Equation (2.2.36)
n	parameter in Equation (2.2.33), dimensionless
P_h	hydraulic pressure in a fibre bed, Pa
P_m	mechanical stress on a layer of a fibre bed, Pa
P_{max}	maximum mechanical stress a fibre bed has experienced, Pa
P_{tot}	local fluid pressure on a fibre bed, Pa
ΔP, ΔP_{pad}	pressure drop across a fibre bed, Pa
ΔP_{max}	maximum pressure drop across a fibre bed, Pa
ΔP_{pipes}	pressure losses in pipes and fittings, Pa
ΔP_{total}	total hydrostatic head driving the flow, Pa
Q	volumetric flowrate of water through a fibre bed, m^3/s
R (Ch. 2)	total filtration resistance of a filter cake, m/m^2
R (Ch. 7)	average filtration resistance of a pulp slurry, cm/g
Re	Reynolds number, dimensionless
Re_p	particle Reynolds number in Ergun Equation, dimensionless
R_w	specific filtration resistance of a pulp suspension, m/kg

r	correlation coefficient of linear regression, dimensionless
r	exponent in Equations (6.3.2) and (6.3.4), dimensionless
S	surface area to volume ratio of particles in a porous bed, m^2/m^3
S_s	specific external surface area of materials in a fibre bed, m^2/kg
t	time, s
u	superficial velocity of water through a fibre bed, m/s
V	cumulative filtrate volume, m^3
V_{sa}	volume of adsorbed moisture and solid in a fibre bed, m^3
V_{tot}	total volume of a compressible fibre bed, m^3
V_v	volume of voids in a fibre bed, m^3
W	mass flowrate of water through a fibre bed, kg/s
W (Ch. 5)	mass flowrate of water through a fibre bed, g/s
w	mass of solid material per unit cross-sectional area of a fibre bed, kg/m^2
w_b	mass fraction of plastic beads in a fibre bed, dimensionless
w_n	mass fraction of nylon fibres in a fibre bed, dimensionless
X	void ratio in a fibre bed, dimensionless
X_m	void ratio in a fibre bed at the reference pressure, dimensionless
y	normalized coordinate in a fibre bed, dimensionless
z	coordinate in a fibre bed, m

Greek Letters

α, α_{sa}	specific swollen volume of materials in a fibre bed, m^3/kg
β	compressibility of material, Pa^{-1}

β	intensive property of materials in a fibre bed (Equation (4.3.4.1))
β_v	compressibility of void volume, Pa^{-1}
ε	porosity in a fibre bed, dimensionless
λ	adjustable parameter in Equation (4.3.2.4), dimensionless
μ	dynamic viscosity of water, Pa.s
μ (Ch. 7)	dynamic viscosity of water, poise
ρ	density of water, kg/m^3
σ	specific external surface area of materials in a fibre bed, m^2/kg
Ω	adjustable parameter in Equation (4.3.2.2), dimensionless

Superscripts

'	reference state

Subscripts

1	constant pressure state in cake filtration
SSF	steady state flow in elastic permeation
b	plastic beads
f	fibres (including both pulp and nylon fibres)
m	mixture
n	nylon fibres
p	pulp fibres

REFERENCES

Abe, E., Hirosue, H. & Yokota, A., "Pressure Drop through a Packed Bed of Binary Mixture", J. Chem. Eng. Jpn., **12** (4), 302 (1979).

Ajersch, M.J., Pelton, R.H., Chan, A.K.T. & Loewen, S.R., "Measuring Dispersed Air in Newsprint Pulp Suspensions", TAPPI, **75** (2), 125 (1992a).

Ajersch, M., Pelton, R., Towers, M. & Loewen, S., "The Characterization of Dispersed Air in Two Newsprint Paper Machines", J. Pulp Pap. Sci., **18** (4), J121 (1992b).

Andersson, N. & Gardh, H., "The Compression and Recovery of a Paper Web in a Felted Press", Svensk Papperstidning, **73** (13-14), 425 (1970).

Andrade, J.S., Benyahia, F., Foumeny, E.A., McGreavy, C. & Rajagopal, K., "On the Permeability of Binary Packings of Spheres", Chem. Eng. Tech., 15, 11 (1992).

Barkowski, E., "Air in Aqueous Stock Suspensions-Method for Determining Air Content", Papiermacher, **28** (3), 44-46 (1978).

Barrett, T. and MacKay, D., "Aeration index measurement of defoamer effectiveness", TAPPSA 3rd Intrn. Tech. Conf. (1986).

Bear, J., **Dynamics of Fluids in Porous Media**, Am. Elsevier Pub. Com., Inc., New York (1972).

Bennett, C.O. & Myers, J.E., **Momentum, Heat and Mass Transfer**, 3rd Edition, McGraw-Hill (1982).

Bennington, C.P.J., Kerekes, R.J. & Grace, J.R., "The yield stress of fibre suspensions", Can. J. Chem. Eng., **68**, 748 (1990).

Bennington, C.P.J., Kerekes, R.J. & Grace, J.R., "Motion of pulp fibre suspensions in rotary devices", Can. J. Chem. Eng., **69**, 251 (1991).

Bird, R.B., Stewart, W.E. & Lightfoot, E.N., **Transport Phenomena**, Wiley, New York (1960).

Boadway, J.D., "Gas in papermaking stock", Pulp Pap. Mag. Can., Convention Issue, (1956).

Brecht, W. & Kirchner, U., "The air content of paper pulp suspensions", Das Papier, **15** (10a), 625 (1961).

Branion, R.M.R., **Drainage of the Paper Machine - A Review**, presented at the 63rd Annual Meeting of the Technical Section, CPPA, Montreal, Feb. (1977).

Brown, J.C., "Determination of the exposed specific surface of pulp fibres from air permeability measurements", TAPPI, **33**, 130 (1950).

Brown, G.G., et al., **Unit Operations**, John Wiley & Sons, Inc., New York (1950).

Cain, C.W., "Filtration theory" & "Filter-aid filtration" in **Handbook of Separation Techniques for Chemical Engineers**, P.A. Schweitzer (Editor), McGraw-Hill (1979).

Campbell, W.B., "The physics of water removal", Pulp Pap. Mag. Can., **48** (conv. issue) (3), 103 (1947).

Carlsson, G., Lindstrom, T. & Floren, T., "Permeability to water of compressed pulp fibre mats", Svensk Papperstidning, **86**, R128 (1983).

Carman, P.C., "Fluid flow through granular beds", Trans. Inst. Chem. Engrs., **15**, 150 (1937).

Carman, P.C., "Fundamental principles of industrial filtration", Trans. Inst. Chem. Engrs. (London), **16**, 168 (1938a).

Carman, P.C., "The action of filter aids", Ind. Eng. Chem., **30**, 1163 (1938b).

Carman, P.C., "The determination of the specific surface of powders, I", J. Soc. Chem. Ind., **57**, 225T (1938c).

Carman, P.C., "The action of filter aids", Ind. Eng. Chem., **31** (8), 1047 (1939a).

Carman, P.C., "Determination of the specific surface of powders, part II", J. Soc. Chem. Ind., **58**, 1T (1939b).

Carman, P.C., "Some physical aspects of water flow in porous media", Discuss. Farad. Soc., **3**, 72 (1948).

Carman, P.C., **Flow of Gases through Porous Media**, Butterworth Scientific Publishers, London (1956).

Carnaby, G.A. & Pan, N., "Theory of the compression hysteresis of fibrous assemblies", Textile Res. J., **59**, 275 (1989).

Casey, J.P. (Editor), **Pulp and Paper: Chemistry and Chemical Technology**, Vol. 1 & 2., 3rd Edition, Wiley-Interscience (1980).

Caulfield, D.F., Young, T.L. & Wegner, T.H., "The role of web properties in water removal by wet pressing: characterization of dewatering time constant", TAPPI, **65** (2), 65 (1982).

Chi, S-M., Klinzing, G.E., Chang, S-H. & Wen, W.W., "Effect of entrapped air bubbles on fine coal dewatering via filtration", Powder Tech., **45**, 25 (1985).

Clarenburg, L.A. & Werner, R.M., "Aerosol filters: pressure drop across multicomponent glass fibre filters", Ind. Eng. Chem., Proc. Des. Dev., **4** (3), 293 (1965).

Clarenburg, L.A. & Schiereck, F.C., "Aerosol filters-II. Theory of the pressure drop across multi-component glass fibre filters", Chem. Eng. Sci., **23**, 773 (1968).

Canadian Pulp and Paper Association Reference Tables (1986).

Darcy, H., "Les Fontaines Publiques de la Ville de Dijon", Dalmont, Paris (1856).

Davies, C.N., "The separation of airborne dust and particles", Proc., Inst. Mech. Eng. (London), **B1**, 185 (1952).

De Cew, J.A., "The adverse function of gases in the manufacture of paper", Paper Trade J., Tech. Asso. Sec., **43**, April 11, (1935).

Dougherty, S.J., "Online entrained-air measurement for brownstock-washer defoamer control", TAPPI, **72** (1), 50 (1989).

Dullien, F.A.L., **Porous Media: Fluid Transport and Pore Structure**, Academic Press, (1979).

Duskin, A.W. & Jenkins, W.B., "The deculator on a kraft paper machine", TAPPI, **36** (11), 490 (1953).

El-Hosseiny, F. & Yan, J.F., "Analysis of Canadian standard freeness, part I. Theoretical considerations", Pulp Pap. Can., **81** (6), 61 (1980a).

El-Hosseiny, F. & Yan, J.F., "Analysis of Canadian standard freeness, part II. Practical implications", Pulp Pap. Can., **81** (6), 67 (1980b).

El-Hosseiny, F., "Mathematical modelling of wet pressing of paper: a review of the literature", Nord. Pulp Pap. Res. J., **6** (1), 30 (1991).

Elias, T.C., "Investigation of the compressive response of ideal unbonded fibrous structures", TAPPI, **50** (3), 125 (1967).

Emersleben, O., Phys. Z., **26**, 601 (1925).

Ethier, C.R., "Flow through mixed fibrous porous materials", AIChE J., **37** (8), 1227 (1991).

Fair, G.M. & Hatch, L.P., "Fundamental factors governing the streamline flow of water through sand", J. Am. Water Works Asso., **25**, 1551 (1933).

Fowler, J.L. & Hertel, K.L., "Flow of a gas through porous media", J. App. Phys., **11**, 496 (1940).

Gavelin, G., "Some effects of gases on properties of fibre suspensions", Can. Pulp Pap. Asso. Tech. Sect., 240 (1954).

Gertjejansen, R.O., "Method for determining the average specific filtration resistance of pulps at constant pressure", TAPPI, **47** (1), 19 (1964).

Gertjejansen, R.O., "Gas-liquid relationships and their effect upon the permeability of wood pulp pads to water", Ph.D. thesis, University of Minnesota (1966).

Gertjejansen, R. & Hossfeld, R., "Gas-liquid relationships and their effect upon the permeability of wood pulp pads to water", TAPPI, **50** (4), 204 (1967).

Goumeniouk, G.I., "The effect of air on drainage and sheet formation on a Fourdrinier paper machine", Pulp Pap. Mag. Can., **99**, Jan., (1954).

Grace, H.P., "Resistance and compressibility of filter cakes, part 1", Chem. Eng. Prog., **49** (6), 303 (1953a).

Grace, H.P., "Resistance and compressibility of filter cakes, part 2", Chem. Eng. Prog., **49** (7), 367 (1953b).

Gurnham, C.F. & Masson, H.J., "Expression of liquids from fibrous materials", Ind. Eng. Chem., **38** (12), 1309 (1946).

Guzy, C.J., Bonano, E.J. & Davis, E.J., "The Analysis of Flow and Colloidal Particle Retention in Fibrous Porous Media", J. Coll. Interf. Sci., **95**, 523 (1983).

Han, S.T., "Compressibility and permeability of fibre mats", Pulp Pap. Mag. Can., **70** (T 134), 65 (1969).

Happel, J., "Viscous flow relative to arrays of cylinders", AIChE J., **5** (2), 174 (1959).

Happel, J. & Brenner, H., **Low Reynolds Number Hydrodynamics**, Noordhoff Int. Pub. (1973).

Hatch, L.P., "Flow through Granular Media", J. Appl. Mech., Sept., A-109 (1940).

Heertjes, P.M., "Industrial filtration", Research (London), **3**, 254 (1950).

Heertjes, P.M. & Zuideveld, P.L., "Clarification of Liquids Using Filter Aids. Part III. Cake Resistance in Surface Filtration", Powder Tech., **19**, 45 (1978).

Higgins, H.G. & DeYong, J., "Visco-elasticity and consolidation of the fibre network during free water drainage", Tech. Sect. BP & BMA, Cambridge (1965).

Hoering, J.F., Ellis, E.R., Jewett, K.B., Ceckler, W.H. & Thompson, E.V., "Dynamic compression of paper. II. Compression behaviour of saturated cellulose mats", J. Pulp Pap. Sci., TR 140, Nov. (1983).

Hoffing, E.H. & Lockhart, F.J., "Resistance to filtration", Chem. Eng. Prog., **47** (1), 3 (1951).

Howells, I.D., "Drag Due to the Motion of a Newtonian Fluid Through a Sparse Random Array of Small Fixed Rigid Objects", J. Fluid Mech., **64**, 449 (1974).

Iberall, A.S., Res. Nat. Bus. Stand., **45**, 398 (1950).

Ingmanson, W.L., "An investigation of the mechanisms of water removal from pulp slurries", TAPPI, **35** (10), 439 (1952).

Ingmanson, W.L., "Filtration resistance of compressible materials", Chem. Eng. Prog., **49** (11), 577 (1953).

Ingmanson, W.L. & Whitney, R.P., "The filtration resistance of pulp slurries", TAPPI, **37** (11), 523 (1954).

Ingmanson, W.L., "Filtration resistance on the Fourdrinier table roll section", TAPPI, **40** (12), 936 (1957).

Ingmanson, W.L. & Andrews, B.D., "The effect of beating on filtration resistance and its components of specific surface and specific volume", TAPPI, **42** (1), 29 (1959a).

Thode, E.F. & Ingmanson, W.L., "Factors contributing to the strength of a sheet of paper: I. external specific surface area & swollen specific volume", TAPPI, **42** (1), 74 (1959b).

Ingmanson, W.L. & Thode, E.F., "Factors contributing to the strength of a sheet of paper: II. relative bonded area", TAPPI, **42** (1), 83 (1959c).

Ingmanson, W.L., Andrews, B.D. & Johnson, R.C., "Internal pressure distributions in compressible mats under fluid stress", TAPPI, **42** (10), 840 (1959d).

Ingmanson, W.L. & Andrews, B.D., "High-velocity water flow through fibre mats", TAPPI, **46** (3), 150 (1963).

Ingmanson, W.L., "Filtration of high-consistency fibre suspensions", TAPPI, **47** (12), 742 (1964).

Isler, W. and Widmer, F., "Creation and removal of air bubbles from technical paper stock suspensions. Part 1: gaseous air content of paper stock suspensions in closed white water systems", Papier, **32** (11), 473 (1978).

Isler, W. and Widmer, F., "Creation of and removal of air bubbles from technical paper stock suspensions. Part 2: bubble separation from pulp suspensions in closed and open flow channels", Papier, **33** (3), 89 (1979).

Jackson, G.W. & James, D.F., "The permeability of fibrous porous media", Can. J. Chem. Eng., **64**, 364 (1986).

Jacobsson, J.J., "Deaeration of paper stock with or without cleaning", TAPPI, **41** (5), 179A (1958).

Jacobsson, J.J., "Complete deaeration as a basic necessity: comparison of energy demands and various applications of the deculator system", Wochen. Papier., **7**, 221 (1981).

Jones, R.L., "The effect of fibre structural properties on compression response of fibre beds", TAPPI, **46** (1), 20 (1963).

Jonsson, B., Petersson, E. & Lindman, B., "Mechanical dewatering of peat", Fuel, **66** (6), 785 (1987).

Jonsson, A-S., "A new method for the estimation of residual lignin content in paper pulp", Ph.D. dissertation, Dept. Chem. Eng., Lund Institute of Technology, Lund, Sweden, (1983).

Jonsson, K.A-S & Jonsson, B.T.L., "Fluid flow in compressible porous media: I. Steady-state conditions", AIChE J., **38** (9), 1340 (1992a).

Jonsson, K.A-S & Jonsson, B.T.L., "Fluid flow in compressible porous media: II. Dynamic behavior", AIChE J., **38** (9), 1349 (1992b).

Karras, M., Pietikainen, T., Kortelainen, H. and Tornberg, J., "Ultrasonic measurement of gaseous air in pulp suspensions", TAPPI, **71** (1), 65 (1988).

Karras, M. & Springer, A., "The influence of aeration and polymer on drainage of pine kraft pulp slurries", TAPPI, **72** (2), 155 (1989).

Komori, T. & Makishima, K., "Numbers of Fibre-to-Fibre Contacts in Generai Fibre Assemblies", Textile Res J., **47**, 13 (1977).

Komori, T. & Makishima, K., "Estimation of Fibre Orientation And Length in Fibre Assemblies", Textile Res. J., **48**, 309 (1978).

Komori, T. & Makishima, K., "Geometrical Expressions of Spaces in Anisotropic Fibre Assemblies", Textile Res. J., **49**, 550 (1979).

Komori, T., Makishima, K. & Itoh, M., "Mechanics of Large Deformation of Twisted-Filament Yarns", Textile Res. J., **50**, 548 (1980).

Komori, T. & Itoh, M., "A New Approach to the Theory of Compression of Fibre Assemblies", Textile Res. J., **61**, 420 (1991a).

Komori, T. & Itoh, M., "Theory of the General Deformation of Fibre Assemblies", Textile Res. J., **61**, 588 (1991b).

Komori, T., M. Itoh and K. Takaku, "A Model Analysis of the Compressibility of Fibre Assemblies", Textile Res. J., **62** (10), 567 (1992).

Kozeny, J., Sitz.-Ber. Wiener Akad., Abt. IIa, **136**, 271 (1927).

Kropholler, H.W. & Sampson, W.W., **Sheet structure and drainage**, manuscript, presented at the "PIRA Flocculation Conference", Luxemburg, March (1992).

Kurtz, K.D., "Deaeration: some practical applications and benefits for pulp and paper mills", TAPPI Eng. Conf. proceedings, (1978).

Kurtz, K.D., "Effect of air on the pulp washer", AIChE symposium, 223, 79 (1983).

Kurtz, K.D., "Deaeration for paper machine", Latin American Tech. Paper Conf., May 29, (1987).

Kyan, C.P., Wasan, D.T. & Kintner, R.C., "Flow of single-phase fluids through fibrous beds", Ind. Eng. Chem. Fund., **9** (4), 596 (1970).

Landmark, P., "A new instrument for determination of entrained air in pulp suspensions", paper given at the Pulp and Paper Technical Convention (1967).

Lewis, W.K. & Almy, C., Ind. Eng. Chem., **4**, 528 (1912).

Lorz, R.H., "Air content, retention and drainage: important parameters in paper/board production", Proceedings 2nd Annual Meeting, (1986).

Macdonald, I.F., El-Sayed, M.S., Mow, K. & Dullien, F.A.L., "Flow through porous media - the Ergun equation revisited", Ind. Eng. Chem. Fundam., **18** (3), 199 (1979).

Operation Manual of Entrained Gas Tester, G.B. Machining Inc., Puyallup, WA, U.S.A.

Mardon, J. & Gavelin, G., Pulp Pap. Mag. Can., **56** (3), 275 (1955).

Mason, S.G., "The specific surface of fibres - its measurement and application", TAPPI, **33** (8), 403 (1950).

May, O.W. and Buckman, S.J., "Practical effects of air in papermaking", TAPPI, **58**, 2 (1975).

McCabe, W.L. & Smith, J.C., **Unit Operations of Chemical Engineering**, 3rd Edition, McGraw-Hill (1976).

Miller, S.A., "Recent Advances in Filtration Theory", Chem. Eng. Prog., **47** (10), 497 (1951).

Miller, B., "The Wetting of Fibres" in **Surface Characteristics of Fibres and Textiles**, M.J. Schick (Editor), Dekker, 428 (1977).

Operation and Maintenance Manual for Model AST-02 Process Air Tester, Product And Process Engineering Concepts (PAPEC), Summer, WA, U.S.A.

Morton, J., "Automatic brown stock defoamer control", PIMA, 11-86, Simpson-Tacoma Kraft, U.S.A.

Neale, G. & Masliyah, J.H., "Flow perpendicular to mats of randomly arranged cylindrical fibres (importance of cell models)", AIChE J., **21** (4), 805 (1975).

Parker, J.D., "The Sheet Forming Process", STAP No. 9, Technical Association of the Pulp and Paper Industry, Atlanta, Ga., (1972).

Pietikainen, T., "On-line air entrainment tests on paper machines", TAPPI, **75** (11), 185 (1992).

Pires, E.C., Springer, A.M. & Kumar, V., "A new technique for specific filtration resistance measurement", TAPPI, **72** (7), 149 (1989).

Quiller, O., "Utpressning av Vann av Cellulose", Papir-J., **26**, 312 (1938).

Radvan, B., Dodson, C. & Skold, C.G., "Detection and cause of the layered structure of paper" in "**Consolidation of the paper web**", Trans. Symp. Oxford, Sept. (1965), F. Bolam (Editor), Technical Section British Paper and Board Makers' Association, London, England, 189-215, (1966).

Rance, H.F. (Editor), **Handbook of Paper Science**, Vol. 1 & 2, Elsevier Scientific Publishing Company (1980).

Robertson, A.A. & Mason, S.G., "Specific surface of cellulose fibres by the liquid permeability method", Pulp Pap. Can., **50** (13), 110 (1949).

Robertson, A.A., "The physical properties of wet webs, part 2. fibre properties and wet web behaviour", Svensk Papperstidning, **66** (12), 477 (1963).

Roux, J.C. & Vincent, J.P., "A proposed model in the analysis of wet pressing", TAPPI, **74** (2), 189 (1991).

Rowe, P.N., "The correlation of engineering data", The Chem. Engr., CE69, Mar., (1963).

Ruth, B.F., Montillon, G.H. & Montonna, R.E., "Studies in filtration: I. Critical analysis of filtration theory", Ind. Eng. Chem., **25** (1), 76 (1933a).

Ruth, B.F., Montillon, G.H. & Montonna, R.E., "Studies in filtration: II. Fundamental axiom of constant-pressure filtration", Ind. Eng. Chem., **25** (2), 153 (1933b).

Ruth, B.F., "Studies in filtration: III. Derivation of General Filtration Equations", Ind. Eng. Chem., **27** (6), 708 (1935).

Ruth, B.F., "Correlating Filtration Theory with Industrial Practice", Ind. Eng. Chem., **38** (6), 564 (1946).

Samson, A., "The compression by liquid stress and the permeability of assemblies of wool fibres", Textile Res. J., **41**, 961 (1971).

Sedivy, O., "Air, an important factor in paper manufacture", Zellstoff und Papier, **8**, 112-118 (1979).

Shirato, M., Sambuichi, M. & Okamura, S., "Filtration behaviour of a mixture of two slurries", AIChE J., **9** (5), 599 (1963).

Shirato, M., Sambuichi, M., Kato, H. & Aragaki, T., "Internal flow mechanism in filter cakes", AIChE J., **15** (3), 405 (1969).

Smith, R.E., Hughson, G.D. & Duncan, R.D., "Determination of per cent air in paper stocks", Pulp Pap. Mag. Can., **52** (5), 107 (1951).

Smith, J.A., "Applications of deculator to fourdrinier papermachines", Pulp Pap. Mag. Can., **53**, con. issue, 169 (1952).

Smook, G.A., **Handbook for Pulp and Paper Technologists**, Joint Textbook Committee of The Paper Industry (1982).

Sparrow, E.M. & Loeffler, A.L., Jr., "Longitudinal laminar flow between cylinders arranged in regular array", AIChE J., **5** (3), 325 (1959).

Sperry, D.R., Chem. Met. Eng., **15**, 198 (1916).

Spielman, L. & Goren, S.L., "Model for predicting pressure drop and filtration efficiency in fibrous media", Environ. Sci. Tech., **2** (4), 279 (1968).

Springer, A.M. & Kuchibhotla, S., "The influence of filler components on specific filtration resistance", TAPPI, **75** (4), 187 (1992).

Sullivan, R.R. & Hertel, K.L., "The flow of air through porous media", J. App. Phys., **11**, 761 (1940).

Sullivan R.R. & Hertel, K.L., "The permeability method for determining specific surface of fibres and powders", **Advances in Coll. Sci.**, K.O. Kraemer (Editor), Vol. 1, 37, (1942).

Thode, E.F. & Ingmanson, W.L., "Factors contributing to the strength of a sheet of paper: I. external specific surface area & swollen specific volume", TAPPI, **42** (1), 74 (1959).

Troland, P., "Measuring suspended air in paper stock", TAPPI, **49**, 9, (1966).

van Wyk, C.M., "Note on the compressibility of wool", J. Textile Inst., **37**, T285 (1946).

Walas, S.M., Trans. Am. Inst. Chem. Engrs., **42**, 783 (1946).

Whitney, R.P., Ingmanson, W.L. & Han, S.T., "Some aspects of permeation, filtration, and fluidization", TAPPI, **38** (3), 157 (1955).

Wilder, H.D., "The compression creep properties of wet pulp mats", TAPPI, **43** (8), 715 (1960).

Woodworth, M.D., "Comparison of practical methods for air-in-stock measurements", TAPPI, **73** (11), 135 (1990).

Zhu, S., Pelton, R.H., Ajersch, M., Towers, M. & Baird, M.H.I., "Measurement of air bubble size using densitometer", Can. J. Chem. Eng., **71**, 269 (1993).

APPENDICES

A.1 Preliminary Experiments Using British Handsheet Machine

Handsheets are sheets of paper made from stock pulp suspensions for testing of sheet properties that usually include bursting strength and air permeability [Casey, 1980]. Since handsheets are used for test purposes, the method of making handsheets is specified in a number of standard procedures to ensure reproducibility in the results. The best known procedure is the TAPPI standard T205 that is based on a report from the Pulp Evaluation Committee of the British Paper and Board Makers Association. The apparatus described in the TAPPI standard for making handsheets is thus termed the British handsheet machine. The British handsheet machine has two main functions; it is the apparatus for preparing handsheets and it is also the apparatus that is most widely used for measuring drainage time of pulp suspensions. Drainage time is measured as the time required to drain away the water in the pulp suspension in the British handsheet machine under controlled conditions. Campbell and Young [Paper Maker, 159 (9), 58 (1969)] had studied the use of the British handsheet machine as a drainage tester. They modified the apparatus to measure the time required to drain a fixed amount of water from the handsheet machine instead of measuring the time required to drain all the water away. Equations were proposed by Campbell and Young to obtain the drainage resistance from corrected drainage time and other experimental parameters.

Brecht and Kirchner had shown experimentally that with increasing air content in a British handsheet machine, air permeability of the finished paper increased while tensile strength, wet-web strength and smoothness decreased [Brecht & Kirchner, 1961]. However, the most remarkable result among all the properties measured was that a considerable increase in drainage time was observed even only a small amount of dispersed air was present. Data presented in the article by Brecht and Kirchner on drainage time, air permeability and tensile strength are presented in Figure A.1.1.

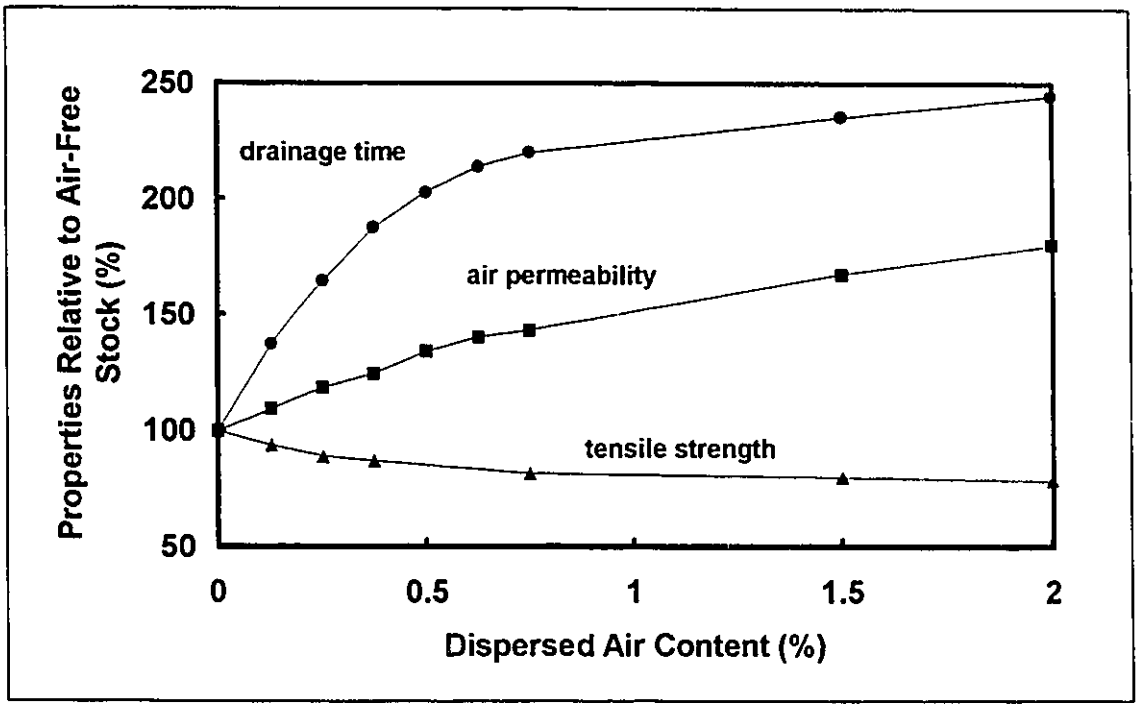

Figure A.1.1 Change in properties of groundwood handsheet relative to air free stock plotted as a function of dispersed air content. All the data are taken from experimental results presented by Brecht and Kirchner in Figure 1 of their paper (W. Brecht & U. Kirchner, Das Papier, 15, 10a, 625-634, 1961).

Before carrying out filtration and permeability experiments, preliminary experiments on a British handsheet machine similar to those performed by Brecht and Kirchner were carried out by the author to study the effects of dispersed air on the drainage of newsprint pulp suspensions. The pulp suspension used was 0.71% consistency TCMP (Thermo Chemi-Mechanical Pulp) obtained from the Abitibi-Price paper mill at Beaupré, Canada.

In a drainage experiment, pulp suspension was first introduced into the British handsheet machine followed by bubbling of air through the pulp suspension using a glass frit manufactured by Fisher Scientific. The pulp suspension was then agitated by a stirrer to ensure homogeneity and allowed to drain in the British handsheet machine. The time required for all the water to drain away was measured and recorded. In the drainage experiments, three different bubbling intervals were used: 0 (no bubbling), 60 and 120 seconds. The volume of pulp suspension introduced into the British handsheet machine took on five different values: 300, 400, 500, 600 and 700 mL.

Preliminary experiments were carried out with pulp suspensions that did not contain any defoamer or surfactant. However, contrary to intuition, bubbling interval showed no effect on the drainage time: that was, there was no difference in drainage time between suspensions that had or had not been aerated by bubbling. A possible reason for this was the instability of the bubbles in the suspensions. Therefore, a surfactant, sodium dodecyl sulphate (SDS), was added to the suspensions at a concentration of 1 g/L in all the later experiments to ensure the stability and presence of bubbles in the suspension during drainage experiments. Experimental results are summarized in Table A.1.1 and Figure A.1.2 below.

Volume of Pulp (mL)	Bubbling Time (s)	Drainage Time (s)
300	0	34
	60	36.5
	120	37
400	0	57
	60	70
	120	76
500	0	91
	60	96
	120	159
600	0	120
	60	143
	120	174
700	0	165
	60	177
	120	360

Table A.1.1 Drainage time of pulp suspension at various bubbling intervals.

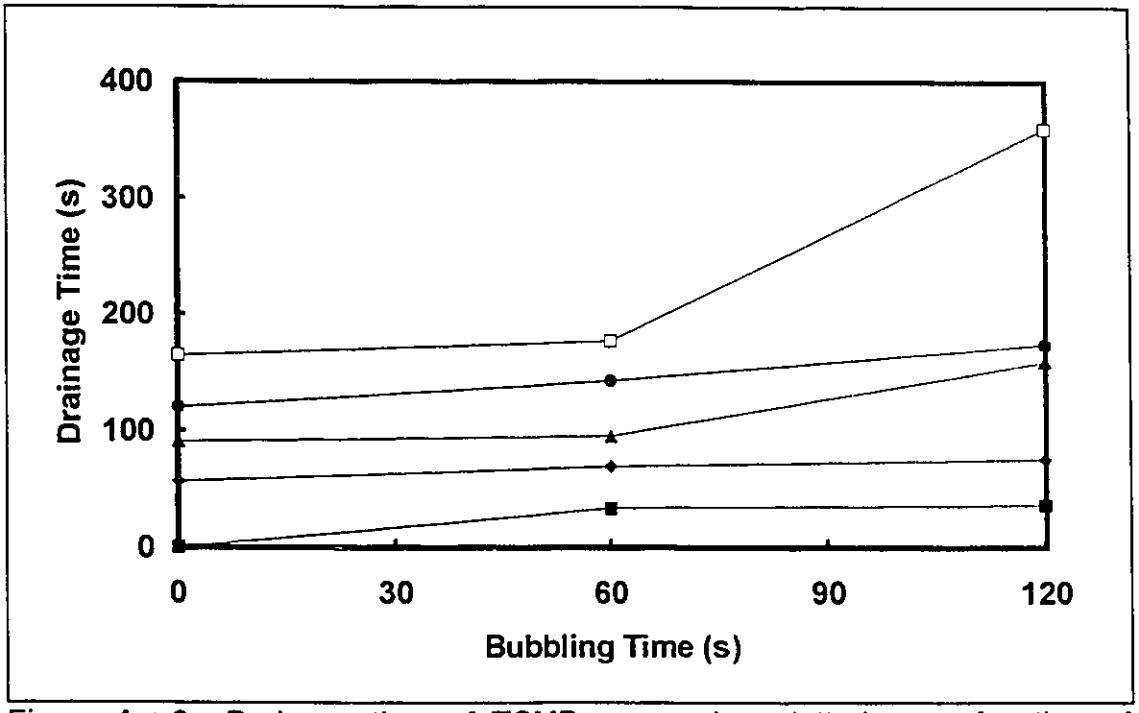

Figure A.1.2 Drainage time of TCMP suspension plotted as a function of bubbling time. The pulp suspensions used contained sodium dodecyl sulphate as a concentration of 1 g/L and bubbling of air was performed with a glass frit. Individual markers represent data from experiments using different total amount of pulp suspensions: ■: 300 mL; ♦: 400 mL; ▲: 500 mL; ●: 600 mL; □: 700 mL.

In Figure A.1.2, drainage times of TCMP suspensions were plotted as a function of bubbling time. At each bubbling time, drainage times of the suspensions exhibited the expected trend; drainage time was proportional to the total volume of suspension in the handsheet machine. When each set of data from a specific volume of pulp suspension was examined individually, another general trend was observed; for a constant volume of suspension, drainage time increased with bubbling time. Ideally, bubbling time should be proportional to the content of dispersed air in the suspensions. However, the amount of air introduced had exceeded the steady state gas holdup of the suspensions with bubbling times of 60 or 120 seconds. Therefore, the amount of dispersed air in the suspensions is not proportional to bubbling time even with the stabilizing effect of the surfactant. Nevertheless, bubbling of air through the suspensions increased the air content in the suspensions and results from the handsheet machine experiments have confirmed the findings of Brecht and Kirchner that the presence of dispersed air hinders the drainage of pulp suspensions.

A.2 Calibration of Pressure Transducer

In the filtration cell, two pressure sensing devices are used to measure the pressure drop across the fibre bed. One is a Celesco DP-30 differential pressure transducer which measures the differential pressure over the range 0 to 2 psi. The pressure transducer is connected to a Celesco CD10D carrier demodulator that produces signals in the range of 0 to 10V DC. The other device consists of two water manometers.

The pressure transducer has been calibrated using the Series 65-120 Portable Pneumatic Calibrator manufactured by the Wallace & Tiernan Division of Pennwalt Corporation. During the calibration, nitrogen from a cylinder was sent to the pneumatic calibrator and then delivered to the pressure transducer. A pressure gauge on the calibrator gave an accurate reading of the pressure of the nitrogen stream while the pressure transducer caused the demodulator to produce an analog electrical signal of 0 to 10 V DC. The analog signal was then sent to the data acquisition system and the 12-bit A/D converter on the data acquisition system gave a digital signal from 0 to 4095. A calibration curve that correlates the digital signal to the actual pressure drop is needed for the operation of the data acquisition system. Therefore, calibration was carried out and the results are presented in Table A.2.1 below.

After calibration, a sand bed was introduced into the filtration cell. Water was allowed to permeate through the sand bed at different flowrates. The corresponding pressure drops across the bed were recorded by both the pressure transducer and the manometer. Measurements from both devices were compared and excellent agreement was obtained. The results are summarized

in Table A.2.2. Error in the measurement provided by the pressure transducer (assuming that the reading by the manometers were 100% accurate) is presented in Figure A.2.1 while pressure drop readings given by the two devices are plotted against each other in Figure A.2.2 to demonstrate the close agreement between the two devices.

Differential Pressure (psi)	Digital Reading
0	-4
0.5	1012
1	2034
1.5	3051
2	4056

Pressure Drop (psi) = Digital Reading × 0.000492 + 0.000993 $r^2 = 0.9999$

Table A.2.1 Calibration results of the Celesco differential transducer and the resulting calibration curve.

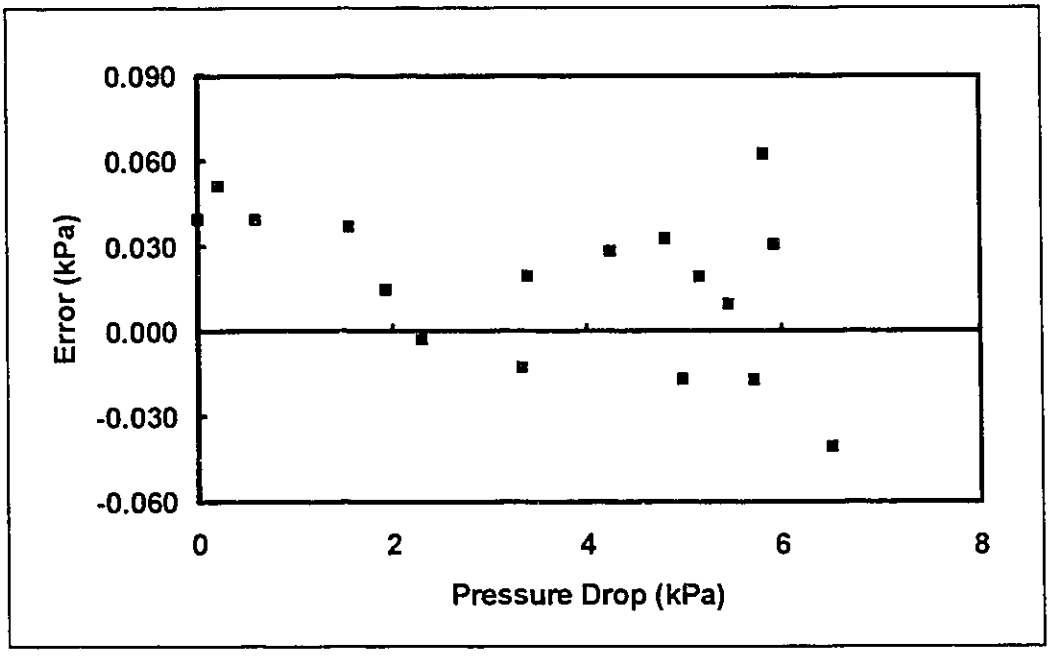

Figure A.2.1 Error in pressure drop measured by the pressure transducer plotted against the pressure drop at which the reading was taken.

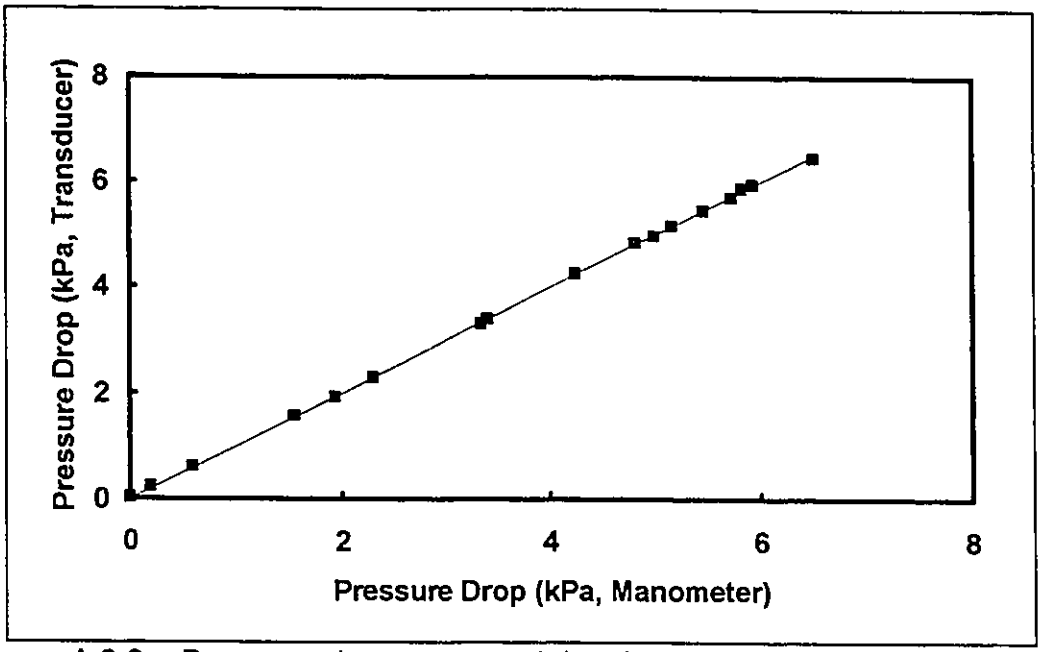

Figure A.2.2 Pressure drop measured by the pressure transducer plotted against the pressure drop measured by the water manometers.

Pressure Drop (kPa, manometer)	Pressure Drop (kPa, transducer)	% Error
0	0.04	NA
0.196	0.247	26.3
0.587	0.627	6.76
1.55	1.58	2.4
1.93	1.94	0.77
2.30	2.30	0.12
3.34	3.32	0.38
3.39	3.41	0.58
4.24	4.27	0.67
4.81	4.84	0.68
4.99	4.97	0.33
5.15	5.17	0.38
5.46	5.47	0.18
5.72	5.70	0.29
5.82	5.88	1.07
5.93	5.96	0.52
6.50	6.46	0.62

Table A.2.2 Comparison between pressure drops measured by the water manometers and the pressure transducer.

A.3 Measurement of Pressure Drop Caused by Porous Brass Plunger and Wire Assembly

Pressure losses across the filtering medium (the porous brass plunger, the paper machine wire and the stainless steel support plate) assembly and in the filtration cell were measured by allowing water to permeate through the pulp pad assembly at various water flowrates. The experimental data are summarized in Table A.3.1 below.

Flowrate of Water (g/s)	Pressure Drop (kPa)
3.72	0.0489
11.94	0.196
25.05	0.538
32.02	0.782
42.4	1.42
66	3.28
82.15	4.76
110.34	7.19
121.74	8.75

Table A.3.1 Summary of data on pressure losses in the filtration cell and across the filtering medium at different flowrates of water.

A.4 Kraft Pulp Fibre Diameter Distribution

The average diameter of wet, swollen kraft pulp fibres was determined from a sample of 96 fibres using image analysis techniques. The number average diameter of the pulp fibres was found to be 26.2 μm with a standard deviation of 8.1 μm. The complete diameter distribution is given in Table A.4.1 below.

Diameter of Beads (μm)	Number of Beads
10	2
12	16
14	31
16	39
18	46
21	56
23	47
25	43
27	27
29	48
31	34
34	31
36	21
38	14
40	8
42	4
44	5
46	4
49	2
51	0
53	2

Table A.4.1 Diameter distribution of polystyrene beads measured by image analysis.

A.5 Verification of The Mathematical Model for Filtration of Suspensions

The approach taken by the author to verify the validity of the mathematical model for filtration here is to apply simplifying assumptions to the model and check if the model is reduced to describe a special case of filtration, namely, filtration of a slurry of incompressible materials.

It has already been mentioned in Chapter 2 that the specific filtration resistance of a slurry of any material is given by,

$$R_w = \frac{5.55 \cdot \sigma^2 \cdot \Delta P}{\int_0^{\Delta P} \left[(1-\alpha c)^3 / c\right] dP} \quad ....(2.3.9)$$

where α, σ, ΔP, c and R_w are the specific swollen volume, specific surface area, pressure drop acting across the fibre bed, the local solid concentration in the bed and the specific filtration resistance of the bed respectively. If the solid materials are incompressible, c is independent of P. Therefore, Equation (2.3.9) becomes,

$$R_w = \frac{5.55 \cdot \sigma^2 \cdot c}{(1-\alpha c)^3}$$

If the slurry contains only one type of solid material that is incompressible, all the mixing rules for the specific surface area, specific swollen volume and equations for the concentration profile in the bed as well as equations for the

average solid concentration in the bed become obsolete. The only pertinent equations remaining are:

Hydrodynamics in the bed: $$\Delta P_{pad} = \int_0^{\Delta P} dP = \frac{Q\mu}{A}\int_0^L \frac{d\ell}{K} = \mu \cdot u \cdot \int_0^L \frac{d\ell}{K} \quad ....(6.3.1)$$

Mass balance over the bed: $$V \cdot c_{min} = A \cdot L \cdot c_{avg} \quad ....(6.3.7)$$

Pressure drop in the equipment: $$\Delta P_{pad} = \Delta P_{total} - f \cdot u^g \quad ....(6.3.10)$$

Definition of volumetric flowrate: $$Q = \frac{dV}{dt} = u \cdot A \quad ....(6.3.8)$$

Kozeny-Carman Equation: $$K = \frac{(1-\alpha c)^3}{5.55\sigma^2 c^2} \quad ....(2.2.9)$$

Since the bed is composed of incompressible materials, the local permeability in the bed and the local solid concentration both become constant. Therefore, Equations (6.3.1) and (6.3.7) become,

$$\Delta P_{pad} = \int_0^{\Delta P} dP = \frac{Q\mu}{A}\int_0^L \frac{d\ell}{K} = \mu \cdot u \cdot \int_0^L \frac{d\ell}{K} = \mu \cdot u \cdot \frac{L}{K}$$

$$V \cdot c_{slurry} = A \cdot L \cdot c$$

Therefore, substitution of Equations (2.2.9), (6.3.7) and (6.3.8) into Equation (6.3.1) yields,

$$\Delta P_{pad} = \frac{\mu \cdot c_{slurry} \cdot 5.55 \cdot \sigma^2 \cdot c}{A^2 \cdot (1-\alpha c)^3} \cdot \frac{VdV}{dt}$$

Integration of the above equation gives,

$$\frac{t - t_1}{V - V_1} = \frac{\mu \cdot 5.55 \cdot \sigma^2 \cdot c_{slurry}}{2A^2 \Delta P_{pad}} \cdot \frac{c}{(1-\alpha c)^3} \cdot (V + V_1)$$

Comparison of the equation above with Equation (2.3.4) which defines the specific filtration resistance gives,

$$R_w = \frac{5.55 \cdot \sigma^2 \cdot c}{(1-\alpha c)^3}$$

which is the special form of Equation (2.3.9). Therefore, it has been demonstrated that the mathematical model reduces to the special form that describes filtration of incompressible materials when the appropriate assumptions are applied. Hence, the verification of the mathematical has been established.

A.6 Listing of Computer Programs

The following is the macro program used in the image analysis of the polystyrene beads to determine the average bead diameter. The macro was kindly supplied and prepared by Mr. Brian Grosse of the McMaster Centre for Pulp and Paper Research.

```
##########################################################################
#     #   PELLET - Brian's Particle Size routine
#     #
#     #   MEASUREMENT OF PELLETS
#     #   Pellets are deagglomerated and the surfaces of
#     #   individual pellets is measured.
#     #
#     #   Images     : pellet (seq of 2 images, size 512x512)
#     #
#     #   LUT        :
#     #   System     : VIDAS 2.1 (standard, no option)
#     #   Author     : MS  27.10.89 / GW  9.02.90
##########################################################################
#  initialization
alpha                                  # alpha mode of menu operation
measstop                               # deactivate old measurement functions
resetpar                               # reset parameters
resetlim                               # reset measskip limits
scalgeom 1,"makro10x",_OFF,_OFF        # scaling in pixel
clearall                               # clear all images
clearallov                             # clear all overlay
setframe "F512"                        # set image size to required format
tvoff                                  # make sure no camera is 'online'
loadlut "grey"                         # black & white look up table
for i=1, i<15, i=i+1 : write ""        # clear message window
##########################################################################
#  initialization of parameters
#
DUMMY = "dummy"
stat1[32]:=0.0
stat2[32]:=0.0
stat3[32]:=0.0
RESP = "y"
write ""
read "Enter the name of your data file  ",DUMMY
write ""
write ""
```

```
write " ... initializing parameters"
InitObj AREA,DMAX,DMIN
measobj 10,DUMMY,_OFF

pell[]=AREA,DMAX,DMIN
AREA=DMAX=DMIN=0.0
######## initialization of database ##########################
dbase = DUMMY
DBerase dbase
DBcreate dbase,"pell"

while(RESP=="y")

###  inputting image  ###################################
loadlut "grey"
write "Cue up focused picture"
write "Press any key to capture image"
tvon
pause
tvinp 1
tvoff
######## image processing loop ##############################
write ""
write " ... processing image "
write " ... image enhancement "
display 1
delin 1,2,180,5,_OFF
write " ... segmentation"
dis?lev 2,3,128,255,_ON,_OFF,1
eraseinside 3,5,255
invert 5,6
fill 6,7
scrap 7,9,_OFF,0,8,_ON,_ON
write " ... erode"
erode 9,10,7,255,2

ANS = "n"
JUNK=500
display 10
while(ANS=="n")
write ""
read "If this is acceptable answer y",ANS
write ""
write ""
read "Enter upper limit on number of pixels to keep ",JUNK
write ""
scrap 10,16,_ON,0,JUNK,_ON,_ON
pause
copy 16,10
endwhile
```

```
write " ... identify with borderline correction"
loadlut "grey"
identframe 10,11,_OFF,1,492,492,10,10,_ON,_OFF,_OFF
write " ... dilate"
erode 11,12,7,0,3
write " ... correction to original size"
display 12
mask 12,9,12,255,0,_ON                    #check mask number
copy 12,13
display 12
measobj 12,DUMMY,_ON
measdbst DUMMY,"AREA",15,_OFF,_ON,0.00,100.00,100.00,"stat1","*"
measdbst DUMMY,"DMIN",15,_OFF,_ON,0.00,100.00,100.00,"stat2","*"
measdbst DUMMY,"DMAX",15,_OFF,_ON,0.00,100.00,100.00,"stat3","*"
display 13
#
outlist DUMMY,_OFF
write ""
read "Enter y if you wish to do another",RESP
write ""
if(RESP=="y")
loadlut "grey"
clearallio
endif
endwhile
######## showing results *##################################*
outlist dbase,_OFF
outhist dbase,"DMIN",15,_OFF,_OFF,0,_ON,_ON,0.00,100,,,"Histogram"
outhist dbase,"AREA",15,_OFF,_OFF,0,_ON,_ON,0.00,100.00,77.00,,"Histogram"
outhist dbase,"DMAX",15,_OFF,_OFF,0,_ON,_ON,0.00,100.00,,,"Histogram"
DBerase dbase
measstop
write
write " end of macro"
stop

#this appears to work well the following that is for discrimination
dis2lev 1,2,64,191,_ON,_ON,1
eraseinside 2,3,255
invert 3,4
fill 4,5
erode 5,6,7,255,2
identframe 6,7,_ON,1,509,431,1,7,_ON,_ON,_ON
erode 7,9,7,0,3
mask 9,5,10,255,0,_ON
copy 4,11
clear 5,0
clovl 5
contour 7,5,13,5,255,_OFF,_ON
loadlut "ident"
initCirc CX,CY,RADIUS
```

```
circdis 13,14,5
clearallio
```

The following is the macro program that was used to determine the average pulp fibre diameter using the image analysis equipment. The macro was again written by Mr. Brian Grosse and modified by the author.

```
alpha
tvon
loadlut "grey"
scalgeom 1,"alexfd",_OFF,_ON
DBerase "PULPDIAM"
DBcreate "PULPDIAM"

while (1)
tvon
loadlut "grey"
write "Cue up video tape"
pause
read "Hit any key to continue",dummy
tvinp 1
display 1
write "Draw your lines on the fiber, Alex."
drawline 1,2,0
clearall 0
display 2
ovlgrey 2,2,3,255
InitObj XMAX,XMIN,YMAX,YMIN
write "locate corners of the frame"
identframe 3,4,_ON,1,512,271,0,18,_ON,_ON,_ON
measobj 4,"PULPDIAM",_ON
outlist "PULPDIAM",_OFF
DBclose "PULPDIAM"
clearall 0
clearallov
endwhile
```

The following is the program written by the author to control the OPTO 22 data acquisition system. The program is written in Microsoft QuickBASIC 4.5. The subroutine OPTOWARE is a subroutine supplied with the OPTO 22 data acquisition system for controlling data input and output between the devices.

```
'    QuickBASIC program for running the OPTO system
'    to monitor the pressure drop and the filtration
'    rate by measuring the weight of filtrate collected
'    ADJUSTABLE READING INTERVAL(12/1/93)
'
'    modifications for QuickBASIC 4.5
'
   REM $STATIC
   DIM positions%(7)      'dimension POSITIONS array to 8 elements
   DIM modifiers%(1)      'dimension MODIFIERS array to 2 elements
   DIM info%(7)           'dimension INFO array to 8 elements
   DECLARE SUB optoware (A%, B%, C%, BYVAL D%, BYVAL E%, BYVAL F%)
   COMMON SHARED errors%, address%, cmd%, positions%(), modifiers%(), info%()
'
'    SYSTEM CONFIGURATION
'
'    host computer : IBM PC/AT
'    serial communication : com 1, 2400 baud
'
'    8 point analog OPTOMUX (B2/PB8AH)
'
'    position     function      type
'      0      pressure drop    input
'
'    AC31 intelligent interface adapter for
'    OPTOMUX network
'
'                function      type
'                weight of     input
'                filtrate
'
'    8 point analog OPTOMUX configuration equates
'
   analog% = 254          'address of analog OPTOMUX = 254
   pressure% = 0
'
'  AC31 Intelligent Interface Adapter configuration equates
'  balance = FF (255)     'address of balance = 255
'
'
'  OPTOMUX command equates
'
   pwrupclr% = 0         'power up clear
   resetopmx% = 1         'reset
   configure% = 7        'configure positions as input/outputs
   readanlin% = 37        'read analog inputs
   setlimits% = 39       'set analog input range
   testlimits% = 41      'read over/under range flags
   clearlimits% = 42     'clear out-of-range limits
```

```
'
'     Dimension and initialize driver parameters
'
    errors% = 0             'initialize errors to 0
    address% = 0            'initialize address to 0
    cmd% = 0                'initialize command to 0
    FOR i% = 0 TO 7         'set all of the POSITIONS and INFO
      positions%(i%) = 0    'array elements to 0
      info%(i%) = 0
    NEXT
    modifiers%(0) = 0       'initialize MODIFIERS array to 0
    modifiers%(1) = 0
'
'     load the driver subroutine
'
    DEF SEG = &H3300        'define segment tells BASIC where to load
    BLOAD "driver.com", 0   'load the driver at segment
'
'     configure the serial port
'
    OPEN "com1:2400,n,8,1,cs,ds,rs,cd" FOR RANDOM AS #1
'
'*************************************************************************
'
'     MAIN SEQUENCER ROUTINE
'
'*************************************************************************
'
'     attempt to initialize the OPTOMUX
'
    KEY OFF: CLS
    INPUT "please enter the file name : ", filen$
    filename$ = filen$ + ".csv"
    OPEN filename$ FOR OUTPUT AS #2
    PRINT ""
    INPUT "please enter interval for data acquisition (in seconds) : ", setint
    PRINT "": PRINT ""
    PRINT "Initialization of OPTOMUX begins..."
    GOSUB 6100              'go initialize OPTOMUX
    IF errors% < 0 THEN
      k = 5
      GOTO 4300             'test for errors
    END IF
'
    PRINT "Finished initialization of OPTOMUX.": PRINT ""
    PRINT "Begins initialization of AC31/balance..."
'
'     attempt to initialize the AC31
'
    GOSUB 8100              'go initialize the AC31
    IF (errors% = -29) THEN
```

```
      PRINT "device timeout error"
      GOTO 5301
    END IF
    IF (LEFT$(response$, 1) <> "A") THEN GOTO 5300
'
    PRINT "Finished initializing AC31."
    PRINT "": PRINT "": PRINT "Press any key to start acquiring data"
    PRINT ""
3000  IF INKEY$ = "" THEN GOTO 3000
    CLS
    PRINT "clearing buffer..."
    PRINT #2, "data left in buffer before start of data acquisition :"
    GOSUB 8850
    PRINT "buffer cleared.": PRINT ""
    PRINT #2, "buffer cleared.": PRINT #2,
    PRINT "To pause or to stop data acquisition, press any key"
    PRINT ""
    PRINT "start reading data..."
    PRINT ""
'
    start = TIMER
    p = 0
    ptime = p * setint
4110  initime = TIMER - start
    IF initime > ptime THEN
      GOSUB 7100                    'read pressure transducer
      IF errors% < 0 THEN GOTO 4300     'test for errors
      GOSUB 8500                    'read data from AC31/balance
      IF (errors% = -29) THEN
        PRINT "device timeout error"
        GOTO 5301
      END IF
      IF (LEFT$(response$, 1) <> "A") THEN GOTO 5300
      p = p + 1
      ptime = p * setint
    END IF
    IF INKEY$ = "" THEN
      GOTO 4110
    ELSE
      INPUT "To pause DA system, enter p; to stop, enter q : ", action$
    END IF
'
    IF action$ = "q" THEN
      GOTO 4280
    ELSE
      PRINT "System halted. Press any key to restart."
    END IF
'
4200  IF INKEY$ = "" THEN GOTO 4200
'
    CLS
```

```
    PRINT "clearing of buffer..."
    PRINT #2, "data left in buffer during pause :"
    GOSUB 8850
    PRINT "buffer cleared.": PRINT ""
    PRINT #2, "buffer cleared.": PRINT #2,
    PRINT "System restarted. Press any key to pause or stop..."
    PRINT ""
    GOTO 4110
'
4280  PRINT #2,
    PRINT #2, "data remaining in buffer after the system has stopped :"
    GOSUB 8850
    PRINT #2, "buffer cleared."
    PRINT #2, : PRINT #2,
    PRINT "Finished reading devices. End of program."
    PRINT #2, "Finished reading devices. End of program."
    END
'
'*************************************************************************
'
'       error recovery code and reinitialization of OPTOMUX
'
'*************************************************************************
'
'       display message indicating error
'
4300  PRINT "error number "; errors%; " encountered at address "; address%
    IF k = 1 THEN
      PRINT "when sending powerup clear": PRINT ""
    ELSEIF k = 2 THEN
      PRINT "when resetting OPTOMUX": PRINT ""
    ELSEIF k = 3 THEN
      PRINT "when configuring I/O rack": PRINT ""
    ELSEIF k = 4 THEN
      PRINT "when reading pressure transducer": PRINT ""
    ELSEIF k = 5 THEN
      PRINT "when setting analog input range": PRINT ""
    END IF
    FOR i% = 1 TO 3         'make noise to signify trouble
      BEEP
    NEXT
'
'       attempt to reinitialize analog OPTOMUX
'
    GOSUB 6100              'go do OPTOMUX initialization
    IF errors% < 0 THEN GOTO 4300
                        'keep trying until successful
    PRINT "system has been reinitialized"
    PRINT "hit return to restart system";
4400  IF INKEY$ = "" THEN GOTO 4400
    GOTO 4110               'go look for start
```

```
'
'*************************************************************************
'
'       error recovery code of AC31/balance
'
'*************************************************************************
'
'       display message indicating error
'
5300  PRINT "not acknowledged error detected in communication with AC31"
5301  IF k = 1 THEN
        PRINT "when sending powerup clear": PRINT ""
      ELSEIF k = 2 THEN
        PRINT "when resetting AC31": PRINT ""
      ELSEIF k = 3 THEN
        PRINT "when returning device type": PRINT ""
      ELSEIF k = 4 THEN
        PRINT "when setting end of text character": PRINT ""
      ELSEIF k = 5 THEN
        PRINT "when specifying device port configuration": PRINT ""
      ELSEIF k = 6 THEN
        PRINT "when getting transmit status from slave": PRINT ""
      ELSEIF k = 7 THEN
        PRINT "when sending ASCII command to request balance data": PRINT ""
      ELSEIF k = 8 THEN
        PRINT "when reading balance data": PRINT ""
      ELSEIF k = 9 THEN
        PRINT "when returning no. of characters waiting in buffer": PRINT ""
      ELSEIF k = 10 THEN
        PRINT "when checking vacancy of slave buffer": PRINT ""
      END IF
'
      IF errors% = -29 GOTO 5400
      PRINT "error message is "; MID$(response$, 2, 2)
5400  FOR i% = 1 TO 3         'make noise to signify trouble
        BEEP
      NEXT
      END
'
'*************************************************************************
'
'       driver calling subroutine
'
'*************************************************************************
'
5580  CALL optoware(errors%, address%, cmd%, VARPTR(positions%(0)),
VARPTR(modifiers%(0)), VARPTR(info%(0)))
5590  RETURN
'
'*************************************************************************
'
```

```
'       initialize the OPTOMUX controllers
'
'*************************************************************************
'
'       initialize analog OPTOMUX
'
6100  address% = analog%        'set the address to analog
    cmd% = pwrupclr%          'first send power up clear
    GOSUB 5580                'call driver to send command
    IF errors% < 0 THEN
      k = 1
      RETURN
    END IF                    'return to main sequencer if there are errors
    cmd% = resetopmx%         'now send a reset command
    GOSUB 5580                'call the driver to send reset
    IF errors% < 0 THEN
      k = 2
      RETURN
    END IF                    'if error return to main sequencer
    cmd% = configure%         'set command to configure
    positions%(0) = pressure% 'put output positions in the array
    positions%(1) = -1        'end of list
    GOSUB 5580                'call driver to send command
    IF errors% < 0 THEN
      k = 3
      RETURN
    END IF
    cmd% = setlimits%         'set analog input range
    positions%(0) = pressure% 'put output positions in the array
    positions%(1) = -1        'end of list
    info%(0) = 4095           'upper limit specified
    info%(1) = -.5            'lower limit specified
    GOSUB 5580                'call driver to send command
    RETURN
'
'*************************************************************************
'
'       read analog pressure transducer output
'
'*************************************************************************
'
7100  address% = analog%        'set address to analog
    cmd% = readanlin%         'set command to read analog inputs
    positions%(0) = pressure% 'specify pressure transducer in POSITIONS
    positions%(1) = -1        'array, -1 marks end of list
    taup = TIMER - start
    GOSUB 5580                'call driver to read pressure
    IF errors% < 0 THEN
      k = 4
      RETURN
    END IF                    'return to main sequencer on error
```

```
    PRINT #2, taup; CHR$(44); (info%(pressure%) * .000744 - 1.01906) * 101.3 / 14.7;
CHR$(44);
    RETURN
'
'*************************************************************************
'
'       initialize the AC31/balance
'
'*************************************************************************
'
8100  PRINT #1, ">FFACD"; CHR$(13);  'send powerup clear
    k = 1
    GOSUB 9100                  'get response from AC31
    IF (LEFT$(response$, 1) <> "A") THEN RETURN 'not acknowledged, error
    PRINT #1, ">FFBCE"; CHR$(13);  'send reset command
    k = 2
    GOSUB 9100
    IF (LEFT$(response$, 1) <> "A") THEN RETURN 'not acknowledged, error
    PRINT #1, ">FFPE7189"; CHR$(13); 'set device port configuration
    k = 5
    GOSUB 9100
    IF (LEFT$(response$, 1) <> "A") THEN RETURN 'not acknowledged, error
    PRINT #1, ">FFEA12"; CHR$(13); 'set end of text character
    k = 4
    GOSUB 9100
    IF (LEFT$(response$, 1) <> "A") THEN RETURN 'not acknowledged, error
    PRINT #1, ">FFFD2"; CHR$(13);  'return device type
    k = 3
    GOSUB 9100
    IF LEFT$(response$, 1) <> "A" THEN
      PRINT ""
      RETURN
    END IF                  'if not acknowledged, print error mssge.
    IF MID$(response$, 2, 2) <> "1F" THEN
      PRINT "device type not properly identified"
      END
    END IF                      'if wrong identification, error
    PRINT #1, ">FFID5"; CHR$(13); 'get transmit status
    k = 6
    GOSUB 9100
    IF LEFT$(response$, 1) <> "A" THEN RETURN
                        'if not acknowledged, print error mssge.
    IF MID$(response$, 2, 1) <> "1" THEN
      PRINT "transmit line busy. Error"
      END
    END IF                      'if busy transmit line, error
    RETURN
'
'*************************************************************************
'
'       reading data from balance
```

```
'
'*************************************************************************
'
8500  PRINT #1, ">FFSSI\r\n13"; CHR$(13);  'write ASCII command to balance
      k = 7
      GOSUB 9100
      IF (LEFT$(response$, 1) <> "A") THEN RETURN 'not acknowledged, error
8550  check = TIMER
      PRINT #1, ">FFRDE"; CHR$(13);              'check buffer vacancy
      GOSUB 9100
      IF MID$(response$, 2, 4) = "0000" THEN GOTO 8550
      taub = check - start
      PRINT #1, ">FFLD8"; CHR$(13);     'ASCII response read from balance
      k = 8
      GOSUB 9100
      IF (LEFT$(response$, 1) <> "A") THEN RETURN 'not acknowledged, error
      PRINT #2, taub; CHR$(44); MID$(response$, 4, 11)
      RETURN
'
'*************************************************************************
'
'       clearing data from buffer
'
'*************************************************************************
'
8850  PRINT #1, ">FFRDE"; CHR$(13);             'check buffer vacancy
      k = 10
      GOSUB 9100
      IF MID$(response$, 2, 4) = "0000" THEN GOTO 8900
      PRINT #1, ">FFLD8"; CHR$(13);     'ASCII response read from balance
      k = 8
      GOSUB 9100
      IF (LEFT$(response$, 1) <> "A") THEN RETURN 'not acknowledged, error
      PRINT #2, CHR$(44); CHR$(44); CHR$(44); MID$(response$, 4, 11)
      GOTO 8850
8900  RETURN
'
'*************************************************************************
'
'      get response from AC31
'
'*************************************************************************
'
9100  response$ = ""                      'initialize input string
      Temp = TIMER
      A$ = "0"                          'initialize input buffer
      errors% = 0                        'clear error variables
      WHILE ASC(RIGHT$(A$, 1)) <> 13          'wait for return
       IF LOC(1) = 0 THEN GOTO 9500
       A$ = ""                         'reinitialize input buffer
       A$ = INPUT$(LOC(1), #1)              'get some characters
```

```
      response$ = response$ + A$
9500   IF (TIMER - Temp) < 2 THEN GOTO 9700
      errors% = -29
      A$ = CHR$(13)
9700  WEND
    RETURN
```

The following is the FORTRAN program for analyzing fixed bed permeation data by nonlinear regression using Marquardt's compromise. The program was originally written by Mr. P. Gloor and later modified by Mr. M. Ajersch, Mr. R. Piette and Mr. M. Towers. The program was finally modified by the author for analysis of fixed bed permeation data. The subroutine MINAME controls the input and output file names, while the subroutine MODEL provides the functional form of the model for the data to be regressed to. The subroutine UWHAUS is the nonlinear least square regression package.

```
        PROGRAM NONLINFT
c this routine was written to use the Nonlinear Least Squares Package
c UWHAUS to estimate the model parameters (p1,p2,p3)
c for a model IN DISCRETE FORMAT
c
c written by P.Gloor, M. Ajersch
c altered by Rich Piette and Mike Towers
c and once again by Richard Piette
c
c References:
c
c   Marquardt, D.L.,
c        J. Soc. Indust. Appl. Math., Vol 2, pp.431-441 (1963)
c
c   "Non-linear Least Squares" D. Meeter, P.J. Wolfe, University of Wisconsin Computing
Center, December 1965
c    UWCC ID Code C0017-00/S00-1700
c
c DECLARATIONS
c
c INTEGERS
        INTEGER NOB,NPROB,NP
c                    number of observations, problem number
c                    and number of parameters
        PARAMETER (NPROB=1,NP=2)
```

```
c
      INTEGER MIT
c                 maximum number of observations
      INTEGER INLUN,OULUN,SCREEN
c                 logical unit numbers
      INTEGER J
c                 a counter
c
c REALS
c
      DOUBLE PRECISION EPS1,EPS2,FLAM,FNU
c                 epsilon 1 and 2 for convergence and
c                 lambda and nu for the method
      DOUBLE PRECISION SIGNS(NP),TH(NP),DIFF(NP)
c                 the signs array, the parameters and the
c                 amount  to perturb each parameter
      DOUBLE PRECISION SCRAT(5*NP+NP*NP+2*100+NP*100)
c                 some scratch space
      DOUBLE PRECISION X1(100),X2(100)
c                 the two measured independent variables
      DOUBLE PRECISION UPPER(NP),LOWER(NP)
c                 the upper and lower values for the
c                 confidence intervals as calculated
c                 by UWHAUS
      DOUBLE PRECISION Y(100),F(100)
c                 the observed and calculated values of
c                 the dependent variable
c
c EXTERNALS
      EXTERNAL MODEL
c                 the subroutine to calculate the model as
c                 a function of x1, x1 and theta
c COMMONS
      COMMON /INDEP/X1,X2
c
c set logical unit numbers
      INLUN=1
      OULUN=2
      SCREEN=6
c
c get input and output names
      CALL MINAME(INLUN,OULUN)
c
c set UWHAUS parameters
c read in input
      READ(INLUN,*)EPS1,EPS2
      READ(INLUN,*)MIT
      READ(INLUN,*)FLAM,FNU
      DO 10,J=1,NP
            READ(INLUN,*)TH(J)
            SIGNS(J)=0.0
```

```
            DIFF(J)=0.1
10      CONTINUE
        READ(INLUN,*)NOB
        DO 20 J=1,NOB
            READ(INLUN,*)X1(J),X2(J),Y(J)
20      CONTINUE
c
c call the Non linear least squares package
c
        WRITE(SCREEN,1005)'Estimation starts...'
        WRITE(*,*)
        CALL UWHAUS(NPROB,MODEL,NOB,Y,NP,TH,DIFF,SIGNS,
     1  EPS1,EPS2,MIT,FLAM,FNU,SCRAT,OULUN,UPPER,LOWER)
c
c write final results
        WRITE(OULUN,1010)'Best Estimate','upper limit','lower limit'
        DO 30 J=1,NP
            WRITE(OULUN,*)TH(J),UPPER(J),LOWER(J)
30      CONTINUE
c
        WRITE(OULUN,*)'  X1          ',
c   1                  '      X2      ',
     2          '    Yexpt     ',
     3          '       Ycalc  '
c
c an optional call to model to get final function values
        CALL MODEL(NPROB,TH,F,NOB,NP)
        DO 40 J=1,NOB
c           WRITE(OULUN,*)X1(J),X2(J),Y(J),F(J)
            WRITE(OULUN,*)X1(J),Y(J),F(J)
40      CONTINUE
        STOP'Successful Completion of regression.'
c
c FORMATS
1000    FORMAT(' ',3(G20.5,1X))
1005    FORMAT(' ',15X,A)
1010    FORMAT(' ',3(A20,1X))
1020    FORMAT(' ',4(1X,A14))
1030    FORMAT(' ',4(1X,G14.5))
        END
```

The following is a listing of the program written by the author in MathCAD 4.0 to simulate elastic permeation based on the Jonsson and Jonsson model.

Modelling Elastic Permeation using Jonsson's Model

Assumptions: - no exchange of solid materials in the bed between adjacent layers of infinitessimal thicknesses
- laminar flow

$s := sec \quad kPa := 1000 \cdot Pa$ Defining the units

$\eta := 8.5 \cdot 10^{-4} \cdot Pa \cdot s \quad \rho := 997 \cdot \frac{kg}{m^3}$

$W := 0.634 \cdot \frac{kg}{m^2} \quad A := 1.96 \cdot 10^{-3} \cdot m^2$

physical properties of the kraft pulp fibres in the pad

$v_{sa} := 3.58 \cdot 10^{-3} \cdot \frac{m^3}{kg} \quad S_s := 3918 \cdot \frac{m^2}{kg}$

specific swollen volume and specific surface area of the fibres

Defining the compressibility equations:

1) experimental (regression)

$M := -0.0444$

$k := 1.86$

$L(P) := \frac{M \cdot P + k}{100} \cdot m$

$C(P) := \frac{1.63 \cdot W}{L(P)}$

2) Jonsson's equation

$N := 0.104$

$P_m := 10.65$

$P_{max} := 10.65$

$X_m := 5.44$

Equation for the local void ratio in the fibre bed

$X(P) := \frac{1 - v_{sa} \cdot C(P)}{v_{sa} \cdot C(P)} \qquad XJ(P) := X_m \cdot \left(\frac{P}{P_m}\right)^{-N}$

Equation for the local permeability in the fibre bed

$KK(X) := \frac{X^3}{5.55 \cdot (1 + X)^2} \qquad XJ2(P) := XJ\left(P_{max}\right) \cdot \exp\left(N - N \cdot \frac{P}{P_{max}}\right)$

Permeation rate of water through the fibre bed

$$J(P) := \frac{v_{sa}}{\eta \cdot W \cdot S_s^{\,2}} \cdot \int_0^P KK(X(P))\, dP \qquad JJ(P) := \frac{v_{sa}}{\eta \cdot W \cdot S_s^{\,2}} \cdot \int_{0.0001}^P KK(XJ(P))\, dP$$

Sample Calculations

Pressure drop varies from 0 to 12 kPa

$p := 0, .5 .. 12$

$p_h := 0.0001, .5 .. 12$

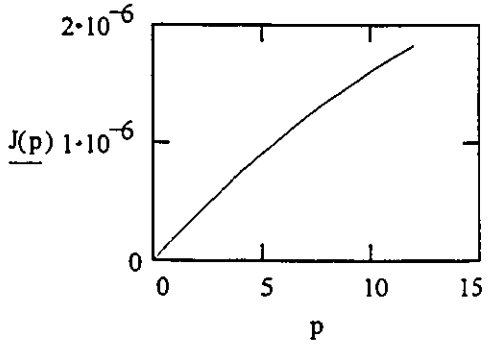

Permeation rate as a function of pressure drop across the pad

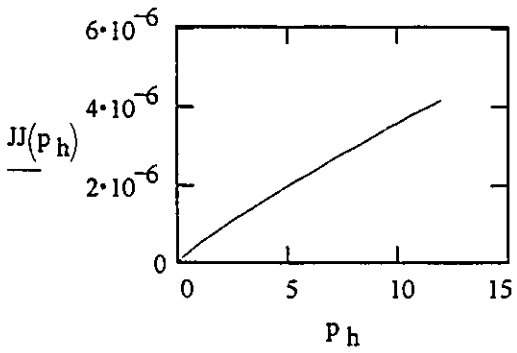

Permeation rate as a function of pressure drop across the pad

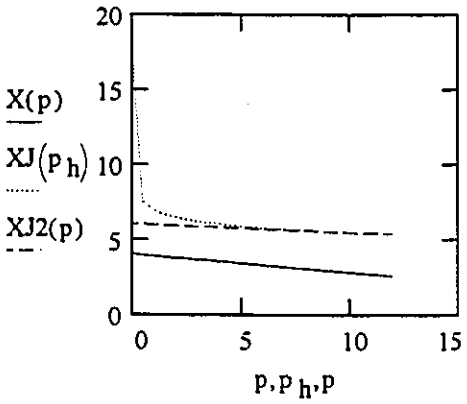

Local void ratio as a function of pressure drop across the pad

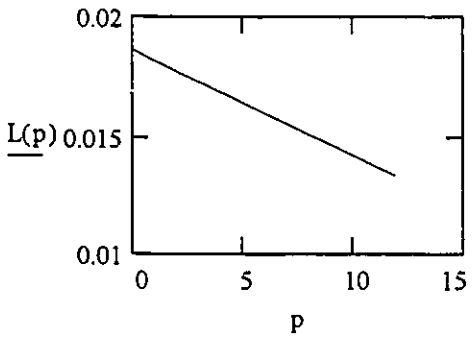

Thickness of the pad as a function of pressure drop across the pad

The following is the FORTRAN program written by Dr. S. Zhu and modified by the author for simulation of the filtration of pulp suspensions. It is based o the equations derived in the model described in Chapter 6.

```
      PROGRAM          CAKE FILTRATION

c     ------------------------------------------------------------
c     Written by Shiping Zhu,
c     modified by Alex Chan to compute VOLUME and PRESSURE
c     as a function of TIME in cake filtration of fiber suspensions
c     Modified version
c     modified on Aug 6, 93 to use actual expt. specific parameters
c     modified on Jan 9, 94 to use revised Kropholler's equation
c     ------------------------------------------------------------

      IMPLICIT DOUBLE PRECISION (A-H,O-Z)
      DIMENSION        Y(1),RWORK(32),IWORK(21)
      EXTERNAL         FUNt,JEXt

      COMMON /ROOM2/          vm,sm,gamma
      COMMON /ROOM3/          eta,A,f,g,Ptot,Cw0,Cmax
      COMMON /ROOM4/          Ppad
      COMMON /ROOM6/          NN

      OPEN                    (UNIT=1,FILE='DATA.CSV',STATUS='NEW')

      NEQ    = 1
      ITOL   = 1
      RTOL   = 1.0D-3
      ATOL   = 1.0D-5
      IOPT   = 1
      RWORK(5) = 1.0D-2
      RWORK(6) = 1.0
      RWORK(7) = 1.0D-5
      ITASK  = 1
      LRW    = 32
      LIW    = 21
      MF     = 22
      ISTATE = 1

c     ------------------------------------------------------------
c     constant parameters used in calculations
c     ------------------------------------------------------------

      eta    = 8.5D-4
      A      = 0.001963
      f      = 1.2941D6
```

```
      g       = 1.78622
c     Ptot    = 10.6D3

      WRITE(*,*)  'INPUT: Particle Weight Fraction, wp'
      READ(*,*)   wp
      WRITE(1,1)  wp
1     FORMAT('wp = ',E20.8)
      WRITE(*,*)  'INPUT: Size of time step, dt'
      READ(*,*)   dt
      WRITE(*,*)  'INPUT: Number of time steps, tn'
      READ(*,*)   tn
      WRITE(*,*)  'INPUT: exponent, r'
      READ(*,*)   gamma
      WRITE(1,2)  gamma
2     FORMAT('r = ',E20.8)
      WRITE(*,*)  'INPUT: slurry solid concentration, Cmin'
      READ(*,*)   Cw0
      WRITE(1,3)  Cw0
3     FORMAT('Cmin = ',E20.8)
      WRITE(*,*)  'INPUT: maximum pad concentration, Cmax'
      READ(*,*)   Cmax
      WRITE(1,4)  Cmax
4     FORMAT('Cmax = ',E20.8)
      WRITE(*,*)  'INPUT: no. of intervals for integration'
      READ(*,*)   NN
      WRITE(*,*)  'INPUT: mixture specific volume, vm'
      READ(*,*)   vm
      WRITE(1,5)  vm
5     FORMAT('vm = ',E20.8)
      WRITE(*,*)  'INPUT: mixture specific area, sm'
      READ(*,*)   sm
      WRITE(1,6)  sm
6     FORMAT('sm = ',E20.8)
      WRITE(*,*)  'INPUT: maximum pressure drop, Ptot'
      READ(*,*)   Ptot
      WRITE(1,7)  Ptot
7     FORMAT('Ptot = ',E20.8)

c     ------------------------------------------------------------------
c     MAIN PROGRAM
c     ------------------------------------------------------------------

      Y(1)    = 0.0
      t       = 0.0
      tout    = 0.0

      DO 100, N = 1, tn
            tout    = tout+dt
            CALL LSODE (FUNt,NEQ,Y,t,tout,ITOL,RTOL,ATOL,ITASK,ISTATE,
     *            IOPT,RWORK,LRW,IWORK,LIW,JEXt,MF)
```

```
              V        = Y(1)
              Ppad = Ppad/1000.0
              V = V*997.0*1000.0
              WRITE(*,*)  t,Ppad,V
              WRITE(1,90)  t,Ppad,V
90            FORMAT(E20.8,',',E20.8,',',E20.8)
              IF (ISTATE .LT. 0) GO TO 110
100     CONTINUE
        STOP
110     WRITE(*,120) ISTATE
120     FORMAT(///22H ERROR HALT.. ISTATE=,I3)
        STOP
        END

c       ------------------------------------------------------------
c       subroutine to calculate the flow velocity using Newton-Raphson
c       algorithm based on pad resistance evaluated by subroutine RESIST
c       ------------------------------------------------------------

        SUBROUTINE          FUNt (NEQ,t,Y,YPRIME)
        IMPLICIT DOUBLE PRECISION (A-H,O-Z)
        DIMENSION           Y(1),YPRIME(1)
        COMMON /ROOM1/          Cwmax,Cwmin
        COMMON /ROOM2/          vm,sm,gamma
        COMMON /ROOM3/          eta,A,f,g,Ptot,Cw0,Cmax
        COMMON /ROOM4/          Ppad

        V       = Y(1)
        Cwmax   = Cmax
        Cwmin   = Cw0
        Cwav    = (gamma*Cwmax+Cwmin)/(gamma+1.0)
        H       = Cw0*V/(A*Cwav)
        CALL      RESIST (H,Rv)

c       ------------------------------------------------------------
c       Newton-Raphson algorithm. The u used as such in line 10 since it is
c       just an initial estimate of the actual flow velocity
c       ------------------------------------------------------------

        u       = (Ptot/f)**(1.0/g)
30      q       = f*(u**g)+eta*Rv*u-Ptot
        qdot    = f*g*(u**(g-1.0))+eta*Rv
        u0      = u-q/qdot
        uERR    = ABS(1.0-u/u0)
        u       = u0
        IF        (uERR.GT.1.0D-5) GO TO 30
        YPRIME(1) =  A*u
        Ppad    = eta*Rv*u
        RETURN
        END
```

```
c     ------------------------------------------------------------
c     subroutine to calculate the filtration resistance by evaluating the
c     the integral form of Darcy's law which is applied to an
c     infinitessimal slice of the pad. Auxiliary information on the
c     local pad consistency and permeability are provided by the
c     subroutine FUNh
c     ------------------------------------------------------------

      SUBROUTINE              RESIST (H,Rv)
      IMPLICIT DOUBLE PRECISION  (A-H,O-Z)
      COMMON /ROOM5/              HH
      COMMON /ROOM6/              NN

      HH      = H
      IF (HH .LE. 0.0) GO TO 300
      CALL SIMP(NN,HH,RvL)
      Rv      = RvL
      GO TO 310
300   Rv      = 0.0
310   RETURN
      END

c     ------------------------------------------------------------
c     subroutine that evaluate the integral using Simpson's rule
c     with NN slices
c     ------------------------------------------------------------

      SUBROUTINE              SIMP(NN,HH,AREA)
      IMPLICIT DOUBLE PRECISION  (A-H,K,O-Z)

      A = 0.0
      B = HH
      HINTV = (B-A)/(2*NN)
      INEND = NN - 1
      SUMEVN = 0.0
      APH = A + HINTV
      CALL Rvh(APH,SUMODD)
      DO 200, IN = 1,INEND
            X = A + 2*IN*HINTV
            XPH = X + HINTV
            CALL Rvh(X,FX)
            CALL Rvh(XPH,FXH)
            SUMEVN = SUMEVN + FX
            SUMODD = SUMODD + FXH
200   CONTINUE
      CALL Rvh(A,FA)
      CALL Rvh(B,FB)
      AREA = (FA + FB + 4.0*SUMODD + 2.0*SUMEVN)*HINTV/3.0
      RETURN
      END
```

```
c     ------------------------------------------------------------
c     subroutine that provides the functional form of the local pad
c     consistency and permeability
c     ------------------------------------------------------------

      SUBROUTINE            Rvh (XLO,KMO)
      IMPLICIT DOUBLE PRECISION  (A-H,K,O-Z)
      COMMON /ROOM1/              Cwmax,Cwmin
      COMMON /ROOM2/              vm,sm,gamma
      COMMON /ROOM5/              HH

      Cw      = Cwmax-(Cwmax-Cwmin)*((XLO/HH)**gamma)
      K       = 1.0-vm*Cw
      K       = K*K*K/(Cw*Cw)
      K       = K/(5.55*sm*sm)
      KMO     = 1.0/K
      RETURN
      END

c     ------------------------------------------------------------
c     subroutines that are not used in this program
c     ------------------------------------------------------------

      SUBROUTINE    JEXt (NEQ,X,Y,ML,MU,PD,NRPD)
      WRITE(*,*)    'NO'
      RETURN
      END
```

A.7 List of Raw Data

List of raw data and supplementary materials are available in computer readable form from A. Chan and Dr. R.H. Pelton. The following is a list of the file names and description of the contents of the files.

File Name	Description
KCS5.XLS	Raw data on the pressure drop across the sand bed at different water flowrates (cf. Ch. 3).
KPB10FBP.XLS	Pressure relaxation data for pads that contained kraft pulp fibres only during fixed bed permeation.
KPB41FBP.XLS	Pressure relaxation data for pads that contained kraft pulp fibres and plastic beads (w_b = 0.2) during fixed bed permeation.
KPB21FBP.XLS	Pressure relaxation data for pads that contained kraft pulp fibres and plastic beads (w_b = 0.33) during fixed bed permeation.
KPB11FBP.XLS	Pressure relaxation data for pads that contained kraft pulp fibres and plastic beads (w_b = 0.5) during fixed bed permeation.
KPB12FBP.XLS	Pressure relaxation data for pads that contained kraft pulp fibres and plastic beads (w_b = 0.67) during fixed bed permeation.
KPB13FBP.XLS	Pressure relaxation data for pads that contained kraft pulp fibres and plastic

	beads (w_b = 0.75) during fixed bed permeation.
KPB14FBP.XLS	Pressure relaxation data for pads that contained kraft pulp fibres and plastic beads (w_b = 0.8) during fixed bed permeation.
KPNF105.XLS	Pressure relaxation data for pads that contained kraft pulp fibres and nylon fibres (w_n = 0.33) during fixed bed permeation.
KPNF110.XLS	Pressure relaxation data for pads that contained kraft pulp fibres and nylon fibres (w_n = 0.49) during fixed bed permeation.
KPNF115.XLS	Pressure relaxation data for pads that contained kraft pulp fibres and nylon fibres (w_n = 0.6) during fixed bed permeation.
KPNF120.XLS	Pressure relaxation data for pads that contained kraft pulp fibres and nylon fibres (w_n = 0.67) during fixed bed permeation.
KPNF125.XLS	Pressure relaxation data for pads that contained kraft pulp fibres and nylon fibres (w_n = 0.71) during fixed bed permeation.
KPNF130.XLS	Pressure relaxation data for pads that contained kraft pulp fibres and nylon fibres (w_n = 0.75) during fixed bed permeation.
KPNF136.XLS	Pressure relaxation data for pads that contained kraft pulp fibres and nylon fibres (w_n = 0.78) during fixed bed permeation.

KPNF150.XLS	Pressure relaxation data for pads that contained kraft pulp fibres and nylon fibres (w_n = 0.83) during fixed bed permeation.
KPNFB140.XLS	Pressure relaxation data for pads that contained kraft pulp fibres, nylon fibres and plastic beads (w_b = 0) during fixed bed permeation.
KPNFB145.XLS	Pressure relaxation data for pads that contained kraft pulp fibres, nylon fibres and plastic beads (w_b = 0.11) during fixed bed permeation.
KPNFB141.XLS	Pressure relaxation data for pads that contained kraft pulp fibres, nylon fibres and plastic beads (w_b = 0.22) during fixed bed permeation.
NONLFITB.XLS	Permeability of the compressed pads during fixed bed permeation calculated by Darcy's law and regressed to the Kozeny-Carman equation. The pads contained kraft pulp fibres and plastic beads.
NONLFITN.XLS	Permeability of the compressed pads during fixed bed permeation calculated by Darcy's law and regressed to the Kozeny-Carman equation. The pads contained kraft pulp fibres and nylon fibres.
NONLFITA.XLS	Permeability of the compressed pads during fixed bed permeation calculated by Darcy's law and regressed to the Kozeny-Carman equation. The pads contained kraft pulp fibres, nylon fibres and plastic beads.
KBEPSUM.XLS	Data on pad thickness and flowrate through the pad at different pressure drops during elastic permeation. The pads contained kraft pulp fibres and plastic beads.

KNEPSUM.XLS	Data on pad thickness and flowrate through the pad at different pressure drops during elastic permeation. The pads contained kraft pulp fibres and nylon fibres.
KNBEPSUM.XLS	Data on pad thickness and flowrate through the pad at different pressure drops during elastic permeation. The pads contained kraft pulp fibres, nylon fibres and plastic beads.
JONMPARA.XLS	Summary of the adjustable parameters used in the Jonsson and Jonsson model to correlate elastic permeation data of all the pads.
KBRW.XLW	Data on pressure drop across the fibre bed and cumulative filtrate weight during filtration of suspensions that contained kraft pulp fibres and plastic beads. Also, specific filtration resistances of the suspensions were calculated from the raw data and the values of the adjustable parameter used in the simulation of filtration were included in the file.
KNRW.XLW	Data on pressure drop across the fibre bed and cumulative filtrate weight during filtration of suspensions that contained kraft pulp fibres and nylon fibres. Also, specific filtration resistances of the suspensions were calculated from the raw data and the values of the adjustable parameter used in the simulation of filtration were included in the file.
KNBRW.XLW	Data on pressure drop across the fibre bed and cumulative filtrate weight during filtration of suspensions that contained kraft pulp fibres, nylon fibres and plastic beads. Also, specific filtration resistances of the suspensions were calculated from the raw data and the values of the adjustable parameter used in the simulation of filtration were included in the file.

A.8 List of Publications Based on This Research

Ajersch, M.J., Pelton, R.H., Chan, A.K.T. & Loewen, S.R., "Measuring Dispersed Air in Newsprint Pulp Suspensions", TAPPI, 75 (2), 125 (1992a).

Chan, A.K.T., Pelton, R.H., Zhu, S. & Baird, M.H.I., "The effects of polystyrene beads and nylon fibres on the permeability of compressed wood fibre pads", submitted to the Canadian Journal of Chemical Engineering in June (1994).

Chan, A.K.T., Pelton, R.H., Zhu, S. & Baird, M.H.I., "The effects of polystyrene beads and nylon fibres on the permeability and filtration resistance of wood fibre pads", in preparation for submission to the Canadian Journal of Chemical Engineering, anticipated date of submission: December (1994).

Chan, A.K.T., Pelton, R.H., Baird, M.H.I. & Kempe, M., a paper on applying the observations made in this research to the area of brownstock washing and investigate the effect of dispersed air on brownstock washing units (planned to be submitted to TAPPI).